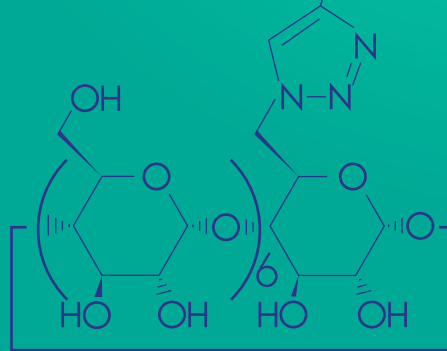


Camilla Facciotti



# Make | it and break it

Stimuli-responsive  
Cyclodextrin-based Complex  
Coacervate Core Micelles

## PROPOSITIONS

1. Host-guest interactions enhance the understanding of assembly and disassembly dynamics of complex coacervate core micelles.  
(this thesis)
2. Significant changes in the structure of cyclodextrin-based complex coacervate core micelles, given specific stimuli, should not be expected by simply including stimuli responsive molecules.  
(this thesis)
3. To benefit from scientific progress, the publication of negative results should be considered as beneficial as the publication of positive results.
4. The race towards personalized nanomedicine will leave low-income countries behind.
5. Support and constructive feedback are the foundation of efficient didactic methods.
6. Equally shared parenting should be mandatory to promote a gender equal society.
7. In politics, the urge for changes, experienced by unsatisfied voters, should not be pursued without the awareness of the possible consequences.

Propositions belonging to the thesis, entitled

Make it and break it. Stimuli-responsive Cyclodextrin-based Complex Coacervate Core Micelles

Camilla Facciotti

Wageningen, 16 December 2019

**Make it and break it**

**Stimuli-responsive Cyclodextrin-based  
Complex Coacervate Core Micelles**

Camilla Facciotti

## **Thesis committee**

### **Promotor**

Prof. Dr Aldrik H. Velders

Professor at the Laboratory of BioNanoTechnology

Wageningen University and Research

### **Co-promotor**

Dr Vittorio Saggiomo

Assistant Professor at the Laboratory of BioNanoTechnology

Wageningen University and Research

### **Other members**

Prof. Dr J. van der Gucht, Wageningen University and Research

Prof. Dr M.M.G. Kamperman, University of Groningen

Dr S. Beeren, Technical University of Denmark, Kongens Lyngby, Denmark

Dr L.M.C. Sagis, Wageningen University and Research

This research was conducted under the auspices of the Graduate School VLAG (Advanced studies in Food Technology, Agrobiotechnology, Nutrition and Health Sciences).

**Make it and break it**  
**Stimuli-responsive Cyclodextrin-based**  
**Complex Coacervate Core Micelles**

Camilla Facciotti

**Thesis**

submitted in fulfilment of the requirements for the degree of doctor  
at Wageningen University  
by the authority of the Rector Magnificus,  
Prof. Dr. A.P.J. Mol,  
in the presence of the  
Thesis Committee appointed by the Academic Board  
to be defended in public  
on Monday 16 December 2019  
at 11.00 am in the Aula.

Camilla Facciotti

Make it and break it

Stimuli-responsive Cyclodextrin-based Complex Coacervate Core Micelles

250 pages

PhD thesis, Wageningen University, Wageningen, the Netherlands (2019)

With references, with summary in English

ISBN: 978-94-6395-152-4

DOI: <https://doi.org/10.18174/501987>





# Make it and break it

## Stimuli-responsive Cyclodextrin-based Complex Coacervate Core Micelles

### Content

<b>Chapter 1</b> General introduction	<b>1</b>
Abstract	
1.1. Nanotechnology towards nanomedicine	
1.2. Polymeric micelles	
1.3. Complex Coacervate Core Micelles	
1.4. Metal-to-ligand-based Complex Coacervate Core Micelles	
1.5. Dendrimicelles	
1.6. Cyclodextrin-based Complex Coacervate Core Micelles	
1.7. Stimuli-responsive Complex Coacervate Core Micelles	
1.8. Motivation, aim and outline of this research	
<b>Chapter 2</b> Cyclodextrin-based Complex Coacervate Core Micelles	<b>39</b>
Abstract	
2.1. Introduction	
2.2. Experimental section	
2.3. Results and discussion	
2.4. Conclusion	
2.5. Supporting information	
2.6. References	

**Chapter 3** Assembly, Disassembly and Reassembly of Cyclodextrin-based Complex Coacervate Core Micelles with Redox-Responsive Supramolecular Cross Linkers **73**

Abstract

3.1. Introduction

3.2. Experimental section

3.3. Results and discussion

3.4. Conclusion

3.5. Supporting information

3.6. References

**Chapter 4** Oxidant-responsive of Ferrocene-based Cyclodextrin Complex Coacervate Core Micelles **117**

Abstract

4.1. Introduction

4.2. Experimental section

4.3. Results and discussion

4.4. Conclusion

4.5. Supporting information

4.6. References

**Chapter 5** Light-responsive Cyclodextrin-based Complex coacervate Core Micelles **149**

Abstract

5.1. Introduction

5.2. Experimental section

5.3. Results and discussion

5.4. Conclusion	
5.5. Supporting information	
5.6. References	
<b>Chapter 6 General Discussions</b>	<b>185</b>
Abstract	
6.1. Main findings	
6.2. Current challenges and future potential	
6.3. Redox stimuli	
6.4. Light stimuli	
6.5. Multi stimuli	
6.6. Encapsulation and release	
6.7. Towards in vitro studies	
6.8. Final considerations	
<b>Chapter 7 Summary</b>	<b>217</b>
<b>Acknowledgments</b>	<b>225</b>
<b>About the author</b>	<b>231</b>
<b>Overview of completed training activities</b>	<b>233</b>
<b>Scientific publications</b>	<b>237</b>



# CHAPTER 1

---

General introduction

---

## ABSTRACT

---

In this chapter we discuss the current challenges in the biomedical field and we introduce nanomedicine as a possible candidate to overcome these challenges. Complex Coacervate Core Micelles have been showing great advances in biomedical applications, due to their ability to solubilize poorly water-soluble drugs, the high stability against salt and dilution, and their great versatility. We focus on the recent progresses towards the achievement of well-controlled Complex Coacervate Core Micelles, by exploiting metal-to-ligand coordination chemistry and dendrimers, as core components. In this thesis, supramolecular host-guest interactions were identified as a promising tool to finely tune the charge of the core-units in Complex Coacervate Core Micelles and their assembly and disassembly behavior, triggered by precise stimuli. At the end of this chapter we present the outline of the thesis.

## 1.1. NANOTECHNOLOGY TOWARDS NANOMEDICINE

The treatment of chronic and severe disorders, such as heart diseases, cancer and diabetes still remains challenging for health care researchers (Figure 1.1).[1-3] Conventional treatments can develop severe side effects and drug resistance, due to the low target specificity, non-selective bio-distribution, and poor water-solubility of the drug.[4] Drugs used nowadays for anticancer treatments, such as paclitaxel and docetaxel, are often toxic and poorly water-soluble, leading to the need of increasing the drug quantity and, thus, also the unwanted side effects.[5-8]

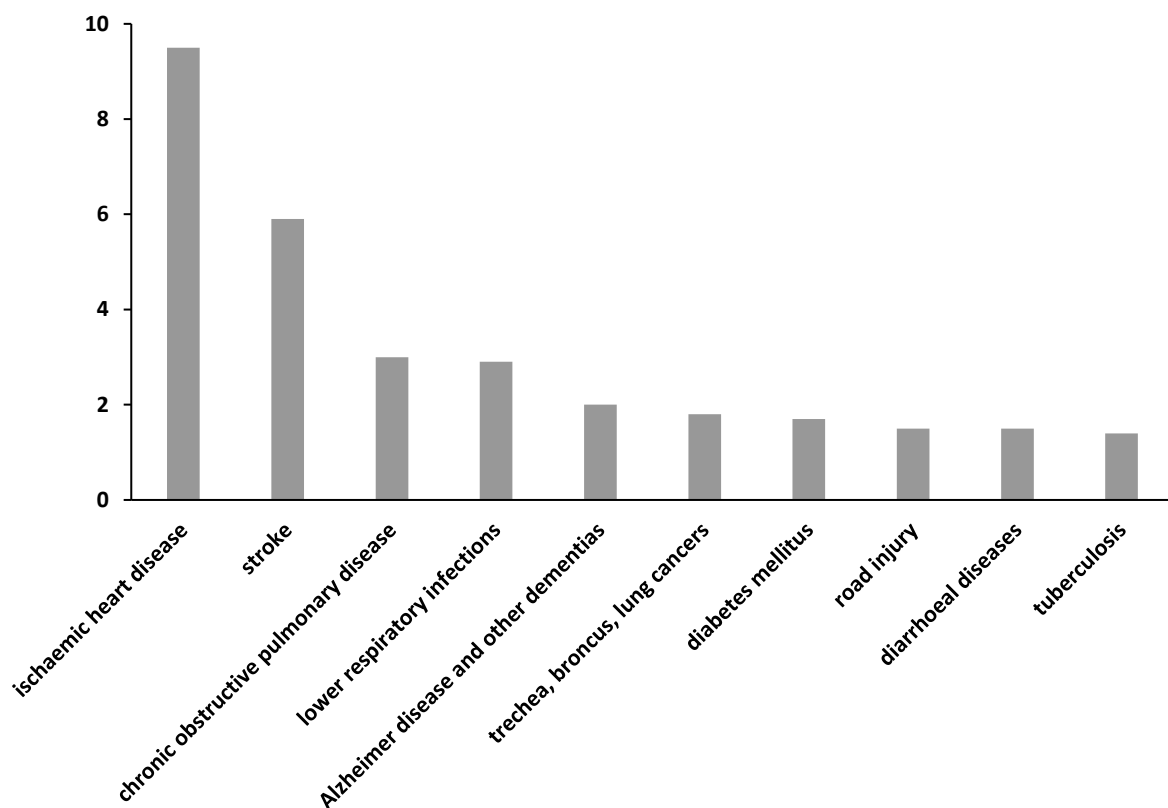


**Figure 1.1.** Top 10 causes of deaths in 2016, according to World health organization's studies. Source: *Global Health Estimates 2016: Deaths by Cause, Age, Sex, by Country and by Region, 2000-2016*. Geneva, World Health Organization; 2018.

Medicine based on nanotechnology, or nanomedicine, is emerging as an alternative (nano-sized) approach for conventional disease treatments, applicable in early diagnosis, therapy monitoring,

drug delivery, and guided surgery.[9-12] The combination of early diagnosis and localized therapy (theranostic) can help in treating the disease in the earliest stage, when it is most likely curable and treatable, lowering costs and risks (Figure 1.2).[4, 6, 13]

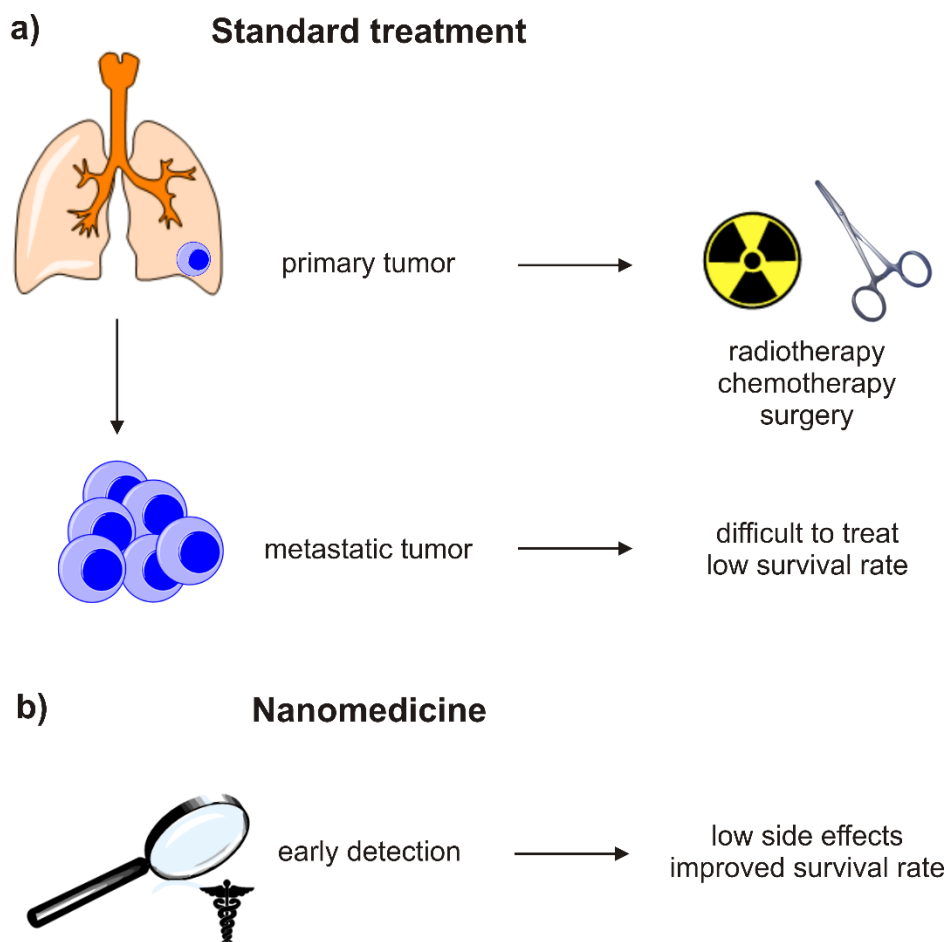


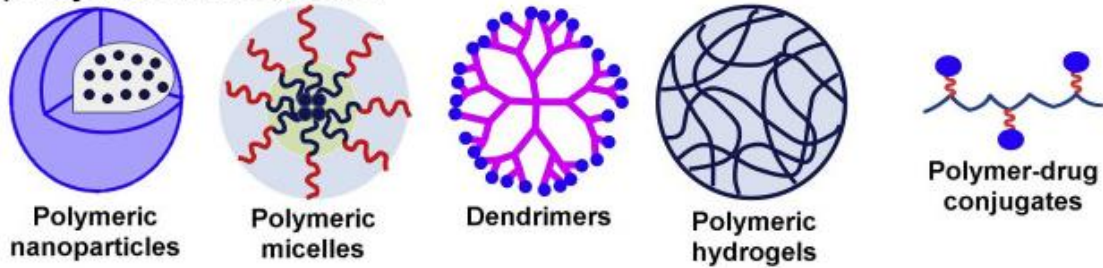
**Figure 1.2.** Representation of standard anticancer treatments a), involving usually surgery, radiotherapy and chemotherapy when the tumor is in the primary phase. When the tumor is in the metastatic phase, the survival rate is low and the tumor remains difficult to treat. Representation of nanomedicine-based approach b), which has the potential advantage of high specificity and drug solubility, that might decrease side effects.

This nanotechnology-based approach relies on the use of nanoparticles or nanocarriers of sub-micron size. Nanocarriers have several advantages compared to conventional treatments, such as i) high surface to volume ratio, ii) favorable and controlled drug release profile, iii) possibility to functionalize the surface and iv) relatively long time of circulation in the blood stream.[3, 6, 14, 15] Those properties allow the nanocarrier to interact more efficiently with tumor cells, release a drug in a precise and localized way and avoid a premature release of the drug or being excreted from the

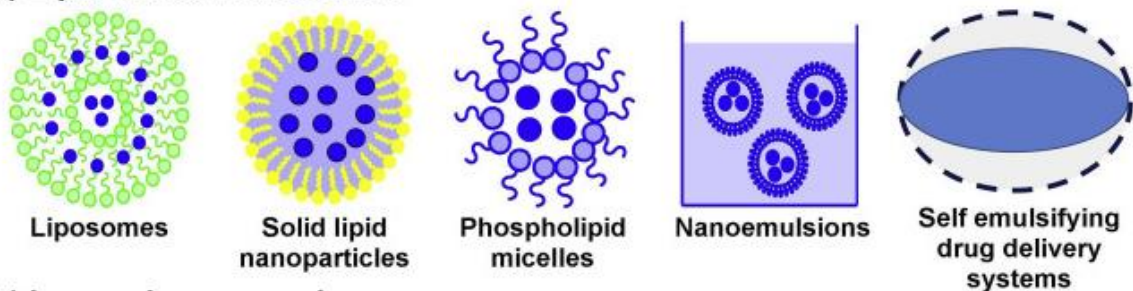
body. Nanocarriers can be categorized in different ways.[6, 10, 14, 16] One way of classifying is to divide them in three categories, based on their composition:

- \* polymer-based (“soft”) nanocarriers, such as polymeric nanoparticles, polymeric micelles, dendrimers, polymeric hydrogels and polymer-conjugated drugs;
- \* lipid-based (“soft”) nanocarriers, such as liposomes, solid-lipid nanoparticles, phospholipid micelles, nanoemulsions and self-emulsifying drug delivery systems;
- \* inorganic-based (“hard”) nanocarriers, such as quantum dots, gold nanoparticles, magnetic nanoparticles, silica nanoparticles, silica nanoparticles and carbon nanotubes.

**(a) Polymeric nanocarriers**



**(b) Lipid-based nanocarriers**



**(c) Inorganic nanocarriers**

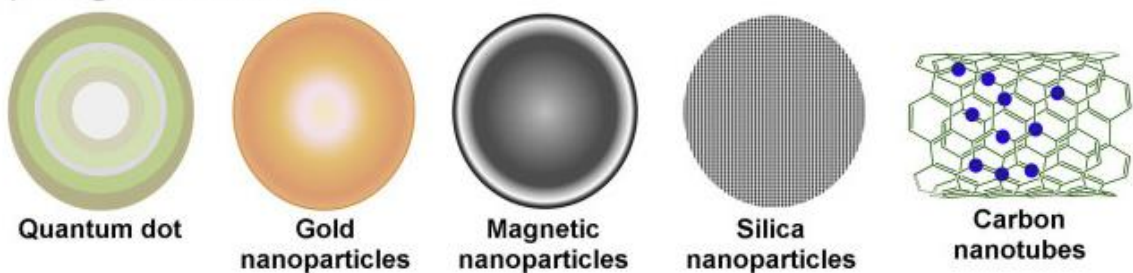


**Figure 1.3.** Classification of nanocarriers in three categories: polymer-based, lipid-based and inorganic-based nanocarriers. This figure was provided by Elsevier and Copyright Clearance center with copyright permission. The figure was published by Arora, D. and S. Jaglan (2016) "Nanocarriers based delivery of nutraceuticals for cancer prevention and treatment: A review of recent research developments." *Trends in Food Science & Technology* 54: 114-126.

Advantages and disadvantages of these nanocarriers are summarized in Table 1.1. The main drawback of magnetic nanoparticles, quantum dots and carbon nanotubes is the potential toxicity of their material, that prevents them from clinical trials. On the other side, those particles have good properties for imaging contrast agents. Supermagnetic based Iron Oxide Nanoparticles, SPIONs, cross-linked and combined with DNA (deoxyribonucleic acid), have shown lower toxicity compared to quantum dots and seem promising for efficient gene delivery and MRI applications.[10, 14] Liposomes and polymeric-based carriers are one of the few nanomaterials already investigated in clinical trials, due to their low toxicity. Especially polymeric micelles have shown biocompatibility, storage stability, solubilization of poorly water-soluble drugs and controllable release. However, a severe disadvantage of these nanocarriers, compared to inorganic nanoparticles, is the risk to undergo degradation before reaching the target site, (Table 1.1).[10, 17]

**Table 1.1.** Summary of the advantages and disadvantages of different nanomaterials. This table was adjusted from Lee, J. J., et al. (2017). "A review on current nanomaterials and their drug conjugate for targeted breast cancer treatment." *Int J Nanomedicine* 12: 2373-2384.

<i>Nanomaterials</i>	<i>Advantages</i>	<i>Disadvantages</i>	<i>Clinical trials for breast cancer treatment</i>
<i>Solid-lipid nanoparticles</i>	Good solubility Good control on drug release kinetic	Low drug loading	Not available
<i>Liposomes</i>	Wide range of drug delivery applications Good drug loading	Cationic lipids cause toxicity Rapid degradation	Liposome-annamycin in phase I/II
<i>Polymeric</i>	Versatility on chemical composition	Degradation	Paclitaxel in polymeric micelles in phase I
<i>Magnetic nanoparticles</i>	Imaging guided	Potential toxicity	Not available
<i>Quantum dots</i>	Imaging guided	Potential toxicity	Not available
<i>Carbon nanotubes</i>	Good penetration at cellular level	Potential toxicity	Not available

Nanocarrier characteristics, such as i) size, ii) morphology, iii) charge and iv) surface properties can influence the diffusion and (bio)distribution inside the body, the toxicity and the drug efficacy (Figure 1.4). [13, 15, 18-21]

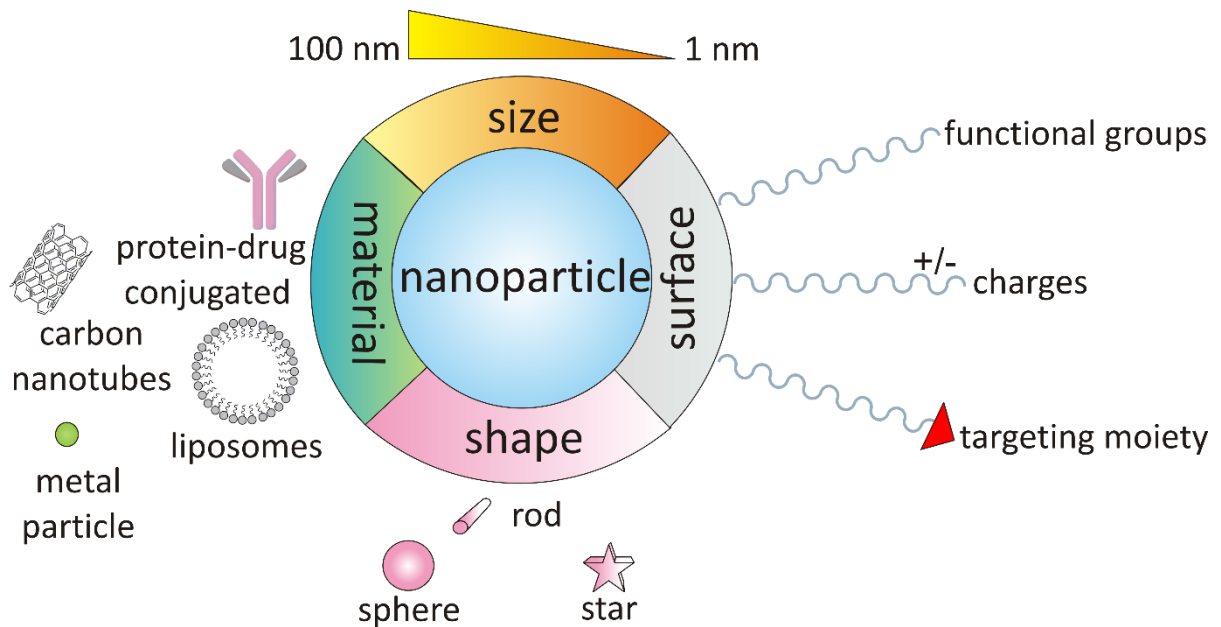


**Figure 1.4.** Representation of nanocarrier' characteristics, such as size, surface functionality, charge, composition and morphology. Those characteristics can influence the nanocarrier biodistribution, toxicity and drug efficiency.

## 1.2. POLYMERIC MICELLES

Hydrophilic and hydrophobic polymers have the ability to self-assemble in water, forming a core-shell micelle structure.[22, 23] The association of the hydrophilic polymers in the shell and the hydrophobic polymers in the core decreases the conformational entropy and the interfacial free energy. The balance between entropy loss and interfacial free energy gain determines the size and shape of thermodynamically stable micelles. After strong interactions have shaped the micellar formation, additional proximity forces, such as Van der Waals and H-bonding, can enhance the core stability.[23-25] Micelles based on self-assembled polymers, or polymeric micelles, are receiving increasing attention over the last decades, especially for biomedical applications.[18, 26, 27] This hype relies on the ability of these micelles, (Figure 1.5.), to solubilize poorly water soluble drugs, on the versatility in controlling their size, shape, surface properties and charge, as explained in the previous section. Figure 1.5. shows the versatility properties of polymeric micelles, such as the ability to encapsulate stimuli-responsive moieties and targeting functionalities and apply them as drug delivery systems or contrast agents.

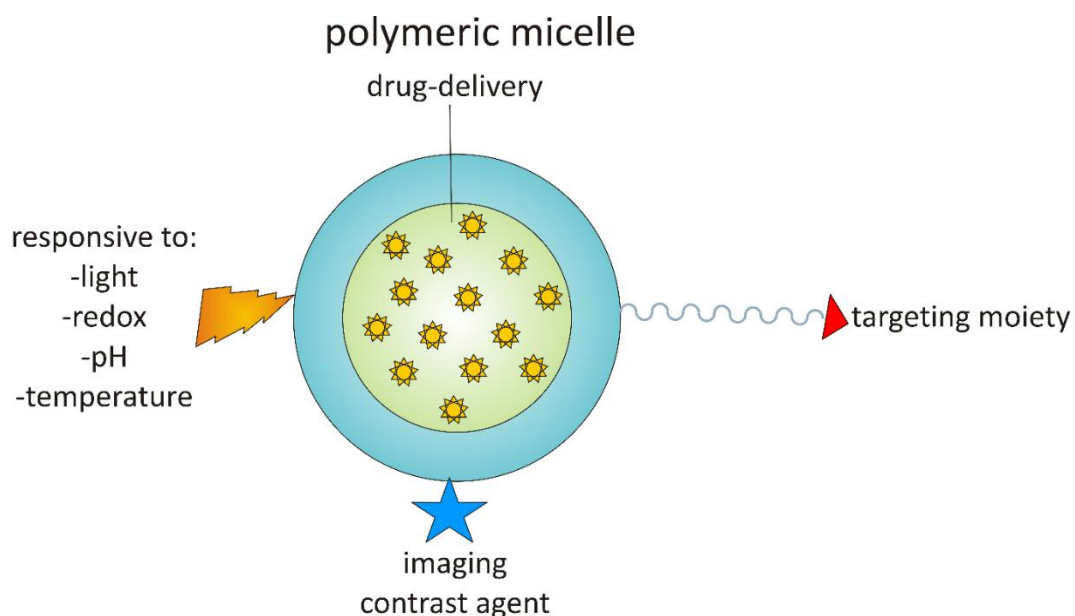


**Figure 1.5.** Representation of polymeric micelle properties. Those micelles seem promising as imaging contrast agents and drug delivery systems. Their versatility relies on the possibility to add targeting agents and/or elements sensitive for light, temperature, redox, or pH.

### 1.3. COMPLEX COACERVATE CORE MICELLES

Coacervation is a liquid-liquid phase separation phenomenon, driven by electrostatic interactions between oppositely charged “macro-ions”. The electrostatic interactions are followed by an entropic gain due to the release of counterions and to the restoration of water molecules. Coacervates are useful in a wide range of applications, such as adhesives, sensors, bioreactors, drug delivery and cartilage mimicking.[28, 29] Attaching these oppositely charged macro-ions to a neutral domain can form a phase separation and, consequently, coacervate micelles. Varying the length of the neutral domain can give rise to different geometries, such as flower-like and vesicles (Figure 1.6.). The assembly of those different coacervate micelles still relies on the self-assembly of oppositely charged polymers, however, there are additional forces that can interfere with the complexation, such as Van der Waals and H-bonding.[30] From the 90's, when the first paper on micelles based on electrostatic interactions was reported, coacervate micelles have gained increasing attention.[31-33] In time, those micelles acquired different names, such as block ionomer complex –BIC (Kabanov),[34, 35] polyion complex micelles-PIC (Harada),[31, 32] Complex Coacervate Core Micelles- C3Ms (Cohen Stuart),[30] and interpolyelectrolyte complexes (Zezin),[36]. All those terms have in common the definition of a water “insoluble” core consisting of oppositely charged units, stabilized by a water-soluble shell.

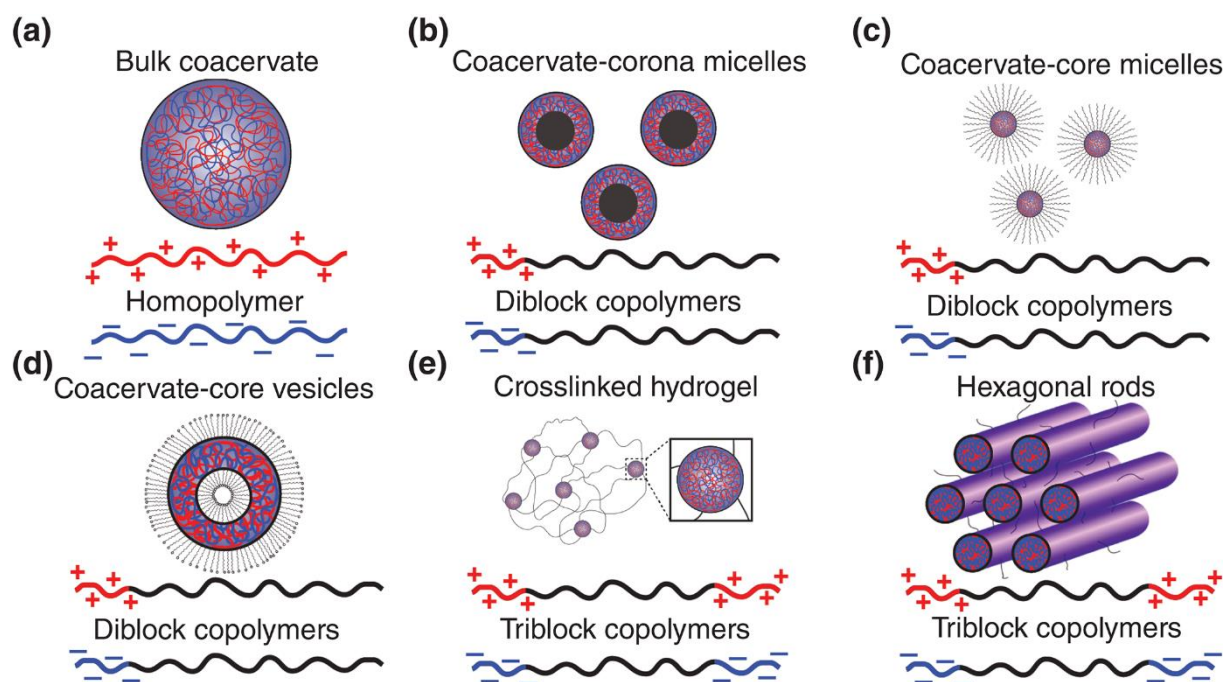


**Figure 1.6.** Representation of bulk coacervate, coacervate corona micelles, coacervate core micelles, coacervate core vesicles, crosslinked hydrogels based on triblock copolymers, hexagonal rods based on triblock copolymers. This figure was provided by John Wiley and Sons with copyright permission. The figure was published by Blocher W.C. and S.L. Perry, "Complex coacervate-based materials for biomedicine" *Wiley Interdiscip Rev Nanomed Nanobiotechnol*, 2017. 9(4).

The first study on this type of micelles was done in the 90's by Harada and Kataoka on poly-lysine and poly-aspartic acid, with a PEO chains.[31] Poly-lysine and poly-aspartic acid were forming micelles of 15 nm size, stable to 350 mM of NaCl. Their following research focused on poly-lysine-PEG-lysozyme micelles, but they were less stable to salt addition (150 mM of NaCl) compared to the previous micelles. Following studies of Cohen Stuart's group tackled fundamental parameters for micelle formation, such as i) CMC (Critical Micelle Concentration), ii) CSC (Critical Salt Concentration), iii) PMC (Preferred Micellar Concentration), iv) pH and v) block copolymer length ratio.[30, 37-40]

- i) CMC is defined as the minimum concentration of micellar monomer required for the formation of a complex micellar structure, by shifting the equilibrium from the monomers to the micelles. Unexpectedly, the CMC is one of the least studied micellar parameters.[30] C3Ms based on metal-to-ligand coordination or on hydrophobic

interactions in the core exhibit a lower CMC, compared to conventional surfactants (10-7 M), making them good candidates for biomedical applications.

- ii) The CSC is defined as the salt concentration until which micelles are stable. By adding salt (and therefore ionic strength), the driving force for micellization diminishes, as electrostatic interactions are screened. Micelles usually adopt a looser structure, their aggregation number decreases and they, finally, swell completely, upon salt addition. A loose structure can end up in a morphological change from spherical micelles to rod like micelles.[38]
- iii) The PMC is defined as the composition at which the mix of positive ( $f^+$ ) and negative ( $f^-$ ) fractions coincides with the overall fraction. By increasing the positive fraction, in a limit  $0 < f^+ < PMC$ , the polymers start to assemble into small complexes and finally into micelles. By increasing, excessively, the positive fraction, the C3Ms dissociate into singular polymers again. Therefore, the PMC corresponds to the ratio of  $f^+$  that would form micelles, without any singular component in excess.[30]
- iv) pH hardly affects the formation when micelles are formed by two strong polyelectrolytes, fully charged in solution, for examples poly-sodium styrene sulfonate. However, when micelles are formed by weak polyelectrolytes, partially charged in solution, for example polyacrylic acid, there might be a critical pH below which the micelle dissociate.[34] If the system is not at the stoichiometric composition, the micelle stability can be easily influenced by the pH variation.
- v) The block copolymer ratio is defined as the optimum ratio of corona/core block polymer length to avoid precipitation.[41] The chemical composition of the corona, the corona solubility and the molecular weight of the block copolymers are also important parameters for the micelle formation.[37, 42]

There are several methods to investigate size, shape and dynamics of C3Ms. The micellar formation is usually confirmed by Static Laser Scattering, Z-potential, viscosimetry and conductometry. Micellar size, structure, morphology and aggregation number are usually studied with Dynamic Laser Scattering, Small Angle X-Ray Scattering, Small Angle Neutron Scattering, cryo-Transmission Electron Microscopy and Atomic Force Microscopy. Most of the studies on micelles

report spherical morphologies.[30] However, to obtain vesicles and other morphologies, additional forces are needed, such as hydrophobic or non-stoichiometric conditions. Most of the micelles present a size range from 10 nm to hundreds and have ideally a polydispersity index (PDI) below 0.1. The PDI is a dimensionless measure of the broadness of the size distribution calculated from the cumulants analysis and it ranges from 0, totally monodispersed sample, to 1, totally polydispersed sample.

Micelles with strong hydrophobic interactions can easily reach a thermodynamic state, in which the size and the polydispersity remain constant in time. A thermodynamically driven assembly usually gives the advantage of highly reproducible, long storing and highly stable properties. By varying the method of preparation, the order of component addition, the titration (or the direct mixing), the results will give the same minimum energy equilibrium state.[30, 41, 43-45] However, micelles consisting of amphiphilic block copolymers can rearrange their structure on different time scales, from milliseconds, to weeks, and therefore, be considered “kinetically frozen”. In a kinetically frozen state, micelles have shape, size and morphology that depends on the preparation protocol and on the time scale.[46-48]

## 1.4. METAL-TO-LIGAND-BASED COMPLEX COACERVATE CORE MICELLES

Cohen Stuart's group has achieved a higher control on the core assembly, compared to the first PIC micelles based on aspartic acid and lysine polymers, by using coordination chemistry. The negatively charged polymer was substituted by a negatively charged metal-to-ligand coordination between dipicolinic acid molecules (DPA) and metal ions (Figure 1.7.). Di-cationic transition metal ions (II), such as Fe, Ni, Co or Zn, can be coordinated by two DPA<sup>2-</sup> molecules.[49] This coordination forms core-units with two residual negative charges in the core (Figure 1.7. d). By adding a neutral and positively charged block copolymer, the residual negative charges can be neutralized, thus, leading to the formation of metal-to-ligand-based C3Ms.

C3Ms, based on these metal-to-ligand coordination structures, are very versatile. By substituting di-cationic transition metal ions with lanthanides (III), core-units become more branched and stable.[50, 51] Changing the ratio between different lanthanides, such as the europium to gadolinium ratio, allows to tune the C3Ms properties from luminescent to magnetic properties (Figure 1.7. e).[52] Velders' group, previously, reported a full study on the coordination structure variation, upon changing the ratio between europium ions to DPA ligand.[53] Upon increasing this ratio, the coordination structure changes from loose oligomeric structure into well-defined polymeric network, highly stable against salt. Yan et al. also reported the formation of a fluorescent and MRI bimodal imaging complex, by using similar Gd-based complex coacervate micelles.[50, 54] Those micelles show a dual channel fluorescence, (in the range of 425-475 nm and 552-617 nm) and an increase of MRI contrast related to the decrease in T1-mode relaxation of the surrounded water molecules. They also proved the negligible cytotoxicity of those micelles in HeLa cells.

By covalently attaching the DPA ligand to the block copolymer, the micelle stability and the lanthanide fluorescence drastically increase (Figure 1.7. f).[55] C3Ms formed using this strategy have similar size, compared to the metal-to-ligand C3Ms discussed above, around 8 nm in core radius and 10 nm in shell.

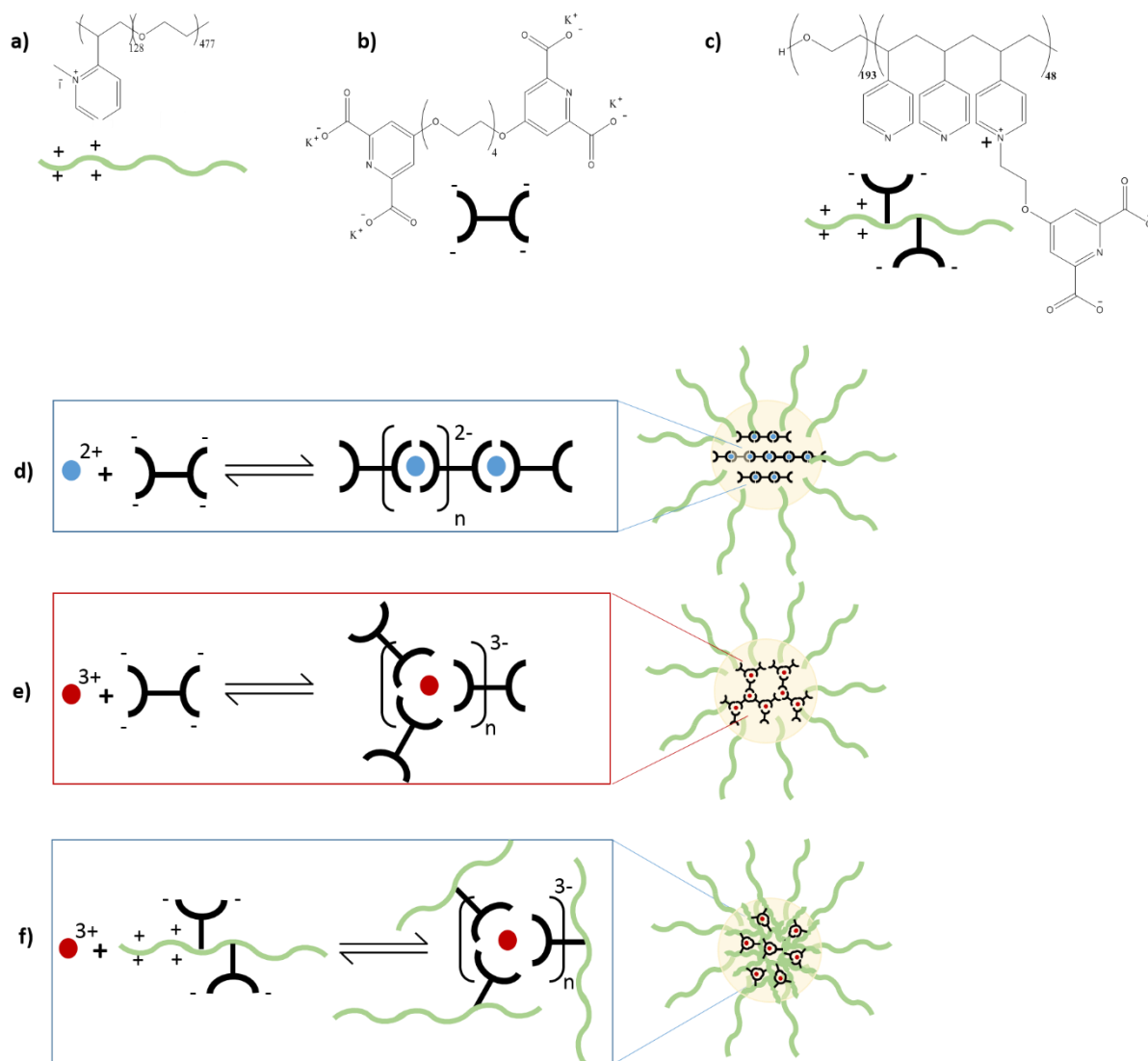


**Figure 1.7.** Schematic representation of block copolymer a), dipicolinic acid bisligand b) and DPA-modified block copolymer c). The coordination between dicationic metal ions (II) and dipicolinic acid ligands forms linear structures that are negatively charged ( $2-$ ). By adding the block copolymer, the coordination structure is neutralized and micelles d) are formed. The coordination between lanthanide ions (III) and dipicolinic acid ligands forms branched polymeric structures that are negatively charged ( $3-$ ). By adding the block copolymer, the coordination structure is neutralized and micelles e) are formed. Mixing the same lanthanide ions and the dipicolinic acid-modified block copolymer in the correct ratio allows the formation of micelles as in f), with good stability and luminescent properties.

## 1.5. DENDRIMCELLES

In 2014 Wang et al. reported an elegant approach to achieve new insight on the assembly of C3Ms, on their aggregation number and their packing density, by encapsulating dendrimers into C3Ms. Negatively-charged PAMAM dendrimers, of different generations, were mixed with neutral and positively charged block copolymer, forming the so-called “dendrimicelles” (Figure 1.8).[56] The results show that the size and the structure of these micelles are independent of the generation of the encapsulated dendrimer. The aggregation number varied from 100 to 1, by increasing the dendrimer generation from 2 to 9. Interestingly, dendrimers of generation below 2 were not able to form any dendrimicelles. This result suggested that there might be a minimum amount of charges required for coacervation. This last hypothesis drove us into a deep study on the ability to finely tune the number of charges, by implementing host-guest interactions into C3Ms (Chapter 2).

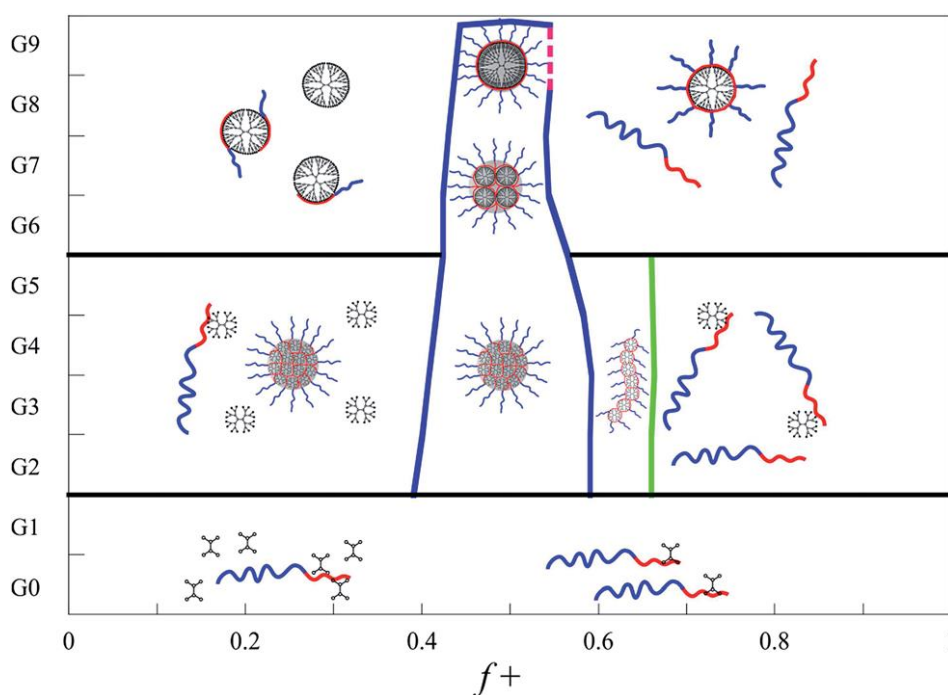


**Figure 1.8.** Schematic representation of dendrimicelles, plotted as dendrimer generation against positive charge fraction. ( $f^+$ ) Below the second generation, dendrimers are not able to form any dendrimicelle structure. Dendrimers of generation 9 to 2 form dendrimicelles with increasing aggregation number (from 1 to 100), at neutral stoichiometric charge. Outside the neutralization stoichiometry, different kind of structures are formed, such as rod like. This figure was taken from Wang, J., et al. (2014). "Controlling the number of dendrimers in dendrimicelle nanoconjugates from 1 to more than 100." *Soft Matter* 10(37): 7337-7345.

A similar approach to the previous one, called “box-in a-box”, was developed by ten Hove et al., to study micellar dynamics and the encapsulation capacity.[57-59] Gold nanoparticles were, firstly, formed inside dendrimers and, secondly, the complex was encapsulated in micelles (AuDENs). This approach allowed a direct counting of the gold nanoparticles and of the dendrimers encapsulated inside the micelles, thanks to the high contrast at the Cryo-TEM. The number of AuDENs per micelle was determined around  $23 \pm 7$ , for G7-based PAMAM. When mixing 50% of empty G7-dendrimers with 50% of fully encapsulated AuDENs, no dynamic exchange was visible in a month-time scale (Figure 1.9).

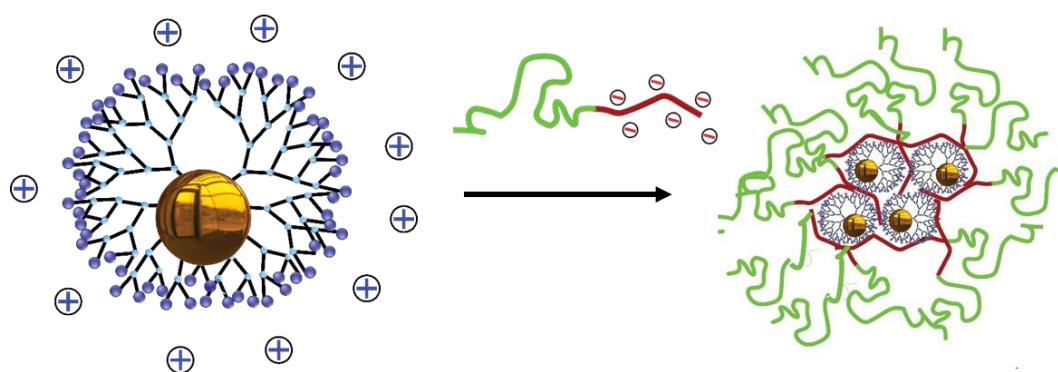


**Figure 1.9.** Representation of “box in a box” structure: gold nanoparticles are synthesized inside dendrimers and this complex is encapsulated inside micelles, by addition an oppositely charged block copolymer.

## 1.6. CYCLODEXTRIN-BASED COMPLEX COACERVATE CORE MICELLES

In the previous sections, we described the self-assembly of Complex Coacervate Core Micelles based on oppositely charged block copolymers. We emphasized the importance of controlling the number of these charges in order to achieve a better understanding of their assembly and disassembly behaviors. Indeed, by encapsulating dendrimers inside a micelle, we discovered that dendrimers of low generations were not able to form any dendrimicelles and therefore, there might be a minimum amount of charges required for coacervation. Besides all the new knowledge that dendrimers brought, the possibility of tuning their charge is strictly limited by the dendrimer generation.[60] Considering a conventional growth approach, every additional reaction yields to a dendrimer with a doubled number of functional groups. According to this, the number of negative charges on the PAMAM dendrimer scales with its generation ( $n$ ) as  $2^n$ , until the starburst limit.

An alternative approach to dendrimers is to combine host-guest interactions inside the core of C3Ms for tuning the charge per core-unit. By fixing the type of host and by varying the charge on the guest, we could finely tune the charge of the core-unit, defined as the smallest unit needed for coacervation. The design and the stability study of this new class of micelles, Cyclodextrin-based Complex Coacervate Core Micelles or C4Ms, are extensively described in Chapter 2.

Several guests have been applied for supramolecular host-guest interactions, such as calixarenes, cucurbiturils, cyclodextrins, etc.[61-63] Especially cyclodextrins have had a pivotal role in supramolecular chemistry in the past 30 years and have been exploited in a wide range of applications, such as food chemistry, catalysis, agriculture, cosmetics, medicine and environment.[62] Cyclodextrins are starch-derived cyclic oligosaccharides, formed by multiple  $\alpha$ -D-glucopyranoside units in a ring linked by  $\alpha$ -1,4-glycosidic bonds (Table 1.2).[62] Cyclodextrins are commonly represented as truncated cones, with a hydrophilic surface and a hydrophobic cavity. Due to the hydrophobic cavity, cyclodextrins are able to host different poor water-soluble guests, such as some anticancer agents (doxorubicin, camptothecin, paclitaxel, fluorouracil) and anti-inflammatory drugs (indomethacin, dexamethasone, ibuprofen). Their insignificant toxicity and the

ability to improve solubility of guest molecules allowed cyclodextrin to be exploited in pharmaceutical applications.[64]

**Table 1.2.** Properties of  $\alpha$ ,  $\beta$ ,  $\gamma$  cyclodextrins in terms of number of glucose units and cavity diameter.[62]

Cyclodextrin	N° of glucose units	Cavity diameter (nm)
$\alpha$	6	0.5
$\beta$	7	0.6
$\gamma$	8	0.8

The forces that influence the complexation between guest molecules and cyclodextrins are mainly four: i) hydrophobic, ii) van der Waals, iii) steric effects and iv) hydrogen bonding. The water present inside the cavity does not affect the complexation.[62] Moreover, the association complex is strongly enhanced by increasing the hydrophobicity of the guest. Usually the hydrophobic part of the guest enters the cyclodextrin cavity and orients in such a way to maximize the interaction between its hydrophobic part and the apolar cavity of the cyclodextrin. One of the most used guest for  $\beta$ -cyclodextrin is adamantane, due to the medium-high association constant ( $10^5 \text{ M}^{-1}$ ). Interestingly, the affinity between hosts and guests can be enhanced by multivalency. Multivalency refers usually to the interaction between multiple host receptors and multiple guest ligands, resulting in the achieving of higher binding affinities, compared to monovalent functionalities.[65] Multivalency plays an important role in many fundamental biological interactions, such as between proteins, antibodies and viruses with cell membranes.[66] These interactions enhance dramatically the ligand ability to bind to a specific target site, compared to weak monovalent binding. The enhancement factor can be calculated as the ratio between the binding constant of a multivalent system with a monovalent system.[65] The binding interaction of a divalent bisadamantane guest on a cyclodextrin-covered surface can be two or three orders of magnitude higher than a mono adamantane guest (Figure 1.10).[67] Multivalency on surfaces, such as flat surfaces,[68] nanoparticles surfaces,[69-71] or cell surfaces, [72] is usually more complicated to study than

multivalency in solution, due to the presence of additional parameters to take into account, such as the orientation, the length and the flexibility of the spacer.[68, 73, 74] There are several techniques to quantify multivalent interactions, such as fluorescence spectroscopy, total internal reflection spectroscopy and microscopy, quartz crystal microbalance, isothermal titration calorimetry and NMR spectroscopy.[65] Multivalent ligands have mainly two advantages, compared to monovalent ones, namely i) the programmability of the number of binding sites, the distance, the rigidity of the linker and ii) the possibility to have hetero-multivalent systems, in which orthogonal binding sites can allow self-sorting studies.[75] In this thesis, we apply the knowledge of surface multivalency to the core of Cyclodextrin-based Complex Coacervate Core Micelles, by using different adamantane bisligands (Chapter 2 and 3).

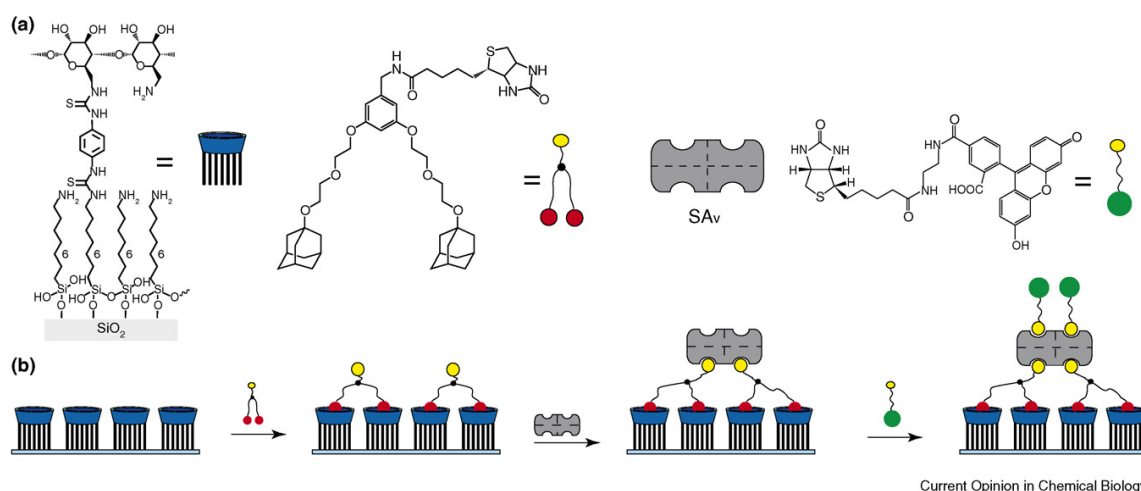


**Figure 1.10.** Representation of building blocks a) and a stepwise assembly of hetero-functional multivalent binding site b). A surface is functionalized with beta cyclodextrins and biotin-modified bisadamantanes guest are added to form multivalent interactions with multiple cyclodextrin hosts. Streptavidines interact with the biotin-modified cyclodextrins and with the biotin-modified dye. The success of those complex hetero-functional multivalent interactions result on a fluorescence signal. This figure was provided by Elsevier and Copyright Clearance center with copyright permission. The figure was published by M. J. Ludden, M. Peter, D. N. Reinhoudt and J. Huskens, *Small*, 2006, 2, 1192.

## 1.7. STIMULI-RESPONSIVE COMPLEX COACERVATE CORE MICELLES

In the previous sections, we reported the ability of C3Ms to encapsulate different cargoes, such as paclitaxel, tamoxifen, camptothecin, DNA, RNA, enzymes, etc, (Figure 1.11.).[18, 23, 28, 30, 39, 76-84] However, the release of these drug from C3Ms, under well-controlled specific stimuli, is still a challenge.

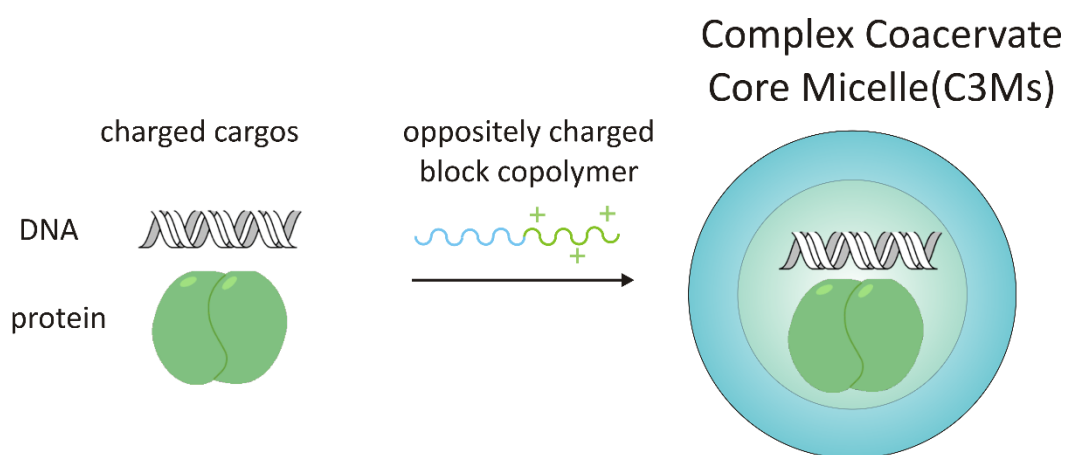


**Figure 1.11.** Representation of coacervate micelles formed by the mixing a charged cargo, such as DNA or protein with an ionic-neutral block copolymer.

An approach to design these specific stimuli-responsive micelles is to combine host-guest interactions. Stimuli-responsive guests can undergo physical or chemical changes in response to specific stimuli, favoring the micelle disassembly and, consequently, the cargo release. The most studied stimuli-responsive host-guest couples are ferrocene-cyclodextrin for redox-responsive-stimuli and azobenzene-cyclodextrin for light responsive-stimuli, Figure 1.12. and Table 1.3.[85-89]

**Table 1.3.** Association constant values between  $\alpha$  and  $\beta$ -cyclodextrin and some of the most common guests.

The brackets underline the ability to form a two to one host-guest complex.

Host/Guest	Adamantane	Ferrocene	Ferrocenium	Azobenzene	Azobenzene
				trans	cis
$\alpha$ CD	(2:1)	(2:1)	(2:1)	$2 \cdot 10^3 \text{ M}^{-1}$	$35 \text{ M}^{-1}$
$\beta$ CD	$10^3 - 10^5 \text{ M}^{-1}$	$3 \cdot 10^3 \text{ M}^{-1}$	$10^1 \text{ M}^{-1}$	$7 \cdot 10^2 \text{ M}^{-1}$	$2 \cdot 10^2 \text{ M}^{-1}$

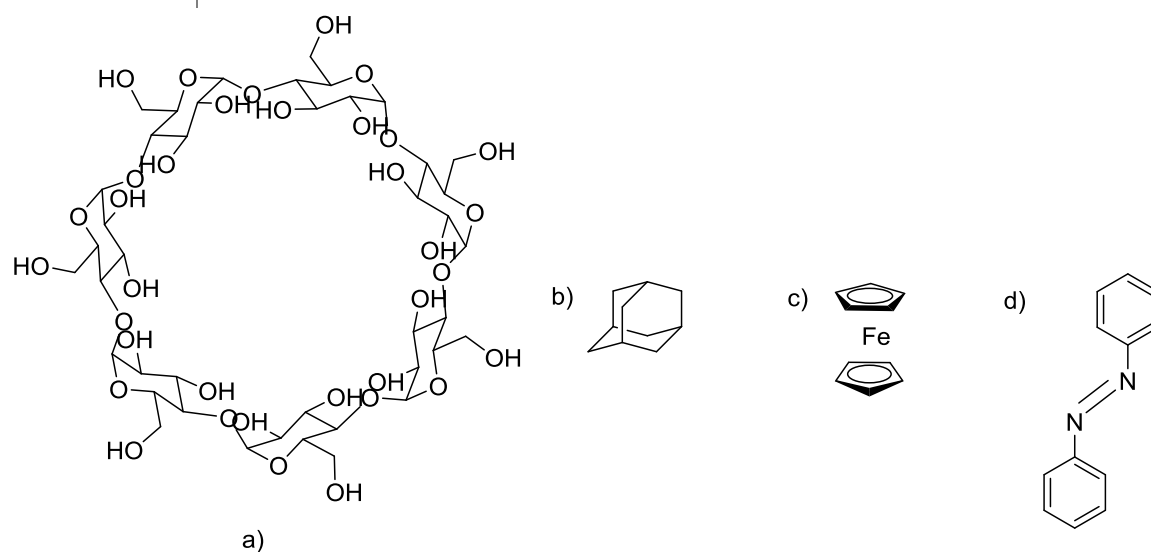


**Figure 1.12.** Representation of a)  $\beta$ -cyclodextrin molecule and different guest molecules, such as b) adamantane, c) ferrocene and d) azobenzene.

Stimuli like (low) pH, reducing environment and high temperature are considered “internal stimuli”, because they are based on intrinsic characteristics of tumor cells. While, stimuli like solvent addition, light and ultrasound are examples of “external stimuli”, regulated by an “external operator” in time and space.[90] Typically, intrinsic characteristics of tumor cells are i) acidic environment (around pH 6.5-7.2), ii) high concentration of glutathione (GSH)[91] and iii) higher temperature [19]. Therefore, designing C3Ms able to disassemble upon acid pH, high GSH concentration and high temperature could be advantageous.[92]



transfection, regulated response and minimal cytotoxicity. Also Li et al. designed redox-responsive micelles able to release DOX under specific stimuli.[97] These micelles were based on polyhydroxylamine polymer containing a redox-sensitive disulfide bond, and a tertiary amine with high buffer capacity in certain pH ranges. DTT triggered the cleavage of the polymeric micelles, leading to the DOX drug release in time. Another approach, to design redox responsive micelles, is to form crosslinked cleavable disulfide bonds on the polymeric shell (Figure 1.14.). Zheng et al. designed crosslinked micelles, based on thiolate polypeptides and siRNA molecules.[102] Upon the addition of GSH reducing agent, the disulfide crosslinks were cleaved and the siRNA was released in the intracellular environment, without compromising their helical structure. The results suggested that disulfide crosslinked micelles can be promising for siRNA cargo release.[102, 103] In Chapter 3, AdSSAd-based C4Ms are introduced. DTT is used to cleave disulfide bonds and trigger the micellar disassembly. The micellar re-assembly was dependent on the time and the DTT concentration.

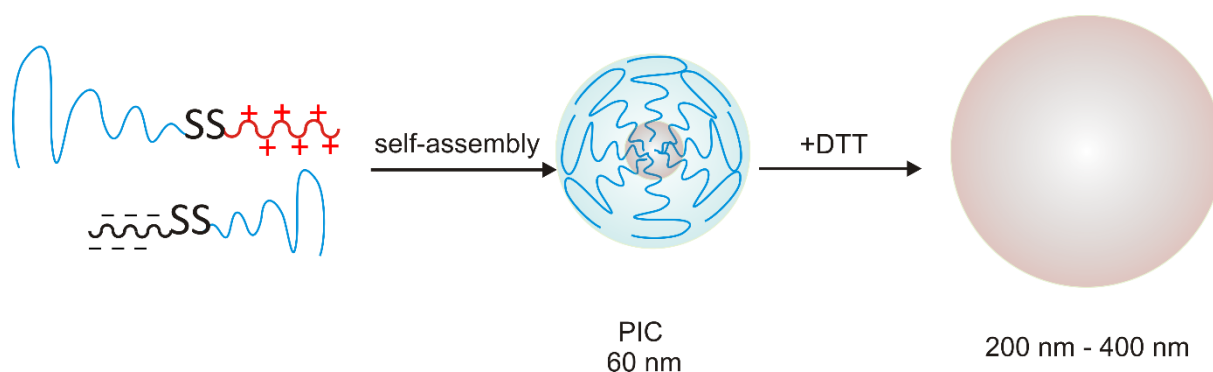


**Figure 1.14.** Schematic illustration of the preparation of PEG-detachable PIC micelle. Upon addition of reducing agent DTT, a morphology transition occurred.

### iii) Temperature

Because of the relatively high temperature of cancer tissues, temperature-responsive micelles can be engineered for hyperthermia applications.[104-107] The change in hydrophobicity/hydrophilicity balance in micelles, due to the high temperature, can cause the micelle to dissociate and release the cargo. [108] One type of thermo-responsive polymeric micelles was introduced into a C6-glioma rat model and showed a drastic tumor inhibition of 83%, without showing toxicity. This type of

micelle is based on DOX encapsulated poly-N-isopropylacrylamide (PNIPAAm) polymers, responsive to temperatures ranging from 30-39°C (Figure 1.15).[18, 109]

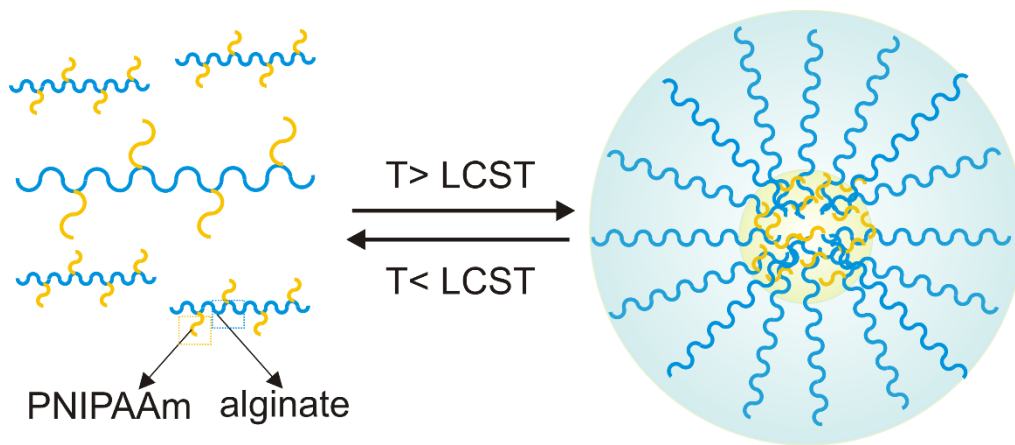


**Figure 1.15.** Schematic representation of thermally reversible alginate-g-PNIPAAm micelle formation. Above a Lower Critical Solution Temperature (LCST) PNIPAAm polymers can form micelles and encapsulate DOX molecules.

#### iv) Light

Light is considered the ideal stimulus, due to i) its non-invasive nature (Near infrared light- NIR especially), ii) the possibility to remotely control it and iii) the high spatio-temporal resolution.[110] Molecules such as azobenzene, pyrene and nitrobenzyl groups are the most commonly used for light responsive molecules. Upon UV-light exposure, those molecules undergo photochemical changes such as photoisomerization, photodimerization or photocleavage, with subsequent disruption of the micelle and release of the cargo.[111-116]

However, NIR light is considered one of the safest wavelength and can penetrate up to 1 cm, without significant damage.[117] Light stimulus is highly versatile and controllable, by varying wavelength, intensity, spot size, exposure time and surface spot-size.[118] Wang et al. reported a surfactant based on an azobenzene molecule. The surfactant was able to assemble in a micellar form under normal conditions.[119] The addition of cyclodextrin caused the disassembly of the micelle. Upon UV-light, the azobenzene molecules were rearranged outside the cyclodextrin cavity

and re-triggered the micelle formation again (Figure 1.16). The formation and light-response of azobenzene-based C4Ms are discussed in chapter 5.

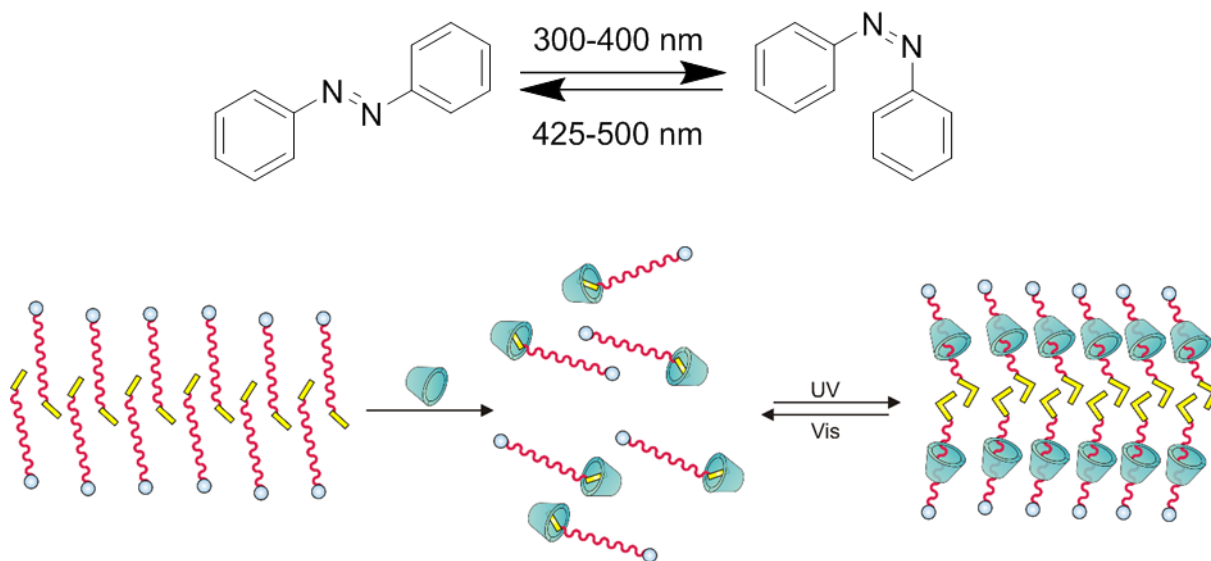


**Figure 1.16.** Top: Chemical representation of the reversible isomerization from trans to cis of azobenzene, under UV and Vis light. Bottom: Representation of photocontrolled assembly and disassembly of azobenzene-based polymeric micelles. The addition of cyclodextrin to the polymer favors the dissociation of the micelle. Upon UV light excitation, the azobenzene is isomerized to its cis form and triggers the re-formation of the micelle.

## 1.8. MOTIVATION, AIM AND OUTLINE OF THIS RESEARCH

The aim of this thesis was to achieve new insight in the assembly and disassembly, encapsulation and release ability of Complex Coacervate Core Micelles, by given specific stimuli. Host-guest interactions were implemented in the core of Complex Coacervate Core Micelles, forming a new class of micelles: Cyclodextrin-based Complex Coacervate Core Micelles or C4Ms, to determine the minimum number of charges per core-unit, required for coacervation. In addition, by adding a responsive guest and by finely tuning the charge, C4Ms can respond in a dynamic way to specific stimuli. Preliminary studies show that C4Ms are able to encapsulate and release a dye, upon reducing agent treatment. Such micelles might be promising for future biomedical applications.

In **chapter 2**, we explore the formation of a new class of Complex Coacervate Core Micelles, called Cyclodextrin-based Complex Coacervate Core Micelles, or C4Ms. This chapter consists of the fundamental investigation of the C4Ms assembly, by finely tuning the core charges. C4Ms stability against salt and dilution can be tuned by the addition of a guest bislinker, able to bridge monomeric core-units into strong polymeric networks.

In **chapter 3**, we present redox-responsive C4Ms, based on the knowledge acquired in chapter 2. Ad-SS-Ad-based C4Ms are designed with a cleavable disulfide bond in the core. Upon the addition of DTT reducing agent, micelles are able to reversibly (dis-)assemble. The rate of re-assembly can be controlled by the DTT concentration and by changing the ratio between responsive and non-responsive bislinker. C4Ms have shown the ability to encapsulate and release methyl red dye under controlled redox stimuli.

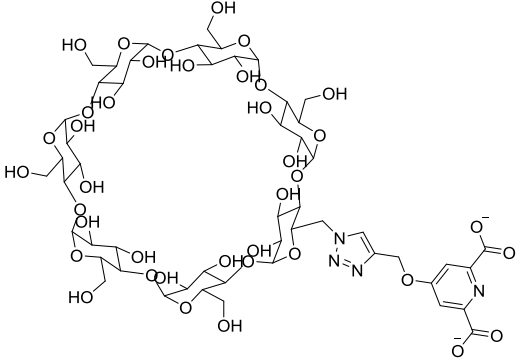
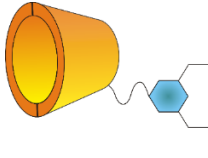
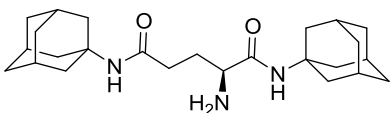
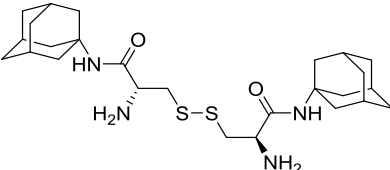
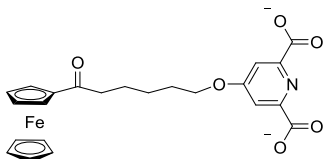
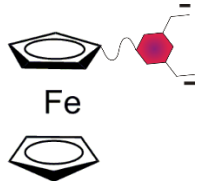
In **chapter 4**, H<sub>2</sub>O<sub>2</sub>-responsive C4Ms are described, based on the knowledge acquired in chapter 2 and chapter 3. Ferrocene-based C4Ms are designed to respond to H<sub>2</sub>O<sub>2</sub> oxidation. By simply changing the europium/ligand ratio, we can tune the core structure from monomeric to oligomeric and, consequently, the oxidant response. The stability of these micelles against H<sub>2</sub>O<sub>2</sub> oxidation can be adjusted in three ways: i) by changing the core-unit from monomeric to oligomeric, ii) by varying the oxidant concentration and iii) by adding a non-responsive guest bislinker.

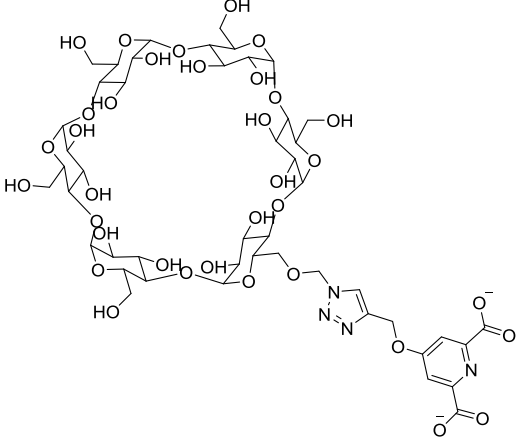
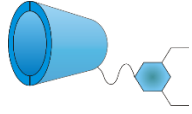
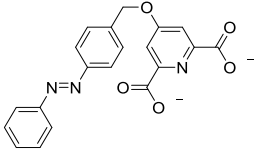
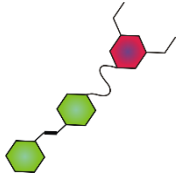
In **chapter 5**, we discuss the challenges related to light-responsive C4Ms. Azobenzene molecules are exploited as a light sensitive switch inside C4Ms. In this case, the knowledge on the charge, acquired in chapter 2 and 3, was essential to weaken Azo-based C4Ms structure and favor the micellar disassembly under light stimuli.

**Chapter 6** summarizes the most important findings of each chapter. Based on these findings, we place our research in perspective and discuss the current challenges and future applications. Additional insight on the ability to control and tune the assembly and disassembly behavior of C4Ms need to be acquired in order to apply these micelles in biomedical field.

Table 1.4. summarizes all the newly synthesized host-guest molecules mentioned throughout the entire thesis and used to develop stimuli-responsive C4Ms. The last figure of this introduction represents an outlook of the projects mentioned in this PhD thesis.

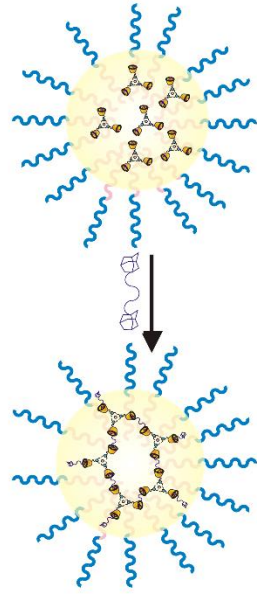
**Table 1.4.** List of newly synthesized compounds discussed throughout this thesis.

Name	Molecular structure	Symbol
<p><b>pyridine-2,6-dicarboxylate-modified <math>\beta</math>-cyclodextrin (<math>\beta</math>CD-DPA)</b></p>		
<p><b>Adamantane-glutamine (Ad-Glu-Ad)</b></p>		
<p><b>Diadamantane-cystine (Ad-SS-Ad)</b></p>		
<p><b>pyridine-2,6-dicarboxylate-modified ferrocene (Fc-DPA)</b></p>		

<p><b>pyridine-2,6-dicarboxylate-modified <math>\alpha</math>-cyclodextrin (<math>\alpha</math>CD-DPA)</b></p>	 <p>The structure shows a cyclodextrin ring with multiple hydroxyl groups. A linker consisting of a methylene group, a diazotized pyridine ring, and another methylene group is attached to one of the hydroxyl groups. The pyridine ring has two carboxylate groups at the 2 and 6 positions.</p>	 <p>A 3D model of the alpha-cyclodextrin molecule, represented as a blue truncated cone, with a smaller blue pyridine ring attached to its side.</p>
<p><b>pyridine-2,6-dicarboxylate-modified Azobenzene (Azo-DPA)</b></p>	 <p>The structure shows an azobenzene molecule (two phenyl rings connected by an azo group) with a pyridine-2,6-dicarboxylate group attached to one of the phenyl rings via a methylene linker.</p>	 <p>A 3D model of the azobenzene molecule, with two green phenyl rings connected by a red azo group, and a red pyridine ring attached to one of the green rings.</p>

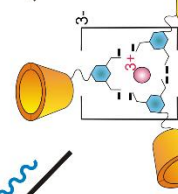
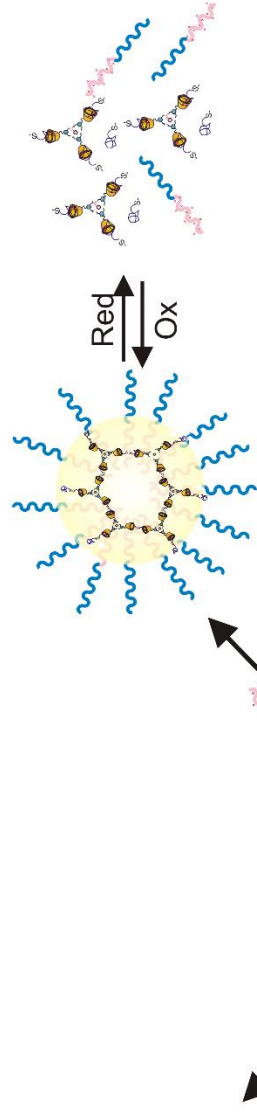
### Chapter 2

Cyclodextrin-based Complex Coacervate Core Micelle with tuneable supramolecular host-guest, metal to ligand and charge interactions.



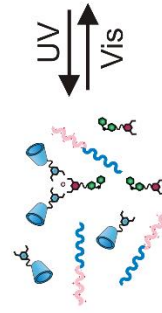
### Chapter 3

Assembly, disassembly and reassembly of Cyclodextrin-based Complex Coacervate Core Micelles with Redox-Responsive Supramolecular Cross Linkers



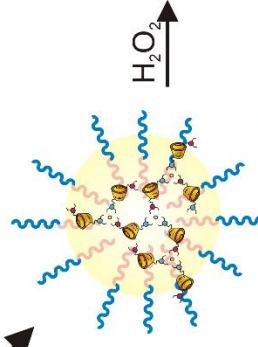
### Chapter 5

Light-responsive Cyclodextrin-based Complex Coacervate Core Micelles



### Chapter 4

Oxidant-responsive Ferrocene-based Cyclodextrin Complex Coacervate Core Micelles



## 1.9. REFERENCES

1. Ferlay, J., Soerjomataram, I., Dikshit, R., Eser, S., Mathers, C., et al., *Cancer incidence and mortality worldwide: sources, methods and major patterns in GLOBOCAN 2012*. Int. J. Cancer, 2015. **136**(5): p. E359-386.
2. Blanco, E., Hsiao, A., Mann, A.P., Landry, M.G., Meric-Bernstam, F., et al., *Nanomedicine in cancer therapy: innovative trends and prospects*. Cancer Sci., 2011. **102**(7): p. 1247-1252.
3. Lee, J.J., Saiful Yazan, L., and Che Abdullah, C.A., *A review on current nanomaterials and their drug conjugate for targeted breast cancer treatment*. Int. J. Nanomedicine, 2017. **12**: p. 2373-2384.
4. Bjornmalm, M., Thurecht, K.J., Michael, M., Scott, A.M., and Caruso, F., *Bridging Bio-Nano Science and Cancer Nanomedicine*. ACS Nano, 2017. **11**(10): p. 9594-9613.
5. Narvekar, M., Xue, H.Y., Eoh, J.Y., and Wong, H.L., *Nanocarrier for poorly water-soluble anticancer drugs--barriers of translation and solutions*. AAPS PharmSci.Tech., 2014. **15**(4): p. 822-833.
6. Tran, S., DeGiovanni, P.J., Piel, B., and Rai, P., *Cancer nanomedicine: a review of recent success in drug delivery*. Clin. Transl. Med., 2017. **6**(1): p. 1-21.
7. Sudhakar, A., *History of Cancer, Ancient and Modern Treatment Methods*. J. Cancer Sci. Ther., 2009. **1**(2): p. 1-4.
8. Cheng, Y., Morshed, R.A., Auffinger, B., Tobias, A.L., and Lesniak, M.S., *Multifunctional nanoparticles for brain tumor imaging and therapy*. Adv. Drug Deliv. Rev., 2014. **66**: p. 42-57.
9. Liu, Y., Miyoshi, H., and Nakamura, M., *Nanomedicine for drug delivery and imaging: a promising avenue for cancer therapy and diagnosis using targeted functional nanoparticles*. Int. J. Cancer, 2007. **120**(12): p. 2527-2537.
10. Muthu, M.S., Leong, D.T., Mei, L., and Feng, S.S., *Nanotheranostics - application and further development of nanomedicine strategies for advanced theranostics*. Theranostics, 2014. **4**(6): p. 660-677.
11. Meershoek, P., van Oosterom, M.N., Simon, H., Mengus, L., Maurer, T., et al., *Robot-assisted laparoscopic surgery using DROP-IN radioguidance: first-in-human translation*. Eur. J. Nucl. Med. Mol. Imaging, 2019. **46**(1): p. 49-53.
12. van Oosterom, M., den Houting, D., van de Velde, C., and van Leeuwen, F., *Navigating surgical fluorescence cameras using near-infrared optical tracking*. J. Biomed. Opt., 2018. **23**(5): p. 1-10.
13. Heinz, H., Pramanik, C., Heinz, O., Ding, Y., Mishra, R.K., et al., *Nanoparticle decoration with surfactants: Molecular interactions, assembly, and applications*. Surface Science Reports, 2017. **72**(1): p. 1-58.
14. S., T.A. and S., G.S., *Nanooncology: The Future of Cancer Diagnosis and Therapy*. CA Cancer. J. Clin., 2019. **63**: p. 398-418.
15. Lembo, D. and Cavalli, R., *Nanoparticulate delivery systems for antiviral drugs*. Antivir. Chem. Chemother., 2010. **21**(2): p. 53-70.
16. Arora, D. and Jaglan, S., *Nanocarriers based delivery of nutraceuticals for cancer prevention and treatment: A review of recent research developments*. Trends Food Sci. Technol., 2016. **54**: p. 114-126.
17. Din, F.U., Aman, W., Ullah, I., Qureshi, O.S., Mustapha, O., et al., *Effective use of nanocarriers as drug delivery systems for the treatment of selected tumors*. Int. J. Nanomedicine, 2017. **12**: p. 7291-7309.
18. Zhou, Q., Zhang, L., Yang, T., and Wu, H., *Stimuli-responsive polymeric micelles for drug delivery and cancer therapy*. Int. J. Nanomedicine, 2018. **13**: p. 2921-2942.
19. Ge, Z. and Liu, S., *Functional block copolymer assemblies responsive to tumor and intracellular microenvironments for site-specific drug delivery and enhanced imaging performance*. Chem. Soc. Rev., 2013. **42**(17): p. 7289-7325.
20. Chiappini, C., De Rosa, E., Martinez, J.O., Liu, X., Steele, J., et al., *Biodegradable silicon nanoneedles delivering nucleic acids intracellularly induce localized in vivo neovascularization*. Nat. Mater., 2015. **14**(5): p. 532-539.
21. Howes, P.D., Chandrawati, R., and Stevens, M.M., *Bionanotechnology. Colloidal nanoparticles as advanced biological sensors*. Science, 2014. **346**(6205): p. 1247390.
22. Blanazs, A., Armes, S.P., and Ryan, A.J., *Self-Assembled Block Copolymer Aggregates: From Micelles to Vesicles and their Biological Applications*. Macromol. Rapid Commun., 2009. **30**(4-5): p. 267-277.
23. Yousefpour Marzbali, M. and Yari Khosroushahi, A., *Polymeric micelles as mighty nanocarriers for cancer gene therapy: a review*. Cancer Chemother. Pharmacol., 2017. **79**(4): p. 637-649.
24. Biswas, S., Kumari, P., Lakhani, P.M., and Ghosh, B., *Recent advances in polymeric micelles for anti-cancer drug delivery*. Eur. J. Pharm. Sci., 2016. **83**: p. 184-202.
25. Ho, K.S. and Shoichet, M.S., *Design considerations of polymeric nanoparticle micelles for chemotherapeutic delivery*. Curr. Opin. Chem. Eng., 2013. **2**(1): p. 53-59.

26. Okesola, B.O. and Smith, D.K., *Applying low-molecular weight supramolecular gelators in an environmental setting - self-assembled gels as smart materials for pollutant removal*. Chem. Soc. Rev., 2016. **45**(15): p. 4226-4251.
27. Talelli, M., Barz, M., Rijcken, C.J., Kiessling, F., Hennink, W.E., et al., *Core-Crosslinked Polymeric Micelles: Principles, Preparation, Biomedical Applications and Clinical Translation*. Nano Today, 2015. **10**(1): p. 93-117.
28. Blocher, W.C. and Perry, S.L., *Complex coacervate-based materials for biomedicine*. Wiley Interdiscip. Rev. Nanomed. Nanobiotechnol., 2017. **9**(4): p. 1-28.
29. Dompe, M., Cedano-Serrano, F.J., Heckert, O., van den Heuvel, N., van der Gucht, J., et al., *Thermoresponsive Complex Coacervate-Based Underwater Adhesive*. Adv. Mater., 2019. **31**(21): p. 1-6.
30. Voets, I.K., de Keizer, A., and Cohen Stuart, M.A., *Complex coacervate core micelles*. Adv. Colloid Interface Sci., 2009. **147-148**: p. 300-318.
31. Harada, A. and Kataoka, K., *Formation of Polyion Complex Micelles in an Aqueous Milieu from a Pair of Oppositely-Charged Block Copolymers with Poly(ethylene glycol) Segments*. Macromolecules, 1995. **28**(15): p. 5294-5299.
32. Harada, A. and Kataoka, K., *Polyion complex micelle formation from double-hydrophilic block copolymers composed of charged and non-charged segments in aqueous media*. Polym. J., 2017. **50**(1): p. 95-100.
33. Lee, Y. and Kataoka, K., *Biosignal-sensitive polyion complex micelles for the delivery of biopharmaceuticals*. Soft Matter, 2009. **5**(20): p. 3810-3817.
34. Kabanov, A.V., Bronich, T.K., Kabanov, V.A., Yu, K., and Eisenberg, A., *Soluble Stoichiometric Complexes from Poly(N-ethyl-4-vinylpyridinium) Cations and Poly(ethylene oxide)-block-polymethacrylate Anions*. Macromolecules, 1996(29): p. 6797-6802.
35. Kim, J.O., Nukolova, N.V., Oberoi, H.S., Kabanov, A.V., and Bronich, T.K., *Block Ionomer Complex Micelles with Cross-Linked Cores for Drug Delivery*. Polym. Sci. Ser. A Chem. Phys., 2009. **51**(6): p. 708-718.
36. Karpushkin, E.A., Kechek'yan, A.S., and Zezin, A.B., *Interpolyelectrolyte reaction between the particles of oppositely charged microgels*. Polym. Sci. Ser. B, 2006. **48**(6): p. 301-303.
37. Hofs, B., Voets, I.K., de Keizer, A., and Cohen Stuart, M.A., *Comparison of complex coacervate core micelles from two diblock copolymers or a single diblock copolymer with a polyelectrolyte*. Phys. Chem. Chem. Phys., 2006. **8**(36): p. 4242-4251.
38. van der Kooij, H.M., Spruijt, E., Voets, I.K., Fokkink, R., Cohen Stuart, M.A., et al., *On the stability and morphology of complex coacervate core micelles: from spherical to wormlike micelles*. Langmuir 2012. **28**(40): p. 14180-14191.
39. Rumyantsev, A.M., Zhulina, E.B., and Borisov, O.V., *Scaling Theory of Complex Coacervate Core Micelles*. ACS Macro Letters, 2018. **7**(7): p. 811-816.
40. Stefan van der Burgh, Keizer, A.d., and Stuart, M.A.C., *Complex Coacervation Core Micelles. Colloidal Stability and Aggregation Mechanism*. Langmuir, 2004. **20**: p. 1073-1084.
41. Cohen Stuart, M.A., Hofs, B., Voets, I.K., and de Keizer, A., *Assembly of polyelectrolyte-containing block copolymers in aqueous media*. Curr. Opin. Colloid Interface Sci., 2005. **10**(1-2): p. 30-36.
42. Aloï, A., Guibert, C., Olijve, L.L.C., and Voets, I.K., *Morphological evolution of complex coacervate core micelles revealed by iPAINT microscopy*. Polymer, 2016. **107**: p. 450-455.
43. Voets, I.K., *Electrostatically Driven Assembly of Polyelectrolytes*. 2016. **16**: p. 65-89.
44. Bodnar, K., Fegyver, E., Nagy, M., and Meszaros, R., *Impact of Polyelectrolyte Chemistry on the Thermodynamic Stability of Oppositely Charged Macromolecule/Surfactant Mixtures*. Langmuir, 2016. **32**(5): p. 1259-1268.
45. Laaser, J.E., Jiang, Y., Petersen, S.R., Reineke, T.M., and Lodge, T.P., *Interpolyelectrolyte Complexes of Polycationic Micelles and Linear Polyanions: Structural Stability and Temporal Evolution*. J. Phys. Chem. B, 2015. **119**(52): p. 15919-15928.
46. Bourouina, N., Cohen Stuart, M.A., and Kleijn, J.M., *Complex coacervate core micelles as diffusional nanopores*. Soft Matter, 2014. **10**(2): p. 320-331.
47. Wu, H., Ting, J.M., Werba, O., Meng, S., and Tirrell, M.V., *Non-equilibrium phenomena and kinetic pathways in self-assembled polyelectrolyte complexes*. J. Chem. Phys., 2018. **149**(16): p. 163330-163339.
48. Yan, Y., Huang, J., and Tang, B.Z., *Kinetic trapping - a strategy for directing the self-assembly of unique functional nanostructures*. Chem. Commun. (Camb), 2016. **52**(80): p. 11870-11884.
49. Wang, J., de Keizer, A., Fokkink, R., Yan, Y., Cohen Stuart, M.A., et al., *Complex coacervate core micelles from iron-based coordination polymers*. J. Phys. Chem. B, 2010. **114**(25): p. 8313-8319.
50. Yang, L., Ding, Y., Yang, Y., Yan, Y., Huang, J., et al., *Fluorescence enhancement by microphase separation-induced chain extension of Eu<sup>3+</sup> coordination polymers: phenomenon and analysis*. Soft Matter, 2011. **7**(6): p. 2720-2724.

51. Hernandez-Garcia, A., Velders, A.H., Stuart, M.A., de Vries, R., van Lent, J.W., et al., *Supramolecular Virus-Like Nanorods by Coassembly of a Triblock Polypeptide and Reversible Coordination Polymers*. Chemistry, 2017. **23**(2): p. 239-243.
52. Wang, J., Velders, A.H., Gianolio, E., Aime, S., Vergeldt, F.J., et al., *Controlled mixing of lanthanide(III) ions in coacervate core micelles*. Chem. Commun. (Camb), 2013. **49**(36): p. 3736-3738.
53. Wang, J., Groeneveld, A., Oikonomou, M., Prusova, A., Van As, H., et al., *Revealing and tuning the core, structure, properties and function of polymer micelles with lanthanide-coordination complexes*. Soft Matter, 2016. **12**(1): p. 99-105.
54. Yan, Y., Besseling, N.A., de Keizer, A., and Stuart, M.A., *Characteristic differences in the formation of complex coacervate core micelles from neodymium and zinc-based coordination polymers*. J. Phys. Chem. B, 2007. **111**(21): p. 5811-5818.
55. Wang, J., Cohen Stuart, M.A., Marcelis, A.T.M., Colomb-Delsuc, M., Otto, S., et al., *Stable Polymer Micelles Formed by Metal Coordination*. Macromolecules, 2012. **45**(17): p. 7179-7185.
56. Wang, J., Voets, I.K., Fokkink, R., van der Gucht, J., and Velders, A.H., *Controlling the number of dendrimers in dendrimicelle nanoconjugates from 1 to more than 100*. Soft Matter, 2014. **10**(37): p. 7337-7345.
57. Ten Hove, J.B., Wang, J., van Leeuwen, F.W.B., and Velders, A.H., *Dendrimer-encapsulated nanoparticle-core micelles as a modular strategy for particle-in-a-box-in-a-box nanostructures*. Nanoscale, 2017. **9**(47): p. 18619-18623.
58. Ten Hove, J.B., Wang, J., van Oosterom, M.N., van Leeuwen, F.W.B., and Velders, A.H., *Size-Sorting and Pattern Formation of Nanoparticle-Loaded Micellar Superstructures in Biconcave Thin Films*. ACS Nano, 2017. **11**(11): p. 11225-11231.
59. Ten Hove, J.B., van Oosterom, M.N., van Leeuwen, F.W.B., and Velders, A.H., *Nanoparticles reveal Extreme Size-Sorting and Morphologies in Complex Coacervate Superstructures*. Sci. Rep., 2018. **8**(1): p. 13820-13827.
60. Sowinska, M. and Urbanczyk-Lipkowska, Z., *Advances in the chemistry of dendrimers*. New J. Chem., 2014. **38**(6): p. 2168-2203.
61. Langton, M.J. and Beer, P.D., *Rotaxane and catenane host structures for sensing charged guest species*. Acc. Chem. Res., 2014. **47**(7): p. 1935-1949.
62. Crini, G., *Review: a history of cyclodextrins*. Chem. Rev., 2014. **114**(21): p. 10940-10975.
63. Liu, Y., Li, C.-J., Guo, D.-S., Pan, Z.-H., and Li, Z., *A Comparative Study of Complexation of  $\beta$ -Cyclodextrin, Calix[4]arenesulfonate and Cucurbit[7]uril with Dye Guests: Fluorescence Behavior and Binding Ability*. Supramol. Chem., 2007. **19**(7): p. 517-523.
64. Hu, Q.D., Tang, G.P., and Chu, P.K., *Cyclodextrin-based host-guest supramolecular nanoparticles for delivery: from design to applications*. Acc. Chem. Res., 2014. **47**(7): p. 2017-2025.
65. Fasting, C., Schalley, C.A., Weber, M., Seitz, O., Hecht, S., et al., *Multivalency as a chemical organization and action principle*. Angew. Chem. Int. Ed. Engl., 2012. **51**(42): p. 10472-10498.
66. Huskens, J., *Multivalent interactions at interfaces*. Curr. Opin. Chem. Biol., 2006. **10**(6): p. 537-543.
67. Ludden, M.J., Peter, M., Reinhoudt, D.N., and Huskens, J., *Attachment of streptavidin to beta-cyclodextrin molecular printboards via orthogonal host-guest and protein-ligand interactions*. Small, 2006. **2**(10): p. 1192-1202.
68. Hsu, S.-H., Yilmaz, M.D., Blum, C., Subramaniam, V., Reinhoudt, D.N., et al., *Expression of Sensitized Eu<sup>3+</sup> Luminescence at a Multivalent Interface*. J. Am. Chem. Soc., 2009. **131**(9): p. 12567-12569.
69. Oikonomou, M., Wang, J., Carvalho, R.R., and Velders, A.H., *Ternary supramolecular quantum-dot network flocculation for selective lectin detection*. Nano Research, 2016. **9**(7): p. 1904-1912.
70. Dorokhin, D., Hsu, S.-H., Tomczak, N., Reinhoudt, D.N., Huskens, J., et al., *Fabrication and Luminescence of Designer Surface Patterns with Cyclodextrin Functionalized Quantum Dots via Multivalent Supramolecular Coupling*. ACS Nano, 2010. **4**(1): p. 137-142.
71. Dorokhin, D., Hsu, S.H., Tomczak, N., Blum, C., Subramaniam, V., et al., *Visualizing resonance energy transfer in supramolecular surface patterns of beta-CD-functionalized quantum dot hosts and organic dye guests by fluorescence lifetime imaging*. Small, 2010. **6**(24): p. 2870-2876.
72. Rood, M.T.M., Spa, S.J., Welling, M.M., ten Hove, J.B., van Willigen, D.M., et al., *Obtaining control of cell surface functionalizations via Pre-targeting and Supramolecular host guest interactions*. Sci. Rep., 2017. **7**: p. 39908-39919.
73. Hsu, S.H., Yilmaz, M.D., Reinhoudt, D.N., Velders, A.H., and Huskens, J., *Nonlinear amplification of a supramolecular complex at a multivalent interface*. Angew. Chem. Int. Ed. Engl., 2013. **52**(2): p. 714-719.
74. Hsu, S.-H., Yilmaz, M.D., Blum, C., Subramaniam, V., Reinhoudt, D.N., et al., *Expression of Sensitized Eu<sup>3+</sup> Luminescence at a Multivalent Interface*. J. Am. Chem. Soc., 2009. **131**: p. 12567-12569.
75. Willems, S.B.J., Schijven, L.M.I., Bunschoten, A., van Leeuwen, F.W.B., Velders, A.H., et al., *Covalently bound monolayer patterns obtained by plasma etching on glass surfaces*. Chem. Commun. (Camb), 2019. **55**(53): p. 7667-7670.

76. Lueckheide, M., Vieregg, J.R., Bologna, A.J., Leon, L., and Tirrell, M.V., *Structure-Property Relationships of Oligonucleotide Polyelectrolyte Complex Micelles*. Nano Lett., 2018.
77. Obermeyer, A.C., Mills, C.E., Dong, X.H., Flores, R.J., and Olsen, B.D., *Complex coacervation of supercharged proteins with polyelectrolytes*. Soft Matter, 2016. **12**(15): p. 3570-3581.
78. Oishi, M., Nagatsugi, F., Sasaki, S., Nagasaki, Y., and Kataoka, K., *Smart polyion complex micelles for targeted intracellular delivery of PEGylated antisense oligonucleotides containing acid-labile linkages*. Chembiochem., 2005. **6**(4): p. 718-725.
79. S., L., R., d.V., W., N., and A., C.S.M., *Structure and Stability of Complex Coacervate Core Micelles with Lysozyme*. Biomacromolecules, 2007. **8**: p. 2219-2227.
80. Montree Jaturanpinyo, Atsushi Harada, Yuan, X., and Kataoka, K., *Preparation of Bionanoreactor Based on Core-Shell Structured Polyion Complex Micelles Entrapping Trypsin in the Core Cross-Linked with Glutaraldehyde*. Bioconjugate Chem., 2004. **15**: p. 344-348.
81. Nolles, A., van Dongen, N.J.E., Westphal, A.H., Visser, A., Kleijn, J.M., et al., *Encapsulation into complex coacervate core micelles promotes EGFP dimerization*. Phys. Chem. Chem. Phys., 2017. **19**(18): p. 11380-11389.
82. Nolles, A., Westphal, A.H., de Hoop, J.A., Fokkink, R.G., Kleijn, J.M., et al., *Encapsulation of GFP in Complex Coacervate Core Micelles*. Biomacromolecules, 2015. **16**(5): p. 1542-1549.
83. Nolles, A., Westphal, A.H., Kleijn, J.M., van Berkel, W.J.H., and Borst, J.W., *Colorful Packages: Encapsulation of Fluorescent Proteins in Complex Coacervate Core Micelles*. Int. J. Mol. Sci., 2017. **18**(7): p. 1-19.
84. Bourouina, N., de Kort, D.W., Hoeben, F.J., Janssen, H.M., Van As, H., et al., *Complex Coacervate Core Micelles with Spectroscopic Labels for Diffusometric Probing of Biopolymer Networks*. Langmuir, 2015. **31**(46): p. 12635-12643.
85. Yamaguchi, H., Kobayashi, Y., Kobayashi, R., Takashima, Y., Hashidzume, A., et al., *Photoswitchable gel assembly based on molecular recognition*. Nat. Commun., 2012. **3**: p. 603.
86. Moozyckine, A.U., Bookham, J.L., Deary, M.E., and Davies, D.M., *Structure and stability of cyclodextrin inclusion complexes with the ferrocenium cation in aqueous solution: 1H NMR studies*. J. Am. Chem. Soc. , 2001(9): p. 1858-1862.
87. Sadrerafi, K., Moore, E.E., and Lee, M.W., *Association constant of  $\beta$ -cyclodextrin with carboranes, adamantane, and their derivatives using displacement binding technique*. J. Incl. Phenom. Macrocycl. Chem., 2015. **83**(1-2): p. 159-166.
88. Granadero, D., Bordello, J., Perez-Alvite, M.J., Novo, M., and Al-Soufi, W., *Host-guest complexation studied by fluorescence correlation spectroscopy: adamantane-cyclodextrin inclusion*. Int. J. Mol. Sci., 2010. **11**(1): p. 173-188.
89. Osella, D., Carretta, A., Nervi, C., Ravera, M., and Gobetto, R., *Inclusion Complexes of Ferrocenes and Cyclodextrins Critical Appraisal of the Electrochemical Evaluation of Formation Constants*. Organometallics 2000. **19**: p. 2791-2797.
90. Katayose, S. and Kataoka, K., *Water-Soluble Polyion Complex Associates of DNA and Poly(ethylene glycol)-Poly(L-lysine) Block Copolymer*. Bioconjug. Chem., 1997. **8**: p. 702-707.
91. Giustarini, D., Galvagni, F., Tesei, A., Farolfi, A., Zanoni, M., et al., *Glutathione, glutathione disulfide, and S-glutathionylated proteins in cell cultures*. Free Radic. Biol. Med., 2015. **89**: p. 972-981.
92. Mura, S., Nicolas, J., and Couvreur, P., *Stimuli-responsive nanocarriers for drug delivery*. Nat. Mater., 2013. **12**(11): p. 991-1003.
93. Bae, Y., Fukushima, S., Harada, A., and Kataoka, K., *Design of Environment-Sensitive Supramolecular Assemblies for Intracellular Drug Delivery: Polymeric Micelles that are Responsive to Intracellular pH Change*. Angew. Chem. Int. Ed. Engl., 2003. **115**(38): p. 4788-4791.
94. Chen, Y.C., Lo, C.L., Lin, Y.F., and Hsiue, G.H., *Rapamycin encapsulated in dual-responsive micelles for cancer therapy*. Biomaterials, 2013. **34**(4): p. 1115-1127.
95. Ohno, S., Ishihara, K., and Yusa, S., *Formation of Polyion Complex (PIC) Micelles and Vesicles with Anionic pH-Responsive Unimer Micelles and Cationic Diblock Copolymers in Water*. Langmuir, 2016. **32**(16): p. 3945-3953.
96. Duan, Z., Gao, Y.-J., Qiao, Z.-Y., Fan, G., Liu, Y., et al., *A photoacoustic approach for monitoring the drug release of pH-sensitive poly( $\beta$ -amino ester)s*. J. Mater. Chem. B, 2014. **2**(37): p. 6271-6282.
97. Li, D., Bu, Y., Zhang, L., Wang, X., Yang, Y., et al., *Facile Construction of pH- and Redox-Responsive Micelles from a Biodegradable Poly(beta-hydroxyl amine) for Drug Delivery*. Biomacromolecules, 2016. **17**(1): p. 291-300.
98. Tayo, L.L., *Stimuli-responsive nanocarriers for intracellular delivery*. Biophys. Rev., 2017. **9**(6): p. 931-940.
99. Wang, H., Tang, L., Tu, C., Song, Z., Yin, Q., et al., *Redox-responsive, core-cross-linked micelles capable of on-demand, concurrent drug release and structure disassembly*. Biomacromolecules, 2013. **14**(10): p. 3706-3712.

100. Bhattacharya, S., Ganivada, M.N., Dinda, H., Das Sarma, J., and Shunmugam, R., *Biodegradable Copolymer for Stimuli-Responsive Sustained Release of Doxorubicin*. ACS Omega, 2016. **1**(1): p. 108-117.
101. Dong, W.-F., Kishimura, A., Anraku, Y., Chuanoi, S., and Kataoka, K., *Monodispersed Polymeric Nanocapsules: Spontaneous Evolution and Morphology Transition from Reducible Hetero-PEG PICmicelles by Controlled Degradation*. J. Am. Chem. Soc., 2009. **131**: p. 3804-3805.
102. Zheng, N., Song, Z., Liu, Y., Zhang, R., Zhang, R., et al., *Redox-responsive, reversibly-crosslinked thiolated cationic helical polypeptides for efficient siRNA encapsulation and delivery*. J. Control. Release, 2015. **205**: p. 231-239.
103. Zhu, C., Zheng, M., Meng, F., Mickler, F.M., Ruthardt, N., et al., *Reversibly shielded DNA polyplexes based on bio-reducible PDMAEMA-SS-PEG-SS-PDMAEMA triblock copolymers mediate markedly enhanced nonviral gene transfection*. Biomacromolecules, 2012. **13**(3): p. 769-778.
104. Gao, Y. and Dong, C.-M., *Triple redox/temperature responsive diselenide-containing homopolypeptide micelles and supramolecular hydrogels thereof*. Journal of Polymer Science Part A: Polymer Chemistry, 2018. **56**(10): p. 1067-1077.
105. Jochum, F.D. and Theato, P., *Thermo- and light responsive micellation of azobenzene containing block copolymers*. Chem. Commun. (Camb), 2010. **46**(36): p. 6717-6719.
106. Lin, Y.-K., Yu, Y.-C., Wang, S.-W., and Lee, R.-S., *Temperature, ultrasound and redox triple-responsive poly(N-isopropylacrylamide) block copolymer: synthesis, characterization and controlled release*. RSC Advances, 2017. **7**(68): p. 43212-43226.
107. Voets, I.K., Moll, P.M., Aqil, A., me, C.J., Detrembleur, C., et al., *Temperature Responsive Complex Coacervate Core Micelles With a PEO and PNIPAAm Corona*. J. Phys. Chem. B, 2008. **112**: p. 10833-10840.
108. Ishii, S., Kaneko, J., and Nagasaki, Y., *Dual Stimuli-Responsive Redox-Active Injectable Gel by Polyion Complex Based Flower Micelles for Biomedical Applications*. Macromolecules, 2015. **48**(9): p. 3088-3094.
109. Ahn, D.G., Lee, J., Park, S.Y., Kwark, Y.J., and Lee, K.Y., *Doxorubicin-loaded alginate-g-poly(N-isopropylacrylamide) micelles for cancer imaging and therapy*. ACS Appl. Mater. Interfaces, 2014. **6**(24): p. 22069-22077.
110. Liu, G., Liu, W., and Dong, C.-M., *UV- and NIR-responsive polymeric nanomedicines for on-demand drug delivery*. Polym. Chem., 2013. **4**(12): p. 3431-3443.
111. Gohy, J.F. and Zhao, Y., *Photo-responsive block copolymer micelles: design and behavior*. Chem. Soc. Rev., 2013. **42**(17): p. 7117-7129.
112. Harnoy, A.J., Slor, G., Tirosh, E., and Amir, R.J., *The effect of photoisomerization on the enzymatic hydrolysis of polymeric micelles bearing photo-responsive azobenzene groups at their cores*. Org. Biomol. Chem., 2016. **14**(24): p. 5813-5819.
113. Huang, Y., Dong, R., Zhu, X., and Yan, D., *Photo-responsive polymeric micelles*. Soft Matter, 2014. **10**(33): p. 6121-6138.
114. Pearson, S., Vitucci, D., Khine, Y.Y., Dag, A., Lu, H., et al., *Light-responsive azobenzene-based glycopolymer micelles for targeted drug delivery to melanoma cells*. Eur. Polym. J., 2015. **69**: p. 616-627.
115. Wang, G., Tong, X., and Zhao, Y., *Preparation of Azobenzene-Containing Amphiphilic Diblock Copolymers for Light-Responsive Micellar Aggregates*. Macromolecules, 2004. **37**(24): p. 8911-8917.
116. Zhao, Y., *Light-Responsive Block Copolymer Micelles*. Macromolecules, 2012. **45**(9): p. 3647-3657.
117. Verbeek, F.P., van der Vorst, J.R., Schaafsma, B.E., Hutteman, M., Bonsing, B.A., et al., *Image-guided hepatopancreatobiliary surgery using near-infrared fluorescent light*. J. Hepatobiliary Pancreat. Sci., 2012. **19**(6): p. 626-637.
118. Zou, H., Yuan, W., Lu, Y., and Wang, S., *UV light- and thermo-responsive supramolecular aggregates with tunable morphologies from the inclusion complexation of dendritic/linear polymers*. Chem. Commun. (Camb), 2017. **53**(16): p. 2463-2466.
119. Wang, Y., Ma, N., Wang, Z., and Zhang, X., *Photocontrolled reversible supramolecular assemblies of an azobenzene-containing surfactant with alpha-cyclodextrin*. Angew. Chem. Int. Ed. Engl., 2007. **46**(16): p. 2823-2826.

# LIST OF ABBREVIATIONS

AFM: Atomic Force Microscopy

AuDENs: Au Dendrimer Encapsulated  
Nanoparticles

BIC: Block Ionomer Complex

CMC: Critical Micelle Concentration

cryo-TEM: cryo-Transmission Electron  
Microscopy

CSC: Critical Salt Concentration

CT: Computed Tomography

C3Ms: Complex Coacervate Core Micelles

C4Ms: Cyclodextrin-based Complex Coacervate  
Core Micelles

DNA: deoxyribonucleic acid

DLS: Dynamic Laser Scattering

DPA: Dipicolinic Acid

DOX: DOXorubicin

DTT: DiThioThreitol

FI: Fluorescent Imaging

GSH: Glutathione

NIR: Near Infrared

MRI: Magnetic Resonance Imaging

LMWG: Low Molecular Weight Gelator

Ln: Lanthanides

NMR: Nuclear Magnetic Resonance

as-ODNS: antisense Oligonucleotides

PAMAM: PolyAmidoAmine

PEG: polyethyleneglycol

PEO-PAsp: polyethyleneoxide-Poly-aspartate

PDI: PolyDispersity Index

PIC: Polyion Complex Micelles

PMC: Preferred Micellar Concentration

PNIPAAm: PolyNIsoPropylAcrylAMide

RNA: RiboNucleic Acid

SANS: Small Angle Neutron Scattering

SAXS: Small Angle X-Ray Scattering

SLS: Static Laser Scattering

SPIONS: SuperParamagnetic based Iron Oxide  
Nanoparticles

WHO: World Health Organization

Z-pot: Z-potential



# CHAPTER 2

---

Cyclodextrin-based Complex Coacervate Core  
Micelles

---

## ABSTRACT

---

Micelles have been recognized as versatile platforms for different biomedical applications, from bioimaging to drug delivery. Complex coacervate core micelles present great advantages compared to traditional micelles, however controlling the number of charges per core-unit and the stability is still a challenge. We here present cyclodextrin-based complex coacervate core micelles where the charge per core-unit can be tuned in a straightforward way by cyclodextrin host-guest interactions. By varying the ratio between two adamantane guest molecules, 1-adamantanecarboxylic acid and 1,3-adamantanediactic acid, the charge of the monomeric core-units can be finely tuned from 6- to 9-. By adding an adamantane bislinker, monomeric core-units can be combined into dimeric and polymeric structures, increasing the micelles' stability. The orthogonal supramolecular host-guest and coordination-chemistry allows for well-controlled cyclodextrin-based complex coacervate core micelles that offer a versatile platform for designing future, e.g., responsive, systems.

---

This chapter has been adjusted from the published form: Camilla Facciotti, Vittorio Saggiomo, Anton Bunschoten, Remco Fokkink, Jan Bart ten Hove, Junyou Wang and Aldrik H. Velders (2018). "Cyclodextrin-based complex coacervate core micelles with tuneable supramolecular host-guest, metal-to-ligand and charge interactions." *Soft Matter* 14(47): 9542-9549.

## 2.1. INTRODUCTION

Micelles provide versatile platforms in adaptive and responsive materials, e.g., for drug delivery, due to the core being capable of solubilizing and incorporating drugs.[1] In the last two decades, there has been a growing interest in Complex Coacervate Core Micelles (C3Ms), which are formed by the electrostatically driven self-assembly of oppositely charged (block co)polymers.[2, 3] Fundamental advantages of C3Ms, compared to, e.g., surfactant micelles, are (i) the high stability, (ii) the relatively hydrophilic core, (iii) the possibility to assemble with almost any charged molecules and (iv) the prolonged circulation in the bloodstream.[4-10] Despite all the advantages and applications of C3Ms, controlling the number of charges of the building blocks and the stability is still a challenge. The first C3Ms, described by Harada and Kataoka, were formed by a rough assembly of oppositely charged polymers, without a precise control on the charge.[11] In further studies Cohen Stuart and coworkers achieved a higher charge control of micelle formation, compared to the polyion micelles, by using coordination chemistry. The coordination between dipicolinic acid molecules and di-cationic transition-metal ions formed negatively-charged coordination polymers in the core,[12] neutralized by a positively-charged and neutral block copolymer (PMVP-PEO), forming metal-to-ligand based C3Ms.[13, 14] By substituting first-row transition metal ions with lanthanide(III) ions, the core coordination polymers change from linear to branched and become more stable.[12, 14] By changing the ratio between different lanthanides in the coordination core, for example Eu/Gd, different properties, such as luminescent and magnetic properties, could be simply introduced.[15]

In recent studies, a better understanding of C3Ms formation and stability was achieved by using different generations of PAMAM dendrimers, which bear a well-defined number of charges. By adding the positively charged-neutral block copolymer (PMVP-b-PEO) several negatively-charged PAMAM dendrimers were encapsulated, forming the so-called dendrimicelles. Each negatively charged PAMAM dendrimer was considered a monomeric core-unit and below a critical number of charges per monomeric core-unit (i.e., 8,) no dendrimicelle could be formed. This suggested that (dendri)micelle formation depends on the number of charges per monomeric-unit in the core and that micelle stability increases with an increase in number of charges per-core unit.[16] A further

understanding of the formation and stability of C3Ms was achieved by including nanoparticles (NP), inside dendrimers, inside micelles, with a so-called box-in-a-box structure.[17-19]

In this chapter, we present a new class of coacervate-core micelles (see scheme 2.1), called Cyclodextrin-based Complex Coacervate Core Micelles (C4Ms), in which the cyclodextrin is covalently tethered to a dipicolinic acid (CD-DPA) unit that can coordinate to metal ions. C4Ms offer the possibility of easy and fine tuning of the charge of the core-unit and the stability of the micelles via orthogonal supramolecular interactions. This possibility allows us to gain insight and control on the lower limit of charge-per-core-unit required for coacervation.

The cyclodextrin/adamantane host-guest pair was selected for its well-known high association constant in water, around  $10^4 \text{ M}^{-1}$ . [20-22] By varying the ratio between the two adamantane guest molecules, 1-adamantanecarboxylic acid (mono-acid, Ad-ma) and 1,3-adamantanediactic acid (bis-acid, Ad-ba), the charge of the Eu-CD-DPA complex can be tuned from 6- to 9-. By adding Ad-ma to the coordination structure, the monomeric unit<sup>6-</sup> was formed with the lowest charge per core-unit. By adding Ad-ba to the coordination structure, the monomeric unit<sup>9-</sup> was formed with the highest charge per core-unit. Intermediate charge per core-unit, such as monomeric unit<sup>7-</sup>, monomeric unit<sup>7.5-</sup>, monomeric unit<sup>8-</sup> were formed by adding Ad-ma and Ad-ba in 2:1, 1:1, 1:2 Ad-ma/Ad-ba ratios (scheme 2.1). The charge per core-unit is a statistic average value, based on the stoichiometric addition of different ratio between Ad-ma and Ad-ba.

C4Ms based on monomeric Eu(III)-complex core-units with charged adamantane guest molecules can be formed by adding a positive-neutral block copolymer P2MVP<sub>128</sub>-b-PEO<sub>477</sub>. The stability of the C4Ms can be further adjusted by adding a double-guest bridging linker molecule. By adding this bislinker, monomeric core-units can be combined in dimeric and polymeric structures, which results in an overall higher charge-per-core-unit. By increasing the bislinker concentration, the micelle stability increases. In this chapter, we present a new class of versatile micelles, C4Ms, in which the orthogonal supramolecular interactions allow for a systematic investigation of the tuneable charge and micelle stability.



## 2.2. EXPERIMENTAL SECTION

Materials and methods, synthesis and micelle preparations are described in the following sections.

### 2.2.1. MATERIALS AND METHODS

Europium nitrate ( $\text{Eu}(\text{NO}_3)_3 \cdot 5\text{H}_2\text{O}$ ), 1,3-adamantanediactic acid, 1-adamantanecarboxylic acid, diisopropylethylamine (DIPEA), amantadine HCl, propargyl bromide, and tris[(1-benzyl-1H-1,2,3-triazol-4-yl)methyl]amine (TBTA) were purchased from Sigma Aldrich and used without further purification. Boc-Glu-OH and (benzotriazol-1-yloxy)tris(dimethylamino)phosphonium hexafluorophosphate (BOP) were purchased from TCI and used without further purification.  $\beta$ -cyclodextrin monoazide was purchased from Cyclodextrin-Shop and used without further purification. All stock solutions were kept at pH 7. The block copolymer, poly(N-methyl-2-vinylpyridinium iodide)-b-poly(ethyleneoxide) (P2MVP<sub>128</sub>-b-PEO<sub>477</sub>), was obtained by quaternization of poly(2-vinylpyridine)-b-poly(ethylene oxide) (PVP<sub>128</sub>-b-PEO<sub>477</sub>) (Polymer Source, Mw/Mn=1.03, Mw= 13.3 k) following a procedure described elsewhere. The degree of quaternization was 90%, as determined by DLS titration.[23]

All NMR measurements were carried out at 298 K on a Bruker Avance III 400 MHz, 500 MHz, or 600 MHz NMR spectrometer. Assignments were aided by COSY, HSQC, NOESY, ROESY and HMBC experiments. All mass spectra were acquired using ES ionization on a Thermo Finnigan LXQ Exactive Mass Spectrometer. Light scattering measurements (dynamic) and zeta potential measurements were carried out on a Malvern NanoSizer ZS, at 173 degree angle, equipped with an argon-helium laser, operating at 632.8 nm at 25°C. Multiangle measurements were performed on an ALV light scattering setup operating with a Cobalt Flamenco 300 mW DPSS laser at 660 nm operated at 100 mW. Titrations were carried out using the Malvern NanoSizer ZS DLS and adding stock solutions stepwise to a 0.5 mL sample volume. All samples were measured at 25°C. UV-vis measurements were carried out on a Hitachi U-2010 Spectrophotometer using quartz cuvettes of 1 cm path length. Fluorescence spectroscopy measurements were carried out on an Agilent Cary Eclipse Fluorescence Spectrophotometer using quartz cuvettes of 1 cm path length, excitation and emission slits were set at 5 nm. Sonication was carried out in the sonication bath Fisherbrand

FB15053. Silica columns were prepared with silica of 40-63  $\mu\text{m}$ , 60  $\text{\AA}$  from Screening Devices BV. Reversed silica phase columns were prepared with C18 functionalized irregular silica of 40-63  $\mu\text{m}$  60  $\text{\AA}$ . For Cryo-TEM, samples were cast on copper grids (400 mesh - 150  $\mu\text{m}$  average hole size, Holey carbon) from Electron Microscopy Sciences (EMS, Hatfield, PA, USA). After blotting, samples were plunged into liquid ethane by using Vitrobot Mark IV instrument. Grids were then transferred to a JEOL 1400 PLUS TEM operating at 120 kV.

## 2.2.2. SYNTHESIS

The synthesis of diethyl 4-(prop-2-yn-1-yloxy)pyridine-2,6-dicarboxylate (**2**), pyridine-2,6-dicarboxylate-modified  $\beta$ -cyclodextrin (**5**) and 1,5-bis(((3s,5s,7s)-adamantan-1-yl)amino)-1,5-dioxopentan-2-aminium (**9**) are described in the following section. The NMR and ROESY spectra can be found in the Supporting information section, Figure S2.1-S2.4.

### SYNTHESIS OF DIETHYL 4-(PROP-2-YN-1-YLOXY)PYRIDINE-2,6-DICARBOXYLATE (**2**)

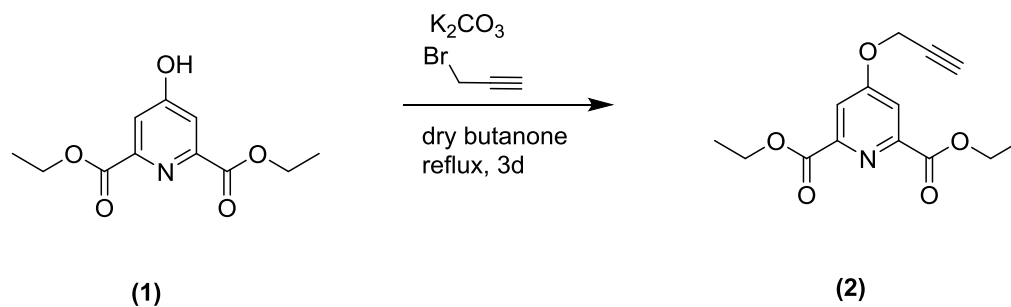
Compound **1**, diethyl 4-hydroxypyridine-2,6-dicarboxylate, was prepared by protecting chelidamic acid following a standard procedure described in literature.[24, 25] Compound **2**, diethyl 4-(prop-2-yn-1-yloxy)pyridine-2,6-dicarboxylate, was prepared following the procedure described in the next section.

Butanone (40 mL) was dried overnight using molecular sieves (4  $\text{\AA}$ ).  $\text{K}_2\text{CO}_3$  (2.0 g, 14.5 mmol), compound **1** (0.5 g, 2.0 mmol), and propargyl bromide (2 mL, 22.0 mmol) were added to the dry butanone. The reaction mixture was heated at 80  $^\circ\text{C}$  to reflux temperature, was refluxed for one night and was monitored with TLC. The reaction was cooled to RT and concentrated in vacuo. The residue was dissolved in DCM (50 mL) and extracted twice with water (50 mL) and once with brine. The organic phase was concentrated in vacuo and the product (**2**) was purified using a silica chromatography column (cyclohexane : ethylacetate from 2:1 to 1:2, as eluent). Yield 0.5 g (94%).

$^1\text{H}$  NMR spectrum (400 MHz,  $\text{CDCl}_3$ )  $\delta$  [ppm]: 7.87 (s, 2H,  $\text{CH-Py}$ ), 4.87 (s, 2H,  $\text{CH}_2\text{C}\equiv\text{CH}$ ), 4.47 (q,  $J=7.2$  Hz, 4H,  $\text{CH}_2\text{CH}_3$ ), 2.62 (s, 1H,  $\text{C}\equiv\text{CH}$ ), 1.44 (t,  $J=7.2$  Hz, 6H,  $\text{CH}_3$ ).

$^{13}\text{C}$  NMR spectrum (100 MHz,  $\text{CDCl}_3$ ),  $\delta$  [ppm]: 165.48 (-C=O), 164.57 (C-Py), 150.34 (2,6-C-Py), 114.61 (3,5 CH-Py), 77.32 (-C $\equiv$  CH), 76.27 (-C $\equiv$  CH), 62.43 (CH<sub>2</sub>CH<sub>3</sub>), 56.34 (-CH<sub>2</sub>C $\equiv$  CH), 14.18 (CH<sub>3</sub>).

Calculated monoisotopic mass ( $[\text{M}+\text{H}]^+$  and  $[\text{M}+\text{Na}]^+$ ) for **2**,  $\text{M} = \text{C}_{14}\text{H}_{15}\text{NO}_5$ , is 278.10 and 300.08. The experimental mass is 278.10 and 300.08.



**Scheme 2.2.** Reaction scheme of the diethyl 4-(prop-2-yn-1-yloxy)pyridine-2,6-dicarboxylate synthesis.

## SYNTHESIS OF PYRIDINE-2,6-DICARBOXYLATE-MODIFIED $\beta$ -CYCLODEXTRIN (**5**)

Compound **5**, pyridine-2,6-dicarboxylate-modified  $\beta$ -cyclodextrin, was prepared by adjusting the procedure in ref [26]. The synthesis was adjusted by using THF and water instead of MeOH, by leaving the reaction overnight instead of 10-30 min and by using CuI as copper catalyst.

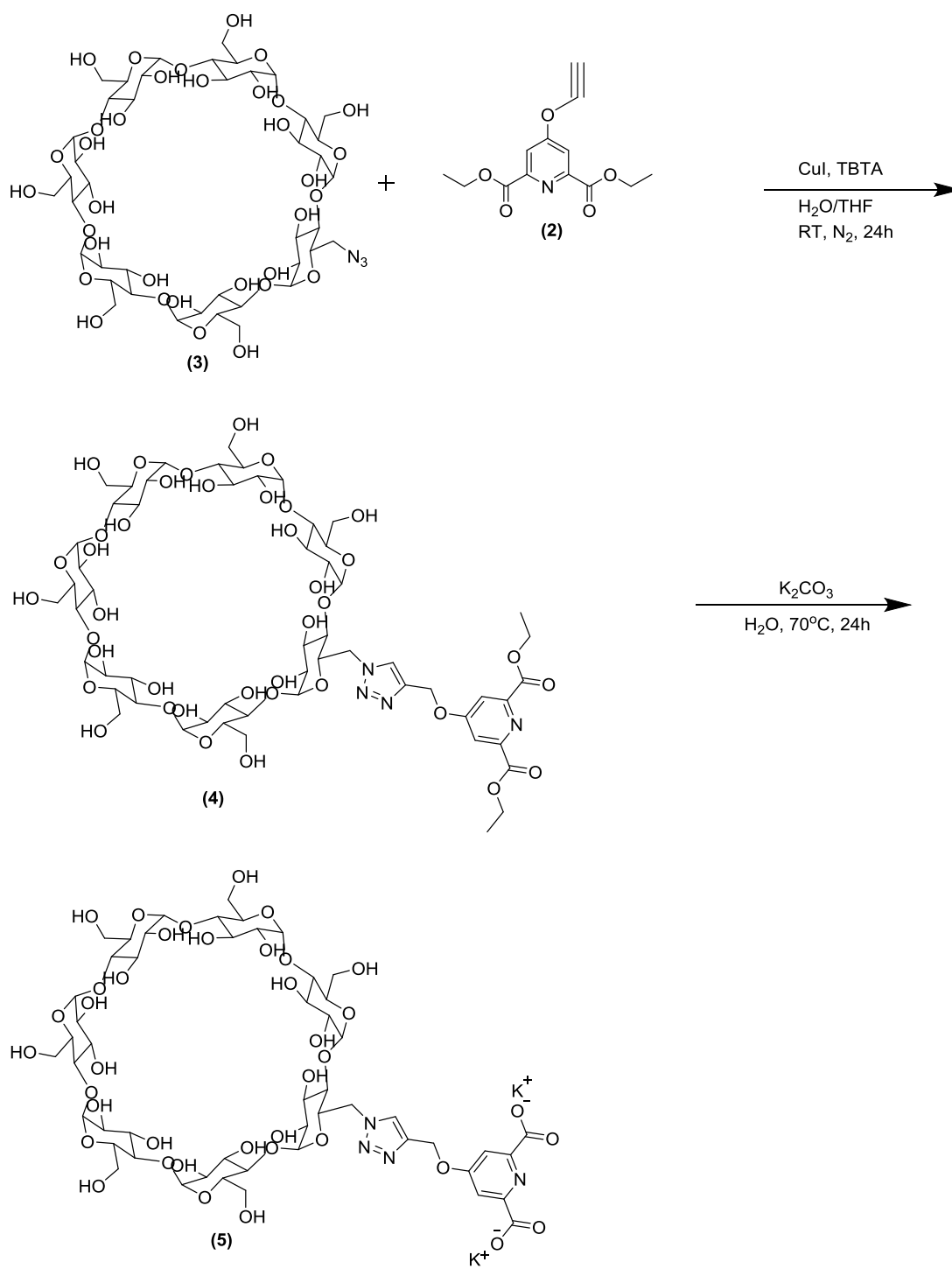
THF and water were purged with nitrogen for two hours.  $\beta$ -cyclodextrin monoazide (**3**) (200 mg, 0.16 mmol) was mixed in a 100 mL round bottom flask with water (20 mL) and THF (10 mL). To this flask, **2** (80 mg, 0.28 mmol), TBTA (6 mg, 0.01 mmol) and CuI (38 mg, 0.20 mmol) were added. The reaction was left stirring under  $\text{N}_2$ -atmosphere at RT overnight and the reaction was monitored with TLC. The volume of the reaction mixture was reduced to 5 mL, by concentrating it in vacuo. The crude reaction mixture was added directly to a reversed phase C18-silica column (water: methanol from 2:1 to 1:1). This yielded 167 mg of **4**.

The deprotection of **4** was performed by dissolving it (167.0 mg, 0.12 mmol) and  $\text{K}_2\text{CO}_3$  (83.5 mg, 1.20 mmol) in water (20 mL). The reaction was heated to 70°C and left stirring overnight. After concentration in vacuo, the product (**5**) was purified by dialysis (MW cut-off 500-1000 kDa) over three days, replacing the water twice a day. Water was evaporated. Yield 153 mg (55%).

$^1\text{H}$  NMR spectrum (400 MHz,  $\text{D}_2\text{O}$ ),  $\delta$  [ppm]: 8.21 (s, 1H, **CH triaz.**), 7.61 (s, 2H, **CH pyr**), 5.41 (s, 2H, pyr O-**CH<sub>2</sub>**), 5.13 (d,  $J=3.6$  Hz, 1H, **H<sub>1''</sub>**), 5.05 (m, 5H, **H<sub>1</sub>**), 5.03 (s, 1H, **1H<sub>6'</sub>**), 4.98-4.94 (m, 1H, **H<sub>1'</sub>**), 4.64 (m, 1H, **H<sub>6''</sub>**), 4.21 (t,  $JJ=10$  Hz, **1H, H<sub>5'</sub>**), 4.04-3.89 (m, 7H, **H<sub>3</sub>**), 3.89-3.78 (m, 18H, **H<sub>6</sub>** **H<sub>5</sub>**), 3.65-3.41 (m, 14H, **H<sub>2</sub> H<sub>4</sub>**), 3.14 (d,  $JJ=12$  Hz, 1H, **H<sub>60'</sub>**), 2.74 (d,  $JJ=12$  Hz, 1H, **H<sub>60''</sub>**).

$^{13}\text{C}$  NMR spectrum (150 MHz,  $\text{D}_2\text{O}$ ),  $\delta$  [ppm]: 172.46 (C=O), 165.98 (C-O pyr.), 155.04 (C C=O), 142.37 (C triaz.), 127.21 (C-H triaz.), 111.6 (CH pyr), 101.88 (1C'', 1C), 101.34 (1C'), 83.07 (4C), 80.79-81.28 (4C), 80.62 (4C''), 73.06-71.48 (2C, 3C, 5C), 70.40 (5C) 60.81 (6C) 51.29 (6C').

Calculated monoisotopic mass ( $[\text{M}-2\text{H}]^2$ ) for **5**,  $\text{M}=\text{C}_{52}\text{H}_{76}\text{N}_4\text{O}_{39}$ , is 689.20. The experimental mass is 689.17.



**Scheme 2.3.** Reaction scheme of the pyridine-2,6-dicarboxylate-modified  $\beta$ -cyclodextrin synthesis.

## SYNTHESIS OF 1,5-BIS(((3S,5S,7S)-ADAMANTAN-1-YL)AMINO)-1,5-DIOXOPENTAN-2-AMINIUM (9)

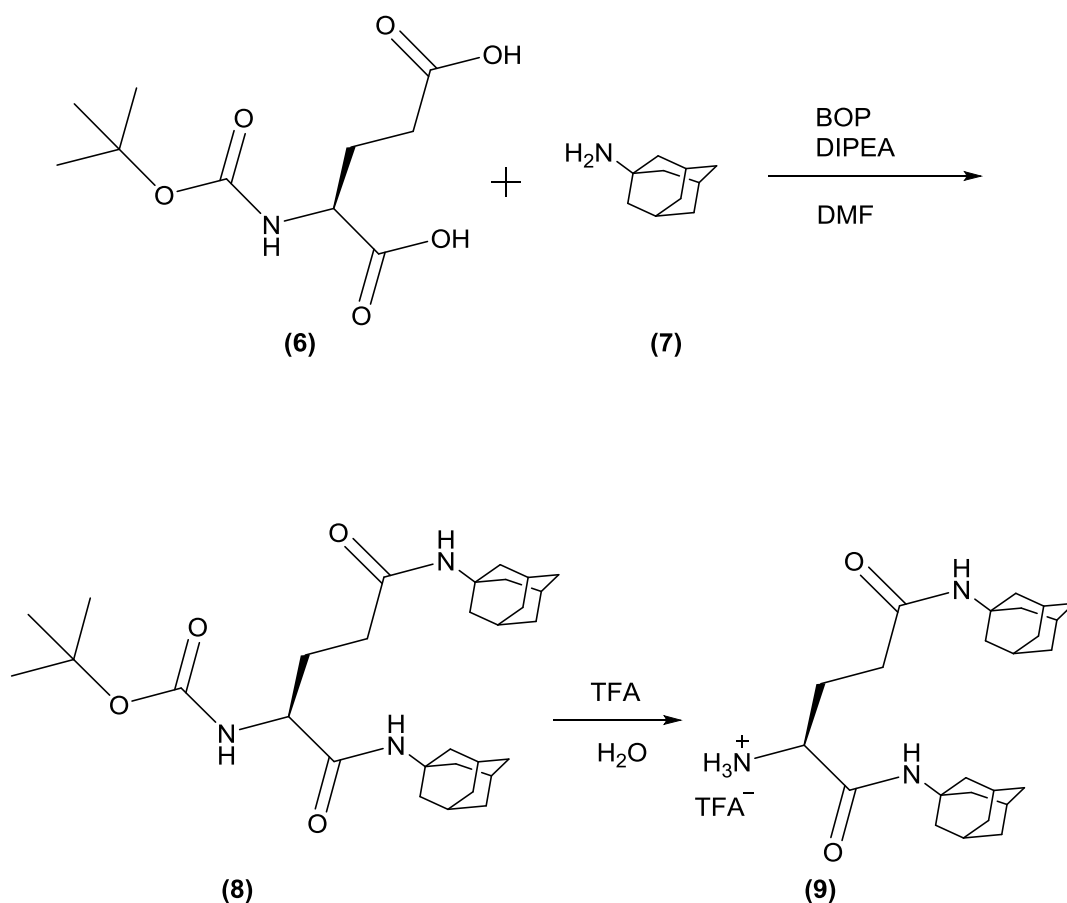
Boc-Glu-OH (**6**) (2.17 g, 10 mmol) was dissolved in DMF (25.0 mL). BOP (11.30 g, 25 mmol) was added. Amantadine HCl (**7**) (4.55 g, 24 mmol) and DIPEA (10.5 mL, 61 mmol) were dissolved in DMF (25.0 mL) and was added to the Boc-Glu-OH solution. This reaction mixture was stirred at RT for three days. The reaction mixture was concentrated in vacuo and the residue was dissolved in ethyl acetate (200.0 mL). The organic phase was extracted with subsequently water, 0.2 M KHSO<sub>4</sub>, water, 5% NaHCO<sub>3</sub>, water and brine. After drying with Na<sub>2</sub>SO<sub>4</sub> the organic phase was concentrated in vacuo. The product (**8**) was purified by a silica column (cyclohexane: ethyl acetate 4:1) resulting in 1.70 g (33 %) product as a clear oil.

Compound **8** was dissolved in 10 mL TFA:H<sub>2</sub>O (95/5) and stirred for 3 h. After thorough concentration in vacuo the product (**9**) was purified by silica column (DCM:MeOH 95:5 as eluent) resulting in 720 mg (41%) product as a white solid.

<sup>1</sup>H NMR spectrum (400 MHz, DMSO), δ [ppm]: 8.09 (s, J, 3H, NH<sub>3</sub>), 7.91 (s, 1H, Ca C=O NH), 7.48 (s, 1H Cg C=O NH), 3.66 (m, 1H, CaH), 2.14 (m, 2H, CgH<sub>2</sub>), 2.02 (m, 4H, Ca C=O Ad NH-C-CH-CH<sub>2</sub>-CH-), 1.99 (m, 4H, Cg C=O Ad NH-C-CH-CH<sub>2</sub>-CH-), 1.95 (m, 6H, Ca C=O Ad NH-C-CH<sub>2</sub>-CH<sub>2</sub>-CH<sub>2</sub>), 1.91 (m, 6H, Cg C=O Ad NH-C-CH<sub>2</sub>-CH<sub>2</sub>-CH<sub>2</sub>), 1.84 (m, 2H, CβH<sub>2</sub>), 1.63 (m, 5H, Ca C=O Ad NH-C-CH<sub>2</sub>-CH-CH<sub>2</sub>), 1.60 (m, 5H, Cβ C=O Ad NH-C-CH<sub>2</sub>-CH-CH<sub>2</sub>).

<sup>13</sup>C NMR spectrum (100 MHz, DMSO), δ [ppm]: 170.55 (Cg C=O), 167.12 (Ca C=O), 52.09 (Ca), 51.39 (Ca C=O C), 50.08 (Cg C=O Ad C), 40.92 (Cg C=O Ad C-CH<sub>2</sub>), 39.49 (Ca C=O Ad C-CH<sub>2</sub>), 36.00 (Cg C=O Ad C-CH<sub>2</sub>-CH-CH<sub>2</sub>), 35.82 (Ca C=O Ad C-CH<sub>2</sub>-CH-CH<sub>2</sub>), 31.32 (Cg), 28.72 (Cg C=O Ad C-CH<sub>2</sub>-CH), 28.34 (Ca C=O Ad C-CH<sub>2</sub>-CH).

Calculated monoisotopic mass ([M+H]<sup>+</sup>) for **9**, M=C<sub>25</sub>H<sub>39</sub>N<sub>3</sub>O<sub>2</sub>, is 414.33. The experimental mass is 414.50.



**Scheme 2.4.** Reaction scheme of the 1,5-bis(((3s,5s,7s)-adamantan-1-yl)amino)-1,5-dioxopentan-2-aminium (Ad-Glu-Ad) synthesis.

### 2.2.3. MICELLE PREPARATION

Stock solutions of europium nitrate (5 mM), P<sub>2</sub>MVP<sub>128</sub>-b-PEO<sub>477</sub> (10 mM charges), βCD-DPA (5 mM), adamantane mono-acid (1 mM), adamantane bis-acid (1 mM) and bis-adamantane (1 mM) were prepared by dissolving the powders into ultrapure water and adjusting the solutions to pH 7. Micelles were prepared under sonication at room temperature in a final volume of 0.5 mL. Micelle preparation consists of three steps (Scheme 2.1.). First, the coordination complex between Eu<sup>3+</sup> and DPA was formed by adding europium ions at a final concentration of 0.2 mM. βCD-DPA was added in a 3:1 ratio of βCD-DPA/Eu. Second, the core-unit was formed by adding adamantane guest molecules to the coordination structure, in a 1:1 ratio Ad/βCD-DPA. The core-unit<sup>6</sup> was formed by adding Ad-ma to the coordination structure at a molar ratio of 3:1 Ad-ma/Eu. The monomeric unit<sup>9</sup> was formed by adding Ad-ba to the coordination structure at a molar ratio of 3:1

Ad-ba/Eu. The intermediately-charged core-unit<sup>7-</sup>, core-unit<sup>7.5-</sup>, core-unit<sup>8-</sup> were formed by adding Ad-ma and Ad-ba to 1 in 2:1, 1:1, 1:2 Ad-ma/Ad-ba ratios (total adamantane concentration was kept at 1:1 Ad/  $\beta$ CD-DPA). Third, the block copolymer P<sub>2</sub>MVP<sub>128</sub>-b-PEO<sub>477</sub> was first sonicated for 10 minutes and then added in the correct amount to neutralize the negative core charges. After the addition of all compounds, the samples were left to equilibrate for 10 min.

C4Ms based on a mix of monomeric core-unit<sup>6-</sup> and dimeric units, called (C4Ms<sup>6.\*</sup>) were formed by adding 90% Ad-ma and 5% of NH<sub>2</sub>-Glu(Ad)-Ad compound **9**, in respect to the  $\beta$ CD-DPA concentration, to the europium complex and the block copolymer.

C4Ms based on polymeric core-units were formed by adding bislinker to the coordination structure at a molar ratio of 3:1 of Ad/Eu and corresponding amount of the block copolymer. During all experiments, the concentration of the components was fixed above the CMC to prevent the equilibrium from shifting from micelles towards monomers (Figure S2.6.).

## 2.3. RESULTS AND DISCUSSION

First, the formation of micelles based on monomeric metal complexes is described, followed by a discussion of the samples that contain bridging ligands connecting core-units.

### 2.3.1. TUNING SIZE AND STABILITY WITH MONOMERIC CORE-UNITS

Scheme 2.1. shows the C4Ms formation in three steps. The starting point for the C4Ms' formation was the coordination complex between  $\text{Eu}^{3+}$  and DPA. Formation of the coordination complex was confirmed by fluorescence spectroscopy, exciting DPA results in  $\text{Eu}^{3+}$  emission from  $5\text{D}_0$  to  $7\text{F}_j$ , confirming the antenna phenomenon and therefore the complex formation (Figure S2.5).[27] The sample presented an  $\text{Eu}^{3+}$  lifetime of 1.5 ms, typical of a fully coordinated structure (data not shown).[28]

The following step for the micelle formation was to form the core-unit by adding adamantane guest molecules to the coordination complex. The charge of the core-unit was adjusted by varying the ratio between the two adamantane species, 1-adamantanecarboxylic acid (mono-acid, Ad-ma) and 1,3-adamantanediactic acid (bis-acid, Ad-ba). By adding Ad-ma to the coordination structure, the core-unit<sup>6-</sup> was formed with the lowest charge per core-unit. By adding Ad-ba to the coordination structure, the core-unit<sup>9-</sup> was formed with the highest charge per core-unit. Intermediate charge per core-unit, such as core-unit<sup>7-</sup>, core-unit<sup>7.5-</sup>, core-unit<sup>8-</sup> were formed by adding Ad-ma and Ad-ba in 2:1, 1:1, 1:2 Ad-ma/Ad-ba ratios. The host-guest interaction between adamantane and  $\beta$  cyclodextrin is already well reported in literature.[20, 29] Notwithstanding, the core-unit formation between cyclodextrin and adamantane molecules was confirmed by ROESY experiments (Figure S2.4).

The final step for micelle formation is the addition of the positive-neutral block copolymer P2MVP<sub>128</sub>-b-PEO<sub>477</sub>. The P2MVP<sub>128</sub>-b-PEO<sub>477</sub> block copolymer was selected for its well-reported properties as micelle counter polyion.[16, 30] C4Ms formation was confirmed by using Zeta-potential and Dynamic Light Scattering (DLS). Upon the addition of block copolymer, all the

samples presented a Zeta-potential of -0.4 (SD 0.2) mV, confirming the neutralization of the core-unit charges.

DLS results confirmed the formation of micelles for C4Ms based on the different core-units. Figure 2.1. shows that the hydrodynamic diameter was 45 (SD 6) nm for C4Ms based on core-unit charge above 6. The core-unit<sup>6-</sup> sample showed micellar aggregates with an apparent diameter of 100 nm, higher compared to the spherical micelles formed with core-units<sup>7-, 7.5-, 8-, 9-</sup>.

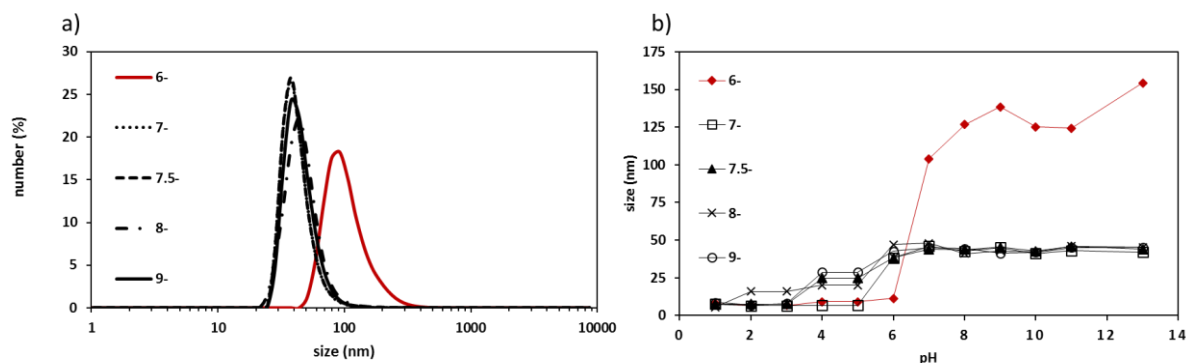


**Figure 2.1.** a) Hydrodynamic diameter distribution of C4Ms, based on different core-unit charges. By adding the block copolymer to the core-unit<sup>7-, 7.5-, 8-, 9-</sup>, stable micelles of 45 nm in hydrodynamic diameter were formed. While by adding the block copolymer to the core-unit<sup>6-</sup> bigger micellar aggregates formed. b) Effect of pH on the hydrodynamic diameter, at different C4Ms core-unit charges. C4Ms based on core-unit<sup>6-</sup> showed lower stability at high pH, compared to higher charged core-units. (Samples prepared at pH 7, final europium concentration is fixed at 0.2 mM).

More investigations were performed using Cryo-TEM and multi-angle DLS with a polarizer. In Figure 2.2. a), cryo-TEM results reveal that core-units<sup>9-</sup> are monodisperse and spherical, as expected. On the other hand, Figure 2.2. b) shows that core-units<sup>6-</sup> micelles are not monodisperse and present a mix of spherical and more elongated shaped aggregates compared to the core-units<sup>9-</sup> micelles. By introducing a 90 degree polarizer between the sample and the DLS detector, the vertical oriented light was rotated by micelles based on core-units<sup>6-</sup>. The polarization ratio of core-units<sup>6-</sup> micelles was calculated around 0.21, confirming their stretched shape, whereas core-units<sup>9-</sup> have the typical depolarization ratio for spherical particles, around 0.01.[30]

The Critical Micelle Concentration (CMC) was determined by titrating water to the core-unit<sup>7-, 7.5-, 8-, 9-</sup> C4Ms, using DLS. The CMC was found around 40  $\mu\text{M}$   $\text{Eu}^{3+}$  ions for all core-unit C4Ms (Figure S2.6.).

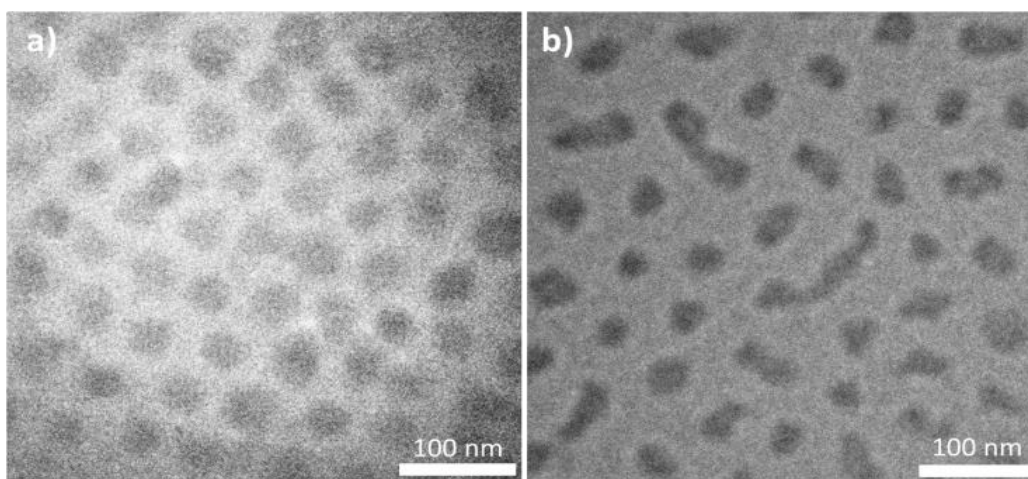


**Figure 2.2.** Size and shape characterization at Cryo-TEM of C4Ms based on the core-unit charge<sup>9-</sup> (a) and C4Ms based on the core-unit charge<sup>6-</sup> (b). The highest core-unit charge C4Ms revealed homogeneously distributed spherical micelles, while the lowest core-unit charge C4Ms showed elongated micelles.

A complete study on C4Ms' stability was performed by investigating them at different times, pH, salt and competitor concentrations. The size and the intensity of C4Ms were monitored over 36 h by using DLS. The size and the intensity of C4Ms based on core-unit<sup>7-, 7.5-, 8-, 9-</sup> were stable up to 36 h (Figure S2.7. and S2.8.). On the other hand, Figure S2.7. and S2.8. show an increase in size and in intensity for core-unit<sup>6-</sup>. The C4Ms' stability was investigated at different pH values. As shown in Figure 2.1. b), C4Ms based on core-unit<sup>7-, 7.5-, 8-, 9-</sup> were stable at basic pH, but they started to dissociate below pH 6. This effect can be related to the protonation of carboxylic acid groups on the adamantanes, as it would result in monomeric europium(III)-DPA coordination complexes with a net charge of 3-, too low to allow micelle formation.[14, 31] Core-unit<sup>6-</sup> was not following the same stable trend and showed high scattered intensity and high size above pH 6.

The C4Ms' stability was also investigated against salt and competing free  $\beta$ CD. By adding salt, or ionic strength, to the C4Ms we expect to screen the charges and, therefore, destabilize the complex. Figure S2.9. shows a positive trend between salt stability and the core-unit charges. By increasing the core-unit charge, the charge stability against salt increased. The Critical Salt Concentration (CSC), the point at which micelles start to dissociate, was determined by adding NaCl to micelles based on the core-unit<sup>6-, 7-, 7.5-, 8-, 9-</sup>. C4Ms dissociated completely at 40 mM of NaCl (Figure 2.3. a) and S9.). The intensity and hydrodynamic diameter of core-unit<sup>9-</sup> C4Ms showed a high peak at around 30 mM NaCl, representing the micellar shape transition from sphere to rod like.[13, 30] Addition

of ionic strength screens the charge interactions between core-units and block copolymers, thus weakening the driving force for micellar formation. The addition of ionic strength might also enhance the hydrophobic association between the adamantane guest and the cyclodextrin host; the latter, however, does not negatively affect the micelle formation.[32] We expect to destabilize C4Ms not only by changing the ionic strength, but also by adding a supramolecular host competitor.  $\beta$ CD competes with the  $\beta$ CD-DPA in the core for hosting adamantane molecules, thereby they destabilize the core of the micelle. Figure 2.3. b) and Figure S2.10 represent the stability of C4MS against free competing  $\beta$ CD. The same figure shows a positive trend between stability against  $\beta$ CD and core-unit charges. Core-unit<sup>9-</sup> C4Ms remained stable upon addition of seven equivalents (5 mM) of  $\beta$ CD compared to  $\beta$ CD-DPA ligand. On the other hand, core-unit<sup>6-</sup> showed the lowest stability against salt and competing  $\beta$ CD (9 mM and 2 mM respectively).

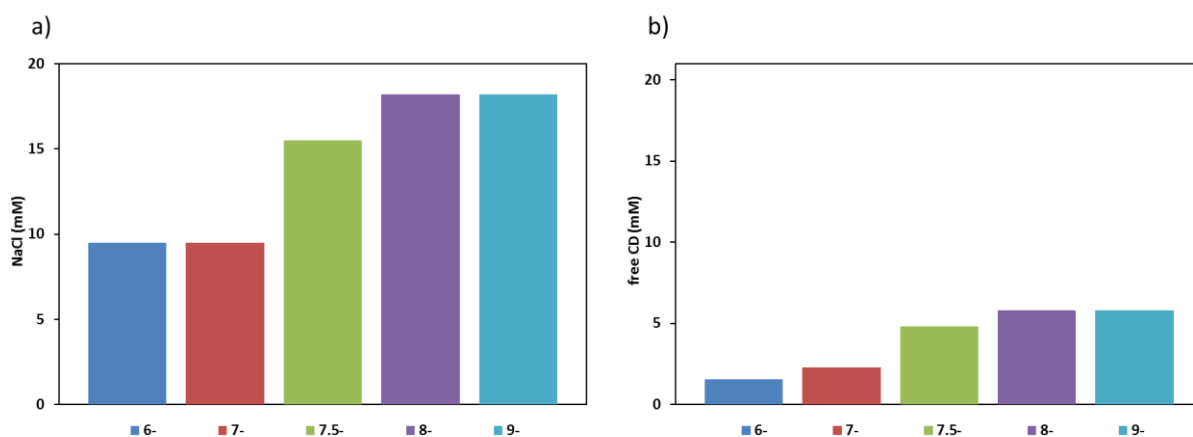
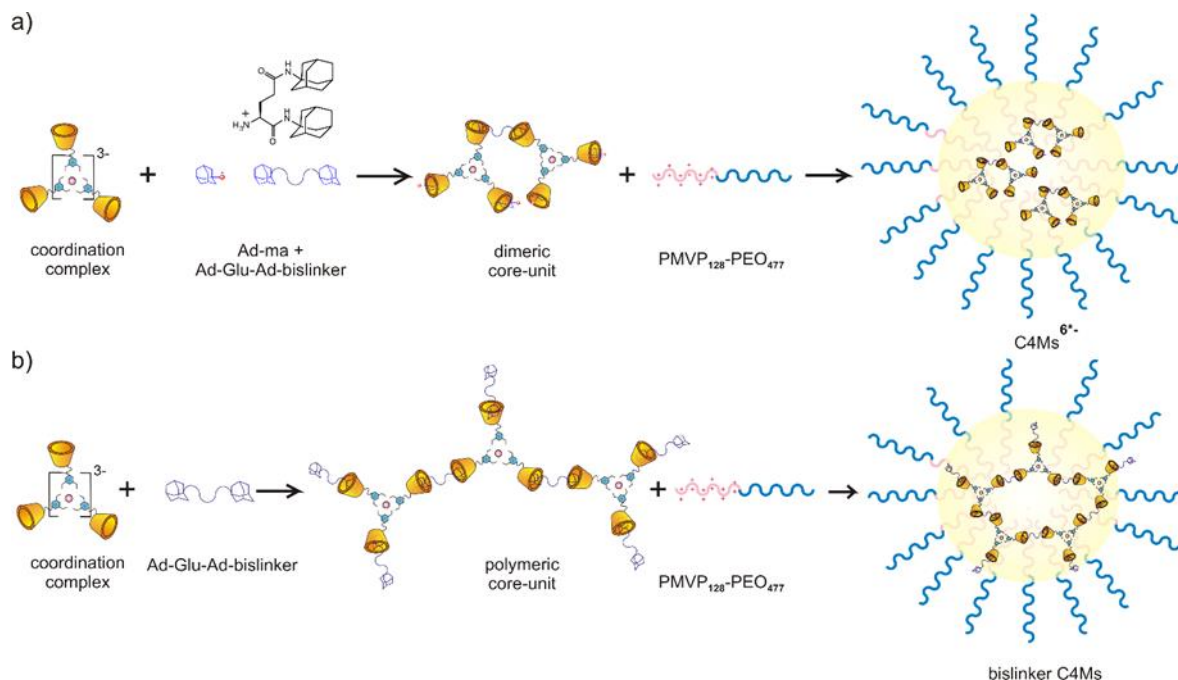


**Figure 2.3.** Salt stability a) and competing free cyclodextrin b) at different core-unit charges. The salt stability and the free-cyclodextrin stability were calculated as the maximum salt and CD concentrations that C4Ms can tolerate, before the DLS intensity and the size decrease. (Micelles were prepared at pH 7, and the final europium concentration was fixed at 0.2 mM.)

The results showed that 6 negative charges per core-unit were not enough to form spherical, monodisperse and stable C4Ms. Therefore, we consider seven negative charges to be the lowest limit of core-unit charge required for proper coacervation of well-defined micelles. Based on these findings, we further exploited the supramolecular interactions to alter the size and the stability of core-unit<sup>6-</sup> samples.

## 2.3.2. TUNING SIZE AND STABILITY OF CORE-UNIT WITH BRIDGING LIGANDS



**Scheme 2.5.** Schematic illustration of C4Ms formation, based on Ad-Glu-Ad bislinker. a) By adding 90% of Ad-ma and 10% of Ad-Glu-Ad bislinker to the coordination complex, dimers can form inside the core. By adding the block polymer to the core dimers, C4Ms<sup>6\*-</sup> can form. b) By adding Ad-Glu-Ad bislinker to the core-unit, polymeric network can form inside the core. By adding the block polymer to the core dimers, Ad-Glu-Ad bislinker based C4Ms can form.

To increase the stability of C4Ms, a supramolecular linker was designed to create crosslinks between monomeric-units, increasing the net charge number per core-unit. The new guest adamantane bislinker (Ad-Glu-Ad) was synthesized and characterized. We investigated the size and the stability of C4Ms with the Ad-Glu-Ad bislinker, by using two different sample preparations. The first method, called “titration”, consisted of preparing one C4Ms sample and titrating increasing amounts of Ad-Glu-Ad bislinker into the just prepared C4Ms. The second method, called “premixing”, consists of the preparation of several samples with increasing stoichiometric ratios between Ad-Glu-Ad bislinker/Ad-ma, prepared before the addition of the block copolymer. A substantial difference between the two methods is that in the titration method, we add an excess of adamantanes to already supramolecularly saturated micelles. However, in the pre-mix a stoichiometric addition of Ad-ma and Ad-Glu-Ad bislinker with respect to the cyclodextrin

concentration is added before block copolymer addition and micelle formation. A change in the titration experiment would therefore moreover confirm the dynamic exchange behavior of the C4Ms' buildingblocks between the core-unit and the environment.

By titrating the Ad-Glu-Ad to the core-unit<sup>6</sup> micellar aggregates, a decrease in the size and intensity became visible already at the very first titration steps (0.03 mM Ad-Glu-Ad over 0.73 mM Ad-ma, thus 4% of Ad-Glu-Ad with respect to Ad-ma, Figure S2.11.). By titrating 0.06 mM of Ad-Glu-Ad (8% of Ad-Glu-Ad respect Ad-ma) to the core-unit<sup>6</sup>, the formation of 59 (SD 5) nm micelles was triggered. The size of those micelles remained constant with the addition of 0.35 mM Ad-Glu-Ad (100% of Ad-Glu-Ad with respect to Ad-ma).

Figure S2.12. shows the effect of pre-mixing Ad-Glu-Ad and Ad-ma on the scattered intensity and size. The results indicate that above 0.04 mM of Ad-Glu-Ad (5% of Ad-Glu-Ad with respect to 90% Ad-ma), intensity and size came in the same range of core-unit<sup>9</sup> C4Ms. Above that value, core-unit<sup>6</sup> forms micelles similar in size to core-unit<sup>9</sup> C4Ms.

Based on the results in Figures S2.11. and S2.12., 5% Ad-Glu-Ad with respect to Ad-ma was chosen as value to improve the stability of the core-unit<sup>6</sup>. By adding Ad-Glu-Ad, we expect, statistically, the formation of new core-unit dimers, defined here as "core-unit<sup>6.\*</sup>" (Scheme 2.5. a). Also, by taking 100% of Ad-Glu-Ad and no monomeric adamantane, a new core-unit based on polymeric structures was formed, which was called "core-unit bislinker" (see Scheme 2.5. b).

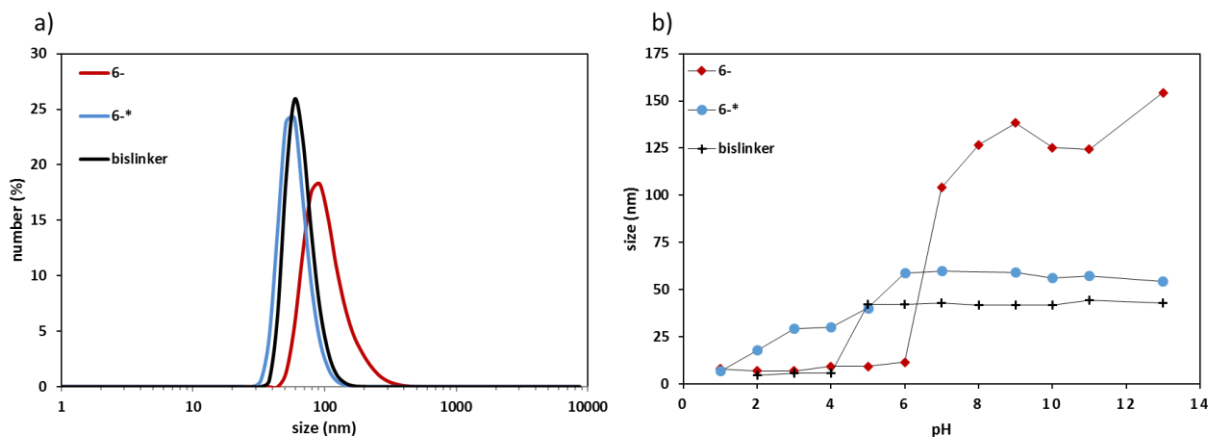


**Figure 2.4.** a) Hydrodynamic diameter distribution of monomeric-unit $6^-$  C4Ms, dimeric unit $6^{*-}$  C4Ms and polymeric unit C4Ms based on the bislinker. Dimeric unit $6^{*-}$  C4Ms and polymeric unit form C4Ms of smaller size compared to the monomeric-unit $6^-$  C4Ms. (Micelles are prepared at pH 7, final europium concentration is fixed at 0.2 mM). b) Effect of pH on the hydrodynamic diameter, at different C4Ms core-unit charges, C4Ms $6^{*-}$ , Ad-Glu\_Ad C4Ms. C4Ms $6^{*-}$ , Ad-Glu\_Ad C4Ms shows stronger stability at high pH compared to monomeric-unit $6^-$  C4Ms.

Core-unit $6^{*-}$  was able to form C4Ms of 59 (SD 7) nm, with a low polydispersity index (PDI) and stable in time (Figure 2.4.). The core-unitbislinker C4Ms showed a size similar to the core-unit $6^{*-}$ , around 60 (SD 7) nm in hydrodynamic diameter, which was stable in time. Micelles based on 100% Ad-Glu-Ad can form even if the residual charge per coordination complex unit is low (1.5-). The reason is due to the fact that the bislinker merges core-units together in polymeric and network structures that crosslinks with each other through the block copolymer, similarly to the bis-DPA lanthanide coordination polymers' core micelles reported before.

The preparation of C4Ms with 5% of bislinker resulted immediately in more stable micelles against pH changes, compared to micelles based on the core-unit $6^-$ . Core-unit $6^{*-}$  based C4Ms stability against salt was comparable with the stability of core-unit $7^{5-}$  C4Ms. Those improvements in the stability of the C4Ms, achieved by adding Ad-Glu-Ad, corroborate the formation of core-unit dimers in the micelle. Interestingly, not all the  $6^-$  core-units need to be crosslinked to form micelles. The addition of small amounts of bislinker (5% in respect to  $\beta$ CD-DPA concentration), that forms dimeric structures with an overall charge of  $9^-$ , suffices.

By preparing micelles based on 100% of bislinker, the core-unit<sup>bislinker</sup> based C4Ms were as stable against pH as core-unit $9^-$  based C4Ms (Figure 2.4. b and S2.13.). The core-unit<sup>bislinker</sup> C4Ms stability

against salt and free  $\beta$ CD was at least double, respectively, four times higher in stability with respect to the other C4Ms prepared with the mono-adamantanes (Figure S2.14).

Combination of orthogonal supramolecular interactions such as cyclodextrin-adamantane host-guest chemistry and lanthanide coordination chemistry has proven a successful strategy to gain insight in complex surface-solute interface chemistry in which multivalency are of importance.[33, 34] The same set of interaction motifs here provides a toolbox to investigate the inside of complex coacervate core micelles, in which the multivalent charge interactions between block copolymer and oppositely-charged supramolecular metal complexes play a crucial role.

## 2.4. CONCLUSIONS

In conclusion, we successfully formed a new class of C3Ms, C4Ms, Cyclodextrin-based Complex Coacervate Core Micelles, based on supramolecular host-guest and metal-to-ligand interactions. We exploited the cyclodextrin-adamantane interaction to finely adjust the core-unit charge of the C4Ms to consecutively investigate the size and the stability of the micelles. The lowest number of charges per core-unit, core-unit<sup>6-</sup>, formed elongated, non-spherical micellar aggregates, around 100 nm in hydrodynamic diameter. These core-unit<sup>6-</sup> based C4Ms aggregates were less stable against salt and free CD, compared to the highest charged core-unit<sup>9-</sup> based C4Ms. The results on intermediate core-unit charges confirmed that stability increases by increasing the core-unit charge. Moreover, by adding an Ad-Glu-Ad bislinker, the size and the stability of core-unit<sup>6-</sup> C4Ms were adjusted, by forming dimeric and polymeric core-units. We showed how to apply supramolecular host-guest chemistry to finely tune charges, size and stability of the important class of coacervate core micelles. A well-controlled cyclodextrin-based complex coacervate core micelle could offer a versatile platform for future responsive systems. **(Chapter 2-5)**

## 2.5. SUPPLEMENTARY INFORMATION

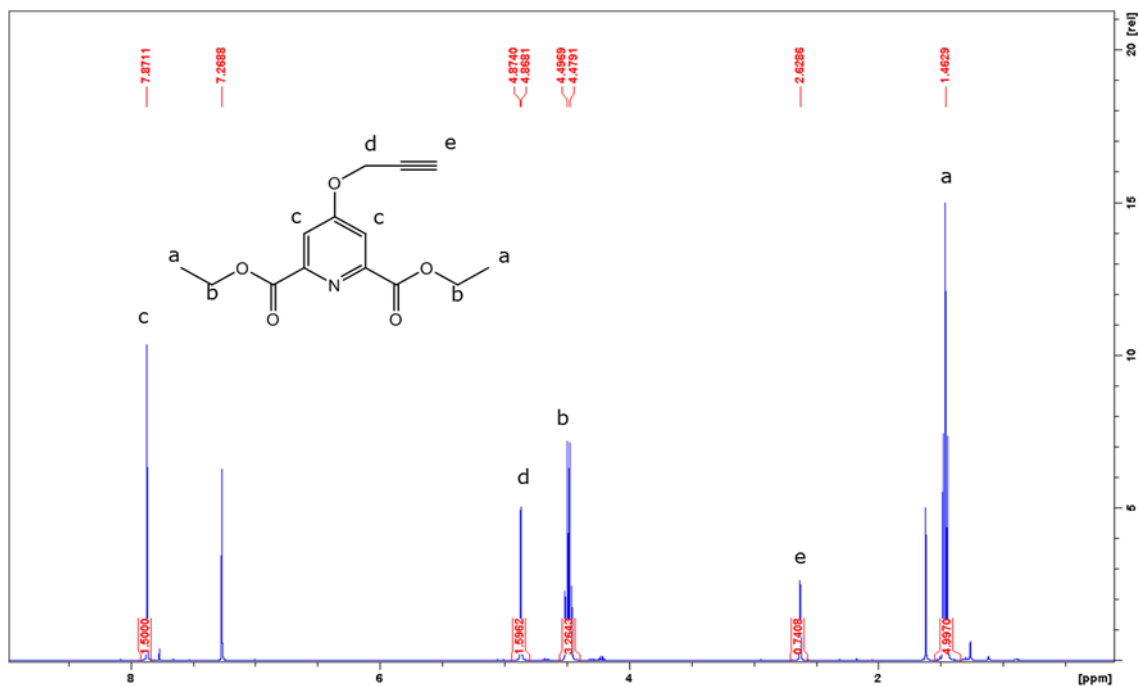


**Figure S2.1.** <sup>1</sup>H-NMR spectrum of diethyl 4-(prop-2-yn-1-yloxy)pyridine-2,6-dicarboxylate (2) (CDCl<sub>3</sub>, 400 MHz).

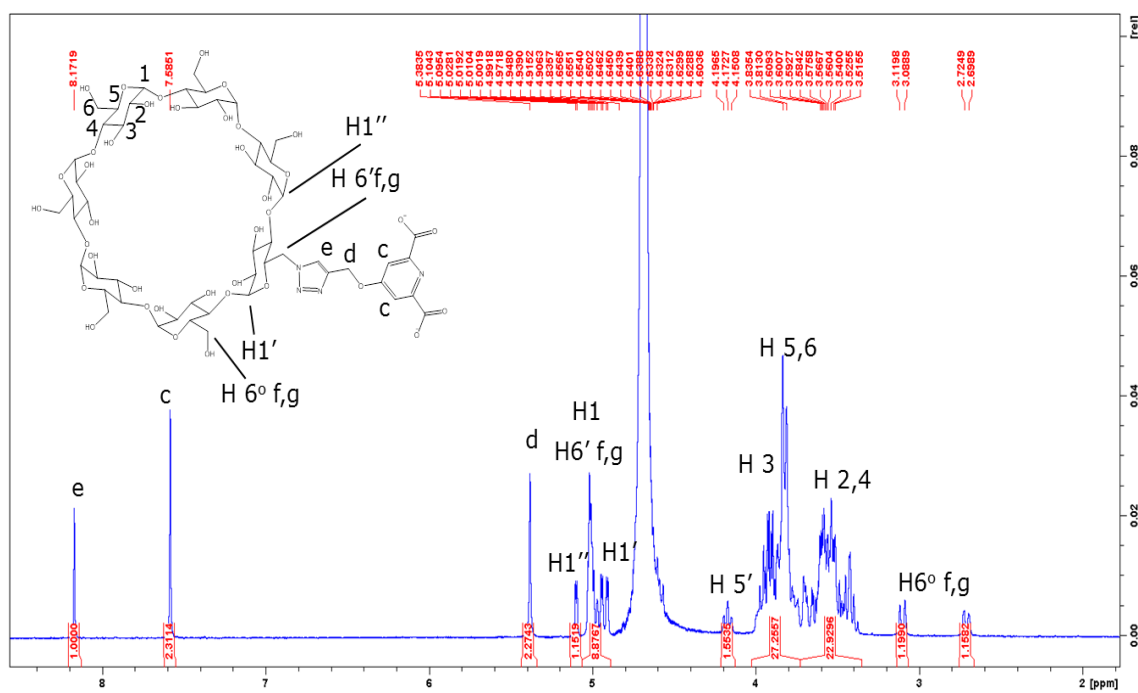


**Figure S2.2.** <sup>1</sup>H-NMR spectrum of pyridine-2,6-dicarboxylate modified β-cyclodextrin (5) (D<sub>2</sub>O, 600 MHz).

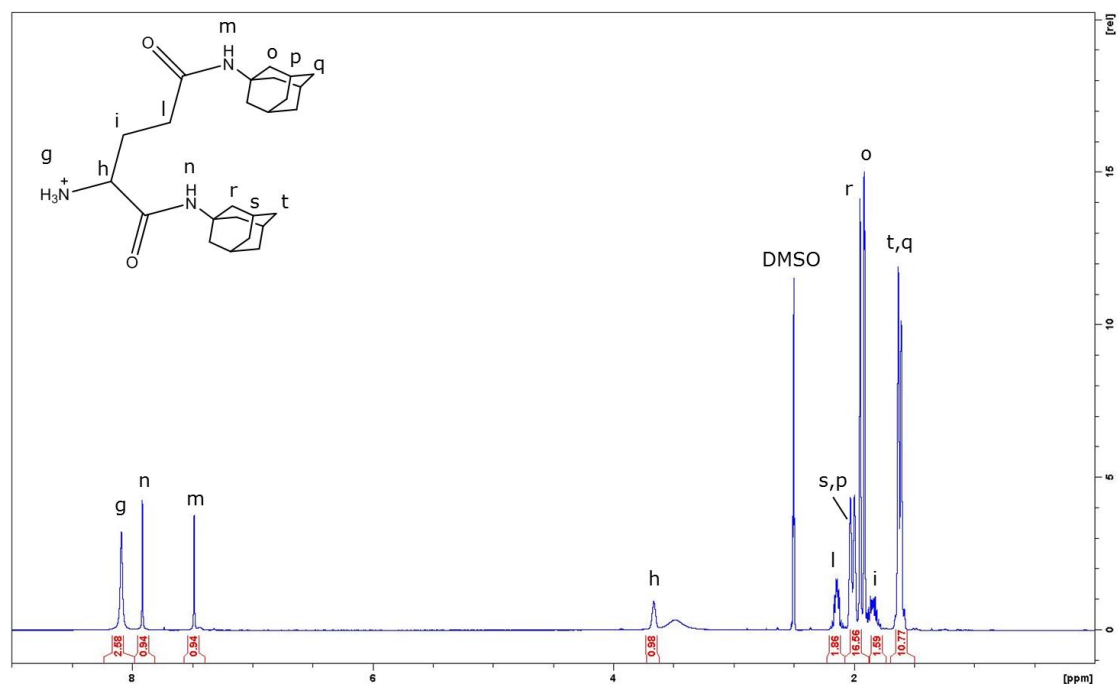


**Figure S2.3.** <sup>1</sup>H-NMR spectrum of 1,5-bis(((3s,5s,7s)-adamantan-1-yl)amino)-1,5-dioxopentan-2-aminium (**9**) (DMSO, 500 MHz).

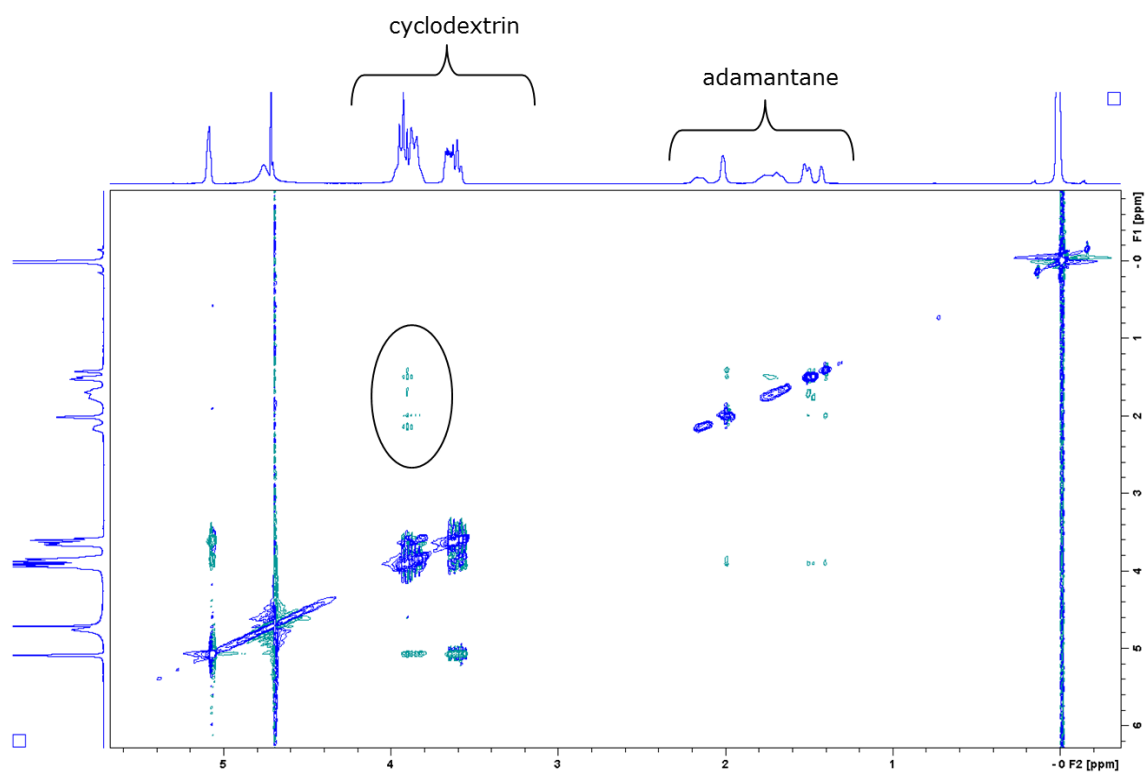


**Figure S2.4.** ROESY spectrum of pyridine-2,6-dicarboxylate modified  $\beta$ -cyclodextrin and 1,3-adamantanediacetic acid ( $D_2O$ , 400 MHz). [29]

*Micelle characterization*

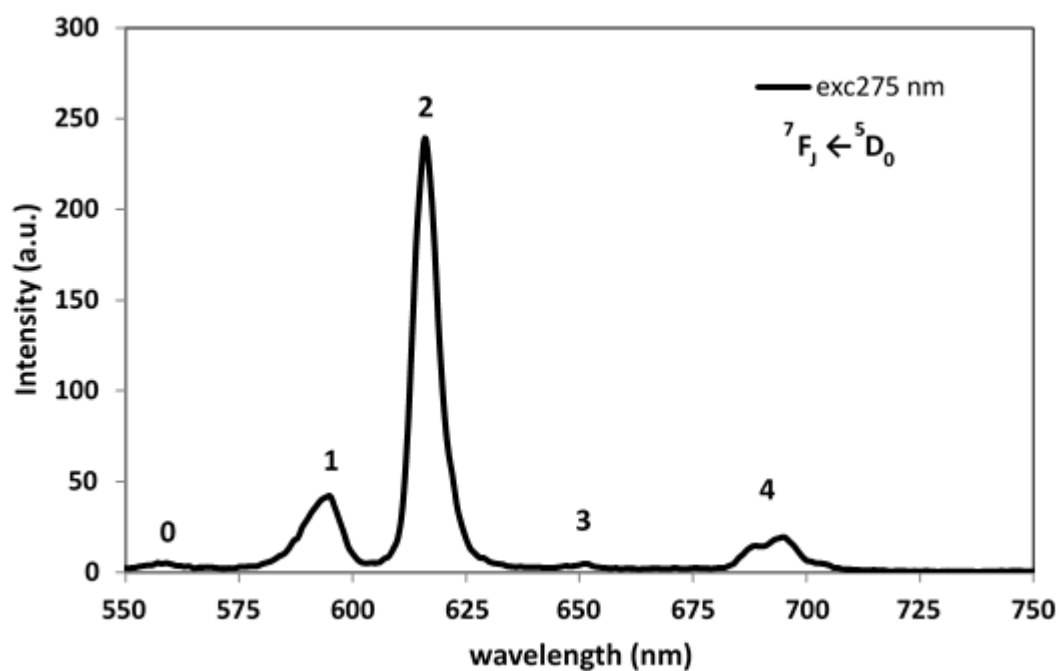


**Figure S2.5.** Fluorescence emission spectrum of core-unit<sup>9</sup> C4Ms, exciting at 275 nm. (micelles were prepared at pH 7, final europium concentration was fixed at 0.2 mM).

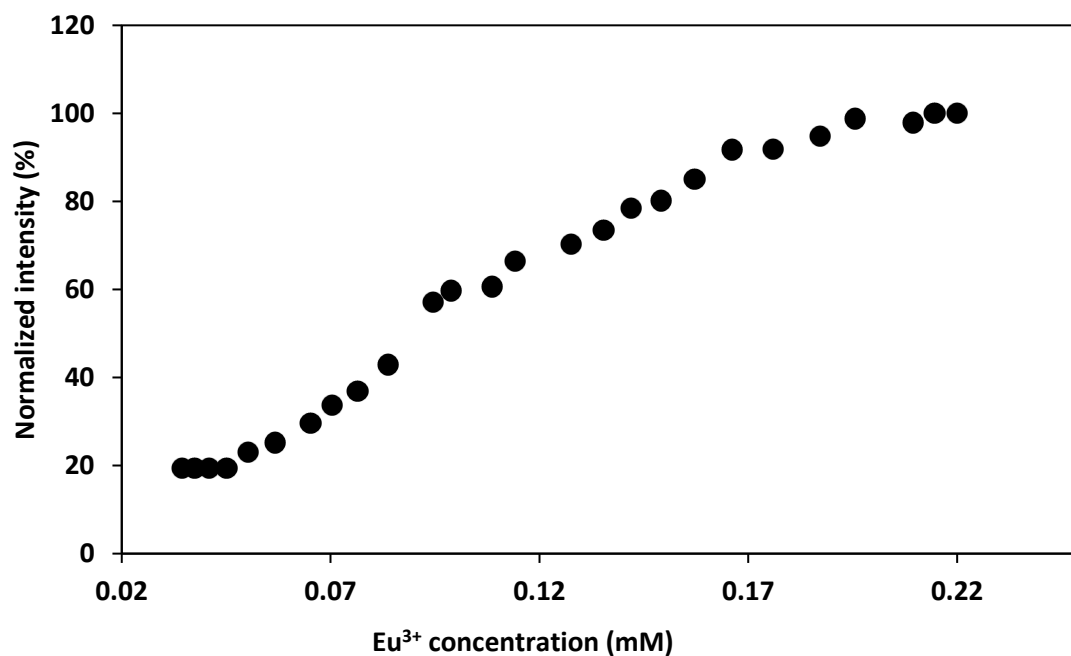


**Figure S2. 6.** Critical Micelle Concentration determination of core-unit<sup>9</sup> depicted as concentration of europium ions. Scattering intensity was monitored after dilution with water. CMC of the other core-unit C4Ms has similar values to the CMC found in the core-unit<sup>9</sup>.

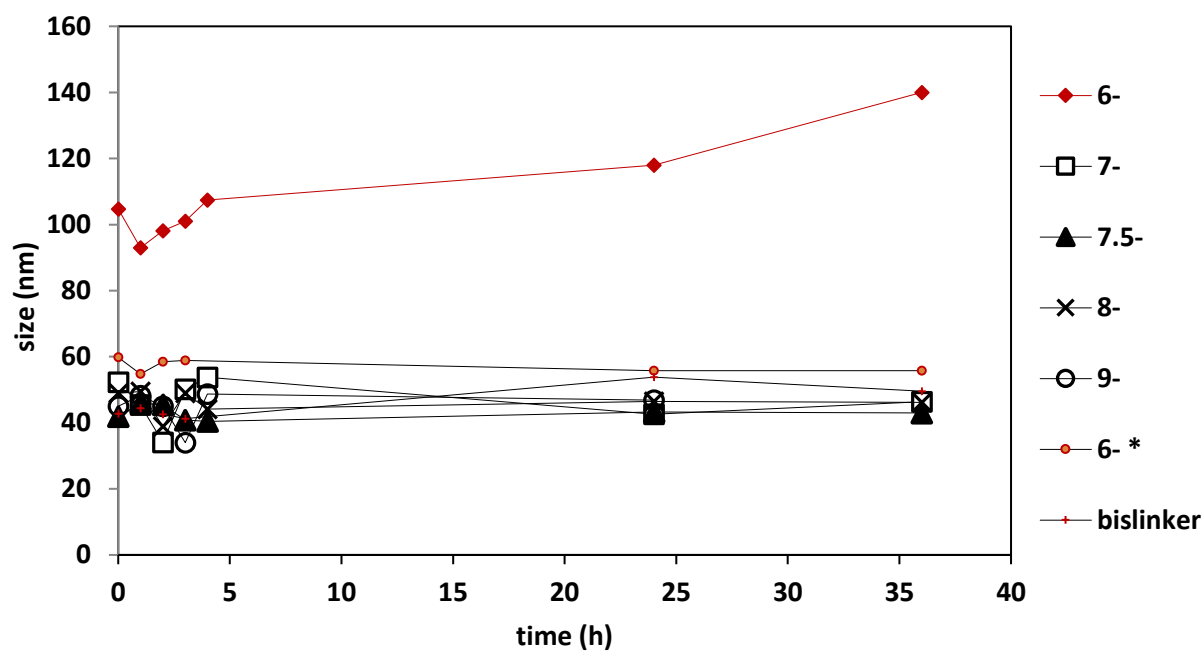


**Figure S2.7.** Effect of time on the hydrodynamic diameter, at different monomeric core-unit charges C4Ms, dimeric unit<sup>6\*</sup> C4Ms and polymeric unit C4Ms based on the bislinker. (micelle are prepared at pH 7, final europium concentration is fixed at 0.2 mM)

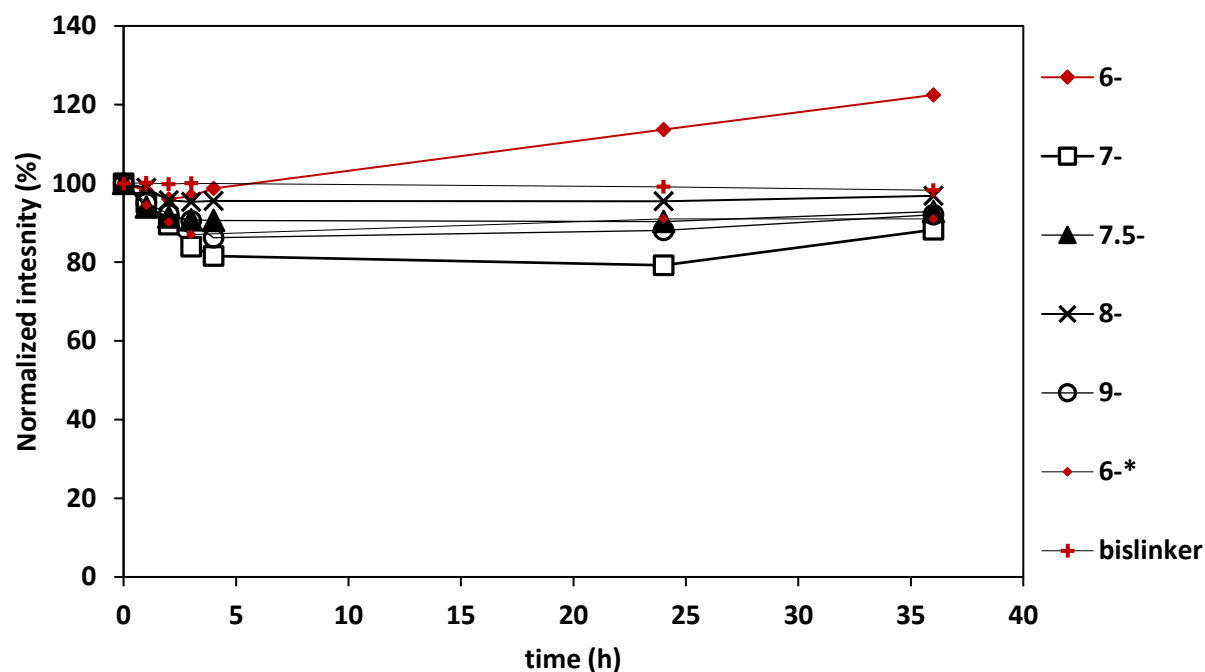


**Figure S2.8.** Effect of time on the scattered intensity, at different monomeric core-unit charges C4Ms, dimeric unit<sup>6\*</sup> C4Ms and polymeric unit C4Ms based on the bislinker (micelles are prepared at pH 7, final metal concentration is fixed at 0.2 mM)

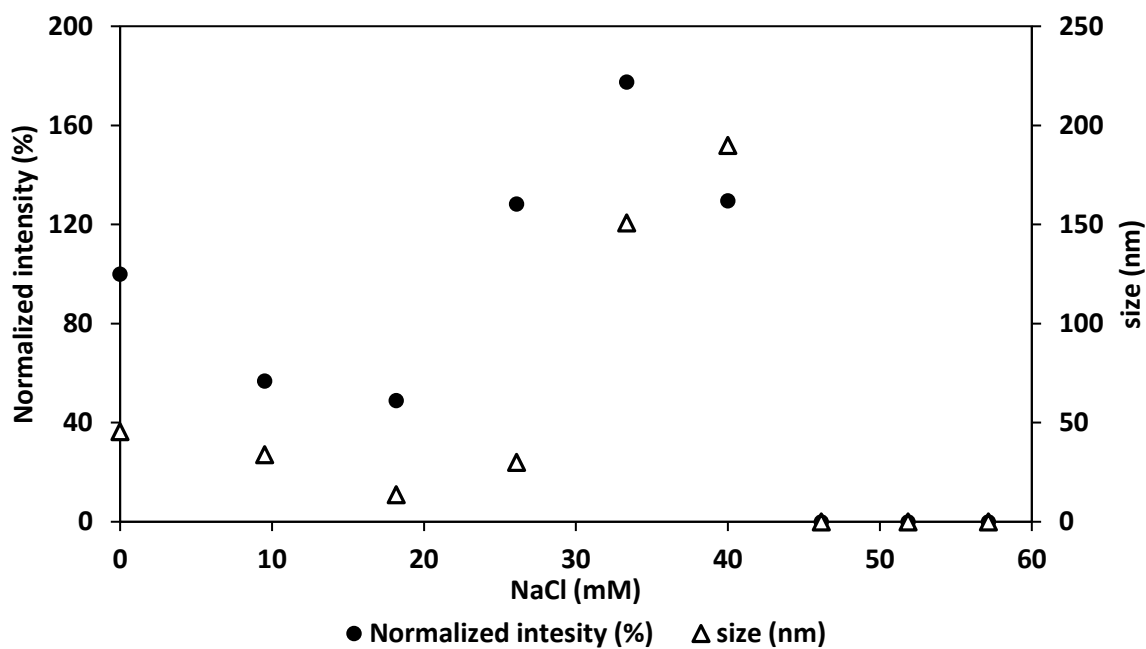


**Figure S2.9.** The effect of salt concentration (NaCl) on scattering intensity and hydrodynamic diameter of monomeric unit<sup>9</sup>- C4Ms. (micelles are prepared at pH 7, final europium concentration is fixed at 0.2 mM)

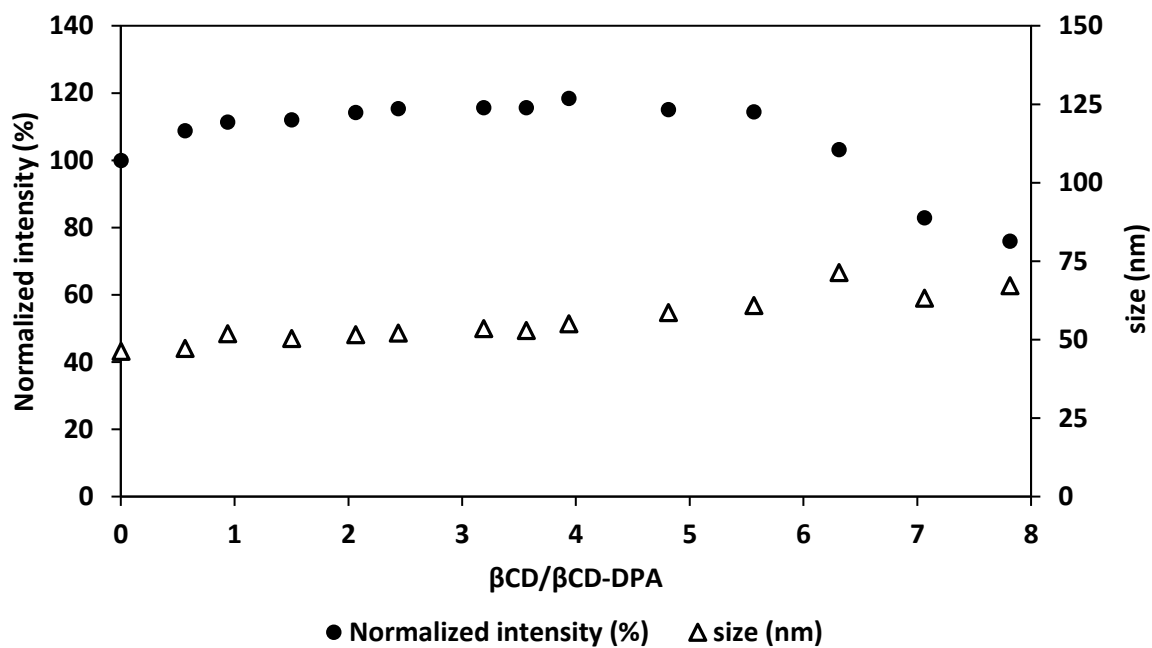


**Figure S2.10.** The effect of competing  $\beta$ -cyclodextrin on the scattering intensity and on the hydrodynamic diameter of monomeric unit<sup>9</sup>- C4Ms. (micelles are prepared at pH 7, final europium concentration is fixed at 0.2 mM)

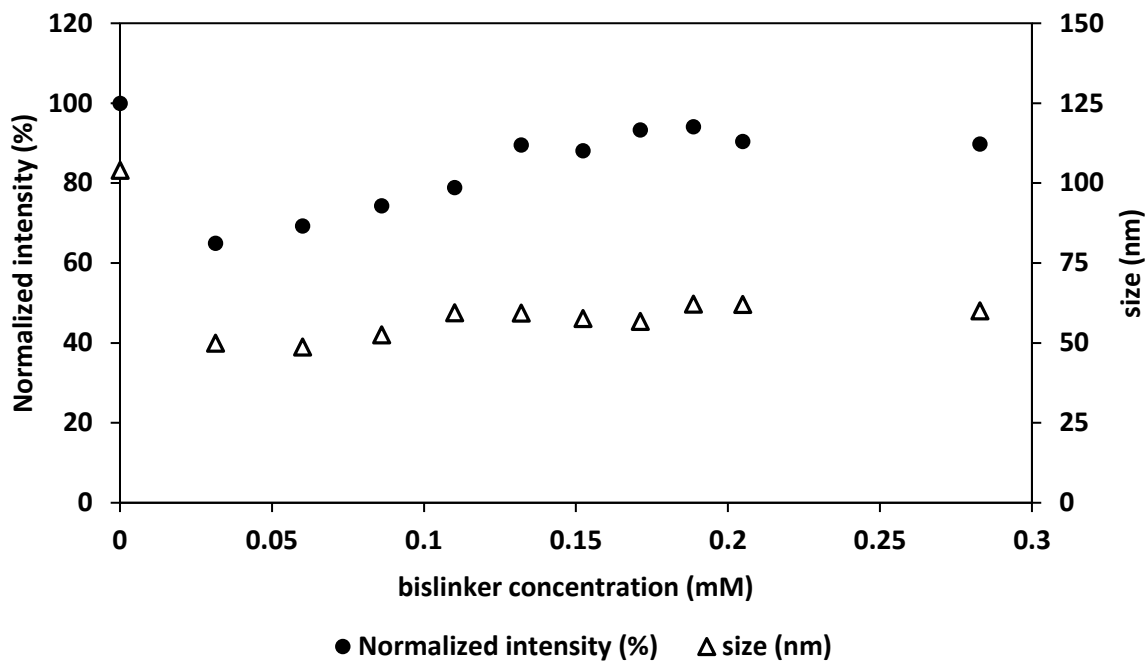


**Figure S2.11.** Effect of Ad-Glu-Ad bislinker (S9) titration on the scattered intensity and hydrodynamic diameter of monomeric unit<sup>6</sup>- C4Ms. 0.1 mM of bislinker corresponds to 16% of bislinker / Ad-ma concentration ratio (final  $\beta$ CD-DPA concentration is fixed at 0.6 mM).

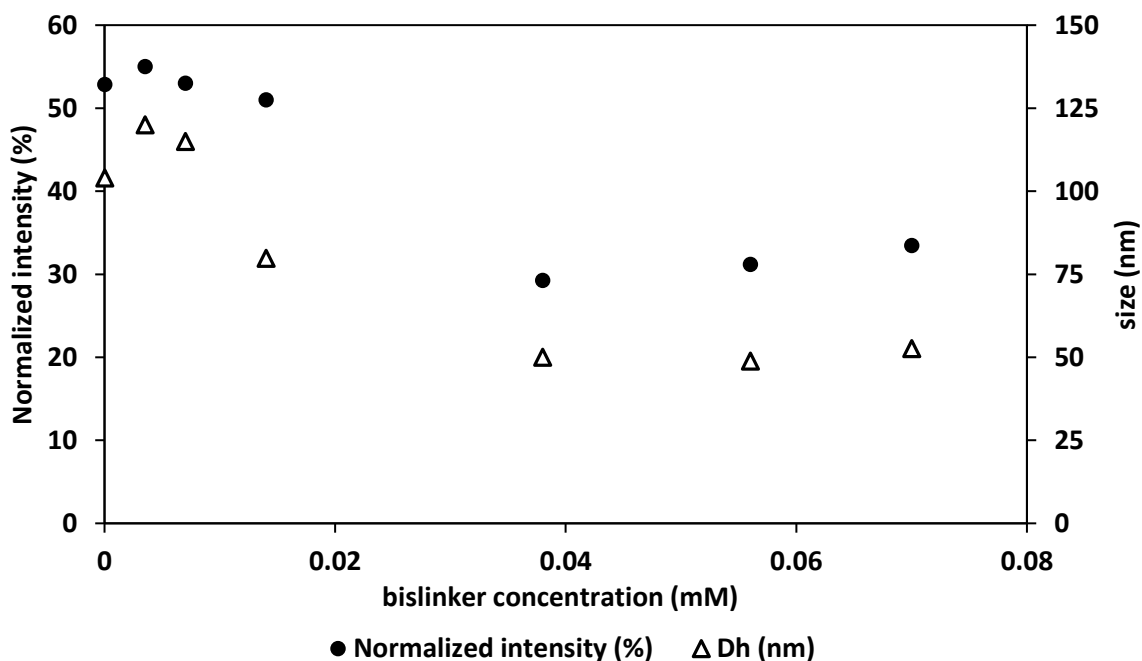


**Figure S2.12.** Effect of Ad-Glu-Ad bislinker (S9) pre-mixing on the scattered intensity and hydrodynamic diameter of monomeric unit<sup>6</sup>- C4Ms. 0.04 mM of bislinker corresponds to 5% of bislinker / Ad-ma concentration ratio (final  $\beta$ CD-DPA concentration is fixed at 0.6 mM).

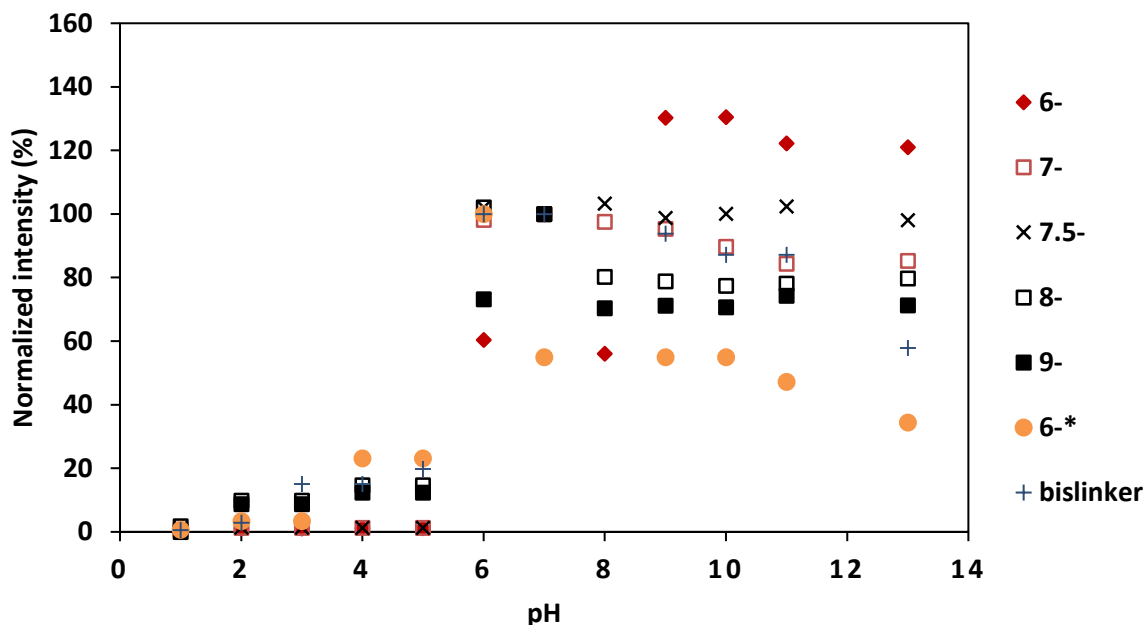


**Figure S2.13.** Effect of pH on the scattered intensity, at different C4Ms core-unit charges, dimeric unit<sup>6-\*</sup> C4Ms and polymeric unit C4Ms (final metal concentration is fixed at 0.2 mM)

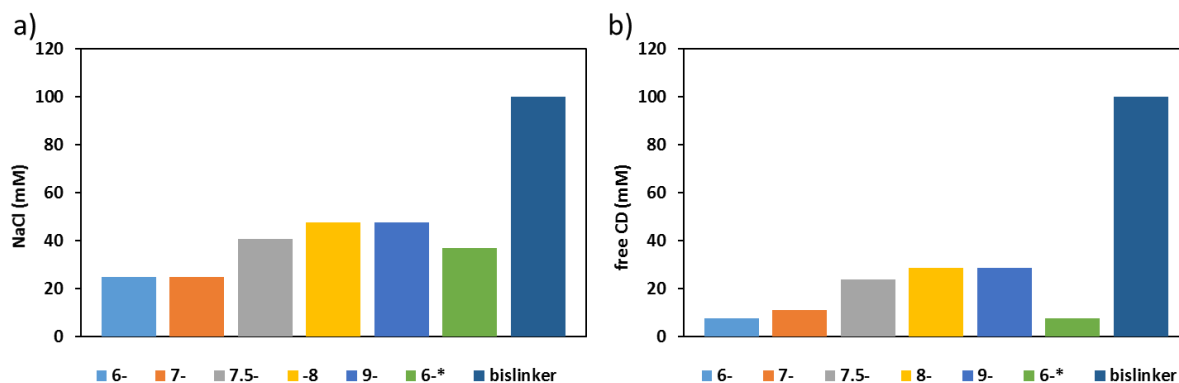


**Figure S2.14.** a) Salt stability at different C4Ms monomeric core-unit charges, dimeric unit<sup>6-\*</sup> C4Ms and polymeric unit C4Ms based on the bislinker. Salt stability experiment was performed by adding NaCl to different charged C4Ms. The salt stability was calculated as the maximum salt concentration that C4Ms can tolerate, before the DLS scattered intensity and the size drop. b) competing  $\beta$ -cyclodextrin stability at different C4Ms monomeric core-unit charges, dimeric unit<sup>6-\*</sup> C4Ms and polymeric unit C4Ms based on the bislinker. The  $\beta$ -cyclodextrin stability was calculated as the maximum  $\beta$ -cyclodextrin concentration that C4Ms can tolerate, before the DLS scattered intensity and the size drop. (micelles are prepared at pH 7, final europium concentration is fixed at 0.2 mM)

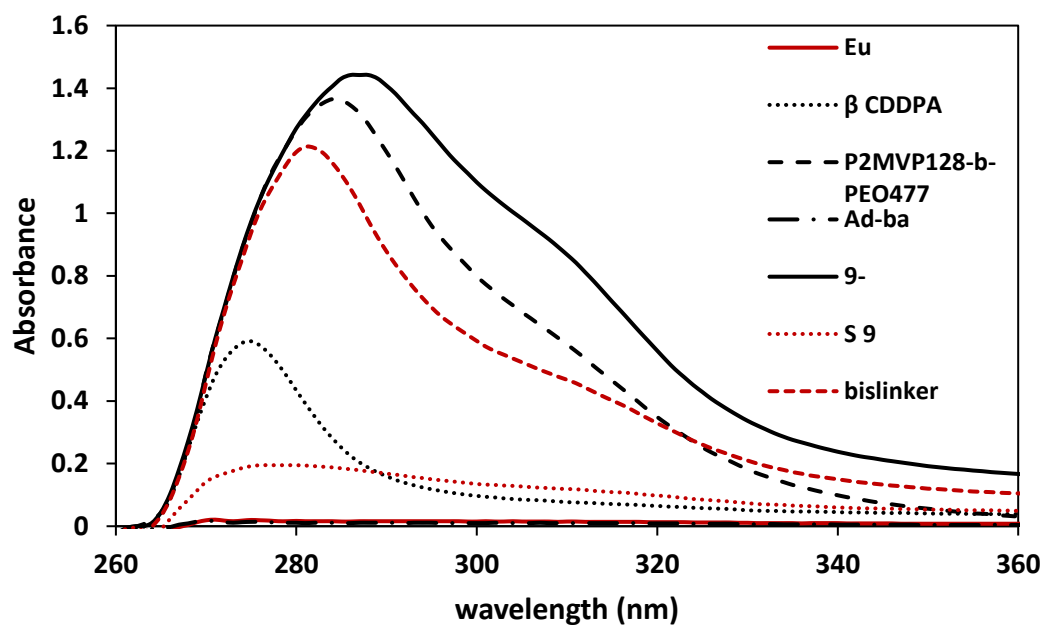


**Figure S2.15.** UV-Vis spectra of building blocks, Eu,  $\beta$ CD-DPA,  $PMVP_{128}$ - $PEO_{477}$ , Ad-ba, monomeric unit 9-C4Ms, S 9 and polymeric C4Ms.

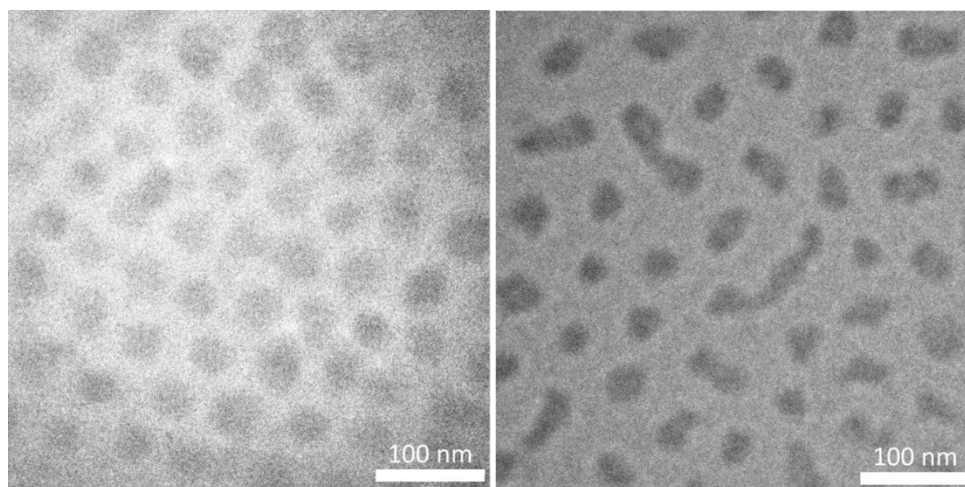


**Figure S2.16.** Original size and shape characterization at Cryo-TEM of C4Ms based on core-unit charge  $9^-$  (left) and C4Ms based on core-unit charge  $6^-$  (right). The highest core-unit charge C4Ms revealed homogeneously distributed spherical micelles, while the revealed core-unit charge C4Ms showed elongated micelles.

**Table S2.1.** DLS intensity for individual building blocks in comparison to the C4Ms. Europium ions (Eu), adamantane mono-acid and bis-acid (Ad-ma and Ad-ba), block copolymer (BP), pyridine-2,6-dicarboxylate-modified  $\beta$ -cyclodextrin ( $\beta$ CD-DPA) and combinations of the components.

<b>Sample name</b>	<b>Intensity (Mcps)</b>
<i>Eu</i>	<i>na</i>
<i><math>\beta</math>CD-DPA</i>	<i>na</i>
<i>AD-ma</i>	<i>0.9</i>
<i>AD-ba</i>	<i>0.9</i>
<i>BP</i>	<i>na</i>
<i>Eu+<math>\beta</math>CD-DPA</i>	<i>1.0</i>
<i>Eu+Ad-ma</i>	<i>2.8</i>
<i>Eu+Ad-ba</i>	<i>2.8</i>
<i>Eu+<math>\beta</math>CD-DPA+Ad-ma</i>	<i>0.8</i>
<i>Eu+<math>\beta</math>CD-DPA+Ad-ba</i>	<i>na</i>
<i>Eu+<math>\beta</math>CD-DPA+BP</i>	<i>na</i>
<i>Eu+BP</i>	<i>na</i>
<i>C4Ms<sup>9</sup></i>	<i>29.0</i>

\* All the controls were investigated at the DLS, keeping the concentrations of the single components the same as the in the final C4Ms.

## 2.6. REFERENCES

1. Ahmad, Z., Shah, A., Siddiq, M., and Kraatz, H.-B., *Polymeric micelles as drug delivery vehicles*. RSC Adv., 2014. **4**(33): p. 17028-17038.
2. Gaucher, G., Dufresne, M.H., Sant, V.P., Kang, N., Maysinger, D., et al., *Block copolymer micelles: preparation, characterization and application in drug delivery*. J. Control. Release, 2005. **109**(1-3): p. 169-188.
3. Cohen Stuart, M.A., Hofs, B., Voets, I.K., and de Keizer, A., *Assembly of polyelectrolyte-containing block copolymers in aqueous media*. Curr. Opin. Colloid Interface Sci., 2005. **10**(1-2): p. 30-36.
4. Bae, Y., Fukushima, S., Harada, A., and Kataoka, K., *Design of Environment-Sensitive Supramolecular Assemblies for Intracellular Drug Delivery: Polymeric Micelles that are Responsive to Intracellular pH Change*. Angew. Chem. Int. Ed. Engl., 2003. **115**(38): p. 4788-4791.
5. Voets, I.K., de Keizer, A., and Cohen Stuart, M.A., *Complex coacervate core micelles*. Adv. Colloid Interface Sci., 2009. **147-148**: p. 300-318.
6. Obermeyer, A.C., Mills, C.E., Dong, X.H., Flores, R.J., and Olsen, B.D., *Complex coacervation of supercharged proteins with polyelectrolytes*. Soft Matter, 2016. **12**(15): p. 3570-3581.
7. Bhattacharya, S., Ganivada, M.N., Dinda, H., Das Sarma, J., and Shunmugam, R., *Biodegradable Copolymer for Stimuli-Responsive Sustained Release of Doxorubicin*. ACS Omega, 2016. **1**(1): p. 108-117.
8. Haag, R., *Supramolecular drug-delivery systems based on polymeric core-shell architectures*. Angew. Chem. Int. Ed. Engl., 2004. **43**(3): p. 278-282.
9. Bourouina, N., Cohen Stuart, M.A., and Kleijn, J.M., *Complex coacervate core micelles as diffusional nanopores*. Soft Matter, 2014. **10**(2): p. 320-331.
10. Katayose, S. and Kataoka, K., *Water-Soluble Polyion Complex Associates of DNA and Poly(ethylene glycol)-Poly(L-lysine) Block Copolymer*. Bioconjug. Chem., 1997. **8**: p. 702-707.
11. Harada, A. and Kataoka, K., *Formation of Polyion Complex Micelles in an Aqueous Milieu from a Pair of Oppositely-Charged Block Copolymers with Poly(ethylene glycol) Segments*. Macromolecules, 1995. **28**(15): p. 5294-5299.
12. Wang, J., de Keizer, A., Fokkink, R., Yan, Y., Cohen Stuart, M.A., et al., *Complex coacervate core micelles from iron-based coordination polymers*. J. Phys. Chem. B, 2010. **114**(25): p. 8313-8319.
13. Yan, Y., Besseling, N.A., de Keizer, A., and Stuart, M.A., *Characteristic differences in the formation of complex coacervate core micelles from neodymium and zinc-based coordination polymers*. J. Phys. Chem. B, 2007. **111**(21): p. 5811-5818.
14. Wang, J., Groeneveld, A., Oikonomou, M., Prusova, A., Van As, H., et al., *Revealing and tuning the core, structure, properties and function of polymer micelles with lanthanide-coordination complexes*. Soft Matter, 2016. **12**(1): p. 99-105.
15. Wang, J., Velders, A.H., Gianolio, E., Aime, S., Vergeldt, F.J., et al., *Controlled mixing of lanthanide(III) ions in coacervate core micelles*. Chem. Commun. (Camb), 2013. **49**(36): p. 3736-3738.
16. Wang, J., Voets, I.K., Fokkink, R., van der Gucht, J., and Velders, A.H., *Controlling the number of dendrimers in dendrimicelle nanoconjugates from 1 to more than 100*. Soft Matter, 2014. **10**(37): p. 7337-7345.
17. Ten Hove, J.B., van Oosterom, M.N., van Leeuwen, F.W.B., and Velders, A.H., *Nanoparticles reveal Extreme Size-Sorting and Morphologies in Complex Coacervate Superstructures*. Sci. Rep., 2018. **8**(1): p. 13820-13827.
18. Ten Hove, J.B., Wang, J., van Leeuwen, F.W.B., and Velders, A.H., *Dendrimer-encapsulated nanoparticle-core micelles as a modular strategy for particle-in-a-box-in-a-box nanostructures*. Nanoscale, 2017. **9**(47): p. 18619-18623.
19. Ten Hove, J.B., Wang, J., van Oosterom, M.N., van Leeuwen, F.W.B., and Velders, A.H., *Size-Sorting and Pattern Formation of Nanoparticle-Loaded Micellar Superstructures in Biconcave Thin Films*. ACS Nano, 2017. **11**(11): p. 11225-11231.
20. Granadero, D., Bordello, J., Perez-Alvite, M.J., Novo, M., and Al-Soufi, W., *Host-guest complexation studied by fluorescence correlation spectroscopy: adamantane-cyclodextrin inclusion*. Int. J. Mol. Sci., 2010. **11**(1): p. 173-188.
21. Webber, M.J., Appel, E.A., Meijer, E.W., and Langer, R., *Supramolecular biomaterials*. Nat. Mater., 2016. **15**(1): p. 13-26.
22. Krieg, E., Bastings, M.M., Besenius, P., and Rybtchinski, B., *Supramolecular Polymers in Aqueous Media*. Chem. Rev., 2016. **116**(4): p. 2414-2477.
23. Biesalski, M., Johannsmann, D., and Ruhe, J., *Electrolyte-induced collapse of a polyelectrolyte brush*. J. Chem. Phys., 2004. **120**(18): p. 8807-8814.
24. Kim, I., Han, B.H., Kim, J.S., and Ha, C.-S., *Allyloxy- and Benzyloxy-Substituted Pyridine-bis-imine Iron(II) and Cobalt(II) Complexes for Ethylene Polymerization*. Macromol. Res., 2005. **13**(1): p. 2-7.
25. Vermonden, T., Branowska, D., Marcelis, A.T.M., and Sudhölter, E.J.R., *Synthesis of 4-functionalized terdentate pyridine-based ligands*. Tetrahedron, 2003. **59**(27): p. 5039-5045.

26. Chamas Zel, A., Guo, X., Canet, J.L., Gautier, A., Boyer, D., et al., *Clicked dipicolinic antennae for lanthanide luminescent probes*. Dalton Trans., 2010. **39**(30): p. 7091-7097.
27. Moore, E.G., Samuel, A.P.S., and Raymond, K.N., *From Antenna to Assay: Lessons Learned in Lanthanide Luminescence*. Acc. Chem. Res., 2009. **42**(4): p. 542-552.
28. Xu, L., Feng, L., Han, Y., Jing, Y., Xian, Z., et al., *Supramolecular self-assembly enhanced europium(III) luminescence under visible light*. Soft Matter, 2014. **10**(26): p. 4686-4693.
29. Tran, D.N., Colesnic, D., Adam de Beaumais, S., Pembouong, G., Portier, F., et al., *Cyclodextrin-adamantane conjugates, self-inclusion and aggregation versus supramolecular polymer formation*. Org. Chem. Front., 2014. **1**(6): p. 703-706.
30. van der Kooij, H.M., Spruijt, E., Voets, I.K., Fokkink, R., Cohen Stuart, M.A., et al., *On the stability and morphology of complex coacervate core micelles: from spherical to wormlike micelles*. Langmuir 2012. **28**(40): p. 14180-14191.
31. Vrettos, E.I., Sayyad, N., Mavrogiannaki, E.M., Stylos, E., Kostagianni, A.D., et al., *Unveiling and tackling guanidinium peptide coupling reagent side reactions towards the development of peptide-drug conjugates*. RSC Adv., 2017. **7**(80): p. 50519-50526.
32. Tao, C., Du, K., Yin, Q., Zhu, J., Yan, H., et al., *Pyridine-2,6-dicarboxylic acid for the sensitization of europium(III) luminescence with very long lifetimes*. RSC Adv., 2015. **5**(72): p. 58936-58942.
33. Hsu, S.H., Yilmaz, M.D., Reinhoudt, D.N., Velders, A.H., and Huskens, J., *Nonlinear amplification of a supramolecular complex at a multivalent interface*. Angew. Chem. Int. Ed. Engl., 2013. **52**(2): p. 714-719.
34. Hsu, S.-H., Yilmaz, M.D., Blum, C., Subramaniam, V., Reinhoudt, D.N., et al., *Expression of Sensitized Eu<sup>3+</sup> Luminescence at a Multivalent Interface*. J. Am. Chem. Soc., 2009. **131**(9): p. 12567-12569.





# CHAPTER 3

---

**Assembly, Disassembly and Reassembly of  
Cyclodextrin-based Complex Coacervate Core  
Micelles with Redox-Responsive Supramolecular  
Cross Linkers**

---

## ABSTRACT

---

Polymer-based micellar assemblies are gaining increasing attention in the smart materials field, yet the design of micelles that show redox-responsive disassembly and, e.g., cargo release is still a challenge. To form redox-responsive micelles, we developed cyclodextrin-based coacervate core micelles that form under interplay of four orthogonal interactions: multivalent electrostatic coacervation, metal-to-ligand coordination chemistry, supramolecular host-guest interactions, and a reversible covalent disulfide metal-complex crosslinker. The cleavage of this crosslinker by dithiotreitol results in the breaking of oligomeric europium(III) structures in the core and results in the disassembly of the 70 nm size micelles. Over hours, due to the oxidation of thiolates to disulfides, monomeric units can re-crosslink into oligomeric core-units, favoring micellar reassembly. The time required to reassemble can be controlled by varying the reducing agent concentration or the ratio between redox-responsive and non-redox-responsive crosslinkers. Controlled Methyl Red encapsulation and release indicate the potential of these micelles, for, e.g., controlled drug uptake and delivery.

---

This chapter has been adjusted from the form: Camilla Facciotti, Vittorio Saggiomo, Anton Bunschoten, Jan Bart ten Hove, Marcus T. M. Rood, Fijs W.B. van Leeuwen and Aldrik H. Velders (2019). "Assembly, Disassembly and Reassembly of Cyclodextrin-based Complex Coacervate Core Micelles with Redox-Responsive Supramolecular Cross Linkers." (under revisions in ChemSystemsChem)

### 3.1. INTRODUCTION

Polymer-based micellar assemblies are gaining increasing attention, for their promising potentials in biomedical applications.[1-8] Among the family of polymer-based micelles, Complex Coacervate Core Micelles (C3Ms) form via electrostatic interactions between oppositely charged polymers. This type of micelles displays high stability under physiological conditions, prolonged blood circulation, high gene transfection efficiency, low cytotoxicity and tunable imaging properties.[9-15] In the past decades, substantial knowledge on the way charged polymers assemble into coacervate micelles has been acquired. For example, it was shown that control over the micellar size and stability can be obtained by varying the individual (block) polymer lengths.[12] Substituting negatively charged polymers with negatively charged metal-to-ligand coordination complexes enabled to control not only the micelle core structure (oligomeric vs. polymeric) and stability, but also, by using different metals, the properties of the final micelle (such as fluorescence or magnetic properties for multimodal, e.g. MR, imaging applications).[14, 16-19] New insights on the aggregation numbers and the minimum amount of charges per core-unit required for coacervate assembly were acquired by encapsulating charged dendrimers into coacervate micelles, forming the so-called dendrimicelles.[20-22] Recently, an even more precise control on the minimum number of charges per core-unit, required for coacervation, was achieved by introducing cyclodextrin-adamantane host-guest interactions in the core of C3Ms, forming Cyclodextrin-based Complex Coacervate Core Micelles (C4Ms), in which monomeric europium(III) complexes can form core-units of the micelles.[23] By varying the ratio between two adamantane guest molecules, 1-adamantanecarboxylic acid and 1,3-adamantanediactic acid, the number of charges of the monomeric units was finely tuned from six to nine, showing that nine negative charges per monomeric core-unit formed spherical and well-monodispersed micelles of 45 nm in diameter, while a lower number of charges per monomeric unit, such as six, were not enough to form well-defined C4Ms, and instead yielded polydispersed aggregates of ca. 100 nm. Upon mixing low charged monomeric units, which are not able to form well-defined stable micelles, with a guest adamantane bislinker (Ad-Glu-Ad), monomeric-units can merge into dimeric and oligomeric core-units, thereby increasing the charge per core-unit and resulting in micelle formation with an increased stability

against salt, pH and competing free  $\beta$ CD. This very subtle control over micelle formation and stability via tuning the charge in monomeric and oligomeric core-units, led us to hypothesize the possibility to incorporate supramolecular stimuli-responsive bridging linkers to allow reversible assembly and disassembly with cyclodextrin-based coacervate-core micelles.

C3Ms, containing stimuli responsive guest molecules, can undergo changes in their morphology and assembly behavior in response to specific stimuli,[24, 25] possibly, releasing their inner content.[26, 27] Among these specific stimuli, redox responsiveness is one of the most enticing one, for example to be exploited in cells and tissue with reducing environments.[11, 28, 29] Based on the concept of redox responsivity, several studies reported the micellar dissociation in response to dithiothreitol (DTT) or glutathione (GSH) and the consequential release of micelle-embedded cargos, such as DNA molecules,[30] doxorubicin,[9-11] and siRNA molecules.[26] However, most of the redox-responsive micelles contain the redox responsive disulfide on the edge between the core and the shell; the cleavage of the disulfide bonds on the shell does not always lead to a fully disassociated micellar core, which decreases the efficiency of the core-embedded drug release.[9, 10, 13, 31-34]

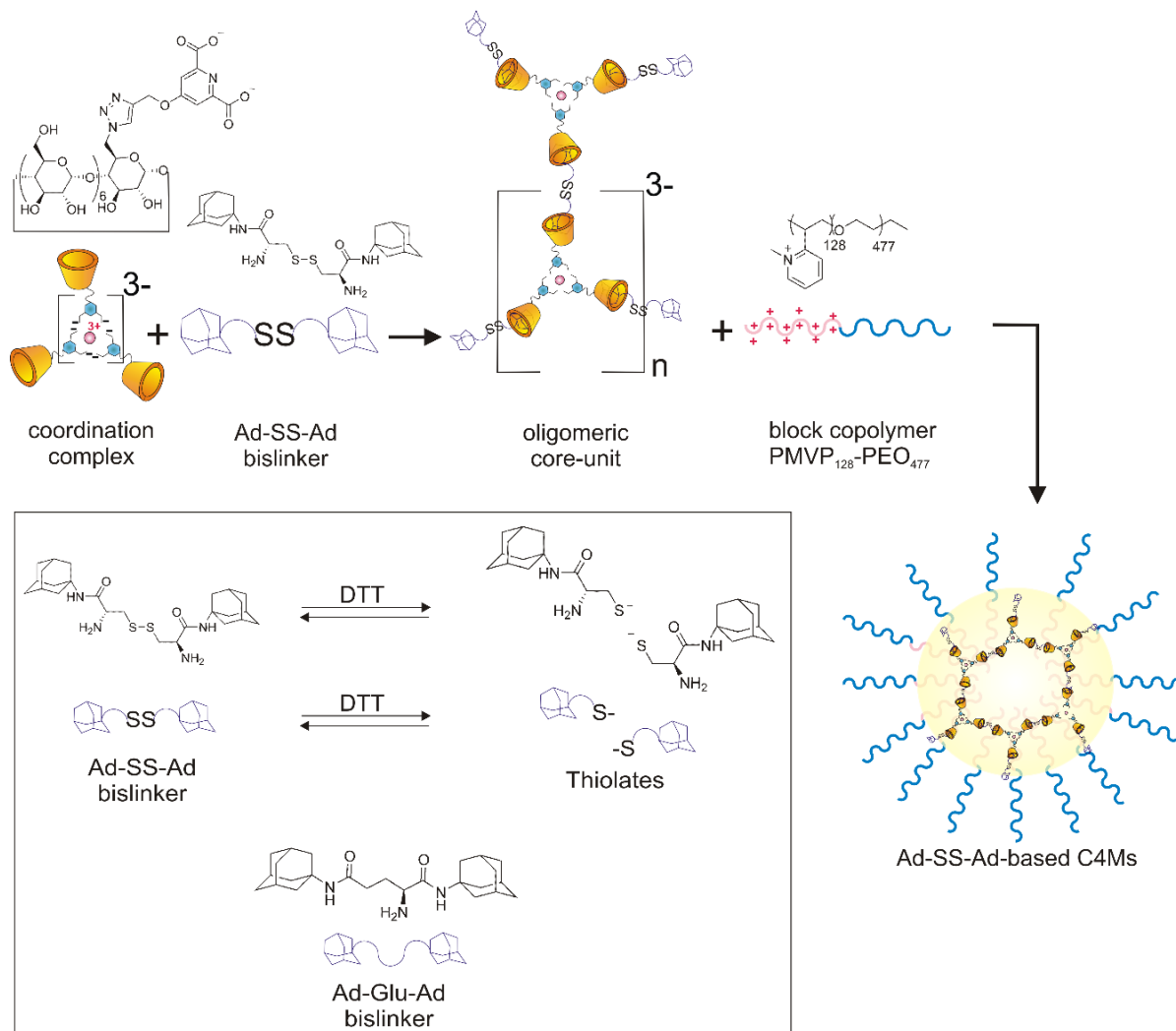
Here, we present the reversible assembly and disassembly of redox-responsive Cyclodextrin-based Complex Coacervate Core Micelles, Ad-SS-Ad-based C4Ms, in which the micellar assembly can be controlled using a disulfide crosslinker, bisadamantadine cystine ligand (Ad-SS-Ad), (Scheme 3.1.) that converts units, incapable of forming micelles, into supramolecular oligomeric core-units that can form the core of coacervate-core micelles. (Scheme 3.1). Uniquely, Ad-SS-Ad-based C4Ms are formed combining four orthogonal interactions, namely: i) electrostatic interactions, ii) metal-to-ligand coordination, iii) host-guest interactions, and iv) reversible covalent disulfide crosslinks (Scheme 3.1). Combining multiple orthogonal supramolecular interactions allows for fine tuning and controlling the formation of these complex hierarchical structures, as we have shown previously with different cyclodextrin systems immobilized on flat surfaces,[35] on nanoparticle surfaces,[36-38] and even cell-surfaces.[39] Here we show the unique control exploiting the supramolecular cyclodextrin chemistry in combination with other orthogonal interactions, in solution and within the inside of nanoscale compartments of a micellar core. The disulfide bond, designed at the center of the redox-responsive bislinker, controls the crosslinking of the multiple

coordination complexes, forming branched structures, that can become “oligomeric core-units” upon micelle formation (Scheme 3.1. and 3.2.).

A coordination complex is formed by a single europium ion (Eu(III)) chelated by three cyclodextrin-modified dipicolinic acid moieties ( $\beta$ CD-DPA); the charge of this complex is 3-, not enough to form micelles.[17] Even when three anionic adamantane-thiolates (Ad-S-) bind, the overall charge of the supramolecular core-unit complex is 6-, which is insufficient for micelle formation. In the oxidized state, and in presence of a block copolymer (PMVP<sub>128</sub>-PEO<sub>477</sub>), the Ad-SS-Ad can crosslink those monomeric units binding to the cyclodextrin, forming oligomeric species with a higher negative charge, capable of stabilizing micelles.

Interestingly, whether or not assembly takes place can be controlled not only prior to the addition of the block copolymer, but also when all subcomponents are present in solution (Scheme 3.2.). In fact, upon addition of DTT to preformed micelles, the Ad-SS-Ad bislinker breaks into two adamantane-thiolates, disrupting the oligomeric core-unit connections into monomeric units with six negative charges per complex hence, converting oligomeric core-units into monomeric units resulting in the micellar disassembly.[23]

Finally, the formed thiolates can oxidize back to disulfides over time, reforming the supramolecular crosslinker leading to the formation of oligomeric core-units and the reassembly of Ad-SS-Ad-based C4Ms. The time required to reassemble can be controlled by varying the DTT concentration or by varying the ratio between redox-responsive and non-redox-responsive bislinker, respectively Ad-SS-Ad (diamantadine cystine) and Ad-Glu-Ad (glutamic acid-modified bisadamantane). The Ad-SS-Ad-based C4Ms allow also for encapsulation and release of Methyl Red dye, which allows possible future drug delivery applications.



**Scheme 3.1.** Schematic illustration and molecular structures of the formation of Cyclodextrin-based Complex Coacervate Core Micelles (C4Ms) with a supramolecular redox-responsive cross-linker (Ad-SS-Ad). Ad-SS-Ad-based C4Ms form by combining four orthogonal interactions: i) metal to ligand coordination between one europium ion and three cyclodextrin-modified dipicolinic acids ( $\beta$ CD-DPA) molecules, ii) host guest interactions between the  $\beta$ CD and the Ad-SS-Ad bislinker, (forming oligomeric core-units), iii) reversible covalent disulfide crosslinks and iv) coacervate interactions, by adding the block copolymer (PMVP<sub>128</sub>-PEO<sub>477</sub>).

## 3.2. EXPERIMENTAL

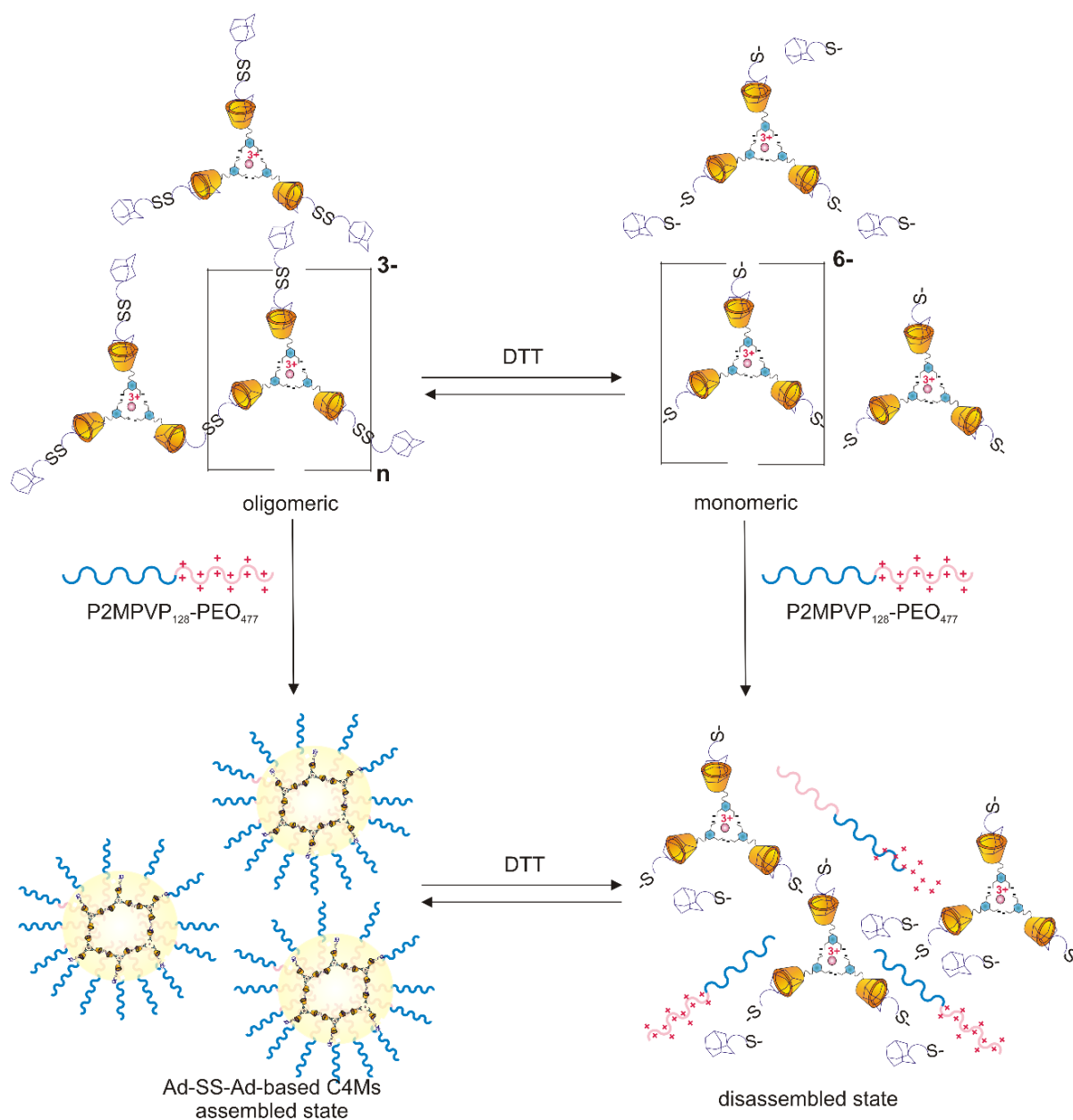
Materials and methods, synthesis and micelle preparations are described in the following sections.

### 3.2.1. MATERIALS AND METHODS

Europium nitrate  $\text{Eu}(\text{NO}_3)_3 \cdot 5\text{H}_2\text{O}$ , N-hydroxysuccinimide, dicyclohexylcarbodiimide, amantadine HCl, N-di-Boc-L-cystine, trifluoroacetic acid, triethylamine, dithiothreitol, dichloromethane and Methyl Red were purchased from Sigma Aldrich and used without further purification. The block copolymer, poly(N-methyl-2-vinyl-pyridinium iodide)-b-poly(ethyleneoxide) ( $\text{P2MVP}_{128}\text{-b-PEO}_{477}$ ), was obtained by quaternization of poly(2-vinylpyridine)-b-poly(ethylene oxide) ( $\text{PVP}_{128}\text{-b-PEO}_{477}$ ) (Polymer Source,  $M_w/M_n = 1.03$ ,  $M_w = 13.3$  k) following a procedure described elsewhere.[40] The degree of quaternization was 90 %, as determined by DLS titration.

NMR measurements were carried out at 298 K on Bruker Avance III 400 MHz, 500 MHz, or 600 MHz NMR spectrometers. Assignments were aided by COSY, HSQC, NOESY, ROESY and HMBC experiments. All mass spectra were acquired using ES ionization on a Thermo Finnigan LXQ Exactive Mass Spectrometer. Light scattering measurements (DLS) were carried out on a Malvern NanoSizer ZS, at 173 degree angle, operating at 632.8 nm at 25 °C. DLS size results are given as number-based size. UV-VIS measurements were carried out on a UV-1601 Shimadzu Spectrophotometer using quartz cuvettes of 1 cm path length. Fluorescence spectroscopy measurements were carried out on an Agilent Cary Eclipse Fluorescence Spectrophotometer using quartz cuvettes of 1 cm path length, excitation and emission slits were set at 5 nm. For cryo-TEM, samples were cast on copper grids (400 mesh - 150  $\mu\text{m}$  average hole size, Holey carbon), from Electron Microscopy Sciences (EMS, Hatfield, PA, USA). After blotting, samples were plunged into liquid ethane by using a Vitrobot Mark IV. Grids were then transferred to a JEOL 1400 PLUS TEM operating at 120 kV.

The diethyl 4-(prop-2-yn-1-yloxy)pyridine-2,6-dicarboxylate and of pyridine-2,6-dicarboxylate modified  $\beta$ -cyclodextrin synthesis was performed following a previously described procedure.[23] The synthesis, NMR assignments, micelle formation, redox-response and Methyl Red release experiments are described in the Supporting Information.



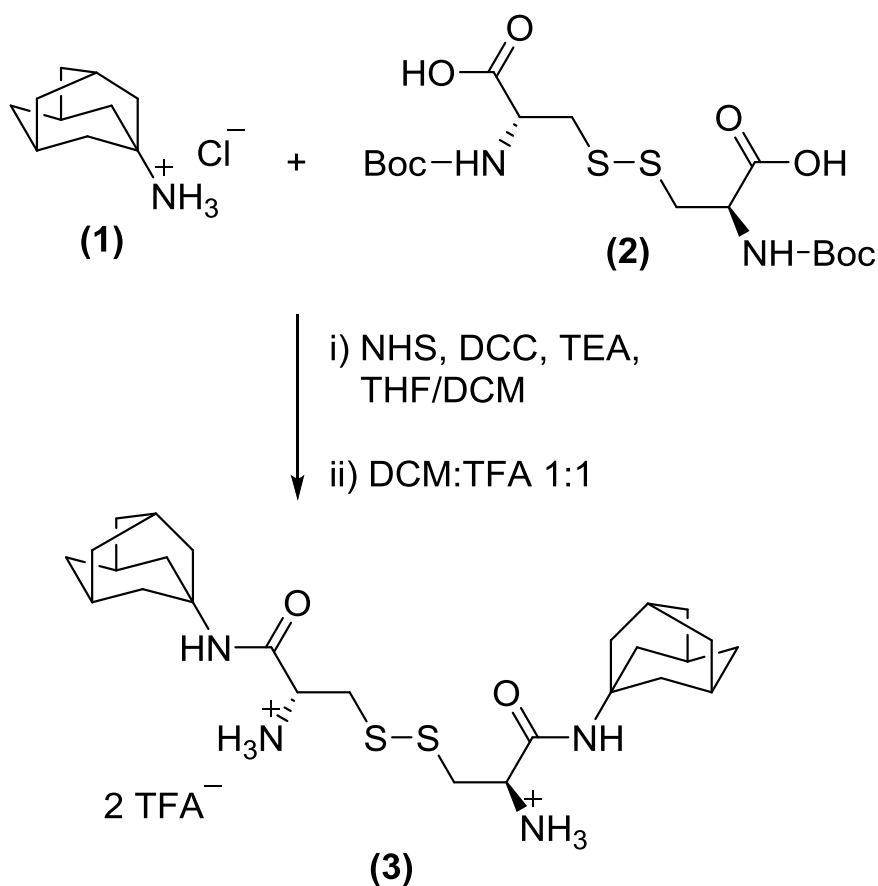
**Scheme 3.2.** Schematic representation of the assembly and disassembly of Ad-SS-Ad-based C4Ms and the sub-components. On the left: by mixing the coordination complex (between europium ions and  $\beta$ CD-DPA) with Ad-SS-Ad bislinker, a branched crosslinked structure was formed, called “oligomeric core-unit. Then, by adding the block copolymer, Ad-SS-Ad-based C4Ms are formed. On the right: by adding DTT reducing agent, the bislinker is cleaved into thiolates. Mixing the cleaved bislinker with the europium-based metal-ligand coordination complex provides monomeric unit complex, with an effective charge of 6-, which does not yield well-defined and stable micelles, upon mixing with an oppositely charged block copolymer. However, over time, the bislinker thiolates re-oxidize to disulfide, favoring the combination of monomeric units into oligomeric core-units, supporting the Ad-SS-Ad-based C4Ms reassembly.

### 3.2.2. SYNTHESIS

#### SYNTHESIS OF DIAMANTADINE CYSTINE (3) (SCHEME 3.3)

Compound **3** (Ad-SS-Ad), (2R,2'R)-3,3'-disulfanediylbis(N-(adamantan-1-yl)-2-aminopropanamide), was prepared from tert-butoxycarbonyl or Boc -protected cystine and amantadine.[41] The NMR spectra can be found in the SI (Figure S3.1-S3.3.).

2.0 mmol (230 mg) N-hydroxysuccinimide (NHS), 2.0 mmol (412 mg) dicyclohexylcarbodiimide (DCC), and 2.2 mmol (414 mg) amantadine HCl were dissolved in a mixture of tetrahydrofuran (THF) and dichloromethane (DCM) (1 mL and 15 mL respectively). 1.0 mmol (440 mg) N-di-Boc-L-cystine and 2.5 mmol (350  $\mu$ L) triethylamine (TEA) were added to this mixture. The reaction was stirred overnight at room temperature. The next day the solvent was removed *in vacuo*. The resulting white solid was stirred in DCM for 30 min. Water was added and the organic phase was separated. The water phase was extracted once more with DCM. The combined organic fractions were dried with sodium sulfate and concentrated *in vacuo*. The resulting white solid was dissolved in 10 ml DCM: trifluoroacetic acid (TFA) (1:1) and left to react overnight. The next day the reaction mixture was precipitated in 90 mL n-hexane: methyl tert-butyl ether (MTBE) (1:1) and centrifuged to collect the white solid product. The product was washed and centrifuged once more with n-hexane:MTBE. The white solid was dried, which resulted in 628 mg of product **3** (82%).



**Scheme 3.3.** Reaction scheme of the diamantadine cystine (Ad-SS-Ad) synthesis from Boc-protected cystine and amantadine.

<sup>1</sup>H-NMR spectrum (600MHz, DMSO),  $\delta$  [ppm]: 8.35-8.21 (s, 4H, NH<sub>2</sub>), 8.05-7.95 (s, 2H, NH), 4.00-3.92 (s, 2H, CH-NH<sub>2</sub>), 3.29-2.98 (m, 4H, CH<sub>2</sub>-CH), 2.05-1.98 (s, 6H, C-CH<sub>2</sub>-CH-CH<sub>2</sub>), 1.98-1.89 (s, 12H, C-CH<sub>2</sub>-CH-CH<sub>2</sub>), 1.69-1.55 (m, 12H, C-CH<sub>2</sub>-CH-CH<sub>2</sub>).

<sup>13</sup>C-NMR spectrum (600MHz, DMSO),  $\delta$  [ppm]: 165.8 (C=O), 158.2 (TFA), 51.7 (C-CH<sub>2</sub>-CH-CH<sub>2</sub>), 51.4 (CH<sub>2</sub>-CH), 40.8 (C-CH<sub>2</sub>-CH-CH<sub>2</sub>), 39.0 (CH<sub>2</sub>-CH), 35.7 (C-CH<sub>2</sub>-CH-CH<sub>2</sub>), 28.6 C-CH<sub>2</sub>-CH-CH<sub>2</sub>).

Calculated monoisotopic mass [M+H]<sup>+</sup> for **3**, M=C<sub>26</sub>H<sub>42</sub>N<sub>4</sub>O<sub>2</sub>S<sub>2</sub>, is 507.28. The experimental mass is 507.49 ([M+H]<sup>+</sup>).

### 3.2.3. MICELLES PREPARATION

Stock solutions of europium nitrate, P2MVP<sub>128</sub>-b-PEO<sub>477</sub>, βCD-DPA, Ad-SS-Ad were prepared by dissolving the solids in ultrapure water and adjusting the pH of the solutions to pH 7 with HCl and/or NaOH. Concentrations of the stock solutions were respectively 5 mM, 10 mM (charge concentration), 5 mM, and 1 mM.

Micelles were prepared under sonication at room temperature in a final volume of 0.5 mL. All the samples were prepared by adding sodium carbonate buffer pH 10 (Na<sub>2</sub>CO<sub>3</sub> and NaHCO<sub>3</sub>, final concentration of 10 mM) to ensure the presence of negative charges in the oligomeric core-units. The coordination complex between Eu<sup>3+</sup> and DPA was formed by adding first europium ions at a final concentration of 0.2 mM. Secondly, βCD-DPA was added in a 1 : 3 ratio of Eu/βCD-DPA, at a final concentration of 0.6 mM. The oligomeric core-unit was formed by adding Ad-SS-Ad guest molecules to the coordination structure, in a 1 : 2 ratio Ad-SS-Ad/βCD-DPA, at a final concentration of 0.3 mM. Ad-SS-Ad-based C4Ms were formed by adding the P2MVP<sub>128</sub>-b-PEO<sub>477</sub> block copolymer to the oligomeric core-unit structure until charge neutralization. During all experiments, the concentration of the components was kept above the CMC to prevent the equilibrium from shifting from micelles towards monomers.

### 3.2.4. REDOX RESPONSE

The redox responsivity studies were performed by exposing Ad-SS-Ad-based C4Ms to DTT. To avoid the inactivation of DTT, each DTT addition was taken from freshly prepared stock solutions. DTT amounts are given as equivalents relative to the disulfide concentration in Ad-SS-Ad molecules.

For the “oxidation/reduction cycle” experiment, 6 equivalents of DTT were repeatedly added to Ad-SS-Ad-C4Ms. Each DTT addition was done after the Ad-SS-Ad-based C4Ms were reassembled. Intensity, size and monodispersity were measured every 10 minutes with DLS.

Two control experiments were performed to confirm that the DTT responsivity was only related to the presence of the disulfide bond in the core of the Ad-SS-Ad-based C4Ms. In the first control experiment, the redox-responsive Ad-SS-Ad bislinker was substituted with a non-redox responsive Ad-Glu-Ad bislinker, (glutamic acid-modified bisadamantane). The preparation of Ad-Glu-Ad-based

C4Ms is described in our previous work.[23] After the formation of Ad-Glu-Ad-based C4Ms, micelles were treated with 6 equivalents of DTT. For the second control experiment, we changed the order of addition of DTT, studying the assembly starting from the monomeric units. The monomeric units were formed first by combining europium ions,  $\beta$ CD-DPA and Ad-SS-Ad bislinker and reducing the disulfide with 6 equivalents of DTT. Next, the block copolymer was added. Intensity, size and monodispersity were measured every 10 minutes with DLS.

### **3.2.5. ENCAPSULATION AND RELEASE STUDY**

A stock solution of 0.15 mM of Methyl Red dye was prepared by dissolving the powder in ultrapure water and adjusting it to pH 10 with HCl and/or NaOH. The encapsulation of Methyl Red inside Ad-SS-Ad-based C4Ms was achieved by mixing Methyl Red and Ad-SS-Ad bislinker before addition to the  $\beta$ CD-DPA (5% Methyl Red and 95% singular adamantane vs.  $\beta$ CD). After the addition of the dye to the oligomeric core-units, the block copolymer was added. For the release experiment, a biphasic system with water/dichloromethane (1:1, 0.5 mL) was prepared in a glass vial. Six different glass vials were prepared: two vials with only Methyl Red, other two with methyl red and  $\beta$ CD-DPA, and the last two with Ad-SS-Ad-based C4Ms and encapsulated methyl red (Figure S3.26.). The concentration of methyl red was kept constant in all the samples, around 37.5  $\mu$ M. To vials B, D and F, 30 equivalents of DTT were added and all the vials were shaken afterwards.

### 3.3. RESULTS AND DISCUSSION

Following the procedures presented in Scheme 3.1 and 3.2, first coacervate core micelles with the bisadamantane cystine linker were prepared, and consecutively the redox responsiveness of the systems under various conditions was tested.

Mixing of europium ions,  $\beta$ CD-DPA, Ad-SS-Ad and P2MVP<sub>128</sub>-b-PEO<sub>477</sub> (or BP) in stoichiometric ratios leads to self-assembled micelles, called Ad-SS-Ad-based C4Ms. The structural integrity of these micelles is based on four orthogonal interaction motifs: i) metal-to-ligand coordination, ii) host-guest interactions, iii) electrostatic interactions and iv) reversible-covalent disulfide bridge. DPA is a well-known ligand for lanthanide ions,[42-44] and the characteristic sharp-lines of the Eu (III) emission at 615 nm after excitation of DPA at 280 nm (antenna effect) corroborate that  $\beta$ CD-DPA coordinates to the metal ion (Figure S3.5.-S3.7.). Ad-SS-Ad linker molecules can connect multiple coordination complexes, driving the formation of branched structures, called “oligomeric core-unit”(Figure S3.8.-S3.9.). The host-guest interaction complex between adamantane guests and  $\beta$ CD hosts has also been demonstrated previously.[45-48] By adding a block copolymer (P2MVP<sub>128</sub>-b-PEO<sub>477</sub>) composed of a positively charged part and a neutral part to the negatively charged oligomeric units, Ad-SS-Ad-based C4Ms were formed, (Figure S3.10.). The size and polydispersity of the Ad-SS-Ad-based C4Ms were studied by DLS and cryo-TEM, resulting in the hydrodynamic diameter of the micelles of around 70 nm (SD 10 nm, PDI 0.12). These results are in good agreement with the cryo-TEM results (around 40 nm core size and around 20 nm shell) (Figure 3.1. and S3.11.). The size and intensity remained stable over at least three days (Figure S3.12.). By diluting a micelle sample with deionized water, the Critical Micelle Concentration (CMC) was determined to be around 50  $\mu$ M of europium ions, comparable with the previous value of Ad-Glu-Ad-based C4Ms (Figure S3.13).[23] The micelles disassemble upon increasing ionic strength due to the screening of the electrostatic charges by salt ions (Figure S3.14.);[12] the Critical Salt Concentration (CSC) is ca. 30 mM of NaCl, which is similar to the CSC found for Ad-Glu-Ad-based C4Ms.[23]

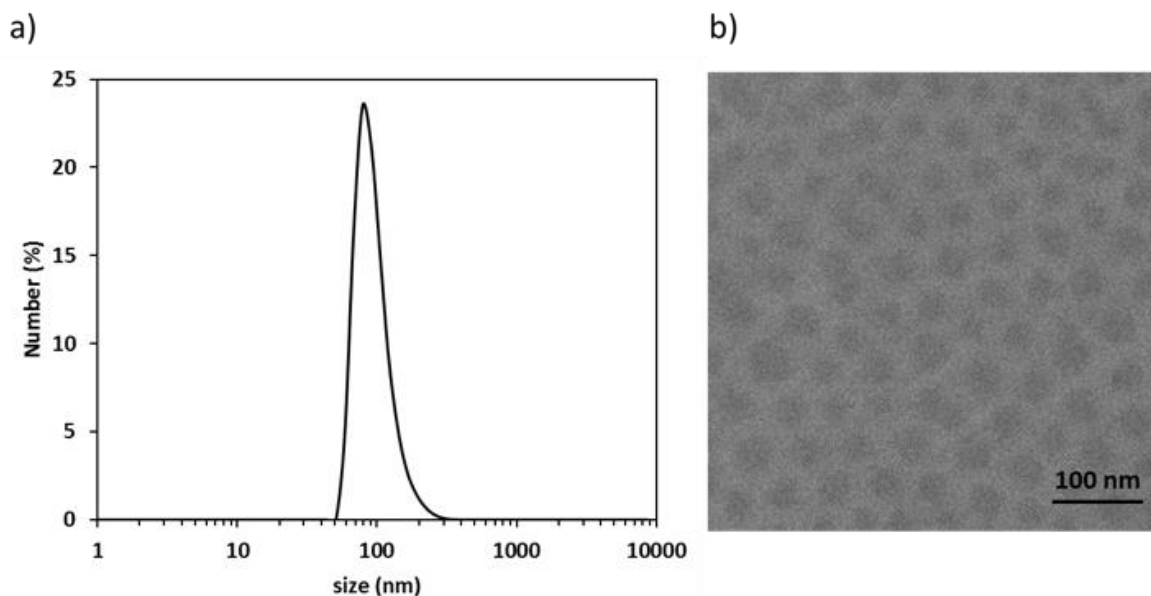


**Figure 3.1.** Size distribution of Ad-SS-Ad-based C4Ms determined by DLS (left) and cryo-TEM image of Ad-SS-Ad-based C4Ms (right). The DLS and cryo-TEM techniques show comparable results, respectively, hydrodynamic diameter of 70 nm (SD 10 nm), specifically core size of ca. 40 nm, with shell of ca. 10 nm.

### 3.3.1. REDOX RESPONSE OF AD-SS-AD-BASED C4MS

In Ad-SS-Ad-based C4Ms, a single europium ion is chelated by three  $\beta$ CD-DPA, forming a coordination complex with a net charge of 3-. The Ad-SS-Ad bislinker, can crosslink multiple coordination complexes into oligomeric core-units, with a higher net-charge, compared to the single coordination complex. Upon the addition of the block copolymer, the solution containing complexes bearing the Ad-SS-Ad bislinker form coacervate micelles (Scheme 3.2. left). Upon DTT treatment, the disulfide crosslinks are reduced into thiols, which are deprotonated to thiolates in the buffer at pH 10 used for the formation of micelles, converting oligomeric core-units into monomeric units with six negative charges. These six negative charges are determined by summing 3- charges of the thiolate guests with 3- net charges of the coordination complex. As previously demonstrated, six negative charges, per monomeric units, are not enough to form stable and well-defined coacervate micelles, but rather unstable and non-uniform aggregates.[23] Therefore, the addition of DTT favors the micellar disassembly (Scheme 3.2. bottom).

To further investigate the ability of disulfide bond cleavage to weaken the cross-linked core and lead to the micelle dissociation, different amounts of DTT, from 1 to 30 equivalents, were added to Ad-SS-Ad-based C4Ms. DLS was used to monitor changes in size and intensity before and after addition of DTT. In the absence of DTT the average micellar size and the scattered intensity remained stable for more than three days (around 70 nm and 160 Mcps respectively). After treatment with 1 or 3 equivalents of DTT, Ad-SS-Ad-based C4Ms did not show any significant change in size or in intensity (Figure S3.15.). However, when Ad-SS-Ad-based C4Ms were treated with higher concentrations of DTT, such as 6, 10, 15, 20 and 30 equivalents, the scattered intensity decreased dramatically, up to 30% of its original value, while the size remained stable (Figures 3.2. and S3.15.-3.16.). The decrease in intensity is caused by a breakage of the oligomeric core-unit into monomeric units, resulting in a loss of stability and disassembly of the micelle. Interestingly, the scattering intensity recovered over time, to its starting value, as shown in Figure 3.2. This phenomenon indicates disulfide bond reformation and the micellar reassembly in time. This process is clearly favored by the presence of oxygen (Figure S3.17.); it is well reported, that in the presence of a small amount of base and oxygen, thiolates tend to form quickly disulfides. Once all the DTT is oxidized the Ad-SS-Ad disulfide can be reformed.[49-53] Obviously, the reassembly time increased by increasing the DTT concentration, as the oxidation of DTT by oxygen competes with the bislinker oxidation. The more DTT is present in its reduced form, the longer the time the oxygen will take to oxidize the thiolates.

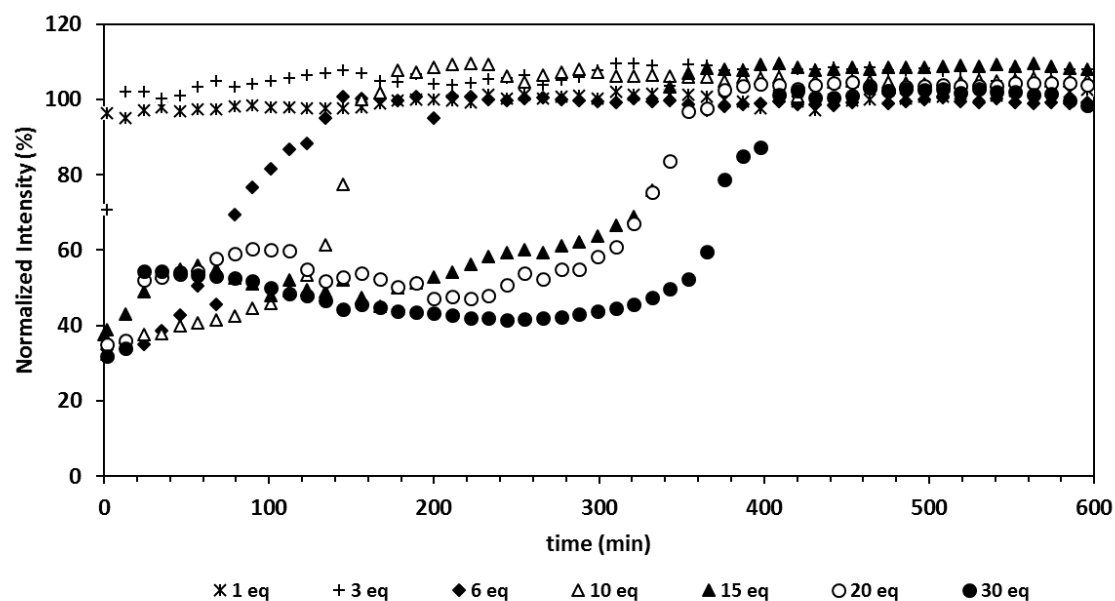


**Figure 3.2.** DLS data of the disassembled micelles after the addition of reducing agent reassembling over time. Micelle disassembly (data points at time = 0) and “reassemble time” graph plotted as normalized scattered intensity against time. Ad-SS-Ad-based C4Ms were treated with 1, 3, 6, 10, 15, 20, 30 equivalents of DTT. The addition of at least 6 equivalents of DTT favors the micelle disassembly. However, over time, micelles can reform, due to the re-oxidation of thiolates into disulfides. Scattered intensity was measured every ten minutes with DLS.

The trend between the reassembly time and the DTT concentration is, indeed, clear in Figure 3.2. A similar behavior was described in literature for poly-hydroxylamine-based micelles.[11] The disulfide cleavage and reformation can be also observed by the naked eye. After treatment with 6 equivalents of DTT, the solution became partially clear due to the cleavage of disulfide bonds and subsequent disassembly of the micelles. However, over time, the solution acquired the same initial turbidity, attributed to the disulfide bond reformation and subsequent reassembly of the micelles (Figure S3.18.). This phenomenon was also observed in other types of micelles and used to confirm the disulfide bond cleavage and, eventually, reformation.[33]

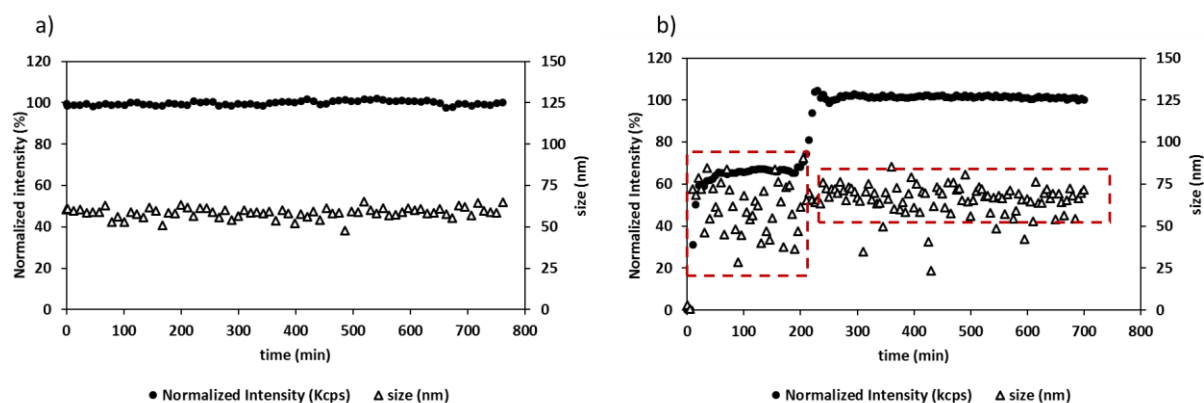


**Figure 3.3.** A control experiment was performed with non-redox-responsive Ad-Glu-Ad-based C4Ms, treated with 6 equivalents of DTT. No difference in size or intensity is noticeable for Ad-Glu-Ad-based C4Ms, after treatment with DTT (left). A second control was performed starting from the thiol-adamantane molecule, by adding first DTT to the Ad-SS-Ad oligomeric core-unit and subsequently the BP (right). In the figure on the right, the first red dashed square underlines the formation of monomeric unit aggregates. The second red dashed rectangular underlines the formation of oligomeric cross-linked core-unit micelles

To tune the stability of the micelles against DTT, we substituted the 10% of the redox-responsive Ad-SS-Ad bislinker with non-redox responsive Ad-Glu-Ad bislinker (Figure S3.19.). In our previous research, we demonstrated that 10% of Ad-Glu-Ad bislinker was enough to increase the stability of C4Ms based on the europium(III)- CD-DPA monomeric units with carboxylated adamantane guest molecules.[23] By substituting 10% of Ad-SS-Ad bislinker with Ad-Glu-Ad bislinker, micelles of similar sizes and intensity were formed (Figure S3.19.). Upon DTT treatment, three main results were noticeable: i) right after the addition of DTT, the intensity drop was less pronounced (from 100% to 50%), compared to C4Ms based on 100% Ad-SS-Ad bislinker (from 100% to 30%), ii) the recovery time was faster (100 minutes rather than 150 minutes) and iii) micelle size remained more monodisperse (70 nm, SD 5 nm), compared to Ad-SS-Ad-based C4Ms (70 nm, SD 10 nm). These results show that the redox response of Ad-SS-Ad-based C4Ms can be tuned by adjusting the ratio between redox-responsive and non-redox-responsive bislinker, i.e. Ad-Glu-Ad bislinker and Ad-SS-Ad bislinker. To confirm that the redox responsivity was only related to the presence of a disulfide bond in the core of the Ad-SS-Ad-based C4Ms, a control experiment with 100% non-redox-responsive bislinker, Ad-Glu-Ad, was performed. Ad-Glu-Ad-based C4Ms were treated with 6 equivalents of DTT. Figure 3.3. on the left shows that no significant change in size or intensity was detected. This result further confirms that the redox-responsivity can be attributed to the presence

of the disulfide bond in the cross-linker. To understand the mechanism of the coacervate micelle formation, an additional experiment was performed studying the assembly starting from monomeric units containing only three negative charges by adding DTT to the supramolecular polymers prior to the addition of the block copolymer, (Scheme 3.2., Figures 3.3.-right and S3.20.-3.22.). In this case, the micellar self-assembly occurred in two steps. The first step between 5 minutes and 3 hours, in which ill-defined aggregates are present with high polydispersity according to the DLS data. The second step occurred after 4 hours and shows stable micellar assemblies, comparable to the previously prepared Ad-SS-Ad-based C4Ms, with a hydrodynamic diameter of c.a. 70 nm (Table S3.1.). We speculate that these two steps can be attributed to the formation of, firstly, aggregates of the block copolymer with monomeric coordination complexes while the second step can be attributed to the formation of crosslinked oligomeric core which then forms the coacervate micelles. The reassembly time, defined as the time required to form stable micelles, could be associated to the disulfide reformation and micelle transition from the monomeric unit structures to the oligomeric cross-linked core-units. We excluded that the lag time was related to the time required for self-assembly of the micelles as, the formation of a standard C3Ms is completed in around 30 seconds. Therefore, we believe that this lag time is mainly related to the reformation of the disulfides and the oligomeric crosslink core-units (Figure S3.24.).

### 3.3.2. OXIDATION/REDUCTION CYCLE OF AD-SS-AD-BASED C4MS

The ability to reversibly disassemble-reassemble multiple times was investigated in a so-called “oxidation/reduction cycle” experiment. Ad-SS-Ad-based C4Ms were first formed and then, repeatedly, treated with 6 equivalents of DTT and exposed to air. Figure 3.4 shows the ability of Ad-SS-Ad-based C4Ms to reassemble up to at least 4 cycles of DTT additions (recovering up to 90% of the original intensity). After each DTT treatment, the intensity decreased due to the micellar disassembly, but it recovered back to the initial values. Figure 3.4. b and S3.25. show the increase in recovery time after the DTT addition. This phenomenon might be explained by the combination of different effects, such as the over oxidation of the sulfur to sulfoxides, which cannot form disulfides anymore, and the increasing concentration of added components and reaction products to the solution with the repeated additions of DTT. [17]

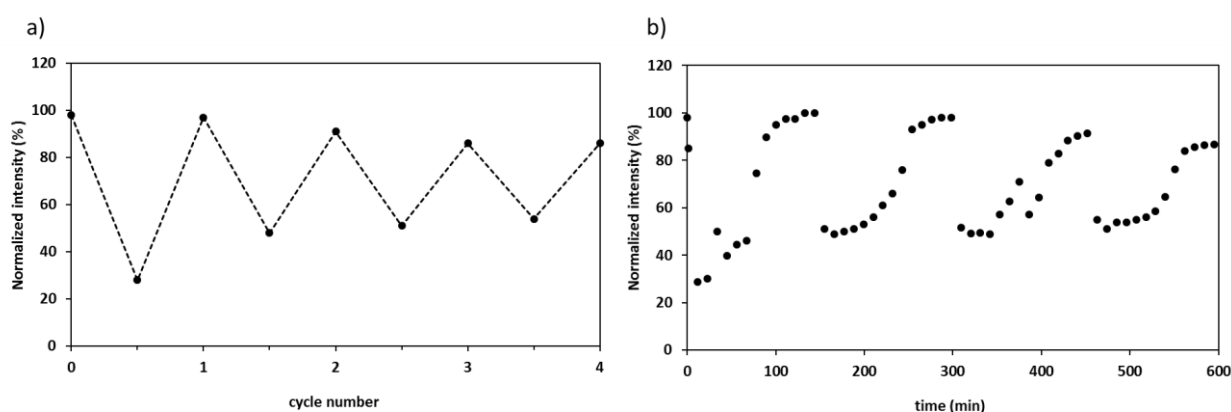


**Figure 3.4.** DLS data of Ad-SS-Ad-based C4Ms oxidation/reduction cycles. In the oxidation/reduction cycle, Ad-SS-Ad-based C4Ms were first formed and then, repeatedly, treated with 6 eq of DTT. Each DTT addition was done after the Ad-SS-Ad-based C4Ms were reassembled (one cycle). Intensity, size and dispersity were detected every 10 minutes with the DLS. In a), the intensity is plotted against the number of cycles. In b), the intensity is plotted against time. From both graphs, it is clear that micelles can disassemble after DTT treatments and reassemble in time.

### 3.3.3. ENCAPSULATION AND RELEASE OF METHYL RED DYE

The goal of this experiment was to prove the encapsulation and the release of Methyl Red (MR) from Ad-SS-Ad-based C4Ms, by using a biphasic system. MR was used as a drug-model, based on its medium-strong association constant with  $\beta$ CD ( $k_a$  around  $5 \cdot 10^3 \text{ M}^{-1}$ ) and the direct visual information.[54-56] Biphasic systems have proven to be very illustrative to study supramolecular interactions involving hydrophobic/hydrophilic building blocks via phase transfer.[57] In a biphasic system based on water and dichloromethane (DCM), MR resides mainly in the DCM layer, due to its hydrophobicity. However, by encapsulating it inside micelles, MR remains in the water phase (Figure 3.5. and S3.26.). This result confirms the ability of C4Ms to solubilize poorly water-soluble molecules. The drug can be released by breaking the coacervate micelle. Figure 3.5 shows that the addition of 30 eq. of DTT to Ad-SS-Ad-based C4Ms provokes the release of the MR dye and its transfer to the organic phase. This result was confirmed by UV-Vis, as upon the DTT addition, the MR absorption peak decreases in the water phase and increases in the organic phase (Figure S3.27.). The peak shift from 420 nm to 520 nm is related to the pH and the MR protonation.[54, 55] Figure S3.27 shows an increase in the absorbance of the dye when it is encapsulated inside the cyclodextrin. This effect is related to the transfer of the guest from a more protic environment to a less protic environment, such as the cavity of the cyclodextrin.[58] From these results it is evident that C4Ms promote the solubilization of MR in water and its release (i.e. to the organic phase) upon micelle dissociation. With this preliminary study, we show that the presence of the  $\beta$ CD, combined with C4Ms can be used to incorporate and release drugs.

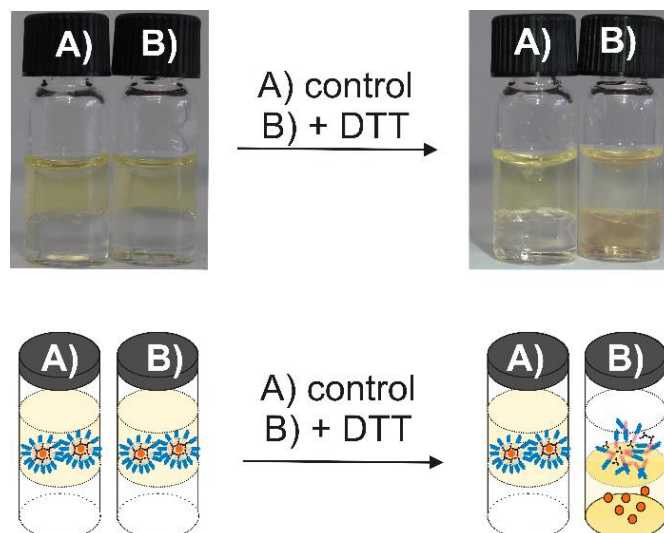


**Figure 3.5.** Pictures and schematic representation of the encapsulation and release experiment. 5% of Methyl Red was encapsulated into Ad-SS-Ad-based C4Ms. A) represents the control and no DTT was added to the vial. B) represents the sample before (left) and after (right) the DTT addition. Without any DTT treatment, the micelle solubilize the Methyl Red in the water phase (upper layer). However, the DTT addition promotes the micellar disassembly and the release of the dye into the organic phase.

### 3.4. CONCLUSION

We successfully developed a core-redox-responsive cyclodextrin-based complex coacervate core micelles, Ad-SS-Ad-based C4Ms, of 70 nm. The assembly and disassembly can be controlled by finely tuning the charge of core-units based on a supramolecular coordination complex, using a redox-responsive bislinker. The disulfide bislinker is able to crosslink multiple monomeric units into stable oligomeric core-units. Upon the addition of 6 or more equivalents of DTT, the disulfide bislinker is cleaved into thiolates, breaking oligomeric core-units into monomeric units, favoring the micellar disassembly. Ad-SS-Ad-based C4Ms disassembly was reversible after two hours, due to the re-oxidation of thiolates to disulfides. Importantly, the ability to be reversibly oxidized and reduced was confirmed up to 4 cycles of DTT treatment. The time required to reassemble can be controlled by varying the DTT concentration or the ratio between redox-responsive and non-redox-responsive bislinker. The ability of the micelles to assemble and disassemble under specific stimuli, and release a cargo was proven in a phase transfer experiment, illustrating the potential for controlled drug delivery applications.

### 3.5. SUPPORTING INFORMATION

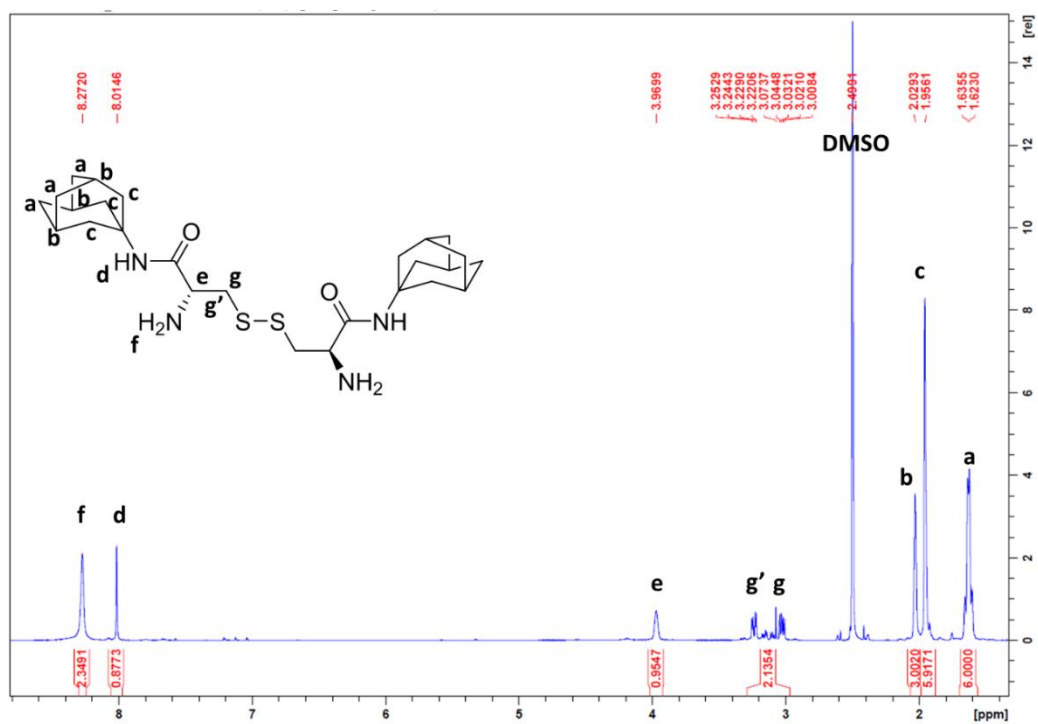


**Figure S3.1.**  $^1\text{H-NMR}$  of Ad-SS-Ad bislinker in DMSO. The concentration of Ad-SS-Ad bislinker was fixed at 0.6 mM.

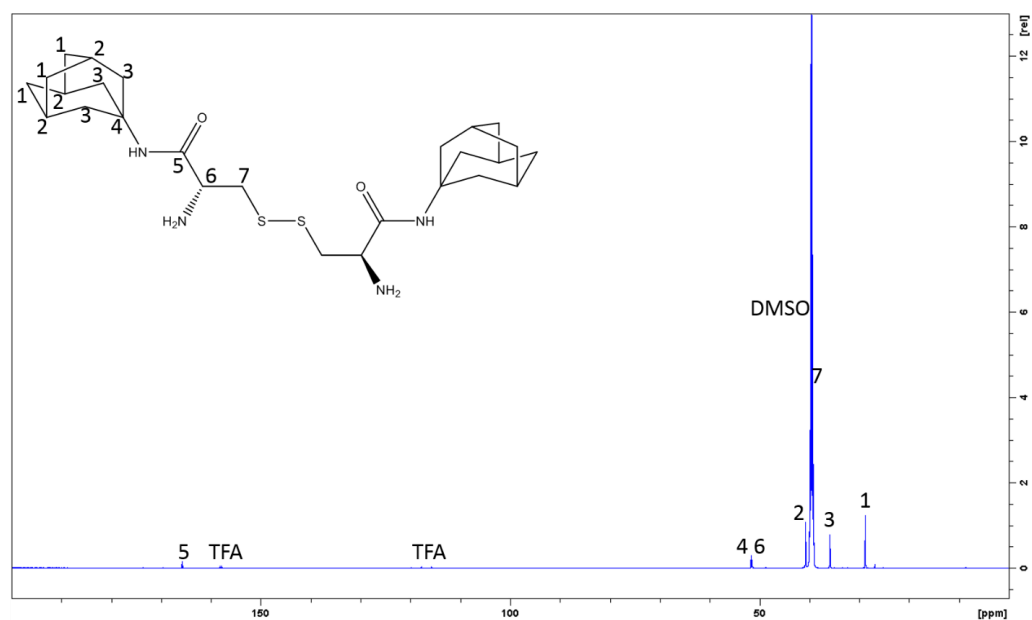


**Figure S3.2.**  $^{13}\text{C-NMR}$  of Ad-SS-Ad bislinker in DMSO. The concentration of Ad-SS-Ad bislinker was fixed at 0.6 mM.

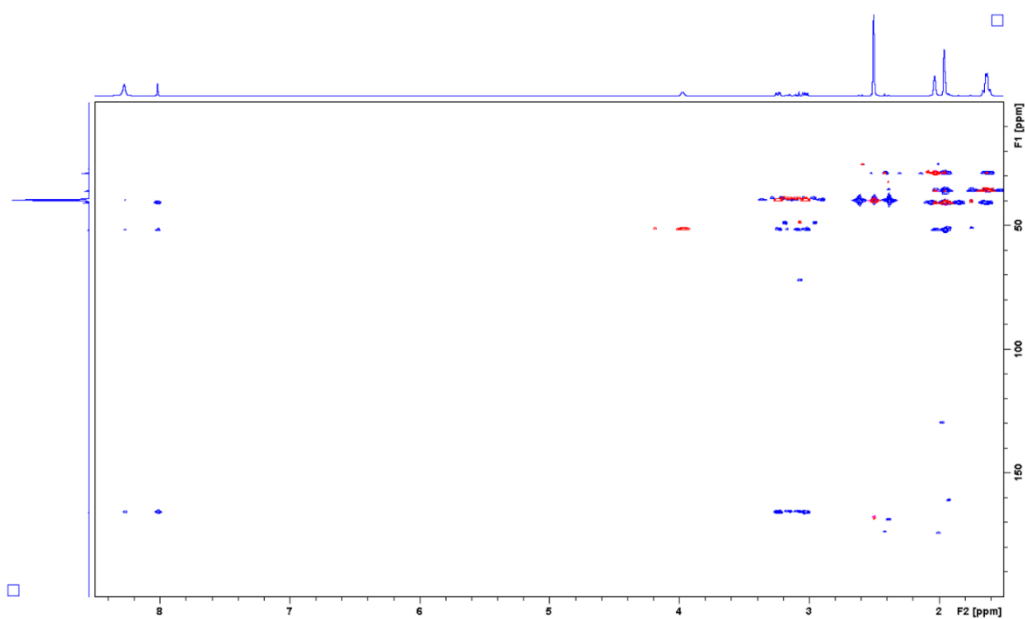


**Figure S3.3.** HMBC (blue) and HSQC (red) spectra of Ad-SS-Ad bislinker in DMSO. The concentration of Ad-SS-Ad bislinker was fixed at 0.6 mM.

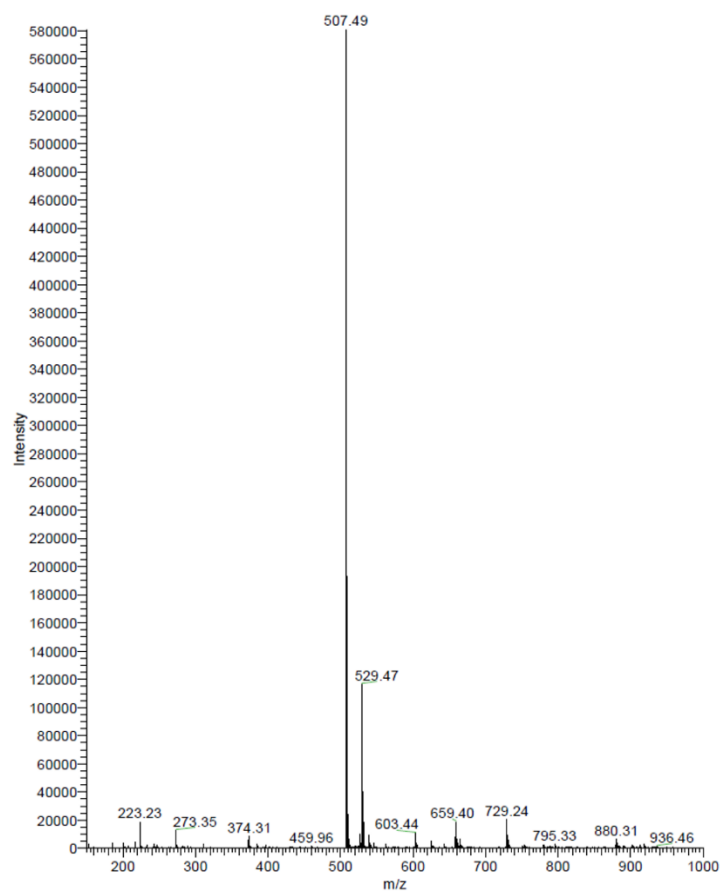


**Figure S3.4.** Mass spectrum of Ad-SS-Ad bislinker in methanol. The experimental mass is 507.49 for  $[M+H]^+$  and 529.47 for  $[M+Na]^+$ .

### Micelle characterization

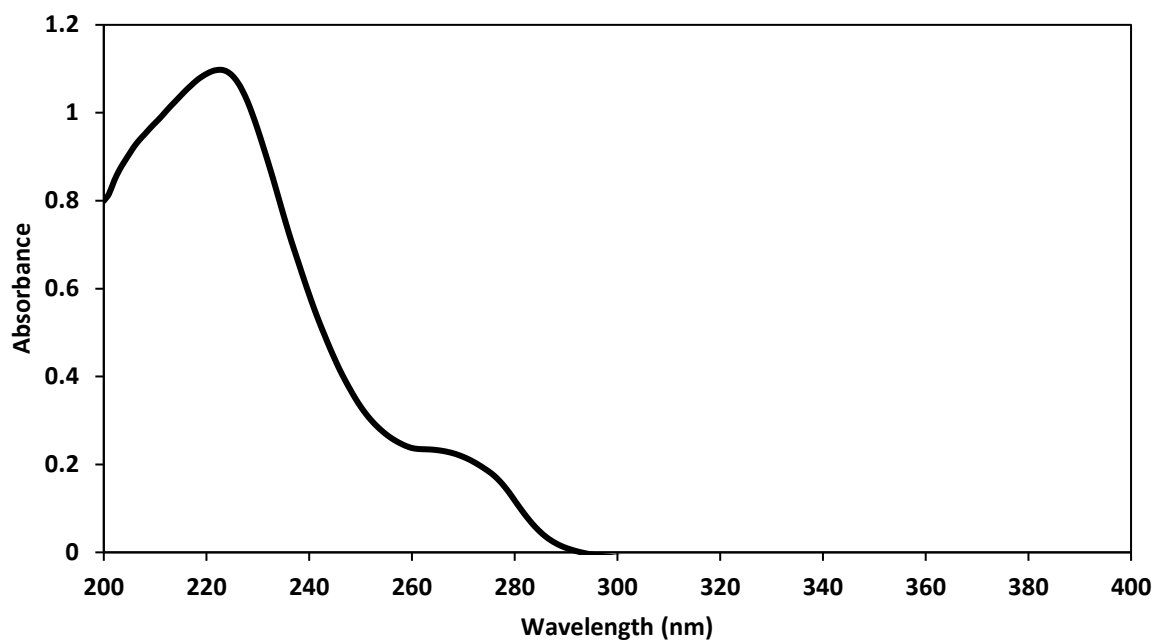


**Figure S3.5.** Absorption spectrum of europium ions,  $\beta$ CD-DPA, Ad-SS-Ad, europium ions final concentration was fixed at 0.2 mM.

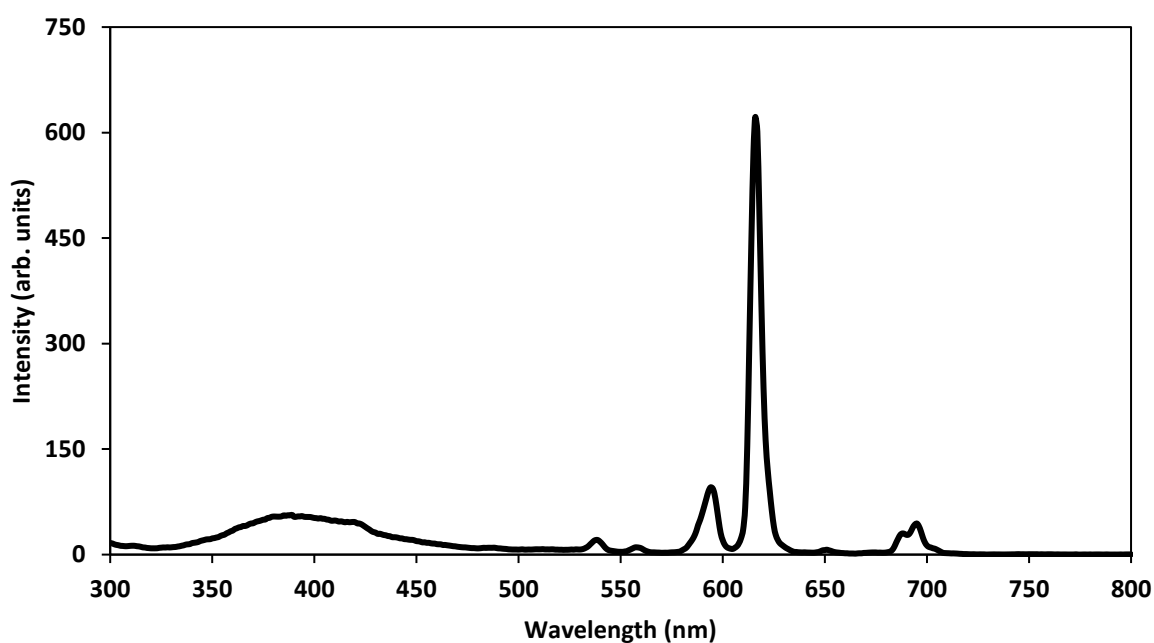


**Figure S3.6.** Emission spectrum of europium ions, in a mixture of  $\beta$ CD-DPA and Ad-SS-Ad, excitation fixed at 280 nm. Observing the europium emission (e.g. 615 nm) upon excitation of the DPA moiety (280 nm) shows the formation of the Eu-DPA complex.

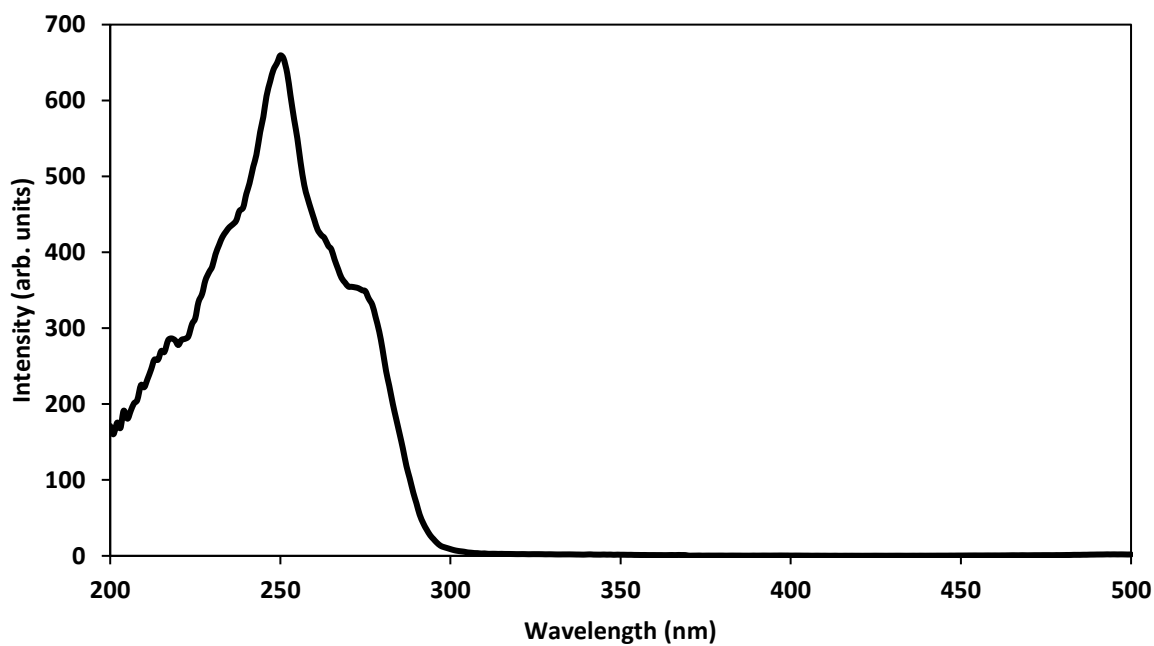


**Figure S3.7.** Excitation spectrum of europium ions, in a mixture of  $\beta$ CD-DPA and Ad-SS-Ad, emission fixed at 615 nm.

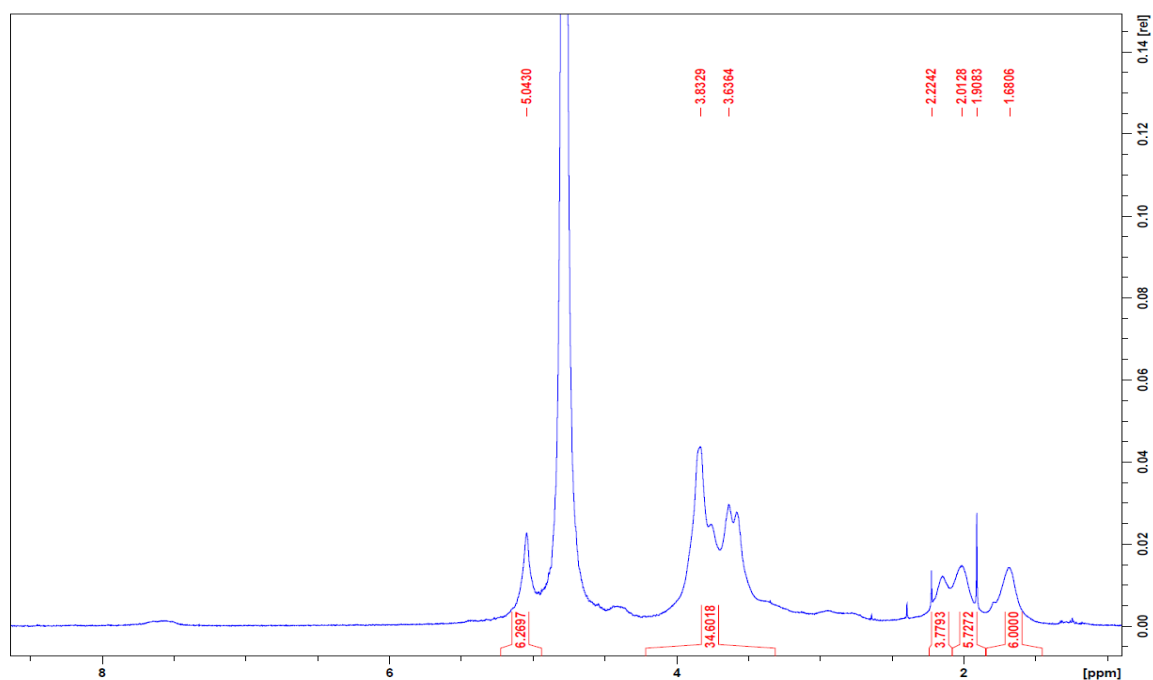


**Figure S3.8.**  $^1\text{H-NMR}$  of europium ions,  $\beta$ CD-DPA, Ad-SS-Ad in  $\text{D}_2\text{O}$ , without the addition of the block copolymer. The measurement was performed in  $\text{D}_2\text{O}$  and carbonate buffer (10 mM, pH 10), at a final europium ion concentration of 0.25 mM, with a 600 MHz, cryo-probe.

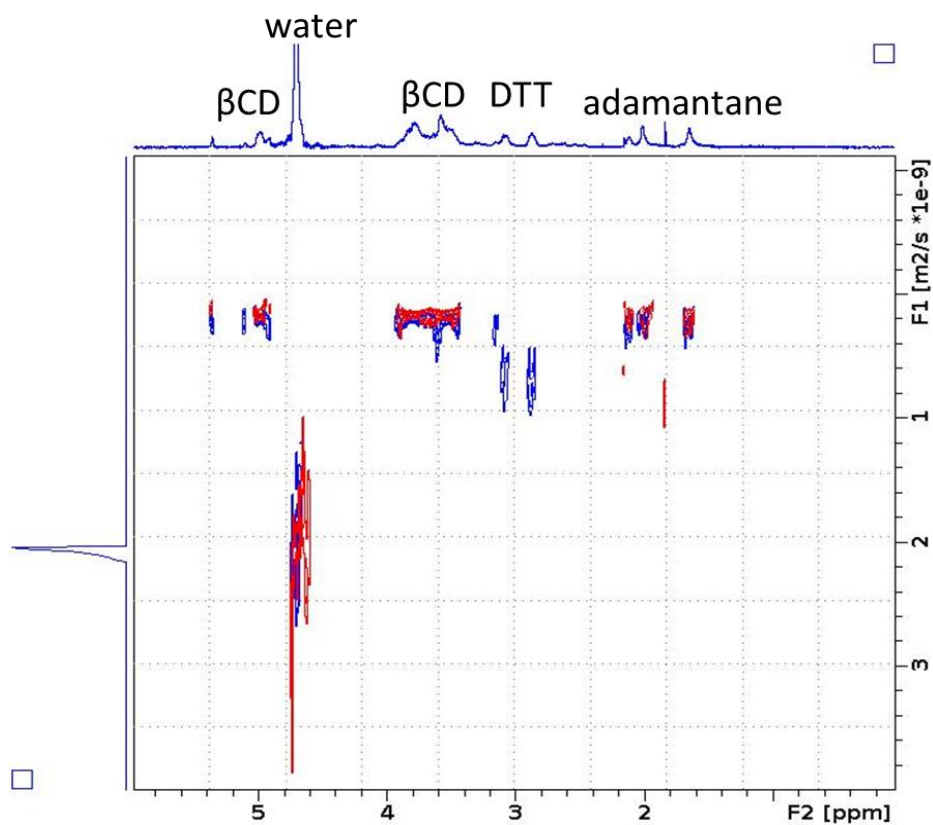


**Figure S3.9.** 500 MHz, DOSY of oligomeric and monomeric core-units. In red, a mixture of monomeric and oligomeric species was formed by mixing europium ions,  $\beta$ CD-DPA, Ad-SS-Ad bislinker. In blue, the monomeric core-units were formed by mixing europium ions,  $\beta$ CD-DPA, Ad-SS-Ad and 6 equivalents of DTT. The measurements were performed in  $D_2O$  and carbonate buffer (10 mM, pH 10), at a final europium ion concentration of 0.25 mM. In the presence of the intact crosslinker (red) a slightly lower diffusion coefficient is noted for the  $\beta$ CD-DPA and the adamantane units, indicating the formation of oligomeric species.

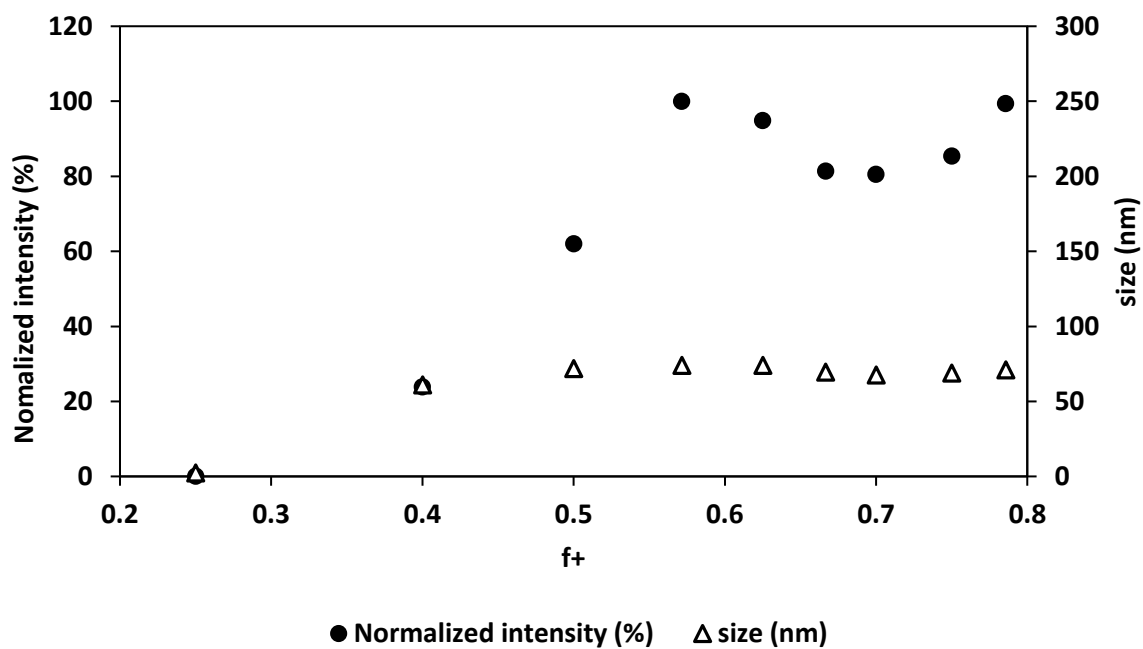


**Figure S3.10.** DLS data showing the determination of the charge fraction  $f_+$ , by titrating the block copolymer to the oligomeric core-units.  $f_+$  was calculated as the amount of positive charges over the amount of total charges. A value of  $f_+$  of 0.57 was used as neutralization optimum of these coacervate micelles.

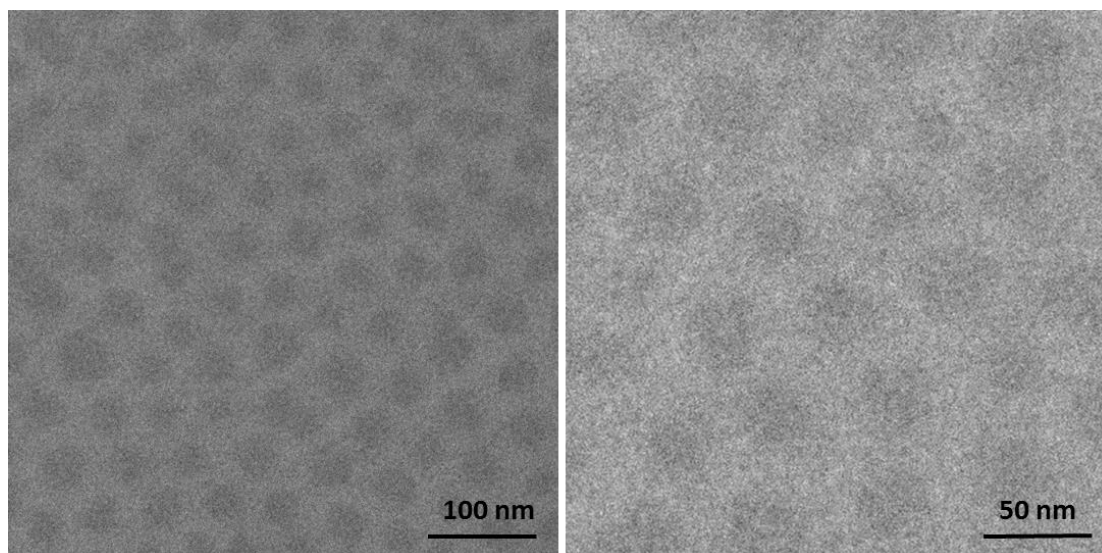


**Figure S3.11.** Cryo-TEM images of Ad-SS-Ad-based C4Ms. The diameter and the shell between micelles are around 40 nm and 20 nm, respectively. The sample was freshly prepared and checked at the DLS. The brightness and contrast of the figure on the right were adjusted by using Image-J.

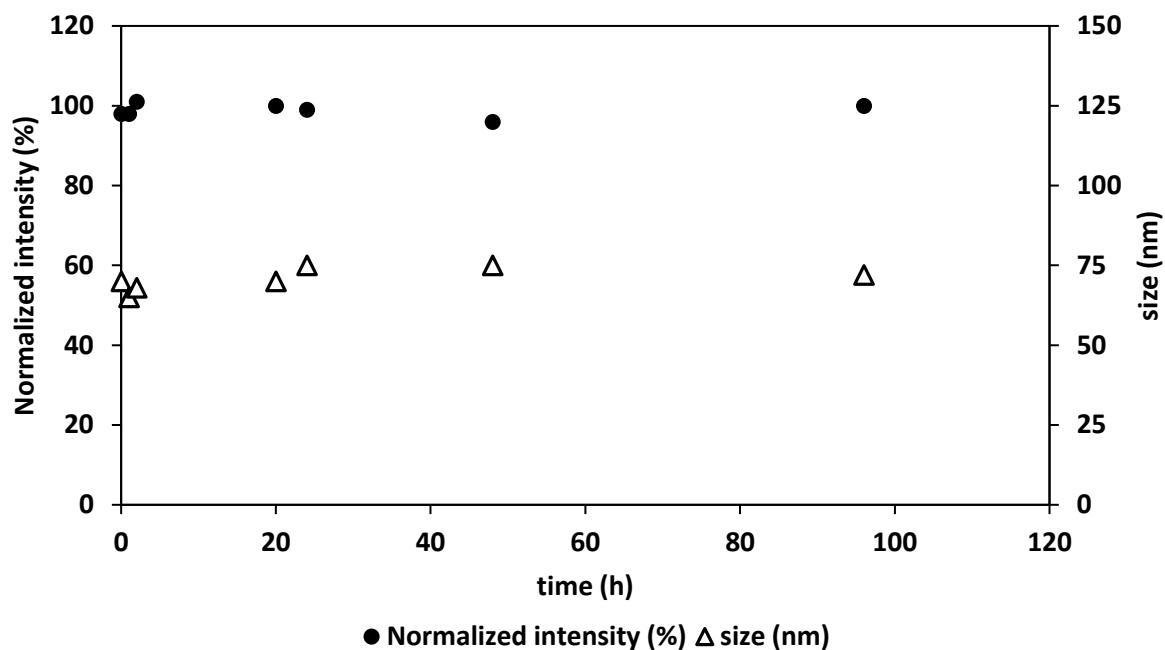


Figure S3.12. Scattered intensity and size stability in time of Ad-SS-Ad-based C4Ms, by using DLS.

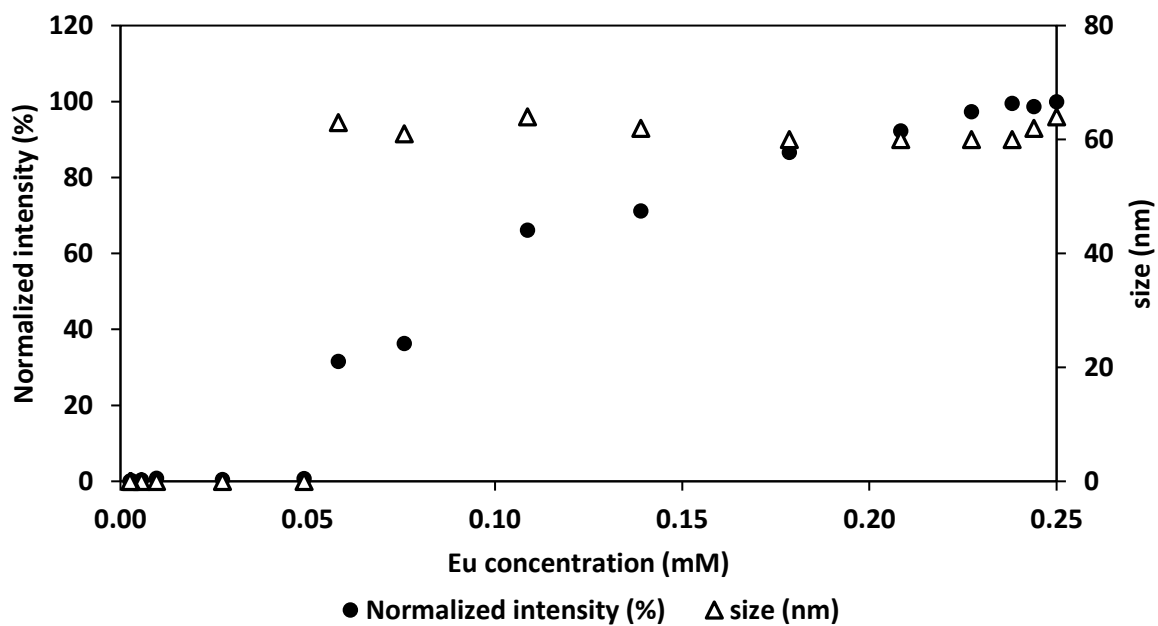
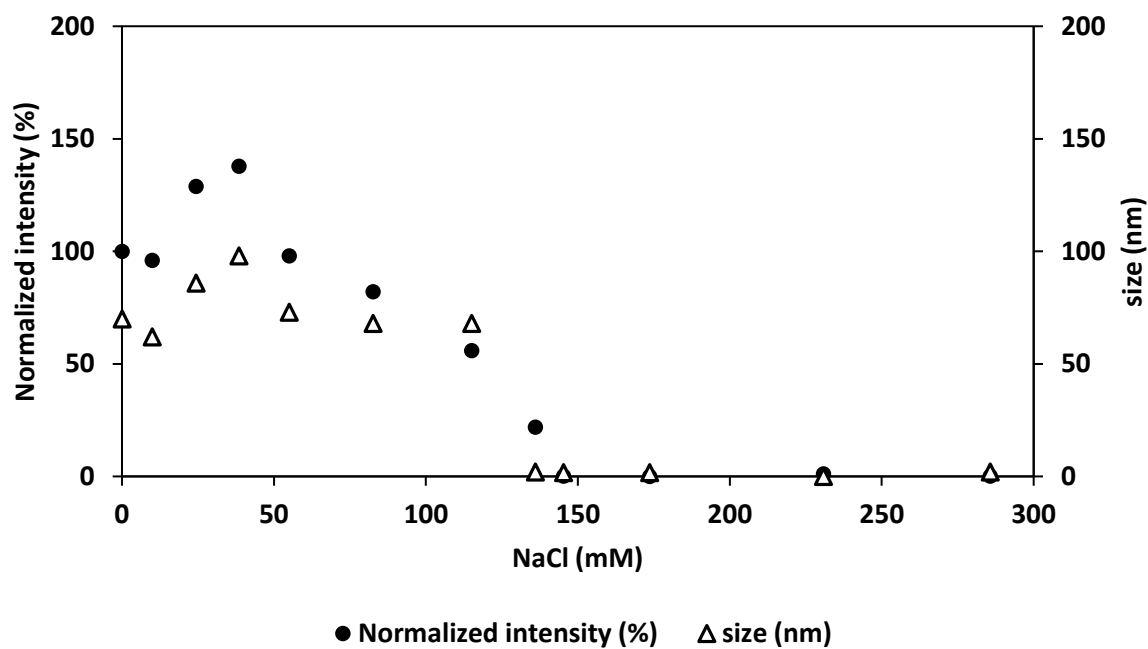
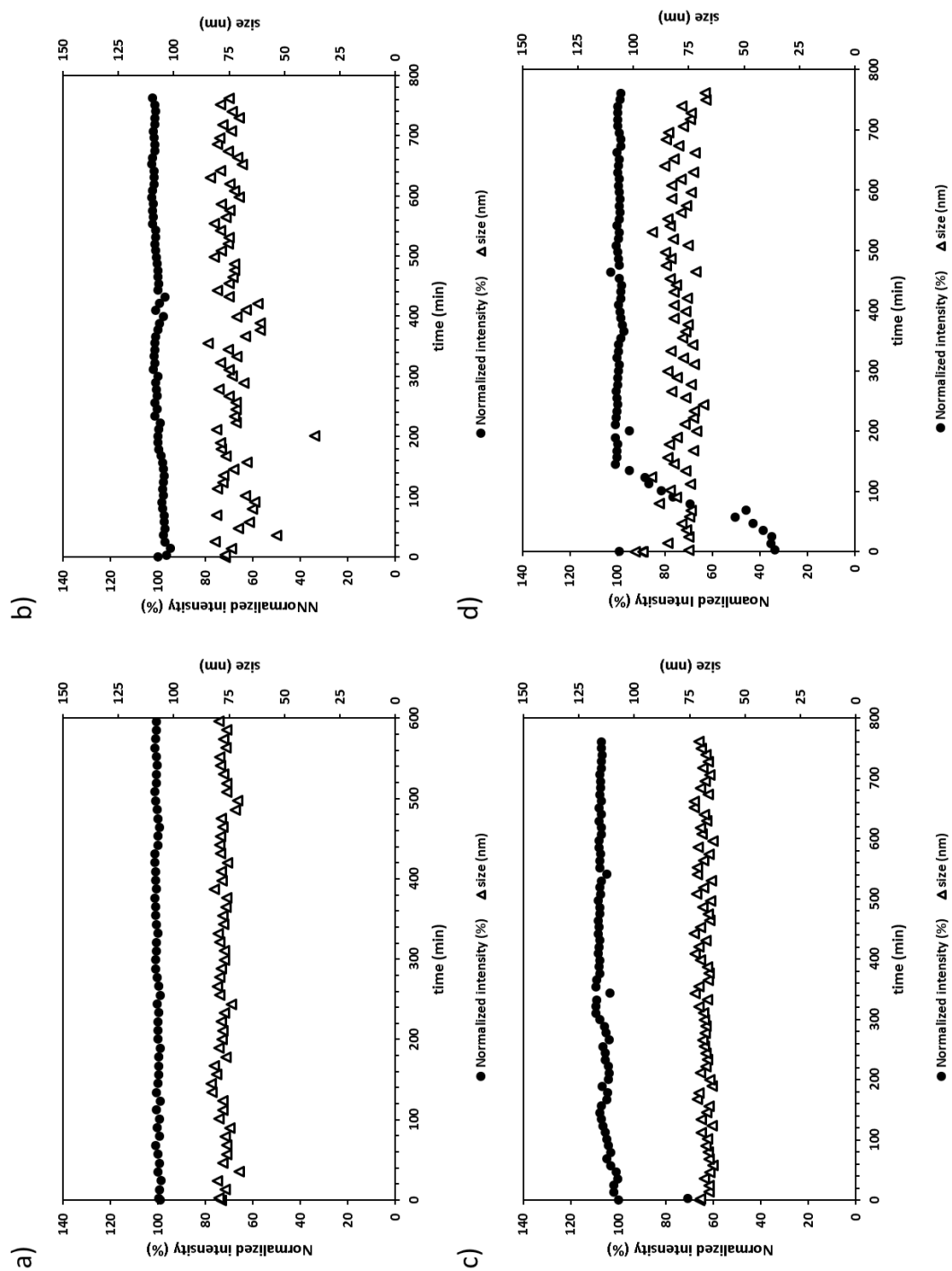


Figure S3.13. Determination of the Critical Micelle Concentration, or CMC, performed by diluting Ad-SS-Ad-based C4Ms with ultrapure water, by using the DLS.



*Figure S3.14. Determination of the Critical Salt concentration, or CSC, performed by adding increasing amounts of NaCl to Ad-SS-Ad-based C4Ms, by using the DLS.*

## Redox response studies



**Figure S3.15.** DLS data of Ad-SS-Ad-based C4Ms treated with different amounts of DTT, respectively 0 equivalent a), 1 equivalents b), 3 equivalents c) and 6 equivalents d). After the DTT addition, the scattered intensity decreases due to the disassembly of Ad-SS-Ad-based C4Ms. However, the intensity recovers in time back to the original values. This phenomenon is attributed to the reformation of Ad-SS-Ad-based C4Ms, in time.

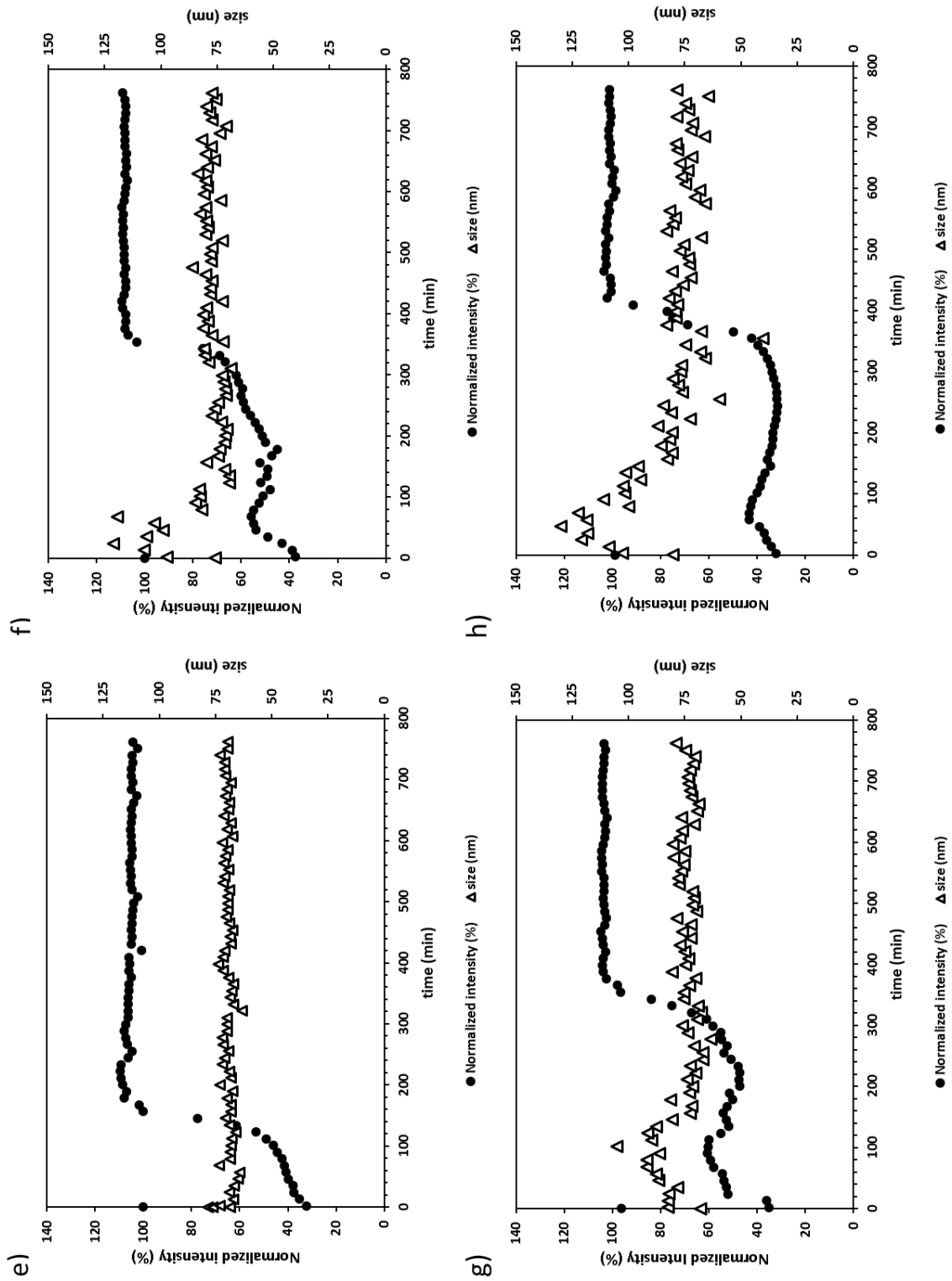


**Figure S3.16.** DLS data of Ad-SS-Ad-based C4Ms treated with different amounts of DTT, respectively 10 equivalents e), 15 equivalents f), 20 equivalents g) and 30 equivalents h). After the DTT addition, the scattered intensity decreases due to the disassembly of Ad-SS-Ad-based C4Ms. However, the intensity recovers in time back to the original values. This phenomenon is attributed to the reformation of Ad-SS-Ad-based C4Ms, in time.

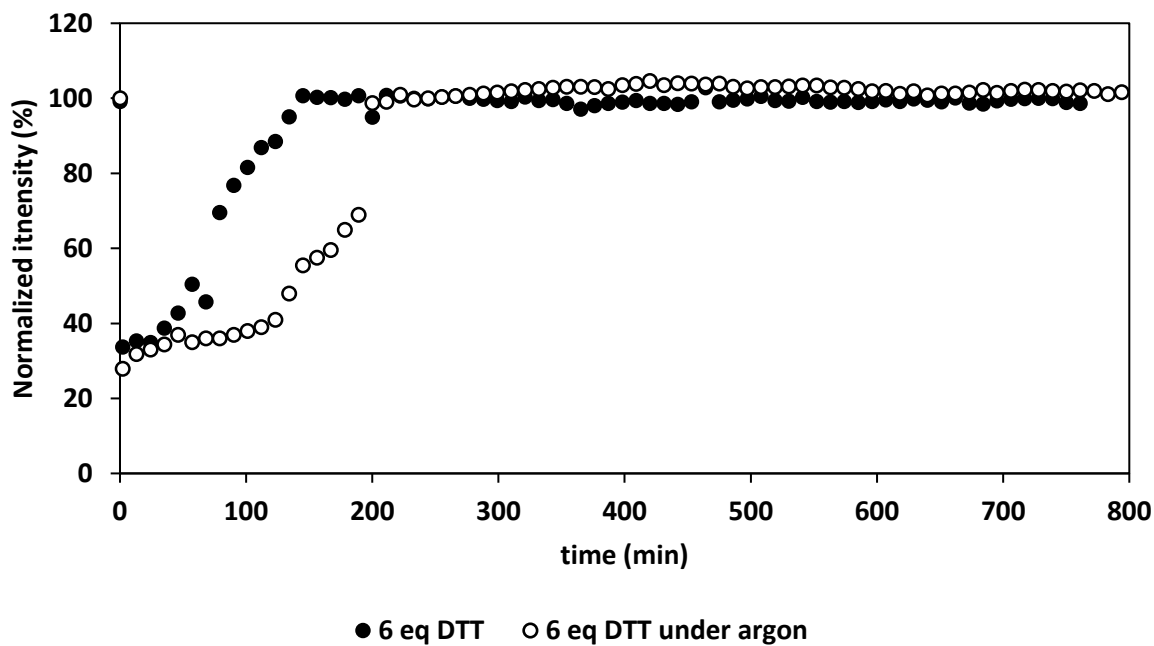


**Figure S3.17.** DLS data showing the comparison between Ad-SS-Ad-based C4Ms treated with 6 equivalents of DTT under regular conditions (black circles) and under argon flux (white circles). The presence of oxygen in the cuvette shortens the “recovery time”.

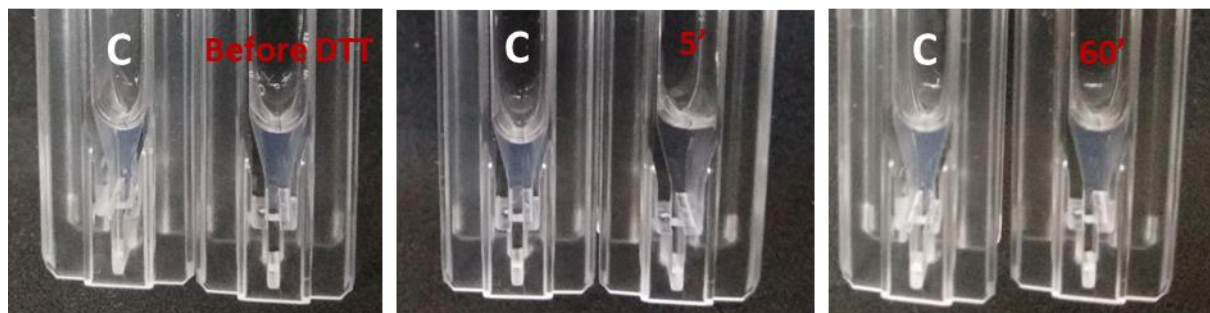


**Figure S3.18.** Picture of Ad-SS-Ad-based C4Ms, before DTT treatment (left), 5 minutes after the treatment (centre) and 1 hour after the treatment (right). The picture taken 5 minutes after the treatment shows a reduced turbidity, compared to the control. In each picture, the control is the left cuvette and marked as “C”.

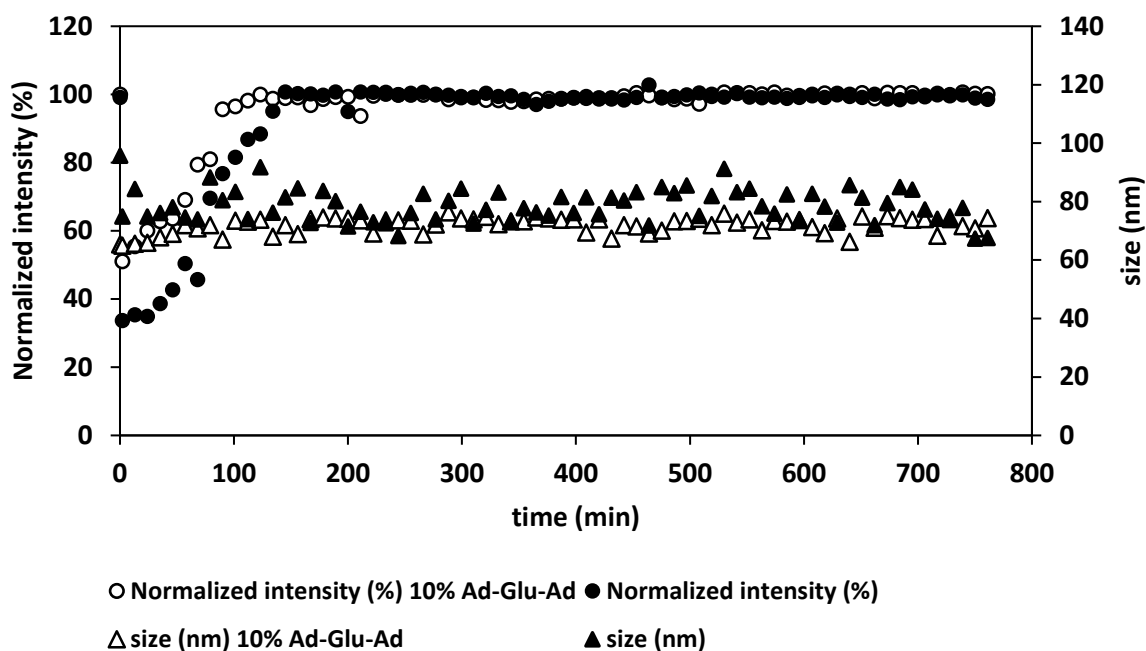


**Figure S3.19.** DLS data of Ad-SS-Ad-based C4Ms formed by mixing 10% of Ad-Glu-Ad bislinker and 90% of Ad-SS-Ad bislinker. Intensity (circles) and size (triangles) of the micelle with 10% Ad-Glu-Ad were compared with Ad-SS-Ad-C4Ms micelles, after the treatment with 6 equivalents of DTT. After the DTT addition, the intensity drops 40%. The Ad-Glu-Ad bislinker was investigated in our previous research as a bridging ligand between monomeric units. (Facciotti, C., et al. (2018), *Soft Matter* 14(47): 9542-9549).

Controls

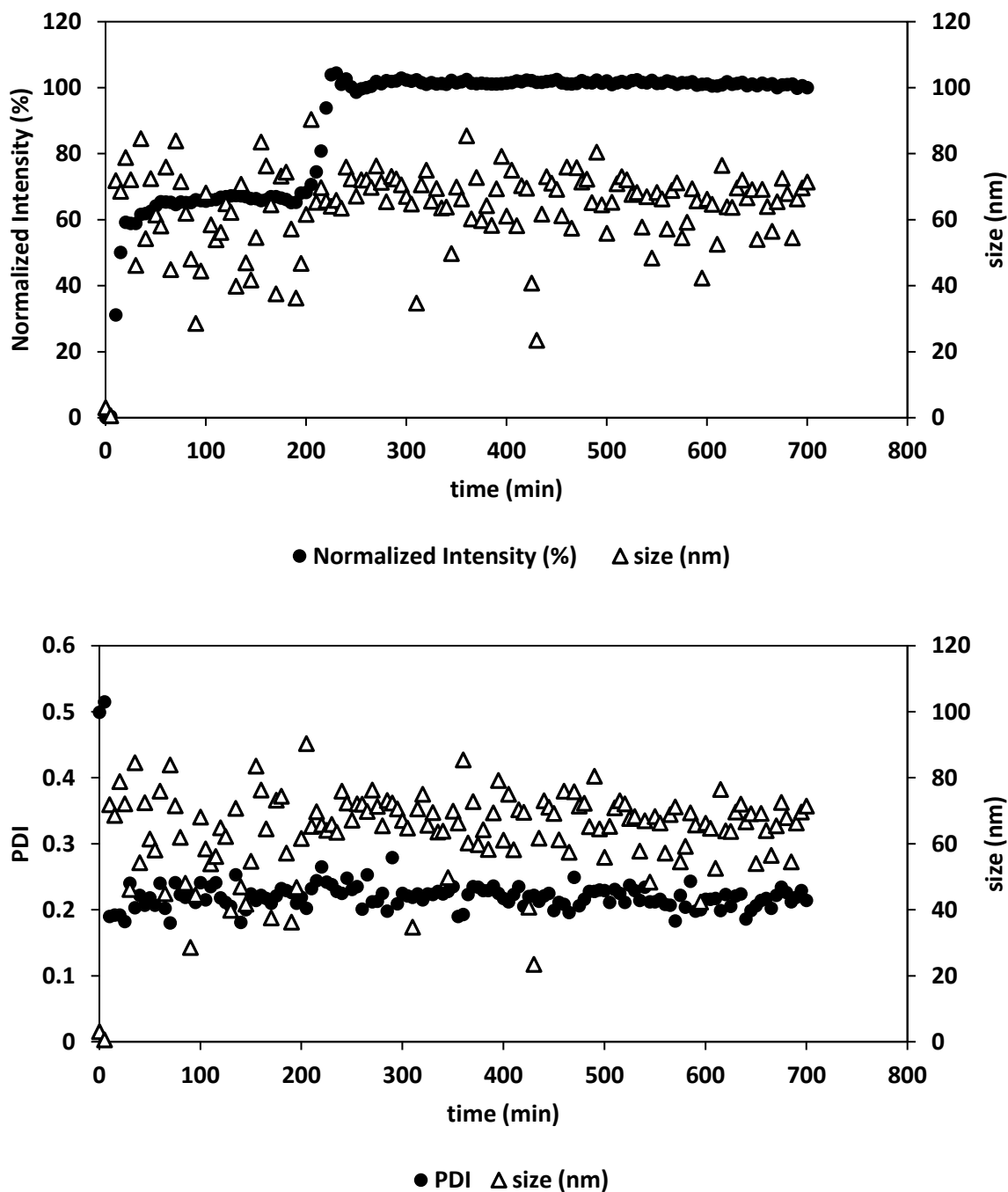


**Figure S3.20.** DLS data of the control of Ad-SS-Ad-based C4Ms formation starting from the thiolate form. In this control 6 equivalents of DTT were added directly to the core-units, before the addition of block copolymer (see the right side of scheme 2 in the main text). In the figure above the variation in intensity and size is plotted against the time, while in the figure below, the variation in size and PDI is plotted against time.

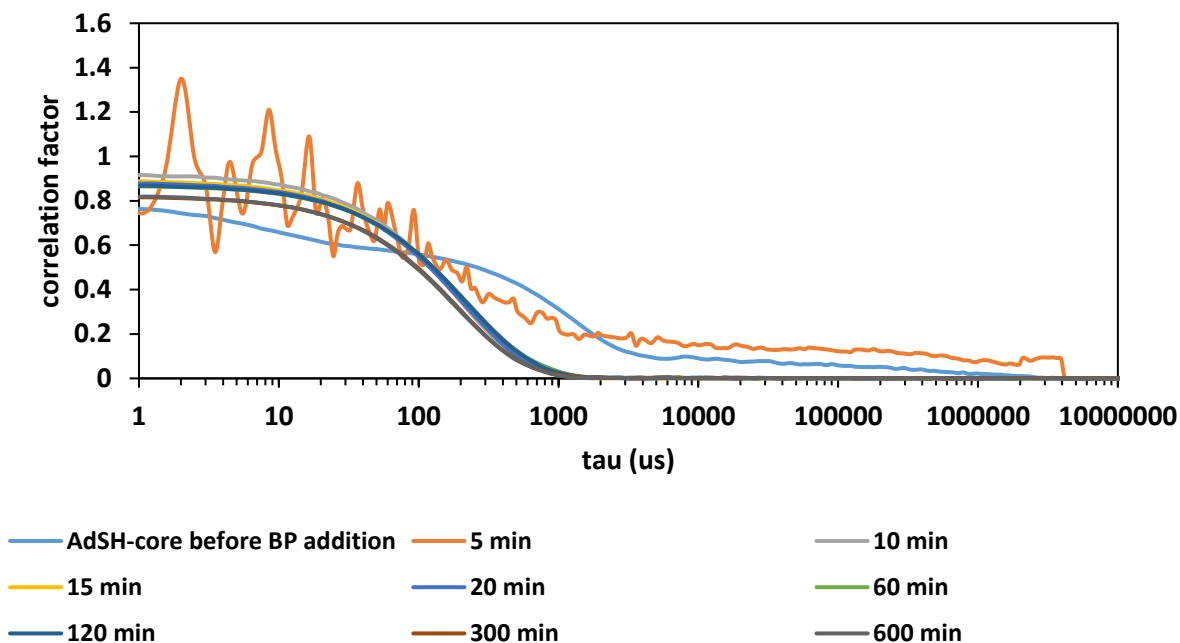


**Figure S3.21.** DLS data of the control of Ad-SS-Ad-based C4Ms formation starting from monomeric units. In this control, 6 equivalents of DTT were added directly to the oligomeric core-units, before the addition of block copolymer. The correlogram was monitored at different times.

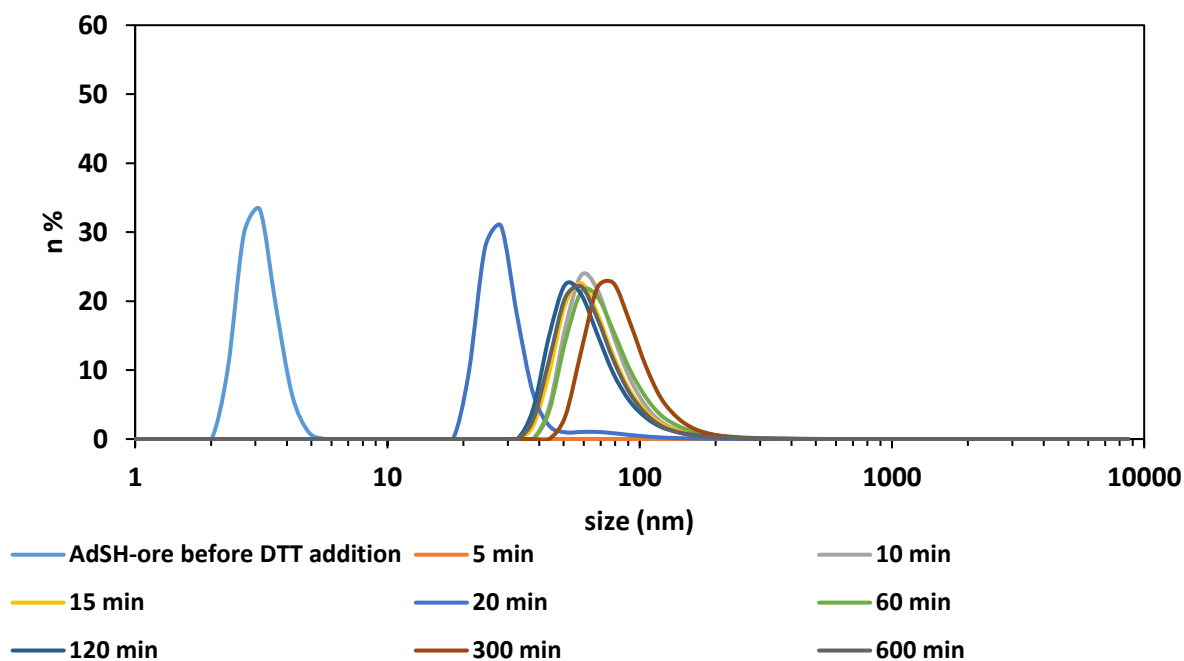


**Figure S3.22.** DLS data of the control of Ad-SS-Ad-based C4Ms formation starting from monomeric units. In this control 6 equivalents of DTT were added directly to the oligomeric core-units, before the addition of block copolymer. The size distribution was monitored at different times.

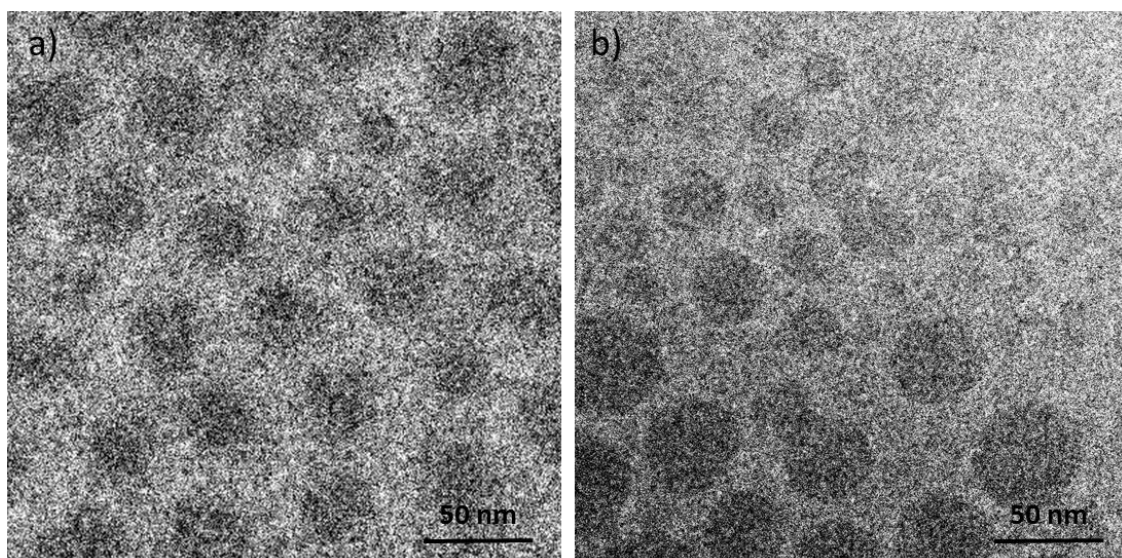


**Figure S3.23.** Cryo-TEM images of Ad-SS-Ad-based C4Ms. Figure a) represents the directly formed Ad-SS-Ad-based C4Ms, while figure b) represent the re-ssembled micelles. The Cryo-TEM of b) was performed after treating the micelle solution with 6 equivalents of DTT and after 2 hours waiting step. The brightness and contrast of both pictures were adjusted by using image-J.

**Table S3.1.** Polydispersity index, size (nm) and intensity (%) values of Ad-SS-Ad-based C4Ms formation starting from the thiolate form in time, by DLS.

<i>Time (min)</i>	<i>Size (nm)</i>	<i>Normalized intensity (%)</i>	<i>PDI</i>
0	na	0	na
5	na	0	na
10	72	31	na
15	69	50	0.19
20	79	59	0.19
60	76	65	0.24
120	65	66	0.22
300	85	101	0.19
600	66	100	0.22

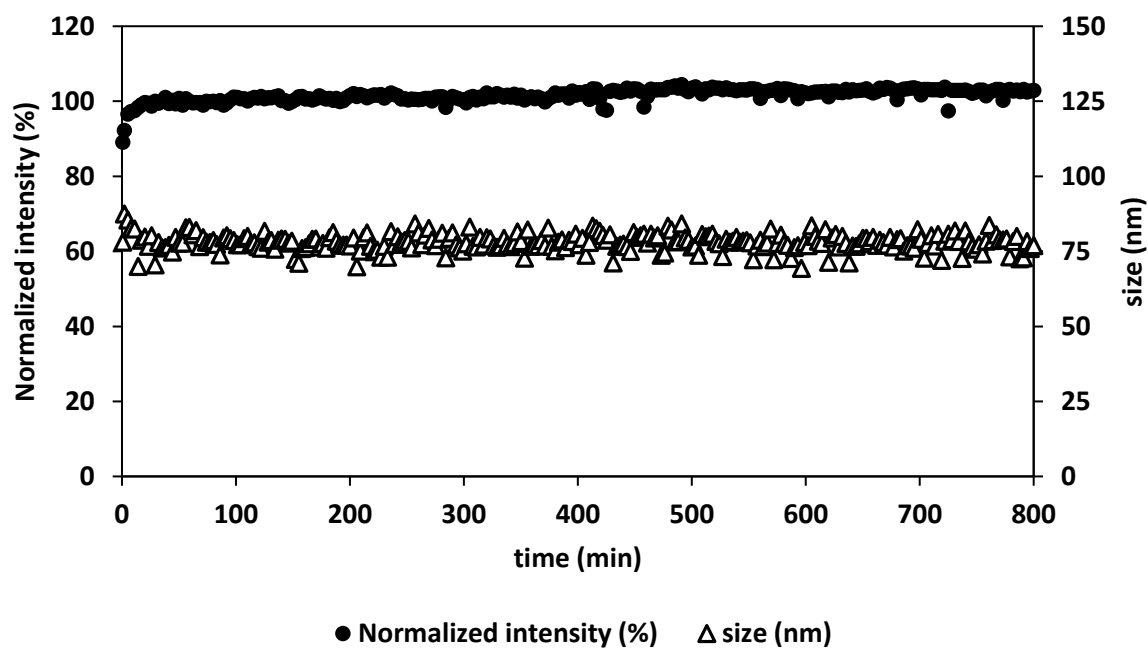


*Figure S3.24. DLS data of Ad-SS-Ad-based C4Ms formation followed in time. The variation of intensity and size is plotted over time, after the micelle formation.*

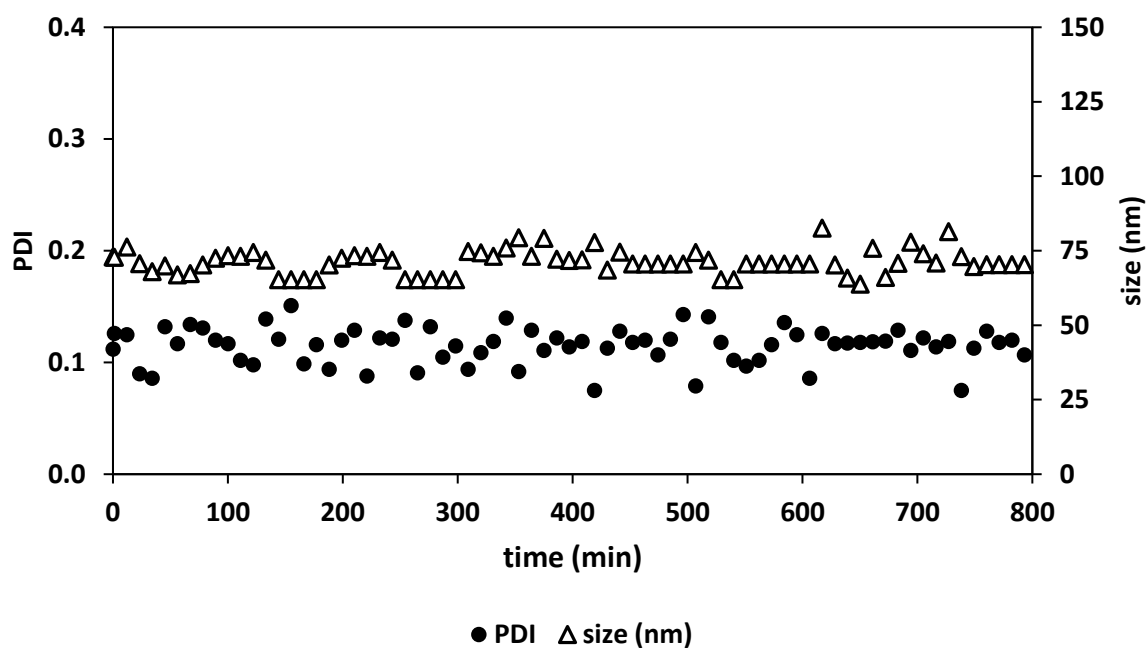
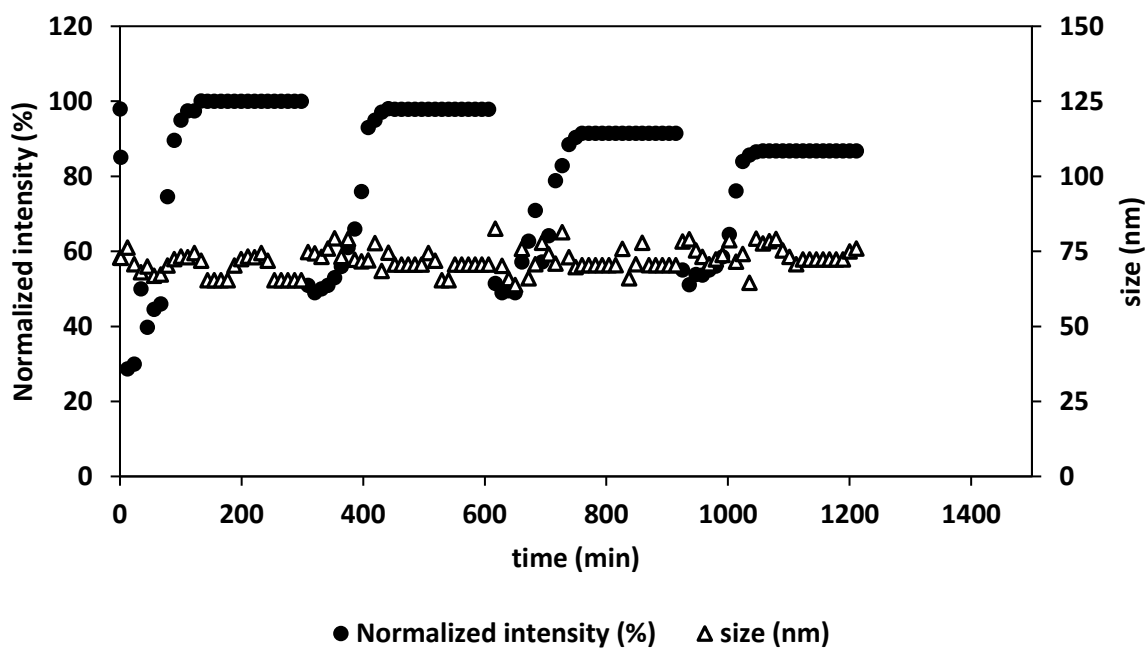


**Figure S3.25.** DLS data of Ad-SS-Ad-based C4Ms reversibility cycles. In the reversibility cycle, Ad-SS-Ad-based C4Ms were first formed and then, repeatedly, treated with 6 equivalents of DTT. Each DTT addition was done after the Ad-SS-Ad-based C4Ms were reassembled and it is called “one cycle”. Intensity, size and monodispersity were measured every 10 minutes with the DLS. On the top, the intensity and the size are plotted against the time. On the bottom, the size and the PDI are plotted against the time.

*Encapsulation studies*

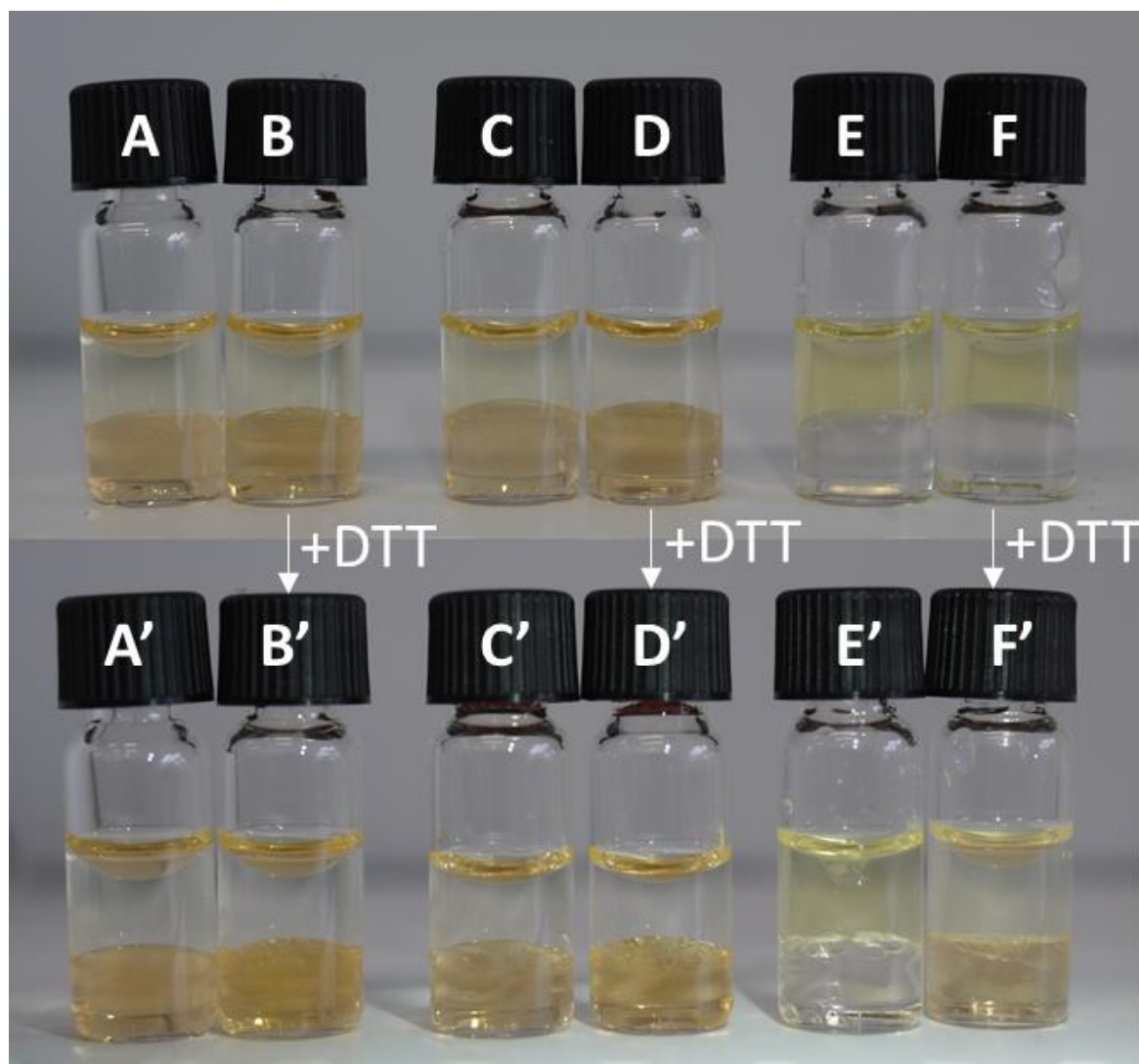


**Figure S3.26.** Pictures of the encapsulation and release study performed in a water/DCM biphasic system. *A* and *B* represent the methyl red, *C* and *D* the Methyl Red complexed with  $\beta$ CD-DPA and *E* and *F* the Methyl Red encapsulated inside Ad-SSAd-based C4Ms. 30 eq. of DTT were added to the vials *B*, *D* and *F*. The water phase includes a carbonate buffer at pH 10.

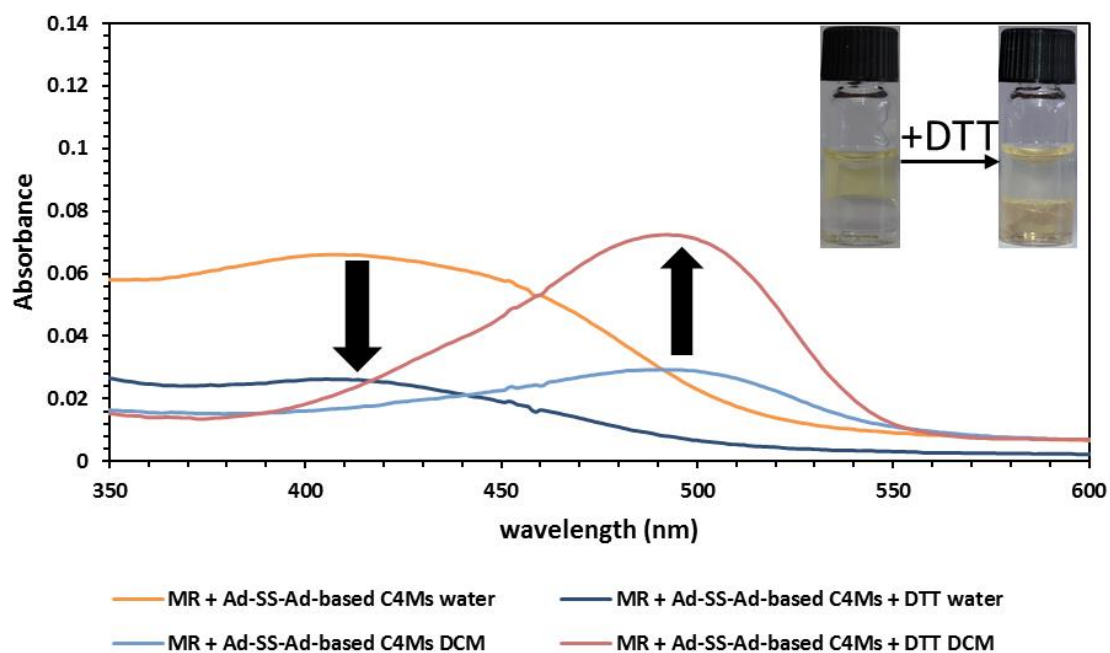


**Figure S3.27.** Absorption spectra of the Methyl Red (MR) encapsulated inside Ad-SS-Ad-based C4Ms, in the water and in the DCM phases, with and without DTT treatment.

**Table S3.2.** Intensity of the Ad-SS-Ad-based C4Ms controls

Name	I (Mcps)
<i>Eu</i>	<i>na</i>
<i>βCD-DPA</i>	<i>na</i>
<i>Ad-SS-Ad</i>	<i>na</i>
<i>BP</i>	<i>na</i>
<i>Eu + βCD-DPA</i>	<i>na</i>
<i>Eu + Ad-SS-Ad</i>	<i>na</i>
<i>Eu + BP</i>	<i>na</i>
<i>Eu + Ad-SS-Ad + BP</i>	13.05
<i>Eu + βCD-DPA + BP</i>	<i>na</i>
<i>Ad-SS-Ad + BP</i>	12.19
<i>Ad-SS-Ad + βCD-DPA</i>	<i>na</i>
<i>βCD-DPA + BP</i>	<i>na</i>
<i>Eu + βCD-DPA + Ad-SS-Ad</i>	<i>na</i>
<i>Ad-SS-Ad-based C4Ms</i>	160

### 3.6. REFERENCES

1. Zhang, Q., Ko, N.R., and Oh, J.K., *Recent advances in stimuli-responsive degradable block copolymer micelles: synthesis and controlled drug delivery applications*. Chem. Commun. (Camb), 2012. **48**(61): p. 7542-7552.
2. Baek, C., Ha, T.-L., Kim, E., Jeong, S., Lee, S., et al., *Bioreducible Micelles Self-Assembled from Poly(ethylene glycol)-Cholesteryl Conjugate As a Drug Delivery Platform*. Polymers, 2015. **7**(11): p. 2245-2258.
3. Ding, J., Chen, L., Xiao, C., Chen, L., Zhuang, X., et al., *Noncovalent interaction-assisted polymeric micelles for controlled drug delivery*. Chem. Commun. (Camb), 2014. **50**(77): p. 11274-11290.
4. Biswas, S., Kumari, P., Lakhani, P.M., and Ghosh, B., *Recent advances in polymeric micelles for anti-cancer drug delivery*. Eur. J. Pharm. Sci., 2016. **83**: p. 184-202.
5. Bae, Y., Fukushima, S., Harada, A., and Kataoka, K., *Design of Environment-Sensitive Supramolecular Assemblies for Intracellular Drug Delivery: Polymeric Micelles that are Responsive to Intracellular pH Change*. Angew. Chem. Int. Ed. Engl., 2003. **115**(38): p. 4788-4791.
6. Katayose, S. and Kataoka, K., *Water-Soluble Polyion Complex Associates of DNA and Poly(ethylene glycol)-Poly(L-lysine) Block Copolymer*. Bioconjugate. Chem., 1997. **8**: p. 702-707.
7. Cabral, H., Miyata, K., Osada, K., and Kataoka, K., *Block Copolymer Micelles in Nanomedicine Applications*. Chem Rev, 2018. **118**(14): p. 6844-6892.
8. Mukerabigwi, J.F., Ge, Z., and Kataoka, K., *Therapeutic Nanoreactors as In Vivo Nanoplatforams for Cancer Therapy*. Chemistry, 2018. **24**(59): p. 15706-15724.
9. Takae, S., Miyata, K., Oba, M., Ishii, T., Nishiyama, N., et al., *PEG-Detachable Polyplex Micelles Based on Disulfide-Linked Block Cationomers as Bioresponsive Nonviral Gene Vectors*. J. Am. Chem. Soc., 2008. **130**: p. 6001-6009.
10. Ge, Z. and Liu, S., *Functional block copolymer assemblies responsive to tumor and intracellular microenvironments for site-specific drug delivery and enhanced imaging performance*. Chem. Soc. Rev., 2013. **42**(17): p. 7289-7325.
11. Li, D., Bu, Y., Zhang, L., Wang, X., Yang, Y., et al., *Facile Construction of pH- and Redox-Responsive Micelles from a Biodegradable Poly(beta-hydroxyl amine) for Drug Delivery*. Biomacromolecules, 2016. **17**(1): p. 291-300.
12. Voets, I.K., de Keizer, A., and Cohen Stuart, M.A., *Complex coacervate core micelles*. Adv. Colloid Interface Sci., 2009. **147-148**: p. 300-318.
13. Zhu, C., Zheng, M., Meng, F., Mickler, F.M., Ruthardt, N., et al., *Reversibly shielded DNA polyplexes based on bioreducible PDMAEMA-SS-PEG-SS-PDMAEMA triblock copolymers mediate markedly enhanced nonviral gene transfection*. Biomacromolecules, 2012. **13**(3): p. 769-778.
14. Wang, J., Velders, A.H., Gianolio, E., Aime, S., Vergeldt, F.J., et al., *Controlled mixing of lanthanide(III) ions in coacervate core micelles*. Chem. Commun. (Camb), 2013. **49**(36): p. 3736-3738.
15. Uchida, S. and Kataoka, K., *Design concepts of polyplex micelles for in vivo therapeutic delivery of plasmid DNA and messenger RNA*. J. Biomed. Mater. Res. A, 2019. **107**(5): p. 978-990.
16. Wang, J., de Keizer, A., Fokkink, R., Yan, Y., Cohen Stuart, M.A., et al., *Complex coacervate core micelles from iron-based coordination polymers*. J. Phys. Chem. B, 2010. **114**(25): p. 8313-8319.
17. Wang, J., Groeneveld, A., Oikonomou, M., Prusova, A., Van As, H., et al., *Revealing and tuning the core, structure, properties and function of polymer micelles with lanthanide-coordination complexes*. Soft Matter, 2016. **12**(1): p. 99-105.
18. Yang, L., Ding, Y., Yang, Y., Yan, Y., Huang, J., et al., *Fluorescence enhancement by microphase separation-induced chain extension of Eu<sup>3+</sup> coordination polymers: phenomenon and analysis*. Soft Matter, 2011. **7**(6): p. 2720-2724.

19. Wang, J., Cohen Stuart, M.A., Marcelis, A.T.M., Colomb-Delsuc, M., Otto, S., et al., *Stable Polymer Micelles Formed by Metal Coordination*. *Macromolecules*, 2012. **45**(17): p. 7179-7185.
20. Ten Hove, J.B., Wang, J., van Leeuwen, F.W.B., and Velders, A.H., *Dendrimer-encapsulated nanoparticle-core micelles as a modular strategy for particle-in-a-box-in-a-box nanostructures*. *Nanoscale*, 2017. **9**(47): p. 18619-18623.
21. Wang, J., Voets, I.K., Fokkink, R., van der Gucht, J., and Velders, A.H., *Controlling the number of dendrimers in dendrimicelle nanoconjugates from 1 to more than 100*. *Soft Matter*, 2014. **10**(37): p. 7337-7345.
22. Ten Hove, J.B., van Oosterom, M.N., van Leeuwen, F.W.B., and Velders, A.H., *Nanoparticles reveal Extreme Size-Sorting and Morphologies in Complex Coacervate Superstructures*. *Sci. Rep.*, 2018. **8**(1): p. 13820-13827.
23. Facciotti, C., Saggiomo, V., Bunschoten, A., Fokkink, R., Hove, J.B.T., et al., *Cyclodextrin-based complex coacervate core micelles with tuneable supramolecular host-guest, metal-to-ligand and charge interactions*. *Soft Matter*, 2018. **14**(47): p. 9542-9549.
24. van der Kooij, H.M., Spruijt, E., Voets, I.K., Fokkink, R., Cohen Stuart, M.A., et al., *On the stability and morphology of complex coacervate core micelles: from spherical to wormlike micelles*. *Langmuir*, 2012. **28**(40): p. 14180-14191.
25. Voets, I.K., Moll, P.M., Aqil, A., me, C.J., Detrembleur, C., et al., *Temperature Responsive Complex Coacervate Core Micelles With a PEO and PNIPAAm Corona*. *J. Phys. Chem. B*, 2008. **112**: p. 10833-10840.
26. Zheng, N., Song, Z., Liu, Y., Zhang, R., Zhang, R., et al., *Redox-responsive, reversibly-crosslinked thiolated cationic helical polypeptides for efficient siRNA encapsulation and delivery*. *J. Control Release*, 2015. **205**: p. 231-239.
27. Wang, Y.C., Wang, F., Sun, T.M., and Wang, J., *Redox-responsive nanoparticles from the single disulfide bond-bridged block copolymer as drug carriers for overcoming multidrug resistance in cancer cells*. *Bioconjug. Chem.*, 2011. **22**(10): p. 1939-1945.
28. Huo, M., Yuan, J., Tao, L., and Wei, Y., *Redox-responsive polymers for drug delivery: from molecular design to applications*. *Polym. Chem.*, 2014. **5**(5): p. 1519-1528.
29. Giustarini, D., Galvagni, F., Tesei, A., Farolfi, A., Zanoni, M., et al., *Glutathione, glutathione disulfide, and S-glutathionylated proteins in cell cultures*. *Free Radic. Biol. Med.*, 2015. **89**: p. 972-981.
30. Dong, W.-F., Kishimura, A., Anraku, Y., Chuanoi, S., and Kataoka, K., *Monodispersed Polymeric Nanocapsules: Spontaneous Evolution and Morphology Transition from Reducible Hetero-PEG PICmicelles by Controlled Degradation*. *J. Am. Chem. Soc.*, 2009. **131**: p. 3804-3805.
31. Zhang, J., Fang, X., Li, Z., Chan, H.F., Lin, Z., et al., *Redox-sensitive micelles composed of disulfide-linked Pluronic-linoleic acid for enhanced anticancer efficiency of brusatol*. *Int. J. Nanomedicine*, 2018. **13**: p. 939-956.
32. Wang, W., Sun, H., Meng, F., Ma, S., Liu, H., et al., *Precise control of intracellular drug release and anti-tumor activity of biodegradable micellar drugs via reduction-sensitive shell-shedding*. *Soft Matter*, 2012. **8**(14): p. 3949-3956.
33. Wang, H., Tang, L., Tu, C., Song, Z., Yin, Q., et al., *Redox-responsive, core-cross-linked micelles capable of on-demand, concurrent drug release and structure disassembly*. *Biomacromolecules*, 2013. **14**(10): p. 3706-3712.
34. Bhattacharya, S., Ganivada, M.N., Dinda, H., Das Sarma, J., and Shunmugam, R., *Biodegradable Copolymer for Stimuli-Responsive Sustained Release of Doxorubicin*. *ACS Omega*, 2016. **1**(1): p. 108-117.
35. Hsu, S.-H., Yilmaz, M.D., Blum, C., Subramaniam, V., Reinhoudt, D.N., et al., *Expression of Sensitized Eu<sup>3+</sup> Luminescence at a Multivalent Interface*. *J. AM. CHEM. SOC.*, 2009. **131**: p. 12567-12569.
36. Oikonomou, M., Wang, J., Carvalho, R.R., and Velders, A.H., *Ternary supramolecular quantum-dot network flocculation for selective lectin detection*. *Nano Research*, 2016. **9**(7): p. 1904-1912.
37. Dorokhin, D., Hsu, S.-H., Tomczak, N., Reinhoudt, D.N., Huskens, J., et al., *Fabrication and Luminescence of Designer Surface Patterns with Cyclodextrin Functionalized Quantum Dots via Multivalent Supramolecular Coupling*. *ACS Nano*, 2010. **4**(1): p. 137-142.

38. Dorokhin, D., Hsu, S.H., Tomczak, N., Blum, C., Subramaniam, V., et al., *Visualizing resonance energy transfer in supramolecular surface patterns of beta-CD-functionalized quantum dot hosts and organic dye guests by fluorescence lifetime imaging*. *Small*, 2010. **6**(24): p. 2870-2876.
39. Rood, M.T.M., Spa, S.J., Welling, M.M., ten Hove, J.B., van Willigen, D.M., et al., *Obtaining control of cell surface functionalizations via Pre-targeting and Supramolecular host guest interactions*. *Sci. Rep.*, 2017. **7**: p. 39908.
40. Biesalski, M., Johannsmann, D., and Ruhe, J., *Electrolyte-induced collapse of a polyelectrolyte brush*. *J. Chem. Phys.*, 2004. **120**(18): p. 8807-8814.
41. Vrettos, E.I., Sayyad, N., Mavrogiannaki, E.M., Stylos, E., Kostagianni, A.D., et al., *Unveiling and tackling guanidinium peptide coupling reagent side reactions towards the development of peptide-drug conjugates*. *RSC Adv.*, 2017. **7**(80): p. 50519-50526.
42. Chamas Zel, A., Guo, X., Canet, J.L., Gautier, A., Boyer, D., et al., *Clicked dipicolinic antennae for lanthanide luminescent probes*. *Dalton Trans.*, 2010. **39**(30): p. 7091-7097.
43. Wang, J., de Kool, R.H., and Velders, A.H., *Lanthanide-Dipicolinic Acid Coordination Driven Micelles with Enhanced Stability and Tunable Function*. *Langmuir*, 2015. **31**(44): p. 12251-12259.
44. Xu, L., Feng, L., Han, Y., Jing, Y., Xian, Z., et al., *Supramolecular self-assembly enhanced europium(III) luminescence under visible light*. *Soft Matter*, 2014. **10**(26): p. 4686-4693.
45. Harada, A., Takashima, Y., and Nakahata, M., *Supramolecular polymeric materials via cyclodextrin-guest interactions*. *Acc. Chem. Res.*, 2014. **47**(7): p. 2128-2140.
46. Takashima, Y. and Harada, A., *Functioning via host-guest interactions*. *J. Incl. Phenom. Macrocycl. Chem.*, 2017. **87**(3-4): p. 313-330.
47. Yuan, Z., Wang, J., Wang, Y., Zhong, Y., Zhang, X., et al., *Redox-Controlled Voltage Responsive Micelles Assembled by Noncovalently Grafted Polymers for Controlled Drug Release*. *Macromolecules*, 2019. **52**(4): p. 1400-1407.
48. Hu, Q.D., Tang, G.P., and Chu, P.K., *Cyclodextrin-based host-guest supramolecular nanoparticles for delivery: from design to applications*. *Acc. Chem. Res.*, 2014. **47**(7): p. 2017-2025.
49. Zen, J.-M., Kumar, A.S., Chen, J.-C., Jayachithra, K., Balamurugan, K., et al., *Electrocatalytic cyclization of dithiothreitol on a chemically modified electrode by analogy with protein action*. *The Analyst*, 2001. **126**(8): p. 1409-1413.
50. Rasmussen, B., Sorensen, A., Gotfredsen, H., and Pittelkow, M., *Dynamic combinatorial chemistry with diselenides and disulfides in water*. *Chem. Commun. (Camb)*, 2014. **50**(28): p. 3716-3718.
51. Otto, S., Furlan, R.L.E., and Sanders, J.K.M., *Dynamic Combinatorial Libraries of Macrocyclic Disulfides in Water*. *J. Am. Chem. Soc.*, 2000. **122**: p. 12063-12064.
52. Hamieh, S., Saggiomo, V., Nowak, P., Mattia, E., Ludlow, R.F., et al., *A "dial- $\alpha$ -receptor" dynamic combinatorial library*. *Angew. Chem. Int. Ed. Engl.*, 2013. **52**(47): p. 12368-12372.
53. Chen, H., Jia, J., Duan, X., Yang, Z., and Kong, J., *Reduction-cleavable hyperbranched polymers with limited intramolecular cyclization via click chemistry*. *Polymer Chemistry*, 2015. **53**(20): p. 2374-2380.
54. Kuwabara, T., Nakajima, H., Nanasawa, M., and Ueno, A., *Color Change Indicators for Molecules Using Methyl Red-Modified Cyclodextrins*. *Analytical Chemistry*, 1999. **71**(14): p. 2844-2849.
55. Khouri, S.i.J., Abdel-Rahim, I.A., and Shamaileh, E.M., *A thermodynamic study of  $\alpha$ -,  $\beta$ -, and  $\gamma$ -cyclodextrin-complexed m-methyl red in alkaline solutions*. *Journal of Inclusion Phenomena and Macrocyclic Chemistry*, 2012. **77**(1-4): p. 105-112.
56. P, T. and J\*, T., *Inclusion complexation of methyl orange and methyl red with  $\alpha$ - and  $\beta$ -cyclodextrin: spectral and theoretical study*. *International Journal of Chemical and Pharmaceutical Sciences*, 2018. **9**(1): p. 25-33.
57. Dorokhin, D., Tomczak, N., Han, M., Reinhoudt, D.N., Velders, A.H., et al., *Reversible phase transfer of (CdSe/ZnS) quantum dots between organic and aqueous solutions*. *ACS Nano*, 2009. **3**(3): p. 661-667.
58. Crini, G., *Review: a history of cyclodextrins*. *Chem. Rev.*, 2014. **114**(21): p. 10940-10975.



# CHAPTER 4

---

Oxidant-responsive Ferrocene-based  
Cyclodextrin Complex Coacervate Core  
Micelles

---

## ABSTRACT

---

Coacervate-core micelle are considered promising materials for several applications, from catalysis to drug delivery. However, oxidant-responsive coacervate-core micelles, able to undergo structural changes upon specific oxidation stimuli, are not well-reported. Here, we present a novel ferrocene-dipicolinic acid derivative as redox responsive subcomponent to be incorporated in cyclodextrin-based coacervate core micelles, C4Ms, with tuneable core structure and responsiveness towards  $\text{H}_2\text{O}_2$  treatment. The Fc-C4Ms are formed combining three orthogonal supramolecular interactions, namely i) metal-to-ligand coordination between europium(III) ions and dipicolinic acid molecules, ii) host-guest interaction between beta cyclodextrins and ferrocenes and iii) electrostatic coacervation interaction. The micelle stability against oxidation can be controlled by varying three main parameters: a) the core-unit structure, from monomeric complexes to supramolecular oligomers, b) the  $\text{H}_2\text{O}_2$  equivalents and c) the ratio between redox-responsive and non-redox-responsive bislinker. The  $\text{H}_2\text{O}_2$ -responsive ferrocene-based systems might have interesting application, e.g. Reactive Oxygen Species (ROS)-mediated drug delivery.

---

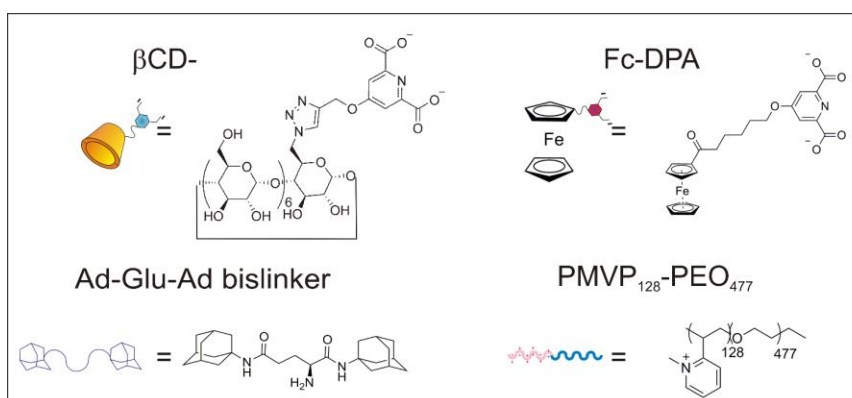
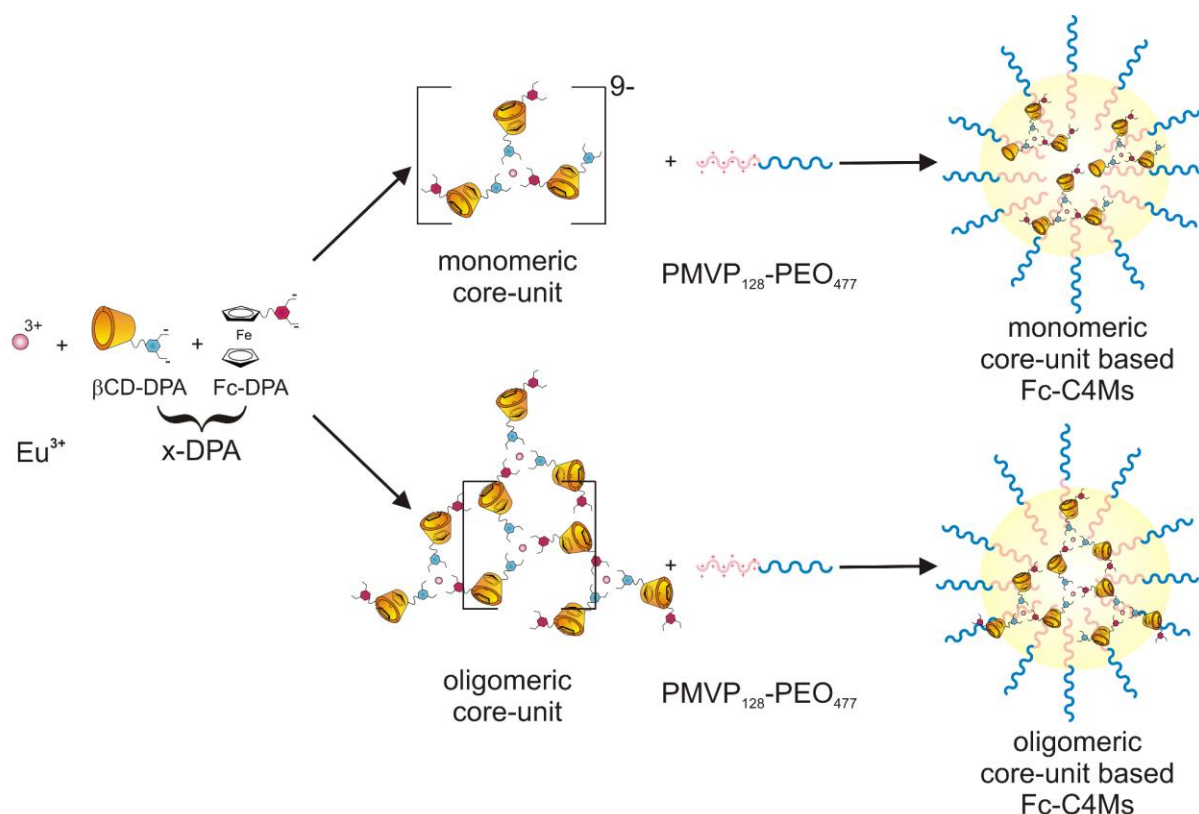
This chapter has been adjusted from the accepted form: Camilla Facciotti, Vittorio Saggiomo, Simon van Hurne, Anton Bunschoten, Rebecca Kaup, and Aldrik H. Velders (2019). "Oxidant-responsive Ferrocene-based Cyclodextrin Complex Coacervate Core Micelles" (accepted in *Supramolecular Chemistry*)

## 4.1. INTRODUCTION

In recent years, Complex Coacervate Core Micelles (C3Ms) have received increasing attention, due to their broad range of applications, from catalysis to drug-delivery.[1-4] Traditionally, C3Ms are formed by electrostatic interactions between oppositely charged polymers.[5-7] By substituting the negatively charged polymers with metal-to-ligand coordination structures, it was possible to form more complex structures in the core of C3Ms, such as branched oligomeric or linear polymeric structures.[8-10] Including a metal-to-ligand coordination structure inside C3Ms allowed a better understanding of the formation process of those micelles and an improved control of their final properties, by changing the coordinated ions.[9, 11] By substituting the metal-to-ligand structures with dendrimers, it was possible to determine the encapsulation capacity and stability of coacervate micelles.[12-14] Recently, host-guest interactions were combined with C3Ms, to investigate, in a subtle way, the minimum number of charges required for coacervate assembly.[15] This minimum value was determined by finely tuning the charges on the adamantane guest molecules in the core of Cyclodextrin-based Complex Coacervate core Micelles (C4Ms). The possibility of changing the guest allowed to adjust the micelle formation, size, stability, and to make them responsive to specific stimuli, such as redox or light. We now wanted to design oxidant-responsive coacervate-core micelles, exploiting supramolecular host-guest interactions, which is of relevance for studying oxidative stress conditions, caused, for example, by Reactive Oxygen Species (ROS) [16-19] production or as H<sub>2</sub>O<sub>2</sub> sensor.[20]

Here, we present ferrocene-based C4Ms, with tuneable core structures and stability against H<sub>2</sub>O<sub>2</sub> stimuli. Uniquely, ferrocene-based C4Ms form by combining three orthogonal supramolecular interactions in the core of C4Ms, namely i) metal-to-ligand coordination between europium ions and dipicolinic acid molecules (DPA), ii) host-guest interaction between beta cyclodextrins ( $\beta$ CD) and ferrocenes (Fc) and iii) electrostatic coacervation interaction (Scheme 4.1.). The metal-to-ligand coordination is formed by mixing europium ions with DPA ligands. In this case, we synthesized two DPA derivatives: i)  $\beta$ CD-DPA, by grafting DPA on the cyclodextrin host and ii) Fc-DPA, by attaching DPA on the ferrocene

guest. Therefore the coordination between the europium and the ligand is based on a dynamic equilibrium between the  $\beta$ CD-DPA and the Fc-DPA ligand, forming these possible structures:  $[\text{Eu} (\text{Fc-DPA})_3]$ ,  $\{\text{Eu} [(\text{Fc-DPA})_2 (\beta\text{CD-DPA})]\}$ ,  $\{\text{Eu} [(\text{Fc-DPA}) (\beta\text{CD-DPA})_2]\}$  and  $[\text{Eu} (\beta\text{CD-DPA})_3]$ . Simply by changing the ratio between Eu/x-DPA, we can tune the core structure from monomeric to oligomeric-based core-unit. A ratio of Eu/x-DPA 1:6 allows the formation of monomeric core-units (Scheme 4.1 top), in which the core-unit charge is 9-, derived from the sum of Eu (3+),  $\beta$ CD-DPA (2-) Fc-DPA (2-) in a 1: (3 + 3) ratio. In the case of oligomeric core-units, a ratio of Eu/x-DPA of 1:3 is required (Scheme 4.1 bottom), and this is achieved by using a ratio of Eu:( $\beta$ CD-DPA + Fc-DPA) 1:(1.5 + 1.5). In our previous work, we found that the stability properties, e.g. fluorescence and magnetic relaxation, of C3Ms could be tuned by changing the core-structures from monomeric to more branched like structures.[11] By introducing host-guest interactions in C3Ms, the stability against salt and competing cyclodextrin could be adjusted by finely tuning the charge of the adamantane guest.[15] Here, we selected ferrocene as guest for its well-known 1:1 inclusion complex with  $\beta$ -CD, with an association constant ( $k_a$ ) around  $4.1 \cdot 10^3 \text{ M}^{-1}$  (in its reduced form)[21-26] and for its responsivity towards mild oxidants, such as  $\text{FeCl}_3$ ,  $\text{AgNO}_3$ ,  $\text{I}_2$ , [27-29] and  $\text{H}_2\text{O}_2$  [16-19, 25, 30-34]. The oxidation reaction of ferrocene to ferrocenium ( $\text{Fc}^+$ ) causes consequently the dissociation of the  $\text{Fc}^+$  from the  $\beta$ -CD ( $k_a 15 \text{ M}^{-1}$ ). In our case,  $\text{H}_2\text{O}_2$  was selected as the oxidant to promote the host-guest dissociation, due to its relevance in biological studies. [26, 35] The addition of  $\text{H}_2\text{O}_2$  to C4Ms favours the disassembly of the host-guest complex, leaving the monomeric core-units with a too low number of charges per core-unit and converting oligomeric core-units into monomeric core-units with low number of charges. In these conditions, core-units with a number of charges below six are not able to form stable coacervate micelles, thus, favouring the micellar aggregation.[15] This destabilization behaviour of Fc-based C4Ms can be finely controlled by varying three parameters: i) the oligomeric structure vs the monomeric core-structure, ii) the  $\text{H}_2\text{O}_2$  equivalents and iii) the addition of a non-responsive bislinker.



**Scheme 4.1.** Representation of the Fc-C4Ms formation. Europium ions (III) are mixed with  $\beta\text{CD-DPA}$  and Fc-DPA molecules to form monomeric or oligomeric core-unit structures. The europium coordination is in dynamic equilibrium between the structures:  $\text{Eu: (Fc-DPA)}_3$ ,  $\text{Eu: [(Fc-DPA)}_2(\beta\text{CD-DPA})]$ ,  $\text{Eu: [(Fc-DPA)(\beta\text{CD-DPA})}_2]$  and  $\text{Eu: (\beta\text{CD-DPA})}_3$ . The formation of the monomeric and oligomeric structures is based on the ratios between  $\text{Eu}/x\text{-DPA}$  or  $\text{Eu}/(\beta\text{CD-DPA and Fc-DPA})$ , respectively 1:6 (top) and 1:3 (bottom) for monomeric and oligomeric core-units. The block copolymer addition, until charge neutralization, allows the formation of the final Fc-C4Ms structure. The bottom part shows the combination of the molecular structures with the schematic representation of the building blocks.

## 4.2. EXPERIMENTAL

Materials and methods, synthesis and micelle preparations are described in the following sections.

### 4.2.1. MATERIALS AND METHODS

Europium(III) nitrate pentahydrate, copper iodide, 30% hydrogen peroxide, 6-bromo-1-oxohexyl)ferrocene, diethyl 4-hydroxy 2,6-pyridinedicarboxylate potassium carbonate and sodium carbonate were purchased from Sigma Aldrich and were used without further purifications. The block copolymer poly(N-methyl-2-vinylpyridine)-b-poly(ethylene oxide) (P2MVP<sub>128</sub>-b-PEO<sub>477</sub>) was purchased from Polymer Source and was quaternised following the procedure described elsewhere.[36] The degree of quaternisation was 80% and was determined by DLS titration.

All NMR measurements were carried out at 298 K on a Bruker Avance III 600 MHz NMR spectrometer. Assignments were aided by COSY, HSQC, NOESY, and HMBC experiments. All mass spectra were acquired using ES ionization on a Thermo Finnigan LXQ Exactive Mass Spectrometer. Samples were prepared as a dilution series in methanol. Measurements were done from lowest to highest concentration until there was sufficient signal. Dynamic Light Scattering measurements (DLS) were carried out on a Malvern NanoSizer ZS, at 173 degree angle, operating at 632.8 nm at 25°C. Samples were incubated for at least two minutes at 25°C before measuring to reduce temperature dependent fluctuations. The size of the particles was determined using number based intensity. UV-vis were measured with UV-1601 Shimadzu Spectrophotometer in 3 mL (1 cm) or 300 µL (1 mm) quartz cuvettes.

Fluorescence spectroscopy measurements were carried out on an Agilent Cary Eclipse Fluorescence Spectrophotometer using quartz cuvettes of 1 cm path length, excitation and emission slits were set at 5 nm. Silica columns were prepared with silica of 40-63 µm, 60 Å. For Cryo-TEM, samples were cast on copper grids (400 mesh - 150 µm average hole size, Holey carbon), from Electron Microscopy Sciences (EMS, Hatfield, PA, USA). After blotting,

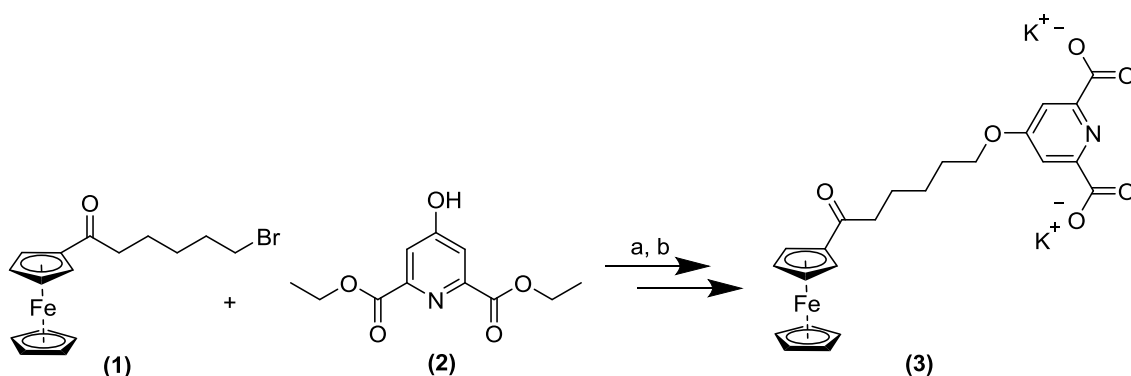
samples were plunged into liquid ethane by using Vitrobot Mark IV instrument. Grids were then transferred to JEOL 1400 PLUS TEM operating at 120 kV.

## 4.2.2. SYNTHESIS

The synthesis of diethyl 4-(prop-2-yn-1-yloxy)pyridine-2,6-dicarboxylate and of pyridine-2,6-dicarboxylate modified  $\beta$ -cyclodextrin were performed following the procedure described in literature.[15] The synthesis of ferrocene-modified dipicolinic acid (**3**) is described in the following paragraph and NMR assignments can be found in the SI (Figure S4.1.-S4.3.).

### SYNTHESIS OF FERROCENE-MODIFIED DIPICOLINIC

### ACID (**3**)



**Scheme 4.2.** Synthesis of ferrocene-modified dipicolinic acid (Fc-DPA). a)  $K_2CO_3$ , butanone, refluxed overnight and b) 2% NaOH, MeOH/ $H_2O$ ,  $N_2$ .

399 mg (1.1 mmol) 6-bromo-1-oxohexylferrocene (**1**) and 250 mg (1.0 mmol) diethyl 4-hydroxy 2,6-pyridinedicarboxylate (**2**) were dissolved in 10 ml butanone with 1.2 equivalents of  $K_2CO_3$ . The mixture was refluxed overnight. The next day the solid was filtered off from the solution and the butanone was evaporated. The crude was purified by column chromatography (1:30 w/w crude/silica) in 2:1 cyclohexane:ethyl acetate.

The product (**3**) was then deprotected by stirring it in a 2% NaOH solution of degassed MeOH/water 98:2. After 2 hours, the orange precipitate was collected by filtration, washed

with a small amount of cold MeOH and dried under vacuum. The overall yield of product **3** was 60%.

$^1\text{H}$  NMR spectrum (600MHz,  $\text{D}_2\text{O}$ ),  $\delta$  [ppm]: 7.53 (s, 2H,  $\text{CH}_{\text{pyr}}$ ), 4.87 (d, 2H,  $\text{H}_{\text{g}}(\text{Fc})$ ), 4.74 (d, 2H,  $\text{H}_{\text{h}}(\text{Fc})$ ), 4.30 (m, 5H,  $\text{H}_{\text{i}}(\text{Fc})$ ), 4.26 (t, 2H,  $J=12.04$  Hz,  $\text{CH}_2\text{-O-pyr}$ ), 3.37 (MeOH), 2.84 (t, 2H,  $J=15.23$  Hz,  $\text{CH}_2\text{-C(=O)-Fc}$ ), 1.89 (m, 2H,  $\text{CH}_2\text{-CH}_2\text{-O-Pyr}$ ), 1.77 (m, 2H,  $\text{CH}_2\text{-CH}_2\text{-C(=O)-Fc}$ ), 1.58 (m, 2H,  $\text{CH}_2\text{-CH}_2\text{-CH}_2\text{-C(=O)-Fc}$ )

$^{13}\text{C}$ -NMR spectrum (600 MHz,  $\text{D}_2\text{O}$ ): ppm 212 ( $\text{C(=O)-Fc}$ ), 172 ( $\text{Pyr-CO}_2$ ), 166 ( $\text{O-C-Pyr}$ ), 154 ( $\text{C(Pyr)-CO}_2$ ), 111 ( $\text{CH-Pyr}$ ), 77.7 ( $\text{C-C(=O)-Fc}$ ), 74 ( $\text{C}_{\text{h}}(\text{Fc})$ ), 70.3 ( $\text{C}_{\text{i}}(\text{Fc})$ ), 69.8 ( $\text{C}_{\text{g}}(\text{Fc})$ ), 68.4 ( $\text{CH}_2\text{-O-pyr}$ ), 39.2 ( $\text{CH}_2\text{-C(=O)-Fc}$ ), 27.7 ( $\text{CH}_2\text{-CH}_2\text{-O-(pyr)}$ ), 24.8 ( $\text{CH}_2\text{-CH}_2\text{-CH}_2\text{-C(=O)-Fc}$ ), 24.5 ( $\text{CH}_2\text{-CH}_2\text{-C(=O)-Fc}$ )

### 4.2.3. MICELLE PREPARATION

The micelles used in these experiments were prepared using a general protocol (Scheme 4.1).[15] Stock solutions of the individual components were prepared:  $\text{Eu}^{3+}$  (5 mM),  $\beta\text{CD-DPA}$  (5 mM), ferrocene-DPA (2 mM), block copolymer  $\text{PMVP}_{128}\text{-PEO}_{477}$  (10 mM charge concentration) and carbonate buffer (200 mM). Micelles were prepared at room temperature in a final volume of 0.2 mL. Firstly, water and carbonate buffer (pH 10) were added, at a final concentration of 20 mM. The Eu coordination complex is formed by adding a fixed amount of DPA. In this case a DPA moiety is attached both on the host (cyclodextrin) and on the guest (ferrocene) making the total amount of DPA (x-DPA) equal to  $\beta\text{CD-DPA} + \text{Fc-DPA}$ . To form monomeric core-units, a ratio of  $\text{Eu/x-DPA}$  1:6 is needed, and this is formed by using a ratio of  $\text{Eu}:(\beta\text{CD-DPA} + \text{Fc-DPA})$  1: (3 + 3). In the second case, a ratio of  $\text{Eu/x-DPA}$  of 1:3 is required to form oligomeric core-units, and this is achieved by using a ratio of  $\text{Eu}:(\beta\text{CD-DPA} + \text{Fc-DPA})$  1:(1.5 + 1.5). Fc-DPA was prepared from a fresh solution and sonication was avoided to prevent ferrocene destabilization. Lastly, the block copolymer was added until charge neutralization, as shown in Scheme 4.1, after the stock solution was sonicated for at least 10 minutes. Each stock solution was vortexed before the addition of the components. Micelles were always prepared freshly before the characterization. During all experiments, the

concentration of the components was fixed to be higher than the CMC to prevent the equilibrium from shifting from micelles towards subcomponents.

#### **4.2.4. H<sub>2</sub>O<sub>2</sub> TREATMENT**

After preparing the micelle solution, specific equivalents of H<sub>2</sub>O<sub>2</sub> were added on top of the solution. No vortexing nor sonication was applied after the treatment as this would create gas bubbles which would interfere with the DLS measurements. Therefore, the treatment can be considered dependent on the diffusion of H<sub>2</sub>O<sub>2</sub> into the micellar solution.

The amounts of H<sub>2</sub>O<sub>2</sub> is given as equivalents with respect to the ferrocene concentration. To prove that the H<sub>2</sub>O<sub>2</sub> response was only related to the presence of ferrocene molecules, other types of micelles, such as metal-to-ligand C3Ms[9] and Ad-Glu-Ad-based C4Ms[15] were treated with 1300 eq. of H<sub>2</sub>O<sub>2</sub>, and their size and intensity was monitored over one day by DLS and Cryo-TEM.

#### **4.2.5. STABILITY EXPERIMENT BY ADDING A NON-RESPONSIVE BISLINKER**

In order to tune the stability of Fc-C4Ms against H<sub>2</sub>O<sub>2</sub>, we introduced a non-responsive bislinker (Ad-Glu-Ad), shown in Scheme 4.1. The synthesis of Ad-Glu-Ad is reported in literature.[15] Increasing percentages of Fc-DPA were substituted with Ad-Glu-Ad. The amounts of substituted guest are given as percentage with respect to the cyclodextrin concentration. DLS and Cryo-TEM were used to measure the size and the polydispersity of the samples.

## 4.3. RESULTS AND DISCUSSION

We synthesized a novel compound, named Fc-DPA, as an addition to the toolbox of components for C4Ms studies. By using the same Fc-DPA (and changing the metal ratio) we are able to form two different structures in the core of C4Ms and to tune the response behavior against H<sub>2</sub>O<sub>2</sub> oxidant. In this section the formation, characterization and oxidant–response of Fc-DPA and Fc-based C4Ms are presented. Further experiments can be found in the Supporting Information.

### 4.3.1. MICELLE CHARACTERIZATION

Fc-C4Ms micelles form by mixing europium ions, βCD-DPA, Fc-DPA and block copolymer in precise stoichiometric amounts. By varying the ratio between europium ions and x-DPA, different monomeric or oligomeric core-unit structures form in the core of coacervate micelles, as previously shown in literature.[11] Wang et al. showed that changing the ratio between europium and DPA ligand from 1:6 to 1:2 increases the number of branches between the singular monomeric core-units, favoring the formation of oligomeric/polymeric core-units. In addition to that, by changing the core-structures of C3Ms, they could adjust the luminescent and magnetic properties.[11] The metal-to-ligand coordination complex between europium ions and x-DPA was confirmed by measuring the europium emission upon DPA excitation (antenna phenomenon), (Figure S4.3.). Finally, the block copolymer was added in stoichiometric amount to the core-units to neutralize the core charges and form the final Fc-C4Ms. The block copolymer concentration was calculated by titrating the block copolymer to the monomeric and oligomeric core-units, (Figure S4.4.).

The formation of Fc-based C4Ms was confirmed by DLS and Cryo-TEM. The hydrodynamic size was determined around 60 nm (SD 8 nm), (Figure 4.1. and S4.5. and S4.6.), comparable with previous C4Ms.[15] The Cryo-TEM results show typical spherical shaped-micelles, with a core around 40 nm (SD 7 nm) and shell around 10 nm. No significance difference in the size is evident between monomeric and oligomeric core-unit-based micelles. This result was

observed also in C3Ms, in which 1:2, 1:3 and 1:6 DPA/Ln ratios were investigated. In all the three cases the micelles had similar sizes, but different aggregation numbers and different lanthanide (III) coordination structures in the core, respectively dimeric, polymeric and monomeric.[11] In our case, although the polydispersity is relatively low, the Cryo-TEM of Fc-based C4Ms shows also the “size sorting” phenomenon (Figure S4.7).[13] This phenomenon consists of the distribution of micelles on different parts of the TEM grid, based on their size. Smaller micelles distribute at the center of the biconcave layer of the TEM grid, while bigger micelles concentrated at the edge.[13, 37]

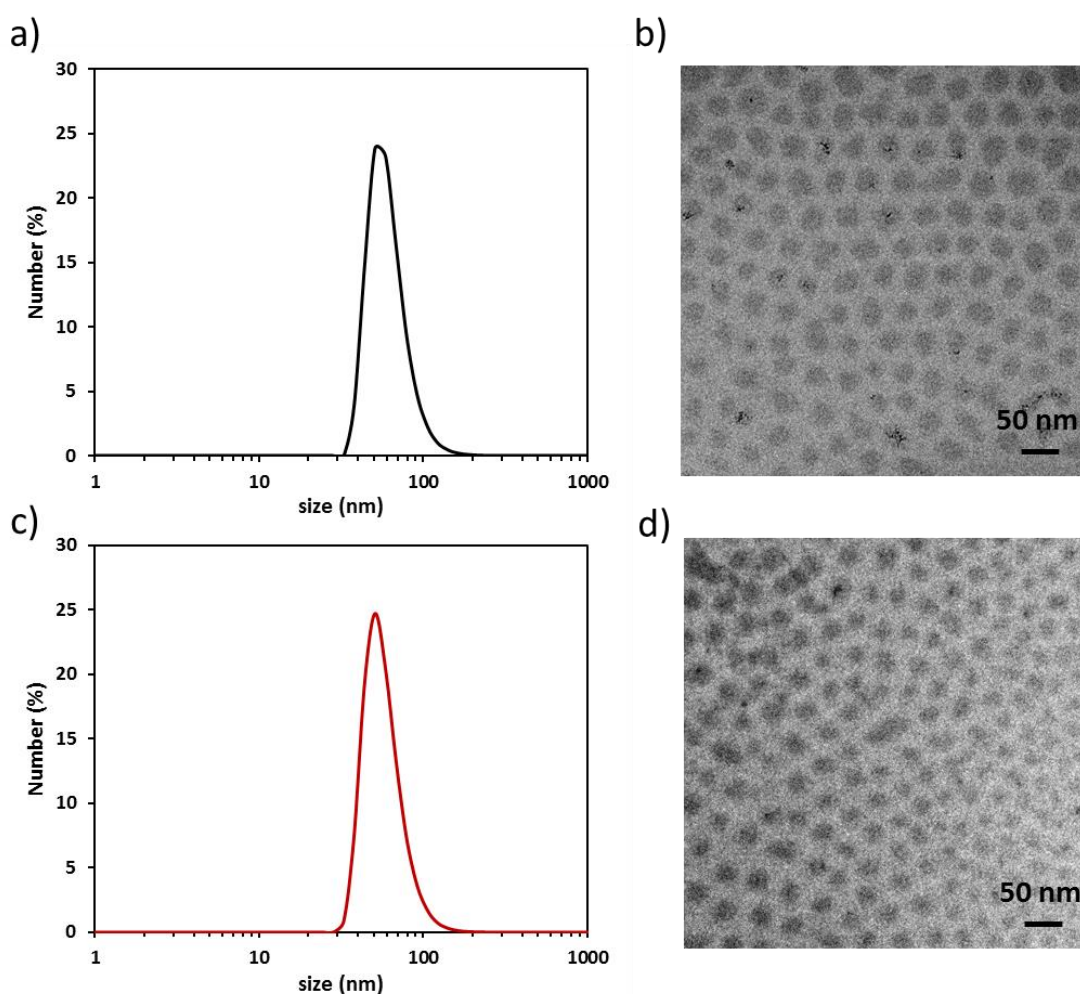


**Figure 4.1.** Size distribution of oligomeric a) and monomeric b) core-unit based Fc-C4Ms at the DLS. Cryo-TEM images of oligomeric c) and monomeric d) core-unit based Fc-C4Ms.

The stability of Fc-C4Ms was investigated by DLS, monitoring size, intensity and polydispersity values over 24 hours. The results did not show any significant variation in

intensity and distribution, confirming that Fc-based C4Ms are stable up to 24 hours (Figures S4.8. and S4.9.). The stability against dilution (CMC) was also investigated with DLS, by monitoring the intensity and size values over the addition of a buffer solution. The CMC was similar for the different core-unit-based micelles around 4  $\mu\text{M}$  of europium ions, (Figures S4.10. and S4.11.). Furthermore, the salt stability is higher for oligomeric core-unit-based micelles compared to monomeric core-unit-based micelles, respectively 100 mM of NaCl and 24 mM of NaCl (Figures S4.12. and S4.13.). These stability results indicate that oligomeric core-unit-based micelles are c.a. four times more stable to salt addition, compared to monomeric core-unit-based micelles. These stability findings are in good agreement with the results found in our previous study, showing that monomeric core-unit C4Ms, based on adamantane bis-acid guest, are less stable than oligomeric core-unit C4Ms, based on an adamantane bislinker.[15]

### 4.3.2. H<sub>2</sub>O<sub>2</sub>-RESPONSE

Increasing equivalents of H<sub>2</sub>O<sub>2</sub> were added to monomeric and oligomeric core-unit-based Fc-C4Ms and the size and intensity were monitored by DLS and cryo-TEM. The addition of 325 equivalents of H<sub>2</sub>O<sub>2</sub> to monomeric core-unit-based Fc-C4Ms did not show any variation in size and intensity up to ca. 8 hours (Figure S4.14.). However, after that time, intensity and size increase, forming large aggregates. This result can be attributed to the oxidation of the ferrocene to ferrocenium by H<sub>2</sub>O<sub>2</sub>, which provokes the disassociation of the host-guest complex. After the host-guest dissociate, the core-unit is left only with three negative charges (per core-unit). As previously demonstrated, three negative charges per core-units are not enough for stable spherical coacervate micelles and then, the micellar destabilization is favoured.[15]

This destabilization process is even more evident at high concentrations of H<sub>2</sub>O<sub>2</sub> (Figures S4.14. and S4.15.). By adding 650 eq. up to 1500 eq. of H<sub>2</sub>O<sub>2</sub>, the monomeric core-unit based micelles form big aggregates of 1500 nm. The aggregation, visible from the intensity drop is subsequent to a slight increase in intensity. This phenomenon is commonly seen for

coacervate micelles and attributed to the change in shape caused by charge mismatches.[38] This aggregation causes the precipitation of the clusters out of solution and, consequently, the drop of the intensity. This phenomenon occurs faster at high H<sub>2</sub>O<sub>2</sub> concentration. On the other hand, oligomeric core-unit based micelles are stable up to 970 eq. of H<sub>2</sub>O<sub>2</sub>. Figure S4.15. shows that no significant change in size and intensity can be detected for oligomeric core-unit-based micelles up to 970 eq. of H<sub>2</sub>O<sub>2</sub>. Above this concentration, oligomeric core-unit based micelles start to aggregate and fall out of solution, similarly to the monomeric core-units. The rate of this phenomenon is, however, slower for oligomeric micelles, compared to monomeric core-unit-based micelles, as shown in Figure 4.2. The oxidant-response results indicate that oligomeric core-unit-based micelles are stable to higher concentrations of H<sub>2</sub>O<sub>2</sub>, compared to monomeric core-unit-based micelles, respectively 970 eq. and 325 eq. and that the time before C4Ms precipitate can be controlled by varying the oxidant concentration. This destabilization process, favoured by the low number of charges per core-unit, was confirmed by adding H<sub>2</sub>O<sub>2</sub> to the core-units prior the block copolymer addition. No micellar structures were detected, confirming that ferrocenium moieties cannot bind to βCD and trigger the formation of stable Fc-based C4Ms. Moreover, to confirm that the H<sub>2</sub>O<sub>2</sub> responsivity is only related to the presence of the ferrocene moieties, we treated other types of coacervate micelles with the same oxidant. By treating Ad-Glu-Ad-based C4Ms[15] with 1300 eq. of H<sub>2</sub>O<sub>2</sub>, no significant variation in size and intensity was visible (Figure S4.16). Therefore, we confirmed that the destabilization of monomeric and oligomeric core-unit-based Fc-based C4Ms is only based on the oxidation of ferrocene molecules.

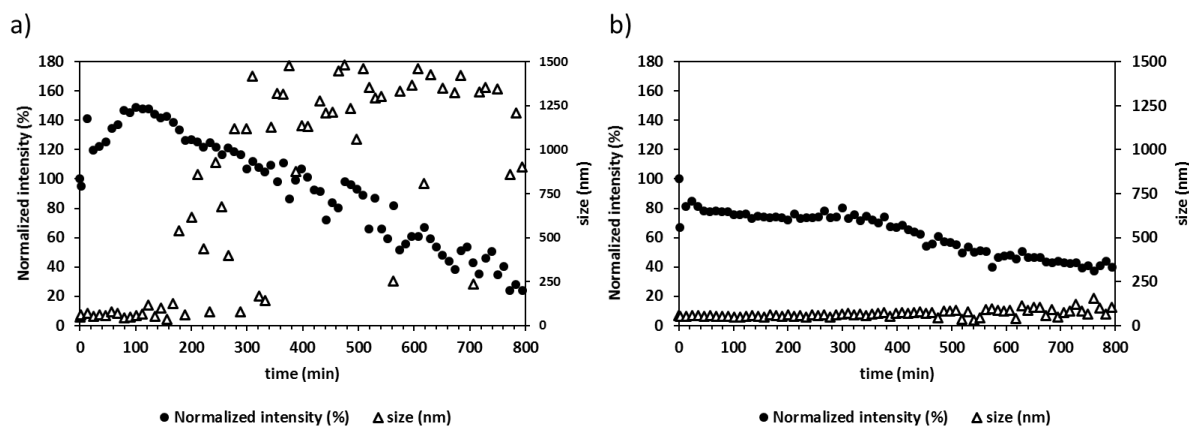


**Figure 4.2.**  $H_2O_2$  response of a) monomeric and oligomeric b) core-unit-based Fc-C4Ms at the DLS, after 1300 eq.  $H_2O_2$  treatment.

### 4.3.3. TUNING THE $H_2O_2$ -RESPONSE BY ADDING A NON-OXIDANT-RESPONSIVE BISLINKER

In order to increase the stability of oligomeric Fc-C4Ms against  $H_2O_2$ , we formed core-units by mixing different percentages of Fc-DPA and the non-responsive Ad-Glu-Ad bislinker, Figure 4.3. The adamantane molecules of Ad-Glu-Ad can combine multiple Eu(CD-DPA) complexes together, forming branched network core-unit structures. Moreover, the association complex between adamantane and  $\beta$ CD ( $k_a$  around  $10^4 M^{-1}$ ), [39] is not dependent on  $H_2O_2$  addition and, therefore, Ad-Glu-Ad should confer more stability to the Fc-based C4Ms (Figure S4.16.).

Increasing amounts of Fc-DPA were substituted with Ad-Glu-Ad. As Figure 4.3. shows, the addition of 10% of non-responsive bislinker did not improve significantly the stability of Fc-based C4Ms against  $H_2O_2$ . In contrast, by adding from 50% to 90% of non-responsive bislinker, micelles are more stable, in time, to the destabilization caused by  $H_2O_2$ . These results indicate that the stability against oxidant can be tuned not only by changing the core

structure from monomeric to oligomeric, but also by including a non-responsive adamantane bislinker.

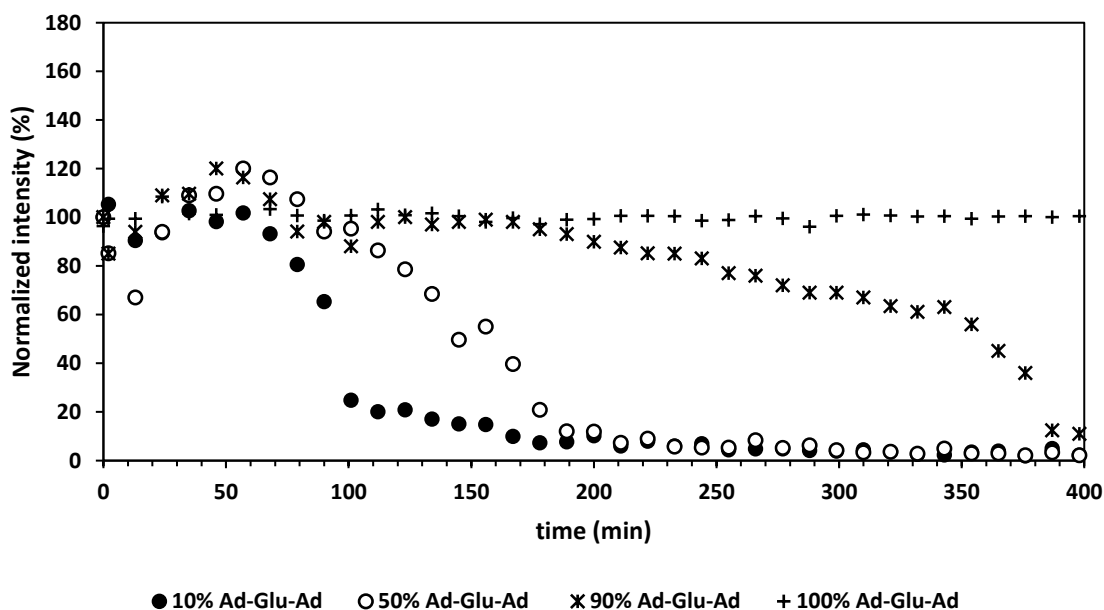


**Figure 4.3.** C4Ms formed by substituting Fc-DPA with increasing ratios of Ad-Glu-Ad non-responsive bislinker. By increasing the concentration of Ad-Glu-Ad from 10% Ad-Glu-Ad bislinker to 100%, C4Ms becomes more stable against oxidant treatment. The normalized intensity is plotted against time, after the addition of 1300 eq. of  $H_2O_2$ .

## 4.4. CONCLUSION

We successfully synthesized a new ligand-guest molecule based on dipicolinic acid-ferrocene molecules, which allowed us to form oxidant-responsive Cyclodextrin-based Complex Coacervate Core Micelles with tuneable core structures and properties. Uniquely, oxidant-responsive Cyclodextrin-based Complex Coacervate Core Micelles were formed by combining three orthogonal supramolecular interactions in the core of C4Ms, namely i) metal-to-ligand coordination between europium ions and dipicolinic acid molecules, ii) host-guest interaction between beta cyclodextrins and ferrocenes and iii) electrostatic coacervation interaction. By simply adjusting the metal-to-ligand ratio, we changed the core structures from monomeric to oligomeric and, consequently, improved the stability against  $H_2O_2$  stimuli. The  $H_2O_2$  response results indicate that oligomeric core-unit-based micelles are stable to higher

concentrations of  $\text{H}_2\text{O}_2$ , compared to monomeric core-unit-based micelles, respectively 970 eq. and 325 eq. By increasing the  $\text{H}_2\text{O}_2$  concentration up to 1500 eq., the micelle aggregation occurs faster, compared to lower oxidant concentrations. The aggregation behaviour of Fc-C4Ms can be controlled by varying three parameters: a) the oligomeric vs monomeric starting structure, b) the concentration of  $\text{H}_2\text{O}_2$  and c) by substituting 50% or more of ferrocene ligand with a non-responsive bislinker. We have shown here how the control at molecular level of the redox state of iron in ferrocene allows the tuning of the micelle formation structure and the stability against  $\text{H}_2\text{O}_2$  oxidant. These  $\text{H}_2\text{O}_2$ -responsive ferrocene-based coacervate micelles might be interesting for Reactive Oxygen Species (ROS)-mediated drug delivery or  $\text{H}_2\text{O}_2$ -sensing applications.

## 4.5. SUPPORTING INFORMATION

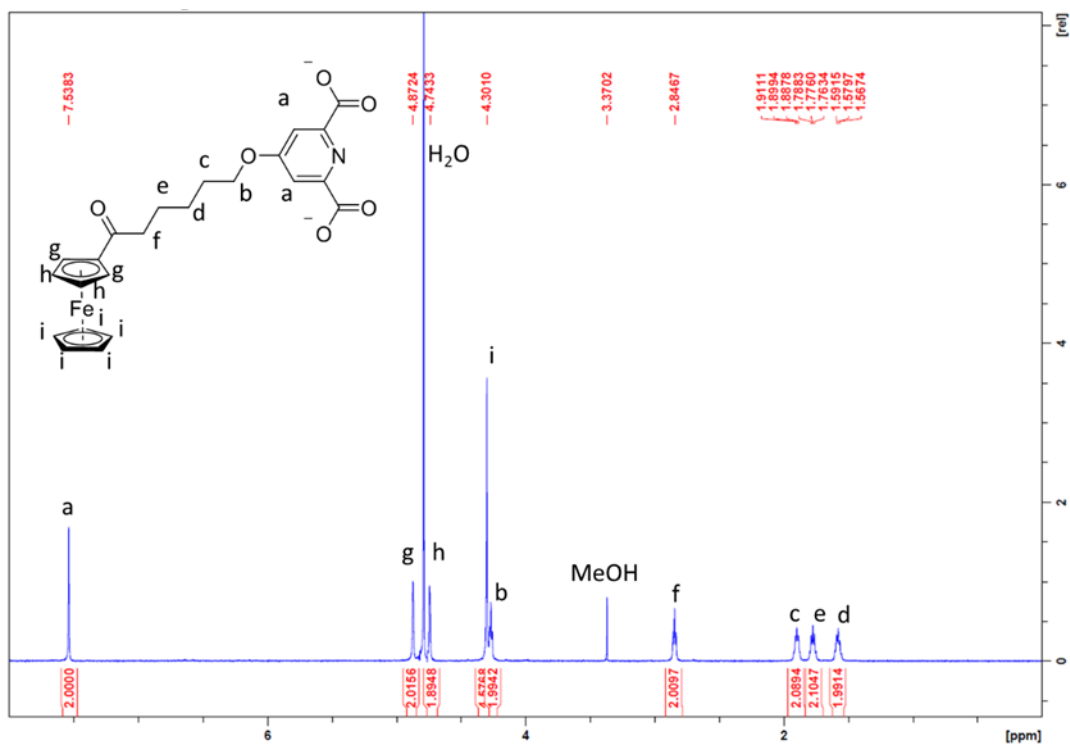


Figure S4.1.  $^1\text{H}$  NMR peak assignment of ferrocene-modified dipicolinic acid (Fc-DPA) in  $\text{D}_2\text{O}$ .

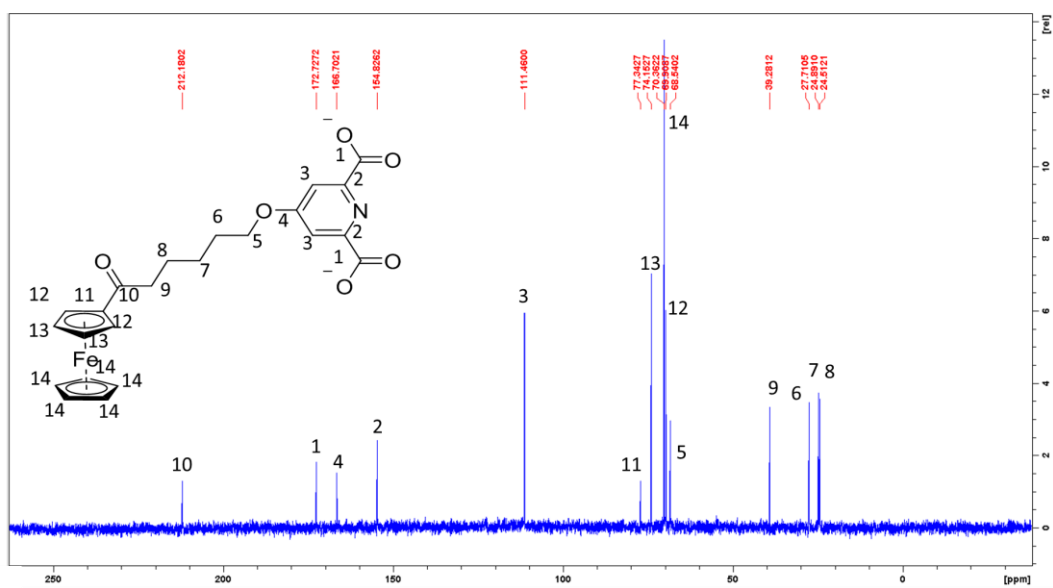
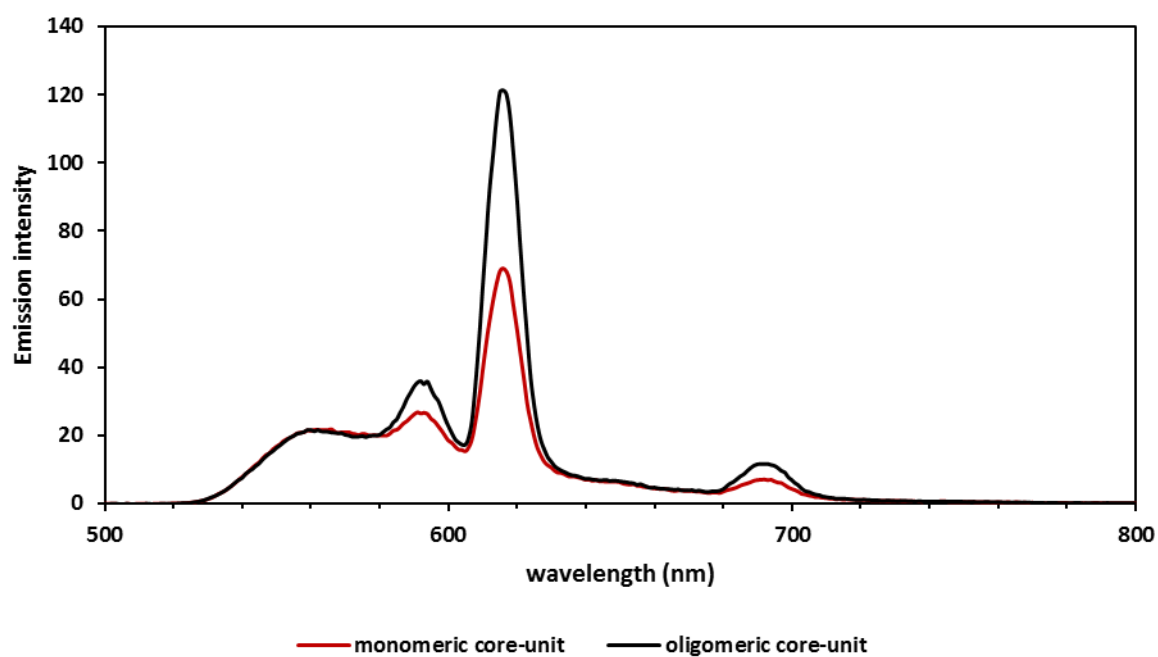
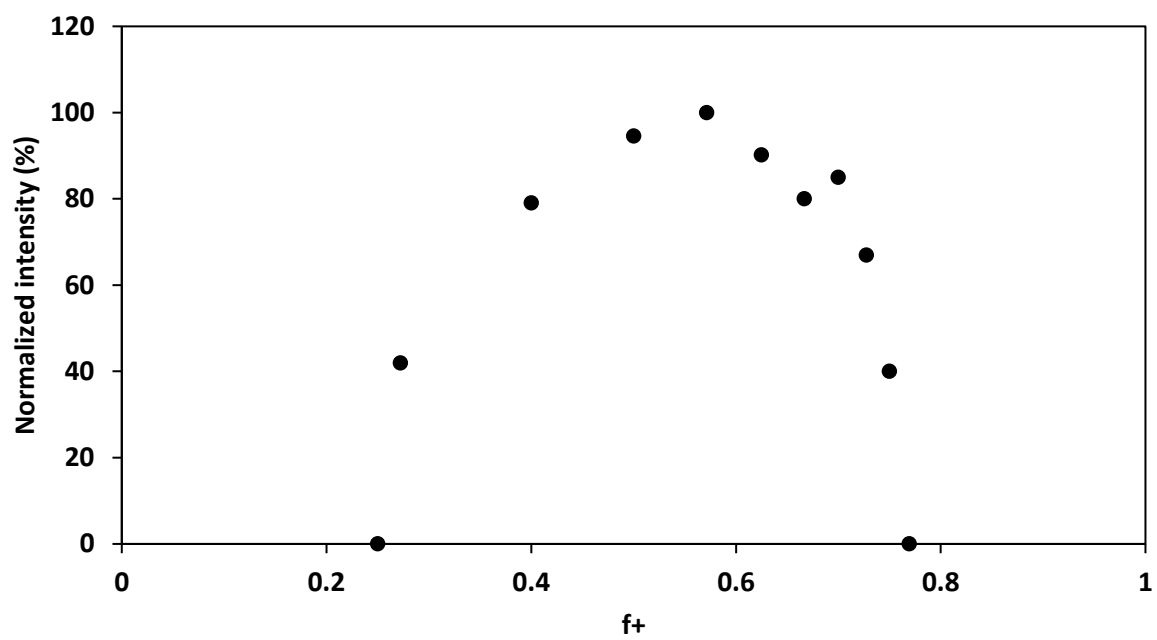


Figure S4.2.  $^{13}\text{C}$  NMR peak assignment of ferrocene-modified dipicolinic acid (Fc-DPA) in  $\text{D}_2\text{O}$ .

*Micelle characterization*



**Figure S4.3.** Emission spectrum of europium ions in the Fc-core-units, exciting the DPA at 280 nm (antenna phenomenon). The europium emission is not normalized for the europium concentration. As mentioned in the main text, the oligomeric core-units contains double the concentration of europium ions, compared to the monomeric core-units.



**Figure S4.4.** Determination of positive fraction ( $f^+$ ), by titrating the block copolymer to the core-units. The  $f^+$  determines the optimum concentration of block copolymer to reach the neutralization of the core-unit charges. In this case, 0.57 mM was determined as the optimum block copolymer concentration.

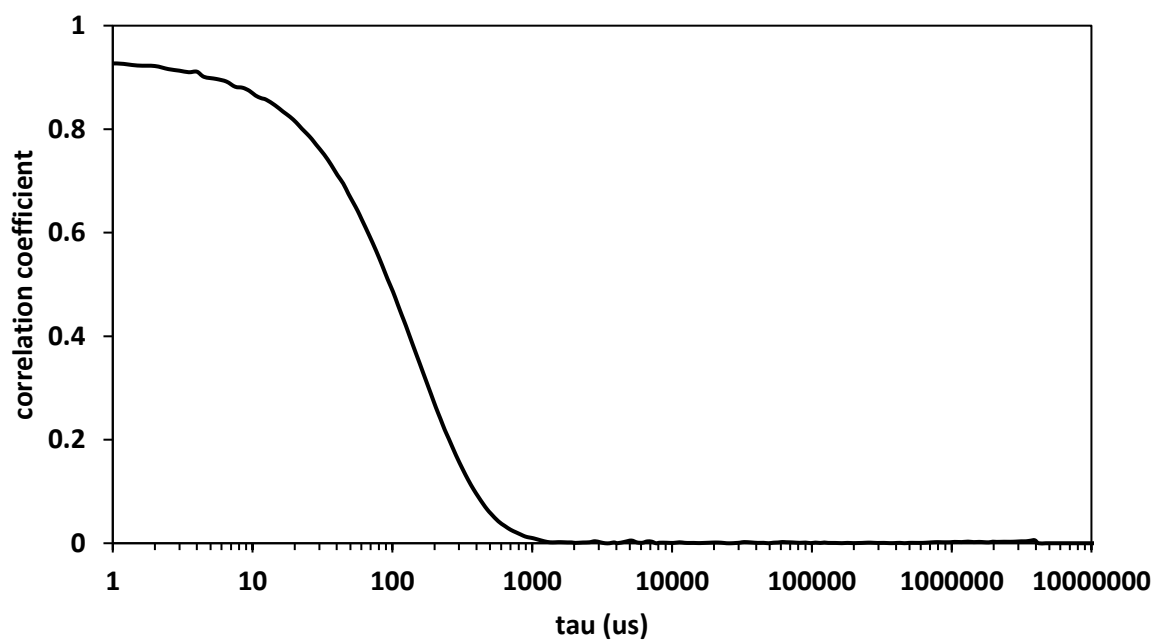
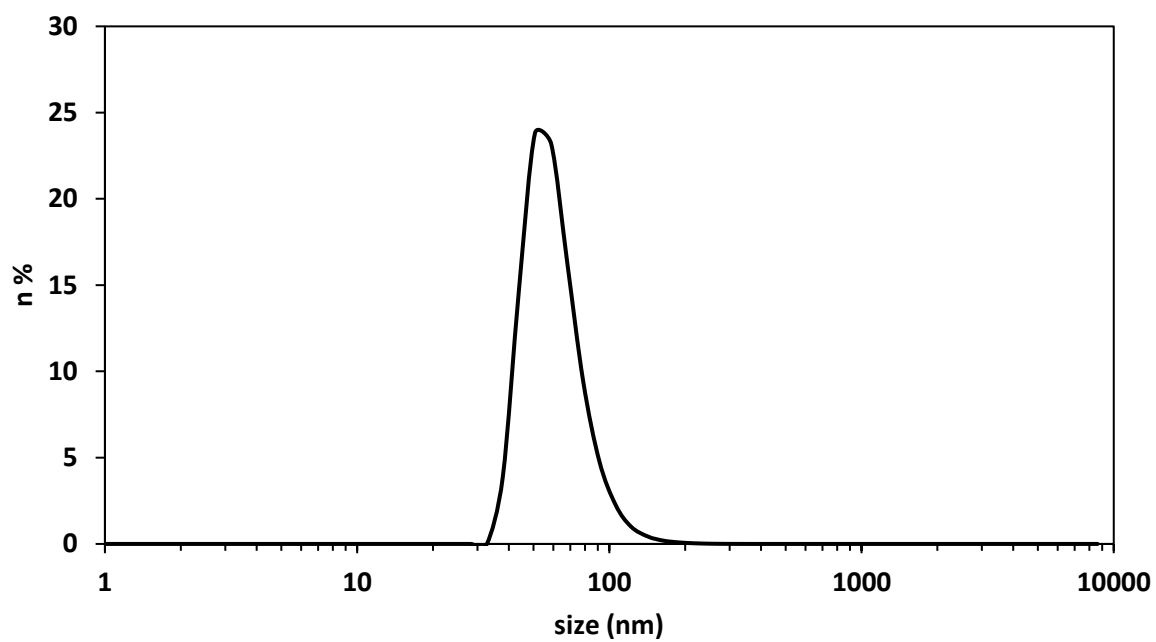


*Figure S4.5. Size distribution (above) and correlogram (below) of oligomeric core-unit based Fc-C4Ms, measured at the DLS.*

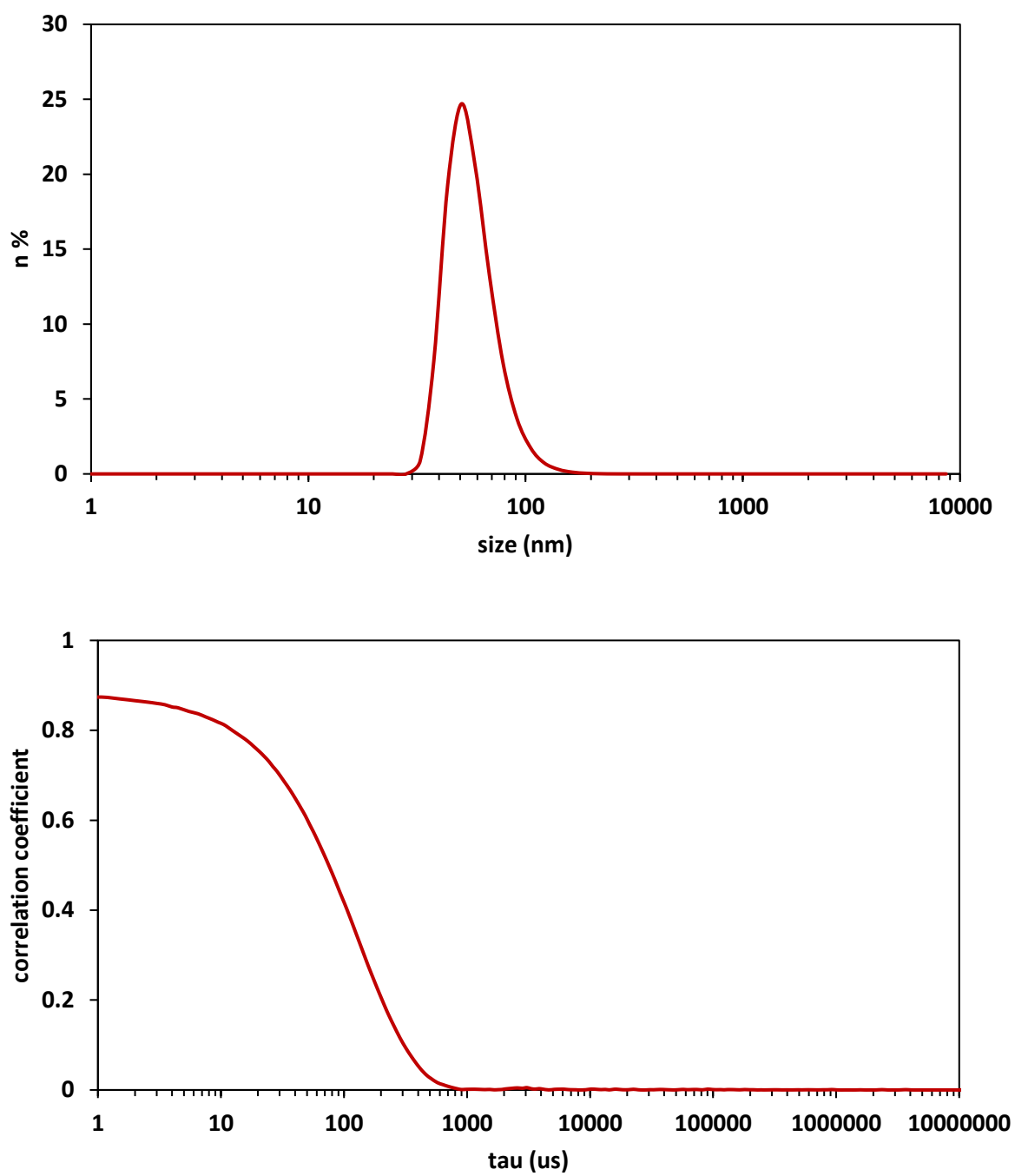


*Figure S4.6. Size distribution (above) and correlogram (below) of monomeric core-unit based Fc-C4Ms, measured at the DLS.*

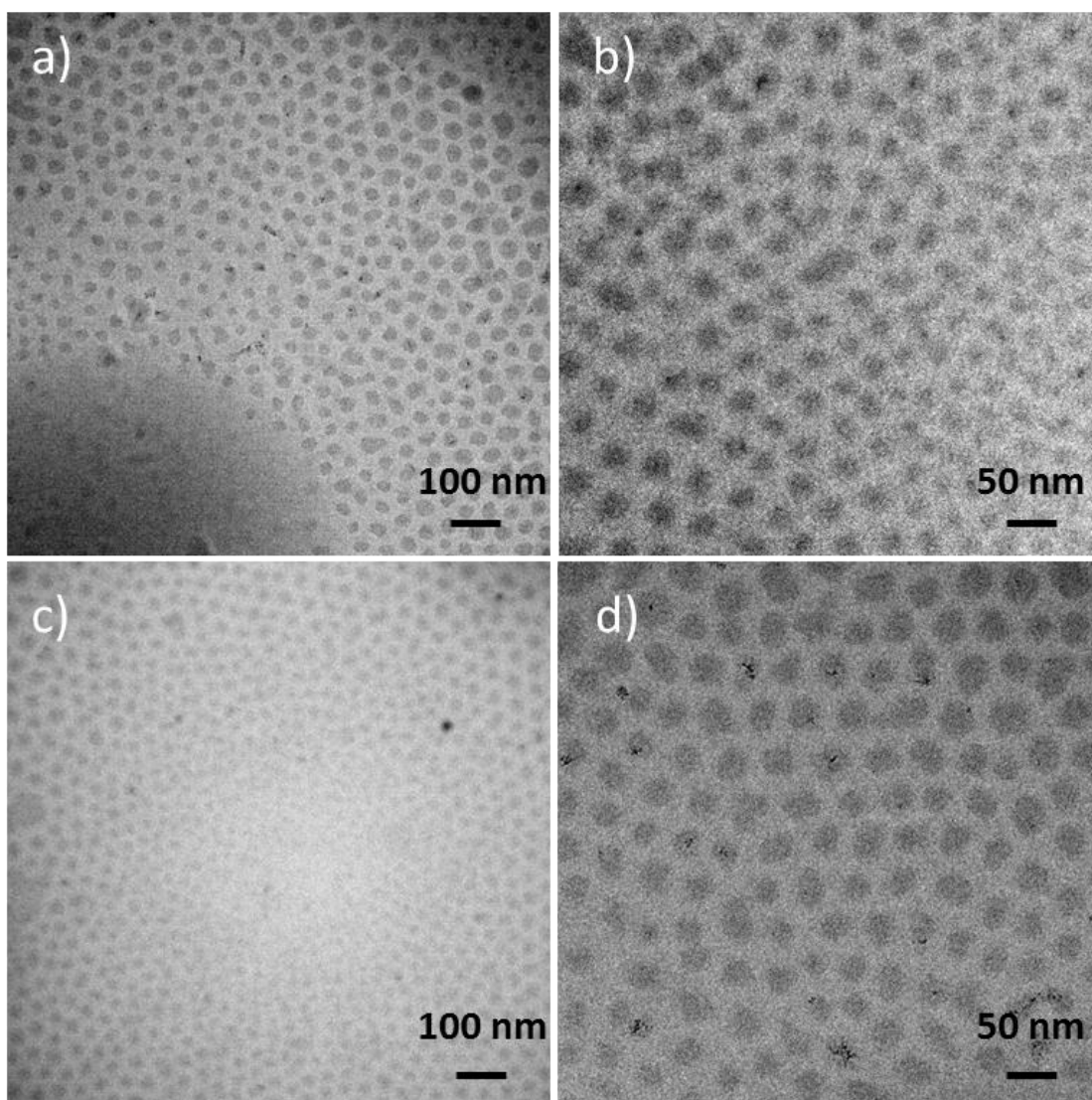


**Figure S4.7.** Cryo-TEM pictures of oligomeric core-unit based Fc-C4Ms a) and b) and monomeric core-unit based Fc-C4Ms c) and d).

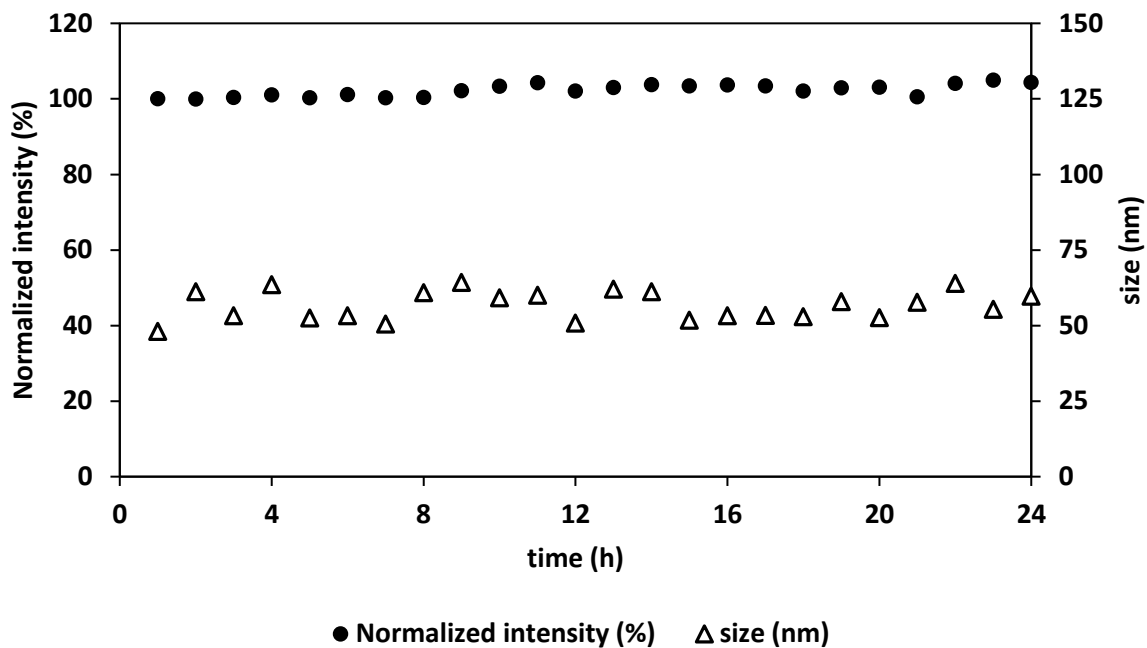


Figure S4.8. Stability in time of oligomeric core-unit based Fc-C4Ms, measured at the DLS.

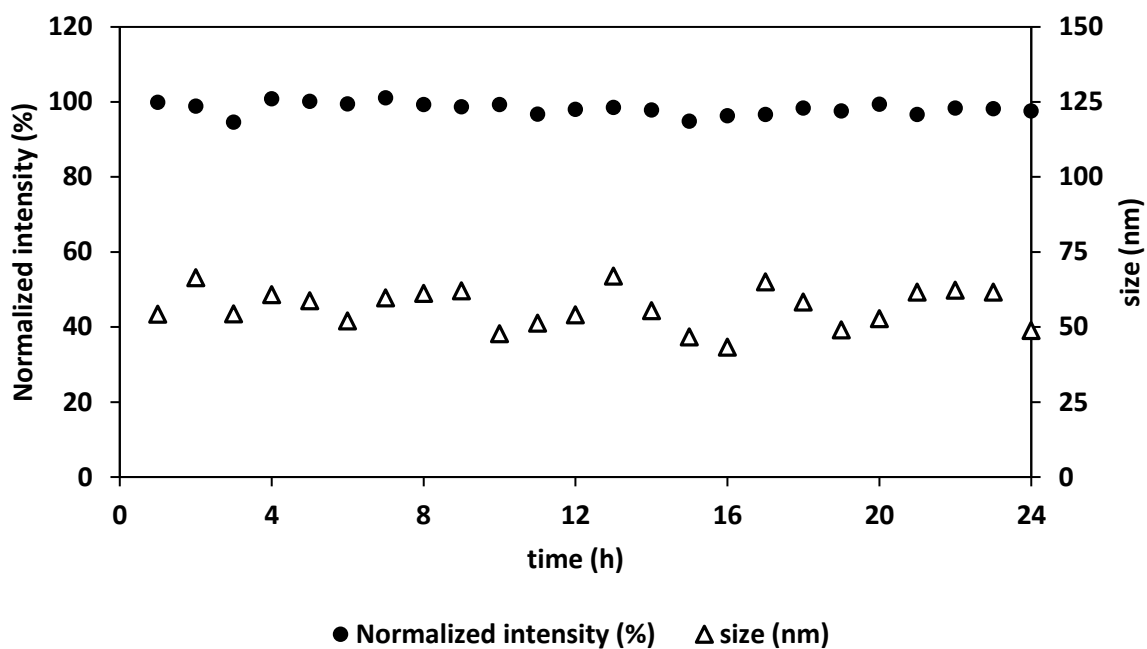
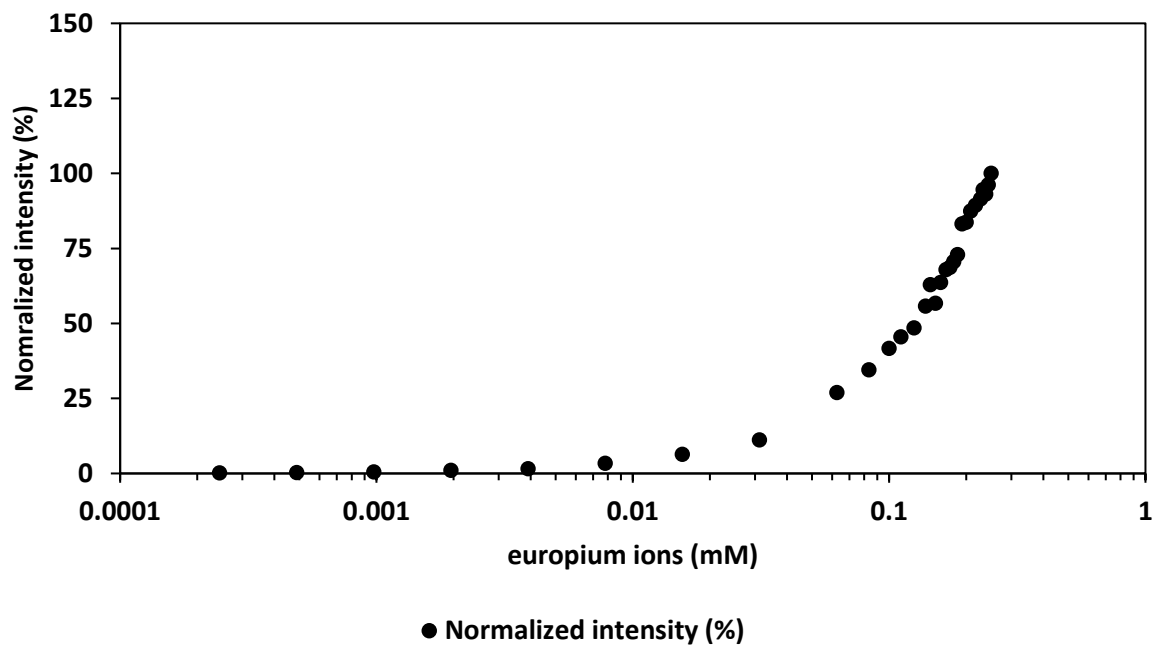
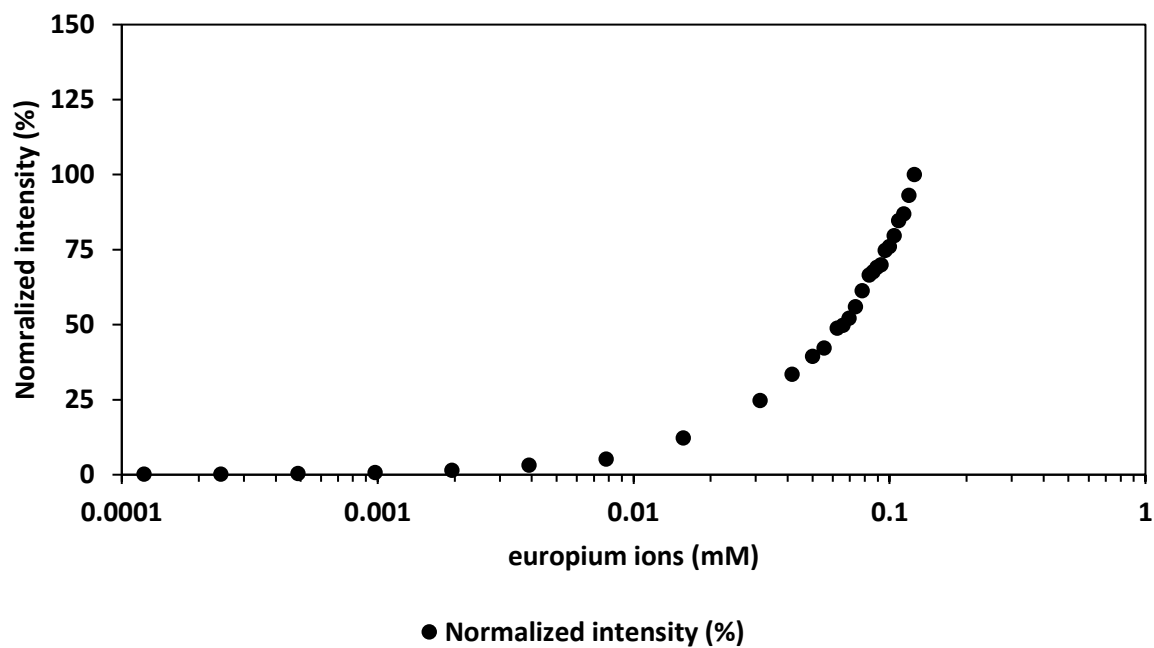


Figure S4.9. Stability in time of monomeric core-unit based Fc-C4Ms, measured at the DLS.



**Figure S4.10.** Critical Micelle Concentration (CMC) determination for the oligomeric core-unit based Fc-CAMs, measured at the DLS.



**Figure S4.11.** Critical Micelle Concentration (CMC) determination for the monomeric core-unit based Fc-CAMs, measured at the DLS.

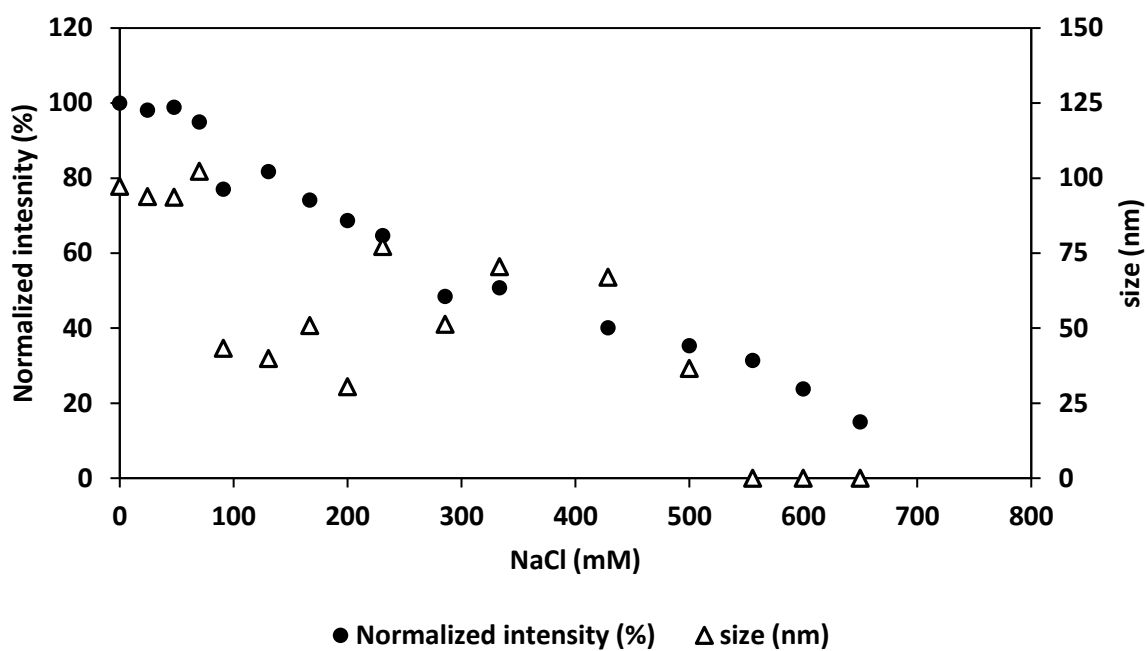


**Figure S4.12.** Critical Salt Concentration (CSC) determination for the oligomeric core-unit based Fc-C4Ms, measured at the DLS.

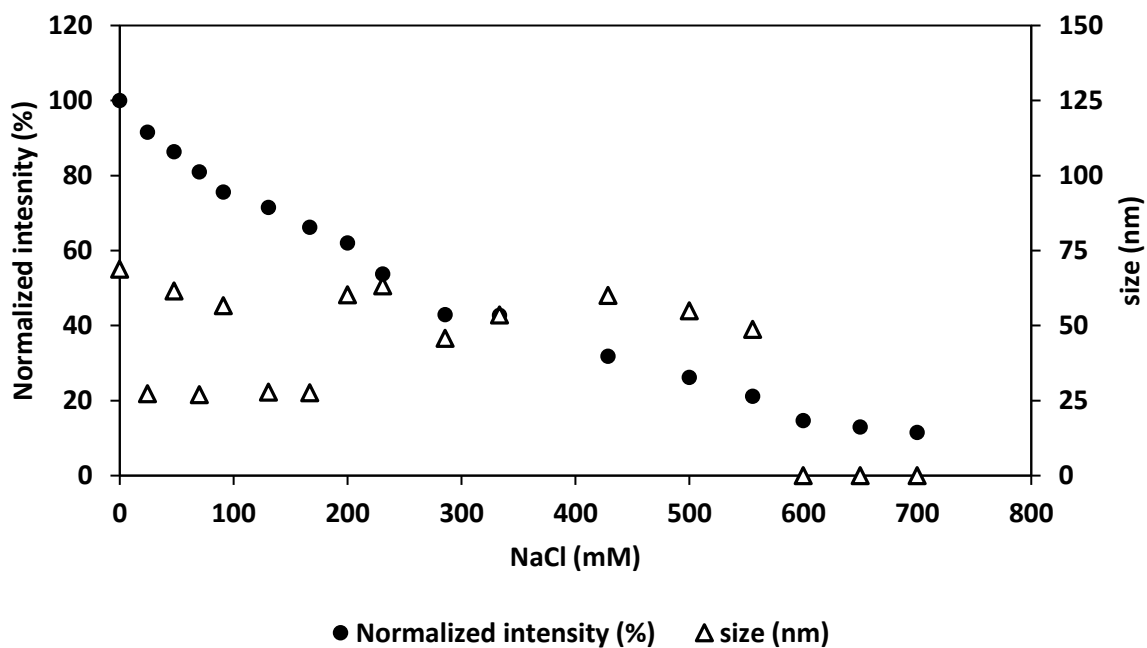


**Figure S4.13.** Critical Salt Concentration (CSC) determination for the monomeric core-unit based Fc-C4Ms, measured at the DLS.

*H<sub>2</sub>O<sub>2</sub>-response studies*

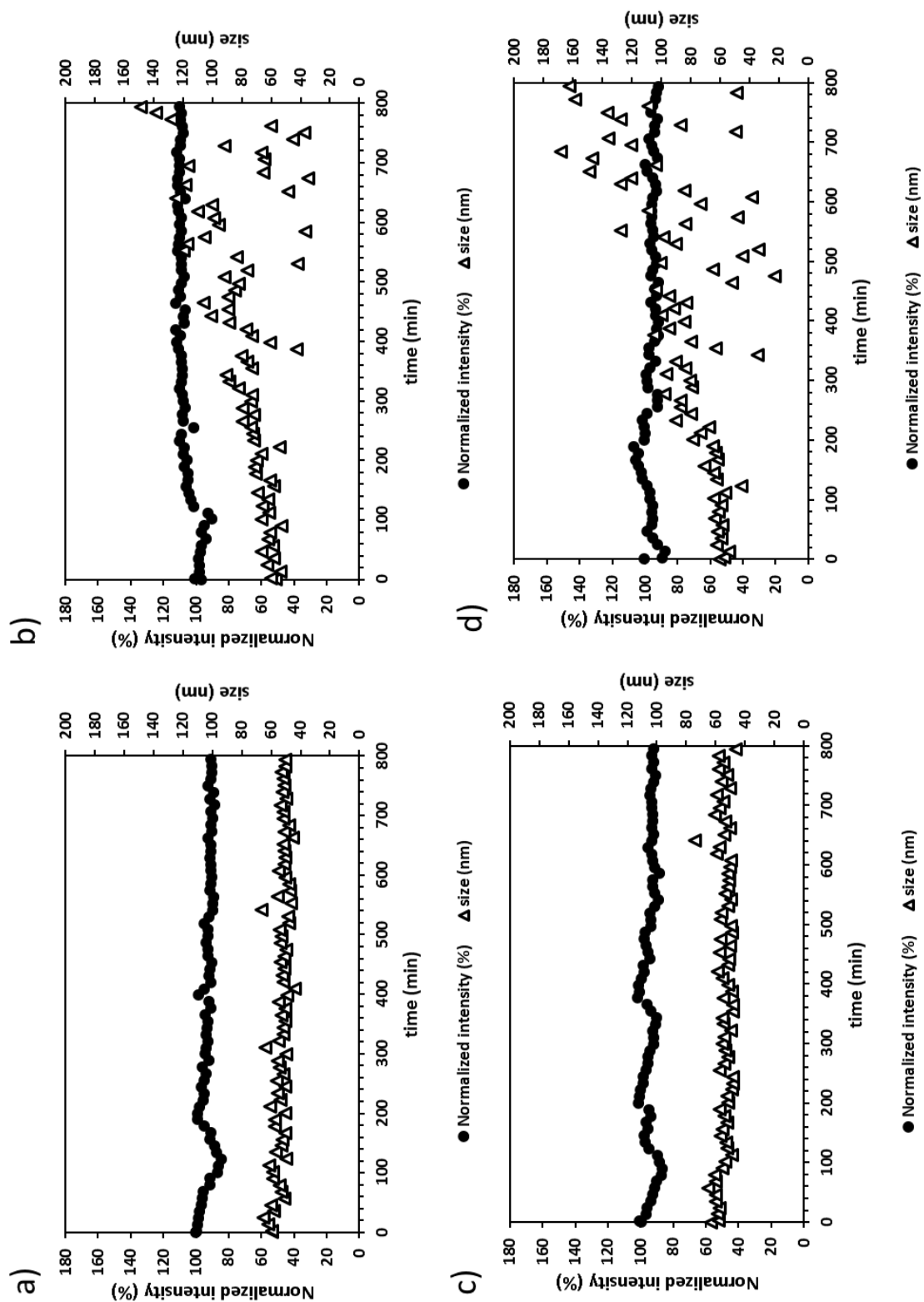


**Figure S4.14.** Normalized intensity and size over time of Fc-C4Ms after the addition of 325 equivalents a) and b) and 650 equivalents c) and d) of H<sub>2</sub>O<sub>2</sub>, for oligomeric core-unit a) and c) and monomeric core-unit based micelles b) and d), measured at the DLS.

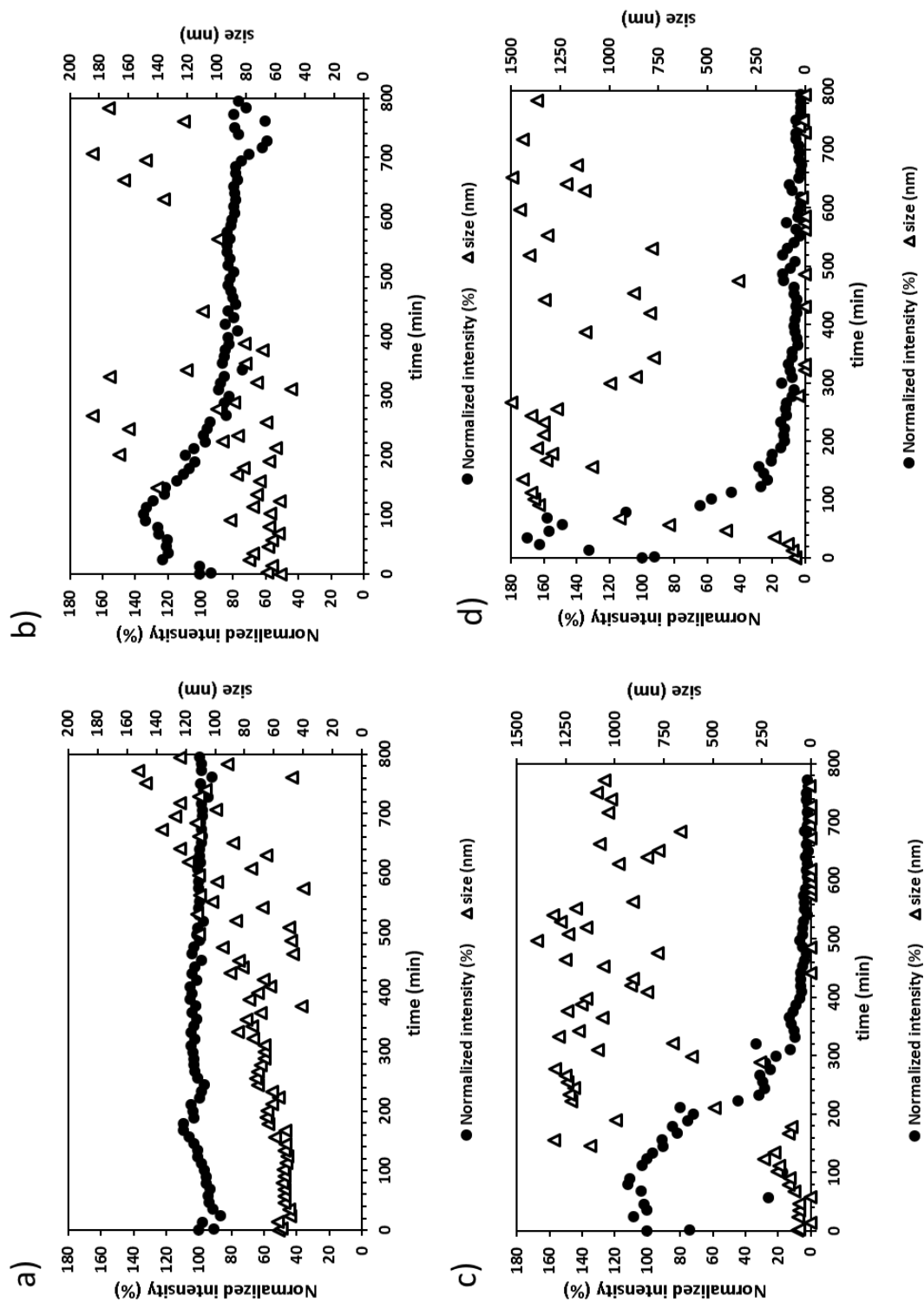


**Figure S4.15.** Normalized intensity and size over time of Fc-C4Ms after the addition of 970 equivalents a) and b) and 1500 equivalents c) and d) of  $H_2O_2$ , for oligomeric core-unit a) and c) and monomeric core-unit based micelles b) and d), measured at the DLS.

*Addition of a non-responsive bislinker*

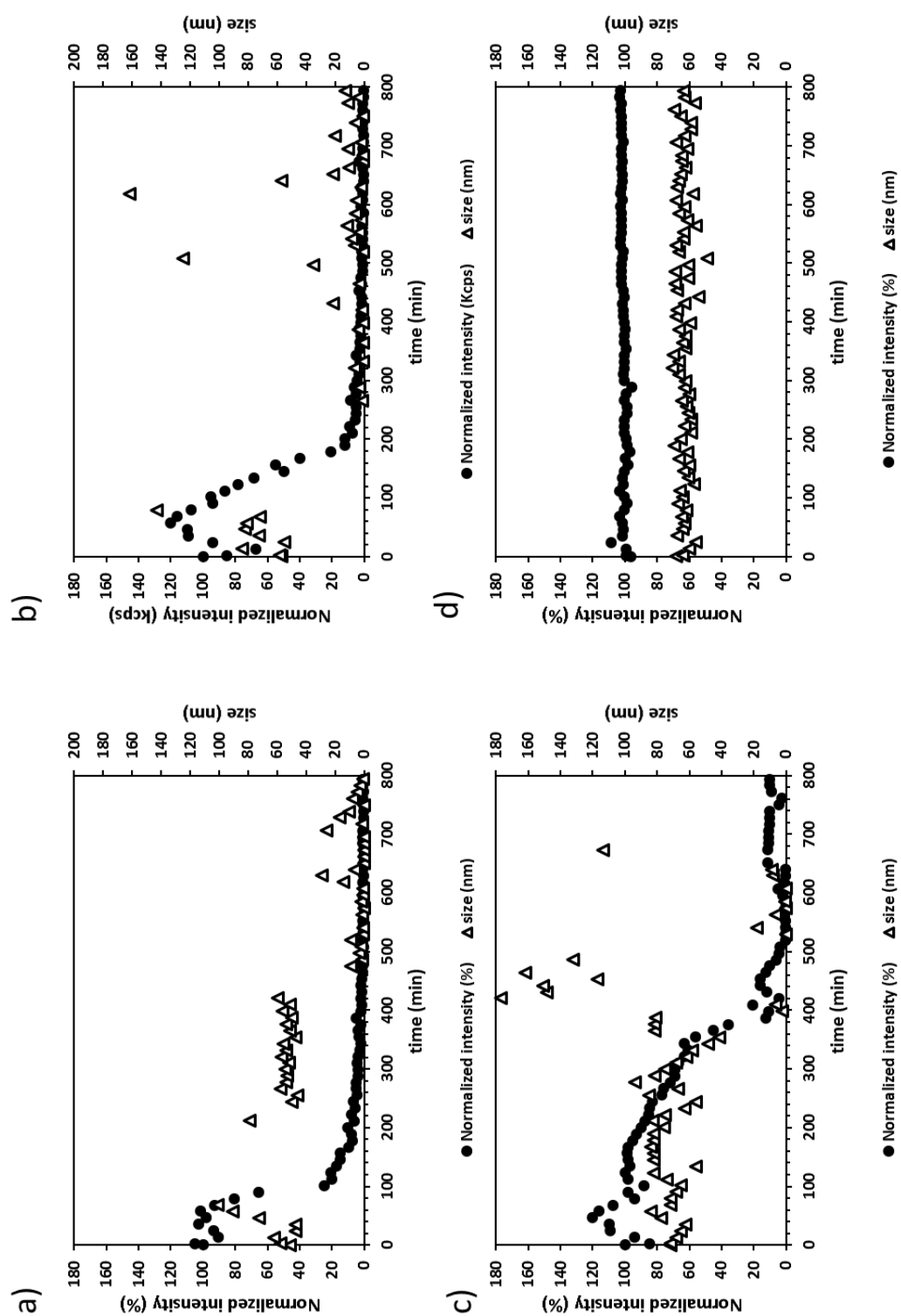


**Figure S4.16.** Normalized intensity and size over time after the addition of 1300 eq of  $H_2O_2$  to a Fc-C4Ms sample, by substituting increasing amount of Fc-DPA with Ad-Glu-Ad bislinker, a) 10%, b) 50 %, c) 90% and d) 100%, measured at the DLS.

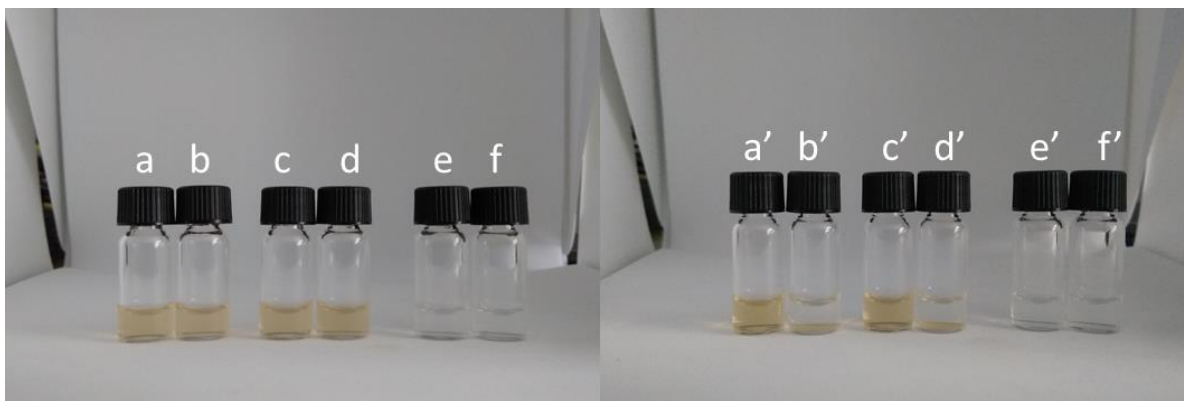


**Figure S4.17.** Pictures of the destabilization study of oligomeric a) and b) and monomeric c) and d) core-unit Fc-C4Ms. The vials e and f represent the control C4Ms, prepared with Ad-Glu-Ad bislinker. The vials b,d and f were treated with 1300 eq of H<sub>2</sub>O<sub>2</sub>.

**Table S4.1.** Intensity of the Fc-based C4Ms controls, measured at the DLS.

Name	I (Mcps)
<i>Eu</i>	<i>na</i>
<i>βCD-DPA</i>	<i>na</i>
<i>Fc-DPA</i>	<i>na</i>
<i>BP</i>	<i>na</i>
<i>Eu βCD-DPA</i>	<i>na</i>
<i>Eu Fc-DPA</i>	<i>na</i>
<i>Eu BP</i>	<i>na</i>
<i>Eu Fc-DPA BP</i>	0.3
<i>Eu βCD-DPA BP</i>	0.4
<i>Fc-DPA BP</i>	0.2
<i>Fc-DPA βCDDPA</i>	<i>na</i>
<i>βCD-DPA BP</i>	<i>na</i>
<i>monomeric core-unit based Fc-C4Ms</i>	22
<i>oligomeric core-unit based Fc-C4Ms</i>	45

## 4.6. REFERENCES

1. Voets, I.K., de Keizer, A., and Cohen Stuart, M.A., *Complex coacervate core micelles*. Adv. Colloid Interface Sci., 2009. **147-148**: p. 300-318.
2. Nolles, A., Westphal, A.H., de Hoop, J.A., Fokkink, R.G., Kleijn, J.M., et al., *Encapsulation of GFP in Complex Coacervate Core Micelles*. Biomacromolecules, 2015. **16**(5): p. 1542-1549.
3. Nakashima, K.K., Baaij, J.F., and Spruijt, E., *Reversible generation of coacervate droplets in an enzymatic network*. Soft Matter, 2018. **14**(3): p. 361-367.
4. Bourouina, N., Cohen Stuart, M.A., and Kleijn, J.M., *Complex coacervate core micelles as diffusional nanoprobos*. Soft Matter, 2014. **10**(2): p. 320-331.
5. Rumyantsev, A.M., Zhulina, E.B., and Borisov, O.V., *Scaling Theory of Complex Coacervate Core Micelles*. ACS Macro Letters, 2018. **7**(7): p. 811-816.
6. Harada, A. and Kataoka, K., *Formation of Polyion Complex Micelles in an Aqueous Milieu from a Pair of Oppositely-Charged Block Copolymers with Poly(ethylene glycol) Segments*. Macromolecules, 1995. **28**(15): p. 5294-5299.
7. Harada, A. and Kataoka, K., *Polyion complex micelle formation from double-hydrophilic block copolymers composed of charged and non-charged segments in aqueous media*. Polym. J., 2017. **50**(1): p. 95-100.
8. Yan, Y., Besseling, N.A., de Keizer, A., and Stuart, M.A., *Characteristic differences in the formation of complex coacervate core micelles from neodymium and zinc-based coordination polymers*. J. Phys. Chem. B, 2007. **111**(21): p. 5811-5818.
9. Wang, J., Velders, A.H., Gianolio, E., Aime, S., Vergeldt, F.J., et al., *Controlled mixing of lanthanide(III) ions in coacervate core micelles*. Chem. Commun. (Camb), 2013. **49**(36): p. 3736-3738.
10. Wang, J., de Keizer, A., Fokkink, R., Yan, Y., Cohen Stuart, M.A., et al., *Complex coacervate core micelles from iron-based coordination polymers*. J. Phys. Chem. B, 2010. **114**(25): p. 8313-8319.
11. Wang, J., Groeneveld, A., Oikonomou, M., Prusova, A., Van As, H., et al., *Revealing and tuning the core, structure, properties and function of polymer micelles with lanthanide-coordination complexes*. Soft Matter, 2016. **12**(1): p. 99-105.
12. Ten Hove, J.B., Wang, J., van Leeuwen, F.W.B., and Velders, A.H., *Dendrimer-encapsulated nanoparticle-core micelles as a modular strategy for particle-in-a-box-in-a-box nanostructures*. Nanoscale, 2017. **9**(47): p. 18619-18623.
13. Ten Hove, J.B., Wang, J., van Oosterom, M.N., van Leeuwen, F.W.B., and Velders, A.H., *Size-Sorting and Pattern Formation of Nanoparticle-Loaded Micellar Superstructures in Biconcave Thin Films*. ACS Nano, 2017. **11**(11): p. 11225-11231.
14. Wang, J., Voets, I.K., Fokkink, R., van der Gucht, J., and Velders, A.H., *Controlling the number of dendrimers in dendrimicelle nanoconjugates from 1 to more than 100*. Soft Matter, 2014. **10**(37): p. 7337-7345.
15. Facciotti, C., Saggiomo, V., Bunschoten, A., Fokkink, R., Hove, J.B.T., et al., *Cyclodextrin-based complex coacervate core micelles with tuneable supramolecular host-guest, metal-to-ligand and charge interactions*. Soft Matter, 2018. **14**(47): p. 9542-9549.
16. Fu, Y.-H., Chen, C.-Y., and Chen, C.-T., *Tuning of hydrogen peroxide-responsive polymeric micelles of biodegradable triblock polycarbonates as a potential drug delivery platform with ratiometric fluorescence signaling*. Polym. Chem., 2015. **6**(47): p. 8132-8143.
17. Lisanti, M.P., Martinez-Outschoorn, U.E., Lin, Z., Pavlides, S., Whitaker-Menezes, D., et al., *Hydrogen peroxide fuels aging, inflammation, cancer metabolism and metastasis: the seed and soil also needs "fertilizer"*. Cell Cycle, 2011. **10**(15): p. 2440-2449.
18. Liu, B., Wang, D., Liu, Y., Zhang, Q., Meng, L., et al., *Hydrogen peroxide-responsive anticancer hyperbranched polymer micelles for enhanced cell apoptosis*. Polym. Chem., 2015. **6**(18): p. 3460-3471.
19. Liu, C., Zhu, X., Wang, X., Miao, D., Liang, X., et al., *Hydrogen peroxide-responsive micelles self-assembled from a peroxalate ester-containing triblock copolymer*. Biomater. Sci., 2016. **4**(2): p. 255-257.
20. Oikonomou, M., Wang, J., Carvalho, R.R., and Velders, A.H., *Ternary supramolecular quantum-dot network flocculation for selective lectin detection*. Nano Research, 2016. **9**(7): p. 1904-1912.
21. Moozyckine, A.U., Bookham, J.L., Deary, M.E., and Davies, D.M., *Structure and stability of cyclodextrin inclusion complexes with the ferrocenium cation in aqueous solution: 1H NMR studies*. J. Am. Chem. Soc., 2001(9): p. 1858-1862.

22. Yuan, Z., Wang, J., Wang, Y., Zhong, Y., Zhang, X., et al., *Redox-Controlled Voltage Responsive Micelles Assembled by Noncovalently Grafted Polymers for Controlled Drug Release*. *Macromolecules*, 2019. **52**(4): p. 1400-1407.
23. Harada, A., Takashima, Y., and Nakahata, M., *Supramolecular polymeric materials via cyclodextrin-guest interactions*. *Acc. Chem. Res.*, 2014. **47**(7): p. 2128-2140.
24. Osella, D., Carretta, A., Nervi, C., Ravera, M., and Gobetto, R., *Inclusion Complexes of Ferrocenes and Cyclodextrins Critical Appraisal of the Electrochemical Evaluation of Formation Constants*. *Organometallics* 2000. **19**: p. 2791-2797.
25. Dong, Z., Kang, Y., Yuan, Q., Luo, M., and Gu, Z., *H<sub>2</sub>O<sub>2</sub>-Responsive Nanoparticle Based on the Supramolecular Self-Assemble of Cyclodextrin*. *Front. Pharmacol.*, 2018. **9**: p. 552-562.
26. Liu, L., Rui, L., Gao, Y., and Zhang, W., *Self-assembly and disassembly of a redox-responsive ferrocene-containing amphiphilic block copolymer for controlled release*. *Polym. Chem.*, 2015. **6**(10): p. 1817-1829.
27. Gu, H., Mu, S., Qiu, G., Liu, X., Zhang, L., et al., *Redox-stimuli-responsive drug delivery systems with supramolecular ferrocenyl-containing polymers for controlled release*. *Coord. Chem. Rev.*, 2018. **364**: p. 51-85.
28. Tsierkezos, N.G., *Cyclic Voltammetric Studies of Ferrocene in Nonaqueous Solvents in the Temperature Range from 248.15 to 298.15 K*. *J. of Solution Chem.*, 2007. **36**(3): p. 289-302.
29. Gagne, R.R., Koval, C.A., and Lisensky, G.C., *Ferrocene as internal standard for electrochemical measurements*. *Inorg. Chem.*, 1980. **19**: p. 2854-2855.
30. Ge, Z. and Liu, S., *Functional block copolymer assemblies responsive to tumor and intracellular microenvironments for site-specific drug delivery and enhanced imaging performance*. *Chem. Soc. Rev.*, 2013. **42**(17): p. 7289-7325.
31. Gu, T. and Hasebe, Y., *Novel amperometric assay for drug-DNA interaction based on an inhibitory effect on an electrocatalytic activity of DNA-Cu(II) complex*. *Biosens. Bioelectron.*, 2012. **33**(1): p. 222-227.
32. Solovev, A.A., Smith, E.J., Bof Bufon, C.C., Sanchez, S., and Schmidt, O.G., *Light-controlled propulsion of catalytic microengines*. *Angew. Chem. Int. Ed. Engl.*, 2011. **50**(46): p. 10875-10878.
33. Harada, A., *Cyclodextrin-based molecular machines*. *Acc. Chem. Res.*, 2001. **34**(6): p. 456-464.
34. Zhao, Y., Huang, Y., Zhu, H., Zhu, Q., and Xia, Y., *Three-in-One: Sensing, Self-Assembly, and Cascade Catalysis of Cyclodextrin Modified Gold Nanoparticles*. *J. Am. Chem. Soc.*, 2016. **138**(51): p. 16645-16654.
35. Huo, M., Yuan, J., Tao, L., and Wei, Y., *Redox-responsive polymers for drug delivery: from molecular design to applications*. *Polym. Chem.*, 2014. **5**(5): p. 1519-1528.
36. Biesalski, M., Johannsmann, D., and Ruhe, J., *Electrolyte-induced collapse of a polyelectrolyte brush*. *J. Chem. Phys.*, 2004. **120**(18): p. 8807-8814.
37. Ten Hove, J.B., van Oosterom, M.N., van Leeuwen, F.W.B., and Velders, A.H., *Nanoparticles reveal Extreme Size-Sorting and Morphologies in Complex Coacervate Superstructures*. *Sci. Rep.*, 2018. **8**(1): p. 13820-13827.
38. van der Kooij, H.M., Spruijt, E., Voets, I.K., Fokkink, R., Cohen Stuart, M.A., et al., *On the stability and morphology of complex coacervate core micelles: from spherical to wormlike micelles*. *Langmuir* 2012. **28**(40): p. 14180-14191.
39. Tran, D.N., Colesnic, D., Adam de Beaumais, S., Pembouong, G., Portier, F., et al., *Cyclodextrin-adamantane conjugates, self-inclusion and aggregation versus supramolecular polymer formation*. *Org. Chem. Front.*, 2014. **1**(6): p. 703-706.



# CHAPTER 5

---

Light-responsive Cyclodextrin-based Complex  
Coacervate Core Micelles

---

## ABSTRACT

---

In the past decades, polymeric micelles have received increasing attention due to their promising applications in several fields, from catalysis to drug delivery. The design of stimuli-responsive polymeric micelles, e.g. controllable with light-triggers, might open a way to design advanced materials and finely controlled cargo release systems. Most of the light-responsive micelles reported in literature disassemble upon a mismatch in the polymer hydrophobic-hydrophilic balance, caused by a light trigger. Here, we present azobenzene and Cyclodextrin-based Complex Coacervate Core Micelles, in which the disassembly is not driven by the hydrophobic/hydrophilic misbalance, but rather by lowering the charge per core-unit. We designed two new micellar-core building blocks,  $\alpha$ cyclodextrin functionalized dipicolinic acid and azobenzene-functionalized dipicolinic acid. Here, we show that we can drive the assembly and the reversible disassembly of azobenzene-based C4Ms, by controlling the charge per core-unit with light-stimuli that changes the azobenzene from *trans* to *cis*, disrupting the supramolecular interaction with the  $\alpha$ cyclodextrin. The response behaviour towards light stimuli can be tuned by changing the core structure from monomeric to oligomeric as well as by mixing in non-DPA functionalized azobenzene moieties. Preliminary studies with methyl red indicate that Azo-based C4Ms can be used to solubilize poor water-soluble dyes and trigger their release under light stimuli. Azobenzene-based Cyclodextrin-based Complex Coacervate Core Micelles might have promising application, e.g. light-controlled drug delivery.

---

This chapter has been adjusted from the form: Camilla Facciotti, Vittorio Saggiomo, Karthik Gangadharaiah, Anton Bunschoten, Rebecca Kaup, Suzanne Jansze and Aldrik H. Velders (2019)." Light-responsive Cyclodextrin-based Complex Coacervate Core Micelles " (manuscript in preparation)

## 5.1. INTRODUCTION

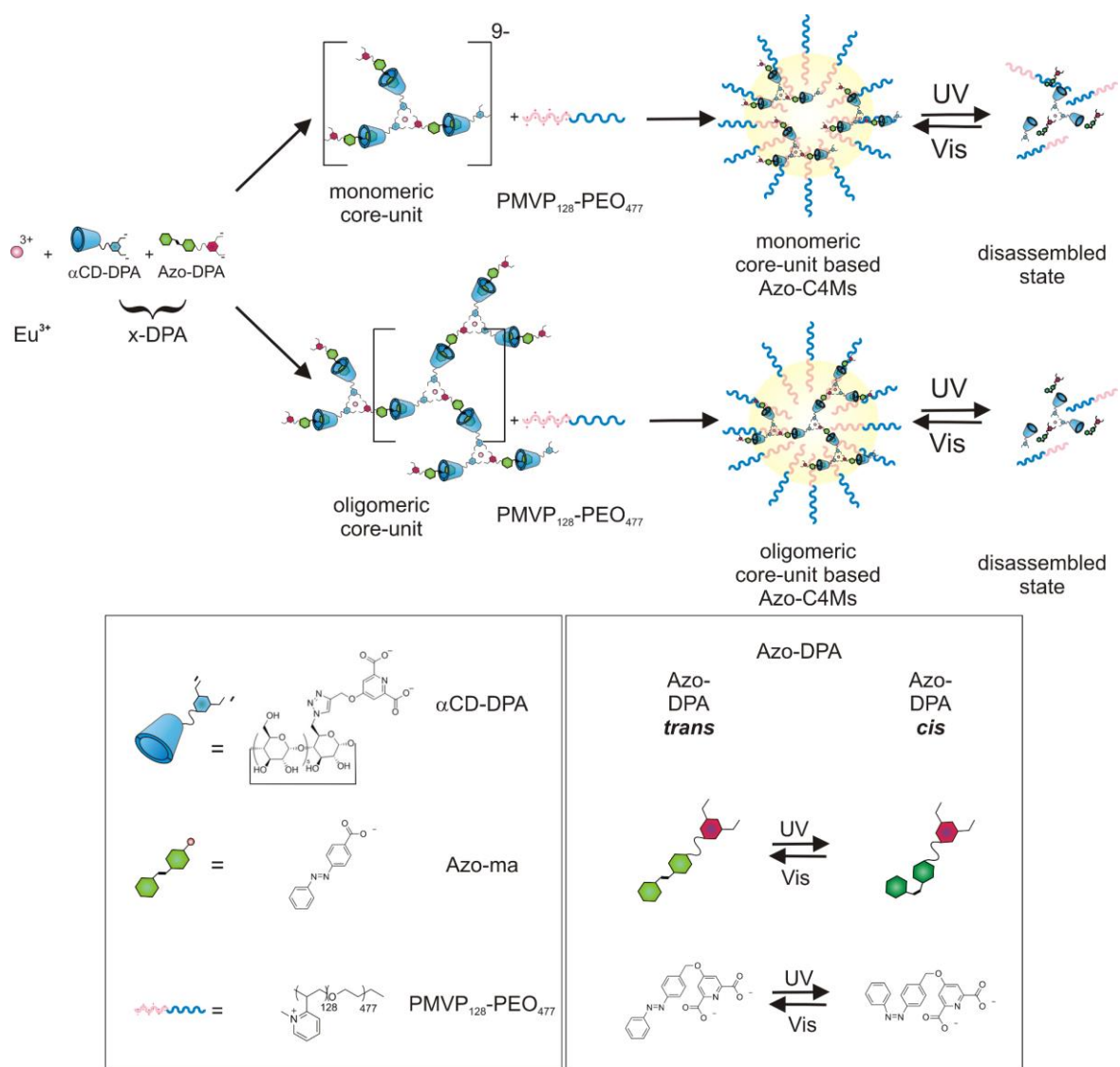
Polymeric micelles, which form through the self-assembly of block copolymers in a specific solvent, are well-investigated due to their potential applications from biomedical diagnostics and therapeutics to catalysis.[1-8] Responsive polymeric micelles, able to disassemble upon external triggers, are of growing interest.[9-11] Understanding the way to program and control these triggers might open a way to design advanced materials and devices, e.g. highly controlled drug delivery systems.[12] Within the available triggers, light has long been recognized as an ideal stimulus for the possibility of controlling in time and space and, in the last decade, the development of light-controllable block copolymer micelles has seen an increasing progress.[1, 13-15] Azobenzene, spiropyrene, nitrobenzyl-ester, coumarin and anthracene groups are the most used photoresponsive molecules for light-responsive micelles.[5, 13, 16] Especially azobenzene is one of the most studied photosensitive molecules, due to its reversible conformational change, activated by irradiating in the UV-Vis range.[17-20] This conformational change consists of an isomerization from *trans* to *cis* isomer, promoted by 365 nm irradiation, associated with a strong polarity change, from a dipole moment of 0 Debye to 3 Debye, respectively in the *trans* and *cis* form.[18] This isomerization can be reversed under visible light, restoring the *trans* isomer. Most of the light-responsive micelles reported in literature exploit this change in polarity to favor a mismatch in the hydrophobic-hydrophilic balance and trigger the micelle disassembly.[9, 21-26] The supramolecular interaction between azobenzene and  $\alpha$ cyclodextrin is well-reported as light-responsive host-guest couple ( $k_a$  ca.  $10^3$  M<sup>-1</sup>), due to the reversible release of the *cis* azobenzene from the  $\alpha$ cyclodextrin cavity, given visible light stimuli.[5, 12]

In this chapter, we synthesized two novel building blocks based on azobenzene and cyclodextrin, namely azobenzene-modified dipicolinic acid (Azo-DPA) and  $\alpha$ cyclodextrin-modified dipicolinic acid ( $\alpha$ CD-DPA), to form Azobenzene-based Cyclodextrin Complex Coacervate Core Micelles (Azo-C4Ms). We can control the assembly, disassembly and re-assembly of these Azo-C4Ms in a photo-controlled and unique fashion, not by changing the hydrophobic/hydrophilic balance, but rather by lowering the charge per core-unit number.

The formation of Azo-C4Ms relies on the combination of three different supramolecular orthogonal interactions, namely i) metal to ligand, between europium ions and dipicolinic acid ligands ii) host-guest, between cyclodextrins and azobenzene molecules, and iii) coacervate interactions between the negative charges in the core and the positively charged part of the block copolymer, (Scheme 5.1). By simply changing the ratio between the metal and the ligand, we can tune the core structure formation, from monomeric to oligomeric-based core-unit and, consequently, the light response.

In chapter 2, we determined the lower limit of the core-unit charge, required to form stable well-defined monomeric-based coacervate micelles.[27] We combine the low number of charges per core-unit with light-stimuli to promote the disassembly of Azo-C4Ms. Upon UV-light irradiation, the azobenzene isomerization to *cis* causes not only the disruption of the host-guest complex, but it also leaves the core with a too low number of charges to form stable and well-defined micelles. As we proved previously, coacervate micelles with a number of charges per core-unit below or equal to six are more prone to disassemble.[27] However, by shining visible-light, the *cis* azobenzene molecules isomerize back to the *trans* form, restoring the host-guest complex with cyclodextrin and, thus, driving the micelle re-assembly.

We show that we can drive, reversibly, the formation and the disassembly of azobenzene-based C4Ms, by controlling the number of charges per core-unit and the light-stimuli. We demonstrated that monomeric and oligomeric-based Azo-C4Ms have different responses towards light stimuli and that we can tune the response by lowering, additionally, the charge introducing an azobenzene-monoacid (Azo-ma). Preliminary studies with methyl red indicate that Azo-based C4Ms can be used to solubilize poorly water soluble dyes and trigger their release under precise light stimuli.



**Scheme 5.1.** Representation of the Azo-C4Ms formation. Europium ions are mixed with  $\alpha\text{CD-DPA}$  and Azo-DPA molecules to form the core-unit structures. The block copolymer addition, until charge neutralization, allows the formation of the final Azo-C4Ms structure. By adding 1:6 ratio of  $\text{Eu}:x\text{-DPA}$ , (with  $x\text{-DPA} = \alpha\text{CD-DPA} + \text{Azo-DPA}$ ), the formation of monomeric core-unit structures is favoured. While, by adding 1:6 ratio of  $\text{Eu}:x\text{-DPA}$ , we favour the formation of branched oligomeric core-unit structures. By shining UV-light, the azobenzene is isomerized to cis and removed from the cyclodextrin cavity, favouring the micelles dissociation. By shining visible light, the azobenzene isomerises back to trans, restoring the host-guest complex and the micelle re-assembly. In the box, all the building blocks, such as  $\alpha\text{CD-DPA}$ , Azo-DPA, Azo-ma, BP, including the reversible isomerization of Azo-DPA, are shown in their molecular structures and symbolic representations.

## 5.2. EXPERIMENTAL SECTION

In the following section, we provide the experimental details regarding Azo-C4Ms formation and reversible disassembly, driven by light-stimuli. Further analysis and controls can be found in the SI.

### 5.2.1. MATERIALS AND METHODS

$\alpha$ -cyclodextrin monoazide, triethylamine, tris[(1-benzyl-1H-1,2,3-triazol-4-yl)methyl]amine (TBTA), 4-(Phenylazo)benzoic acid and (E)-1-(4-(bromomethyl)phenyl)-2-phenyldiazene were purchased respectively from Cyclodextrin Shop, VWR, TCI, Sigma Aldrich and BOC Sciences and used without further purification. Europium(III) nitrate pentahydrate, copper iodide, diethyl 4-hydroxy 2,6-pyridinedicarboxylate, potassium carbonate and sodium carbonate were purchased from Sigma Aldrich and were used without further purifications. The block copolymer poly(N-methyl-2-vinylpyridine)-b-poly(ethylene oxide) (P2MVP<sub>128</sub>-b-PEO<sub>477</sub>) was purchased from Polymer Source and was quaternised following the procedure described elsewhere.[28] The degree of quaternisation was 80% and was determined by DLS titration.

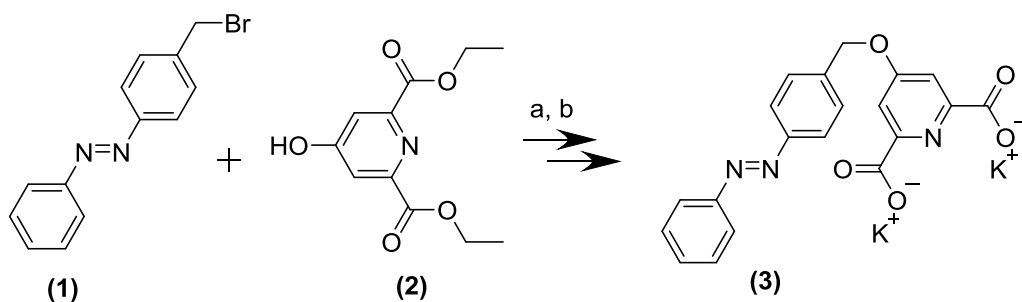
All NMR measurements were carried out at 298 K on a Bruker Avance III 400 MHz, 500 MHz, or 600 MHz NMR spectrometer with cryo-probe. Assignments were aided by COSY, HSQC, NOESY, and HMBC experiments. All mass spectra were acquired using ES ionization on a Thermo Finnigan LXQ Exactive Mass Spectrometer. Samples were prepared as a dilution series in methanol. Measurements were done from lowest to highest concentration until there was sufficient signal. Dynamic Light Scattering measurements (DLS) were carried out on a Malvern NanoSizer ZS, at 173 degree angle, operating at 632.8 nm at 25°C. Samples were incubated for at least two minutes at 25°C before measuring to reduce temperature dependent fluctuations. Measurements were averaged by three runs each consisting of six scans, ten seconds each. The size of the particles was determined using number based intensity. UV-Vis were measured with UV-1601 Shimadzu Spectrophotometer in 3 mL (1 cm) or 300  $\mu$ L (1 mm) quartz cuvettes.

Fluorescence spectroscopy measurements were carried out on an Agilent Cary Eclipse Fluorescence Spectrophotometer using quartz cuvettes of 1 cm path length, excitation and emission slits were set at 5 nm. Silica columns were prepared with silica of 40-63  $\mu\text{m}$ , 60  $\text{\AA}$ . For Cryo-TEM, samples were cast on copper grids (400 mesh - 150  $\mu\text{m}$  average hole size, Holey carbon), from Electron Microscopy Sciences (EMS, Hatfield, PA, USA). After blotting, samples were plunged into liquid ethane by using Vitrobot Mark IV instrument. Grids were then transferred to JEOL 1400 PLUS TEM operating at 120 kV.

## 5.2.2. SYNTHESIS

The synthesis of diethyl 4-(prop-2-yn-1-yloxy)pyridine-2,6-dicarboxylate was performed following the procedure described in literature.[27] The synthesis of azobenzene-modified dipicolinic acid and of pyridine-2,6-dicarboxylate modified  $\alpha$ -cyclodextrin are described in the following section, while their NMR assignments can be found in the SI.

### SYNTHESIS OF AZOBENZENE-MODIFIED DIPICOLINIC ACID (3)



**Scheme 5.2.** Synthesis of azobenzene-modified dipicolinic acid (Azo-DPA); a  $\text{K}_2\text{CO}_3$ , butanone,  $\text{N}_2$ ,  $85^\circ\text{C}$ , b  $\text{K}_2\text{CO}_3$ ,  $\text{H}_2\text{O}/\text{EtOH}$ ,  $80^\circ\text{C}$  refluxed.

Monobromo azobenzene (1) (0.50 g, 1.8 mmol), diethyl 4-hydroxypyridine-2,6-dicarboxylate (2) (1.66 g, 7.0 mmol) and  $\text{K}_2\text{CO}_3$  (1.00 g) were added in a 50 mL flask equipped with a stirring bar. Butanone (25 mL) was added and the mixture was put under  $\text{N}_2$ . The reaction mixture

was stirred at 85°C for 17 h and monitored with TLC (20% DCM in hexane). The butanone was evaporated under reduced pressure, DCM (20 mL) was added, the mixture was filtered and the solid was washed with DCM (20 mL). The liquid phase was evaporated under reduced pressure and the residue was re-crystallised from butanone (10 mL), to yield the pure orange crystals (0.48 g, 1.1 mmol, 60%).

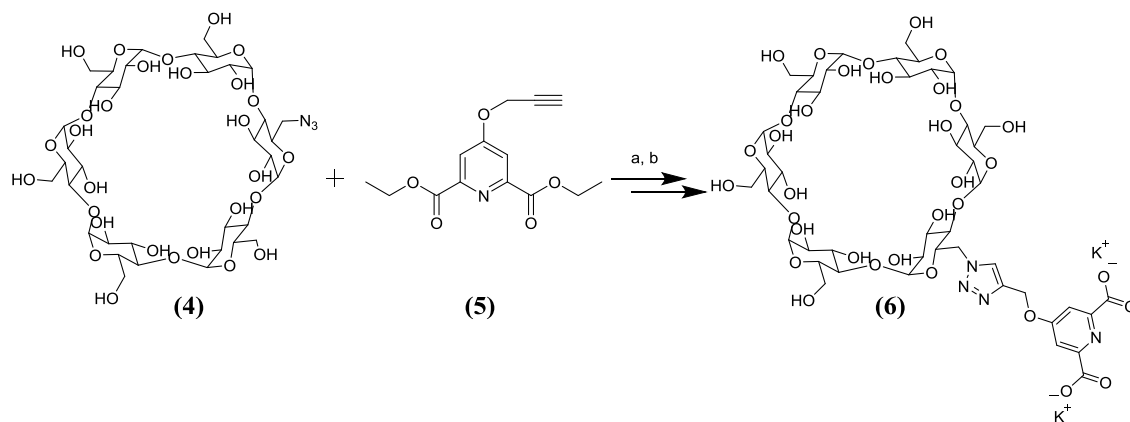
The latter (0.30 g, 0.7 mmol) and K<sub>2</sub>CO<sub>3</sub> (1.00 g) were added in a 50 mL flask equipped with a stirring bar. Water (10 mL) and ethanol (5 mL) were added and the mixture was refluxed at 80 °C for 17 h. To check the completion of the reaction, a small sample of the reaction mixture was taken and DCM was added, this DCM layer was spotted on TLC and run in 20% DCM in hexane to see if there was any starting material present. After the reaction was complete, ethanol was evaporated under reduced pressure and water (200 mL) was added to the reaction mixture until all the solid material was dissolved. The pH was slowly lowered to pH 6.7 with HCl (1 M). Next, the reaction mixture was put on ice and then filtered to yield the pure orange solid of **(3)** (0.12 g, 0.3 mmol, 46%).

<sup>1</sup>H-NMR (600 MHz, D<sub>2</sub>O), δ [ppm]: 7.94-7.84 (m, 4H, CH<sub>2</sub>-(C-2CH-2CH-C(ph))<sub>t</sub>), N-(C-2CH-2CH-CH(ph))<sub>t</sub>, 7.84-7.70 (m, 2H, CH<sub>2</sub>-(C-2CH-2CH-C(ph))<sub>t</sub>), 7.68-7.56 (m, 5H, CH(pyr)<sub>t</sub>, N-(C-2CH-2CH-CH(ph))<sub>t</sub>), N-(C-2CH-2CH-CH(ph))<sub>t</sub>, 7.56-7.51 (s, 2H, CH(pyr)<sub>c</sub>), 7.51-7.43 (m, 2H, CH<sub>2</sub>-(C-2CH-2CH-C(ph))<sub>c</sub>), 7.33-7.22 (m, 3H, N-(C-2CH-2CH-CH(ph))<sub>c</sub>, N-(C-2CH-2CH-CH(ph))<sub>c</sub>), 7.01-6.96 (m, 2H, CH<sub>2</sub>-(C-2CH-2CH-C(ph))<sub>c</sub>), 6.95-6.89 (m, N-(C-2CH-2CH-CH(ph))<sub>c</sub>).

<sup>13</sup>C-NMR (600 MHz, D<sub>2</sub>O), δ [ppm]: 172.5 (pyr-C=O), 166.6 (O-C(pyr)), 155.2 (C(pyr)), 152.1 (CH<sub>2</sub>-(C-2CH-2CH-C(ph))<sub>t,c</sub>), N-(C-2CH-2CH-CH(ph))<sub>t,c</sub>), 139 (CH<sub>2</sub>-(C-2CH-2CH-C(ph))<sub>t</sub>), 131 (N-(C-2CH-2CH-CH(ph))<sub>t</sub>), 129.5 (N-(C-2CH-2CH-CH(ph))<sub>t</sub>), 128.8 (CH<sub>2</sub>-(C-2CH-2CH-C(ph))<sub>t</sub>), 128.5 (CH<sub>2</sub>-(C-2CH-2CH-C(ph))<sub>c</sub>), 122.7 (CH<sub>2</sub>-(C-2CH-2CH-C(ph))<sub>t</sub>), 122.3 (N-(C-2CH-2CH-CH(ph))<sub>t</sub>), 120.9 (CH<sub>2</sub>-(C-2CH-2CH-C(ph))<sub>c</sub>), 120.7 (N-(C-2CH-2CH-CH(ph))<sub>c</sub>), 112 (CH(pyr))<sub>c</sub>, 111.6 (CH(pyr))<sub>t</sub>, 69.7 (CH<sub>2</sub>-O-pyr).

The calculated isotropic mass [M-H]<sup>-</sup> for **3**, M= C<sub>20</sub>H<sub>15</sub>N<sub>3</sub>O<sub>5</sub> is 376.10. The experimental mass is 376.09 ([M-H]<sup>-</sup>).

## SYNTHESIS OF PYRIDINE-2,6-DICARBOXYLATE-MODIFIED $\alpha$ CYCLODEXTRIN (**6**)



**Scheme 5.3.** Synthesis of the pyridine-2,6-dicarboxylate-modified  $\alpha$ -cyclodextrin (**6**); a)  $H_2O$ , THF, TBTA, CuI, b)  $K_2CO_3$ ,  $H_2O$ ,  $70^\circ C$ .

Compound **6**, pyridine-2,6-dicarboxylate-modified  $\alpha$ -cyclodextrin, was prepared by adjusting the procedure in literature for  $\beta$ -cyclodextrin.[27] The synthesis was adjusted by using  $\alpha$ -cyclodextrin instead of  $\beta$ -cyclodextrin and by leaving the reaction for four hours, instead of overnight.

THF and water were purged with nitrogen for two hours. Compound **4** (100 mg, 0.10 mmol) was mixed in a 100 mL round bottom flask with water (20 mL) and THF (10 mL). To this flask, **5** (55 mg, 0.20 mmol), TBTA (6 mg, 0.01 mmol) and CuI (38 mg, 0.20 mmol) were added. The reaction was left stirring under  $N_2$ -atmosphere for four hours and the reaction was monitored with TLC. The volume of the reaction mixture was reduced to 5 mL, by concentrating it *in vacuo*. The crude reaction mixture was added directly to a reversed phase C18 silica column (water: methanol from 2:1 to 1:1).

The purified intermediate (27 mg, 0.02 mmol) was deprotected by dissolving it and  $K_2CO_3$  (41 mg, 0.60 mmol) in water (20 mL). The reaction was heated to  $70^\circ C$  and left stirring overnight. After concentration *in vacuo*, the product (**6**) was purified by dialysis (MW cut-off

500-1000 KDa) over three days, replacing the water twice a day. Water was evaporated. The final yield was 27 mg (21%, 0.02 mmol).

<sup>1</sup>H-NMR spectrum (600 MHz, D<sub>2</sub>O),  $\delta$ [ppm]: 8.17 (s, 1H, CH triaz.), 7.75 (s, 2H, CH pyr), 5.37 (s, 2H, pyr O-CH<sub>2</sub>), 5.09 (d,  $J=3.6$  Hz, 1H, H<sub>1''</sub>), 5.05 (m, 1H, H<sub>6f,g</sub>), 5.03-4.96 (m, 5H, H<sub>1</sub>), 4.95-4.91 (m, 1H, H<sub>1'</sub>), 4.87-4.91 (m, 1H, H<sub>6f,g</sub>), 4.14 (t,  $J=19$  Hz, 1H, H<sub>5'</sub>), 4.0-3.70 (m, 20H, H<sub>6</sub> H<sub>5</sub> H<sub>3</sub>), 3.69-3.39 (m, 16H, H<sub>2</sub> H<sub>4</sub>), 3.10 (d,  $J=13$  Hz, 1H, H<sub>6''f</sub>), 2.74 (d,  $J=11$  Hz, 1H, H<sub>6''g</sub>).

The calculated isotropic mass [M-H]<sup>2-</sup> for **6**, M= C<sub>47</sub>H<sub>68</sub>N<sub>4</sub>O<sub>35</sub> is 623.18. The experimental mass is 623.80 ([M-H]<sup>2-</sup>).

### 5.2.3. MICELLE PREPARATION

The micelles used in these experiments were prepared using a general protocol (scheme 5.1).[15] First stock solutions of the individual components were prepared: Eu<sup>3+</sup> (5 mM),  $\alpha$ CD-DPA (5 mM), Azo-DPA (5 mM), block copolymer P2MVP<sub>128</sub>-b-PEO<sub>477</sub> (10 mM charge concentration) and MES buffer (200 mM). Micelles were prepared at room temperature in a final volume of 0.2 mL, under sonication. First water and MES buffer (pH 7) were added, at a final concentration of 20 mM. The Eu coordination complex is formed by adding a fixed amount of x-DPA. In this case a DPA moiety is attached both on the host (cyclodextrin) and on the guest (azobenzene) making the total amount of DPA (x-DPA) equal to  $\alpha$ CD-DPA + Azo-DPA. The europium coordination complex is, therefore, based on a dynamic equilibrium between the  $\alpha$ CD-DPA and the Azo-DPA ligand, forming these possible structures: [Eu (Azo-DPA)<sub>3</sub>], {Eu [(Azo-DPA)<sub>2</sub> ( $\alpha$ CD-DPA)]}, {Eu [(Azo-DPA) ( $\alpha$ CD-DPA)<sub>2</sub>]} and [Eu ( $\alpha$ CD-DPA)<sub>3</sub>]. To form monomeric core-units, a ratio of Eu/x-DPA 1:6 is needed, and this is formed by using a ratio of Eu:( $\alpha$ CD-DPA + Azo-DPA) 1: (3 + 3). In the second case, a ratio of Eu/x-DPA of 1:3 is required to form oligomeric core-units, and this is achieved by using a ratio of Eu:( $\alpha$ CD-

DPA + Azo-DPA 1:(1.5 + 1.5). Lastly the block copolymer was added until charge neutralization, as shown in Scheme 5.1, after the stock solution was sonicated for at least 10 minutes. Each stock solution was vortexed before the addition of the components. Micelles were always prepared freshly before the characterization. During all experiments, the concentration of the components was fixed to be higher than the CMC to prevent the equilibrium from shifting from micelles towards monomers.

The stability experiment was designed to weaken the structure of monomeric-based Azo-C4Ms and make them more prone to disassemble, by substituting Azo-DPA with Azo-ma. The micelle solution was prepared by mixing europium ions with  $\alpha$ -cyclodextrin-DPA in the same ratio as the procedure for the monomeric based Azo-C4Ms described above. To the coordination complex, Azo-ma/Azo-DPA were added in different ratios, such as 33%, 90% and 100%. Finally, the block copolymer was added to the core-unit, to form the desired micelle. All the parameters, such as pH, order of addition, sonication and temperature were kept the same as the preparation of the conventional Azo-C4Ms. Azo-ma stock solution was prepared at a concentration of 5 mM.

## 5.2.4. LIGHT TREATMENT

UV Irradiation experiments were conducted using a HeroLab UV-8S/L UV-lamp at 365 nm. The UV-Lamp was placed under a home-made box, equipped with a black cover, to avoid external light interference. 1 mL of micelle solution in a quartz cuvette was placed under the UV-lamp 5-10 cm away from the lamp, for different times. For the visible light irradiation, the cuvettes were placed at day light in the open lab space. The micelle size and intensity were monitored by DLS and Cryo-TEM. The isomerization transition was monitored by UV-Vis spectroscopy.

## 5.2.5. METHYL RED ENCAPSULATION

A stock solution of 0.15 mM methyl red was prepared by dissolving the powder in ultrapure water. The encapsulation of methyl red dye was achieved by mixing first europium ions and  $\alpha$ -cyclodextrin-DPA and, secondly, the dye and the Azo-DPA. The block copolymer was added as last component for the micelle formation. For the release experiment, a water/DCM biphasic system (1:1, 2 mL) was prepared in two glass vials. Micelles were added to both vials. One vial was treated with 10 min 365 nm light, while the other was kept in the dark and considered the control.

## 5.3. RESULTS AND DISCUSSION

In this section the formation, characterization and light-response of Azo-based C4Ms are presented. First, we start describing the new micellar subcomponents, the synthesis and characterization of Azo-DPA and  $\alpha$ CD-DPA .

### 5.3.1. MICELLE CHARACTERIZATION

Azo-based C4Ms were first constructed by mixing europium and x-DPA ligands ( $\alpha$ CD-DPA + Azo-DPA) to form the metal-to-ligand coordination, as shown in Scheme 5.1. The coordination between the europium and the ligand is based on a dynamic equilibrium between the  $\alpha$ CD-DPA and the Azo-DPA ligand, forming these possible structures: [Eu (Azo-DPA)<sub>3</sub>], {Eu [(Azo-DPA)<sub>2</sub> ( $\alpha$ CD-DPA)]}, {Eu [(Azo-DPA) ( $\alpha$ CD-DPA)<sub>2</sub>]} and [Eu ( $\alpha$ CD-DPA)<sub>3</sub>]. Fluorescence spectroscopy was used to confirm the metal-to-ligand coordination structure, by showing the europium emission upon DPA ligand excitation at 280 nm (antenna phenomenon, Figure S5.4). The host-guest complex between azobenzene and  $\alpha$ cyclodextrin molecules formed the so called “core-unit” structures. By simply changing the ratio between europium and DPA ligand, the core-unit structure can be tuned between monomeric and oligomeric, as shown in Scheme 5.1.[27, 29] The association constant between azobenzene and  $\alpha$ cyclodextrin molecules is already well-reported in literature ( $k_a$   $3 \cdot 10^4$  M<sup>-1</sup>). [12, 30] We confirmed the complex formation by using DOSY, which showed the same diffusion coefficient between the CD and the *trans* azobenzene molecules (Figure S5.5). In Figure S5.5 the *cis* and the *trans* diffusion coefficients of the azobenzene molecule are well-separated, indicating that only the *trans* molecule form a complex with the cyclodextrin. The addition of the block copolymer to the host-guest complex neutralizes the negative charges in the core and allows the formation of Azobenzene-based Cyclodextrin-based Complex Coacervate core Micelles, or Azo-C4Ms. The size of Azo-C4Ms was measured by using DLS and Cryo-TEM. The hydrodynamic radius was found around 40 nm (SD 8 nm) for both monomeric and

oligomeric-based Azo-C4Ms (Figure 5.1.). The fact that the size does not change by varying the core structure is not uncommon for coacervate micelles. It was already reported that by changing the type of metal-to-ligand coordination or by increasing the dendrimer generation in the core, the size of these coacervate micelles was constant.[29, 31] The Cryo-TEM pictures show similar sizes compared to the DLS and confirmed the spherical shape. Surprisingly, Figure 5.1. c) and d) show a well-organized distribution of micelles, almost perfectly spaced between each other, similarly to a crystal lattice structure. This result is not common for coacervate micelles, that often experience a size-sorting distribution on biconcave layer of the Cryo-TEM grid.[32, 33] Only few comparable structures to the ones in Figure 5.1. were reported in literature and described as micellar photonic crystals (MPC) or micellar photonic fluids (MPF), for their crystalline core structures.[34, 35]

The Critical Micelle Concentration (CMC) for Azo-C4Ms is measured by DLS, by diluting the micelle solution with MES buffer and by monitoring the intensity and size decays (Figures S5.7. and S5.8.). The CMC was found to be ca 32  $\mu\text{M}$  and 47  $\mu\text{M}$  for monomeric and oligomeric, respectively. The Critical Salt Concentration (CSC) was determined by titrating NaCl salt to the two types of Azo-C4Ms and by monitoring the intensity and size changes by DLS, (Figure S5.9. and S5.10.). The CSC results show that oligomeric Azo-C4Ms are twice more stable to salt, compared to monomeric-based Azo-C4Ms, respectively around 600 mM and 300 mM of NaCl. These CMC and CSC results indicate that Azo-C4Ms are more stable against dilution and ionic strength, than similar C4Ms.[27] These improvements in stability can be attributed to the introduction of the azobenzene moiety to the C4Ms, which can increase the driving force of the self-assembly process, resulting in the micelle formation at low component concentration or at high salt concentration.[36]

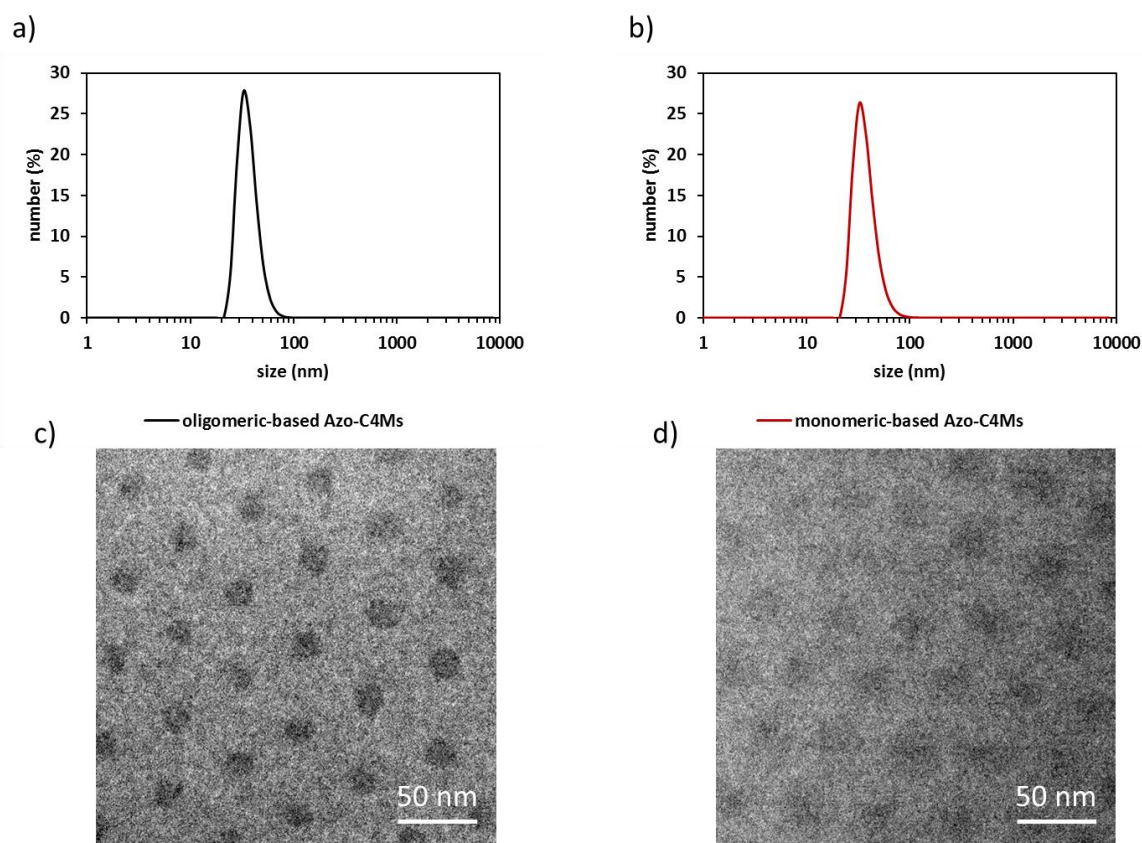


**Figure 5.1.** Size distribution of oligomeric a) and monomeric b) core-unit based Azo-C4Ms at the DLS. Cryo-TEM images of oligomeric c) and monomeric d) core-unit based Azo-C4Ms.

### 5.3.2. LIGHT-RESPONSE

In the following section, the photo-response behavior of Azo-C4Ms was studied upon subsequent exposure to UV and Vis light. Prior to irradiation, the Azo-DPA is present in the solution mainly in its most stable form, the *trans* form. Figure S5.11. shows the two characteristic absorption peaks of the azobenzene, i) at 325 nm belonging to the *trans*  $\pi$ - $\pi^*$  transition and ii) at 430 nm, belonging to the *cis*  $n$ - $\pi^*$  transition.[18] Upon irradiating both micelle solutions for 2 minutes with UV light, the absorption band at 325 nm decreases significantly, while the 430 nm peak increased. This change is attributed to the isomerization of the *trans* peak to *cis* form. By exposing the micelle solutions to 30 min of UV light, no significant additional decrease of the *trans* peak is visible, compared to the 2 minutes irradiation. This result proves that the isomerization required only ca. 2 minutes and that it is not 100% *trans* to *cis* conversion, but rather ca. 80%. Upon consequently exposing it to

visible light for 6 minutes, the absorption band at 325 nm reappeared, indicating that the *cis* peak isomerized back to *trans*. This experiment was repeated for multiple cycles to confirm the isomerization reversibility. Similar kinetics were found for monomeric and oligomeric Azo-C4Ms (Figure S5.11.-S5.13. and S5.15.). These results indicated that the isomerization of the Azo molecule occurs for all the sample and that it is reversible.

After UV-exposure, monomeric and oligomeric Azo-C4Ms were measured with DLS and Cryo-TEM techniques. Both techniques showed similar sizes, compared to the ones prior irradiation, around 42 nm (SD 7 nm), as shown in Figure S5.14. For other types of light-responsive micelles the shift in the hydrophobic/hydrophilic balance can trigger the swelling or the deformation of the micelles, by changing the polarity of the azobenzene.[1, 5, 37] This increase in polarity does not alter significantly the core size structures.[1, 13] However, in some cases this small change could still be exploited to release some cargoes.[24] Despite the fact that the size remained the same, a 20% decrease in intensity was visible for the monomeric-based Azo-C4Ms (Figure 5.2.). While, oligomeric -based Azo-C4Ms showed a difference in intensity of only 10%. The intensity decrease might be caused by the partial cleavage of the micelles, which would lead to a small loss in the count number. These findings suggested that, even if the azobenzene isomerizes to *cis* and the host-guest complex dissociates, Azo-C4Ms cannot be destabilized until complete disassembly.

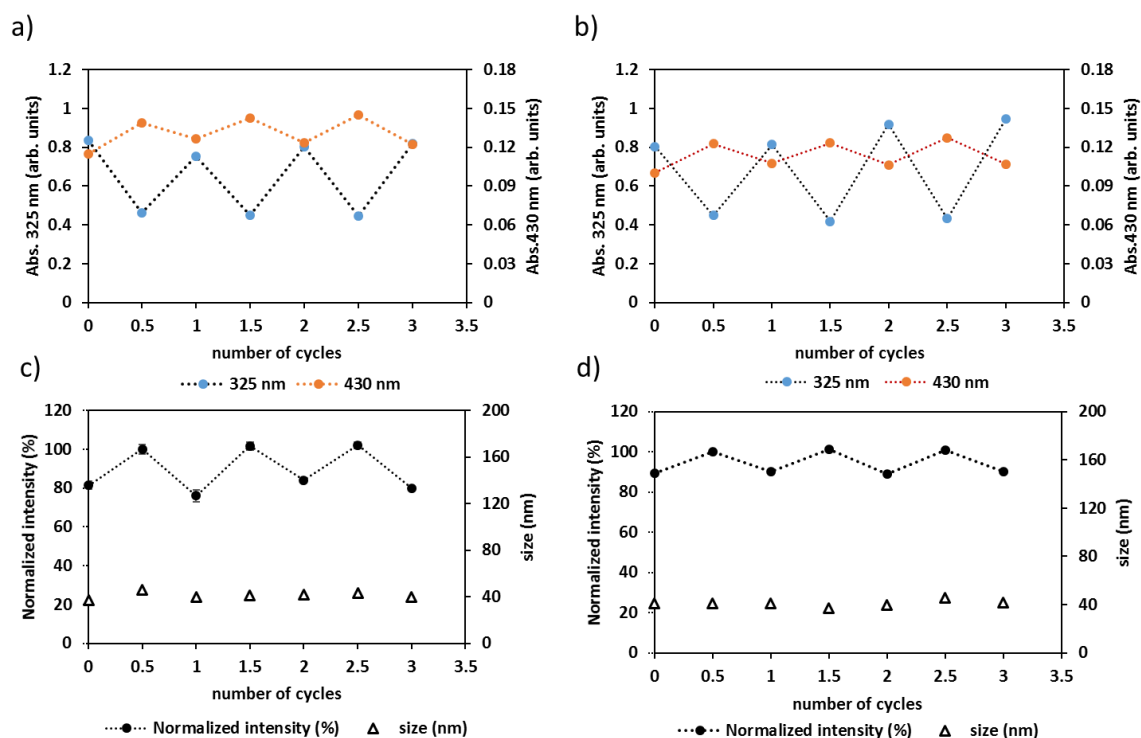


**Figure 5.2.** Light response of a), c) oligomeric and b), d) monomeric core-unit-based Azo-C4Ms at the UV-Vis (top) and at the DLS (bottom),

### 5.3.3. INCREASING DISASSEMBLY

In order to boost the micelle instability and disassembly, we exploited the knowledge acquired on the lower limit of core-unit charges.[27] From our previous work, we determined the lowest limit of core-unit charges required to form stable and well-defined structures. By lowering the number of charges of the monomeric core-unit from 9- to 6-, we can expect to weaken the Azo-C4Ms and favor the micelle disassembly under light stimuli. For this goal, we substituted the Azo-DPA with an azobenzene monoacid (Azo-ma), as shown in Scheme 5.1. The Azo-ma does not allow the formation of branched oligomeric structures and favors the formation of a core-structure with lower number of charges. By increasing the ratio between Azo-ma/Azo-DPA, we can form Azo-C4Ms with a progressively lower number of charges per core-unit. Figure S5.16 shows that by substituting 33% of Azo-DPA with Azo-ma, the difference in intensity between the two isomers is 35%, considerably higher than the difference of the monomeric and oligomeric Azo-C4Ms (Figure 5.3.). By substituting 90% and

100% of Azo-DPA with Azo-ma, the disassembly is even more marked, than at low substitution percentage. However, the results in Figure S5.16. shows that the size does not remain stable over the cycles and is considerably higher, compared to oligomeric and monomeric-based Azo-C4Ms. This result might be related to the formation of not-well defined rather big aggregates, as observed for micelles with low number of charges per core-units.[27]

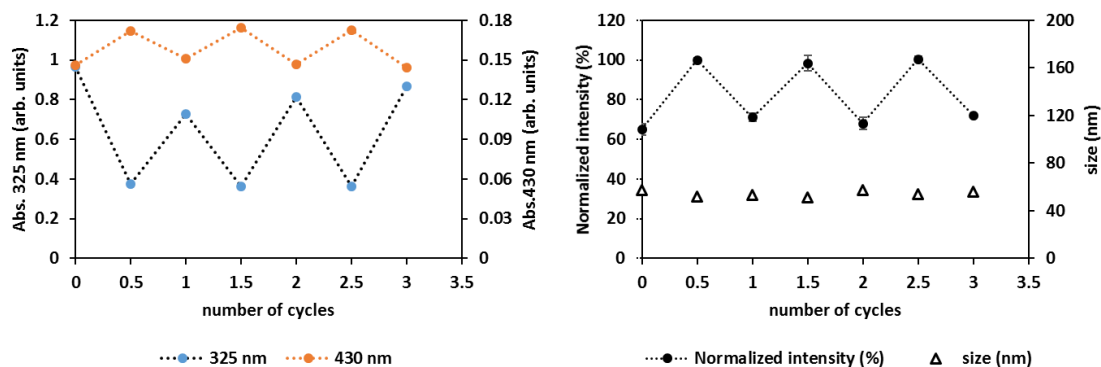


**Figure 5.3.** Left: UV-Vis cycle of Azo-C4Ms in which 33% of Azo-DPA was substituted with Azo-ma; the absorption at 325 nm and 430 nm is plotted over the number of repeated cycles. Right: DLS cycle of Azo-C4Ms in which 33% of Azo-DPA was substituted with Azo-ma, in which the intensity and the size are plotted over the number of repeated cycles.

### 5.3.4. ENCAPSULATION AND RELEASE

Methyl red was selected as a hydrophobic model dye to study the ability of Azo-C4Ms to encapsulate and release cargoes under light stimuli. A water-DCM biphasic system was used as a direct visualization method. First, Figure 5.4. shows that Azo-C4Ms are indeed able to solubilize the MR dye in the water phase (upper part of the vial). Second, given 10 minutes of UV light, the MR was released from the Azo-C4Ms and transferred into the organic phase, Figure 5.4. a. This preliminary result suggested that Azo-C4Ms can encapsulate poor water-soluble dyes and release them upon light stimuli.

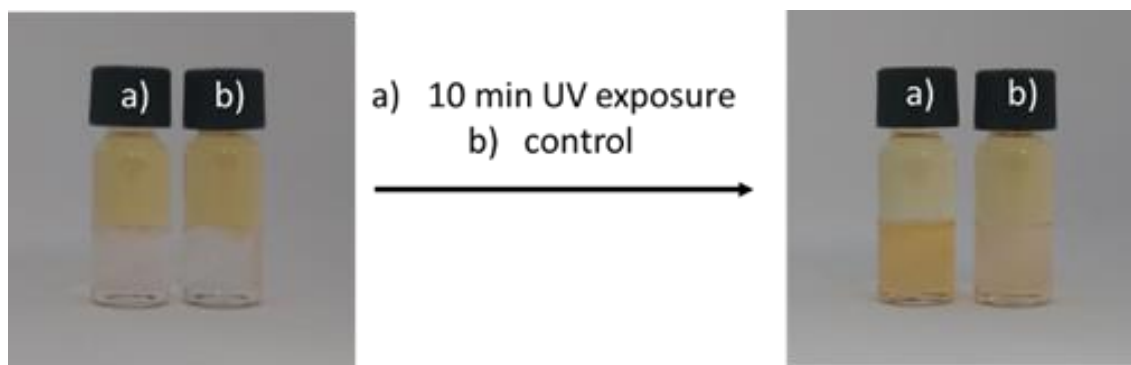


**Figure 5.4.** Sequential pictures of monomeric Azo-C4Ms in a biphasic system of water and DCM, before and after UV-light treatment. Vial a) was treated with UV-light for 10 minutes, while vial b) was kept in the dark for 10 minutes and used as control.

## 5.4. CONCLUSION

Here, a novel azobenzene-modified dipicolinic acid molecule was successfully synthesized to form azobenzene-based Cyclodextrin Complex Coacervate Core Micelles of 40 nm. The disassembly of these micelles was finely controlled by combining a low charge per core-unit with an UV-light trigger. By simply varying the europium to ligand ratio, we tuned the core structure, from monomeric to oligomeric-based core-unit, and, consequently, the stability against light stimuli. Preliminary studies on methyl red indicated that these micelles are able to encapsulate poor water-soluble dyes and to release them upon exposure to UV-light. Azobenzene-based Cyclodextrin-based Complex Coacervate Core Micelles might have promising application, e.g. light-controlled drug delivery.

## 5.5. SUPPORTING INFORMATION

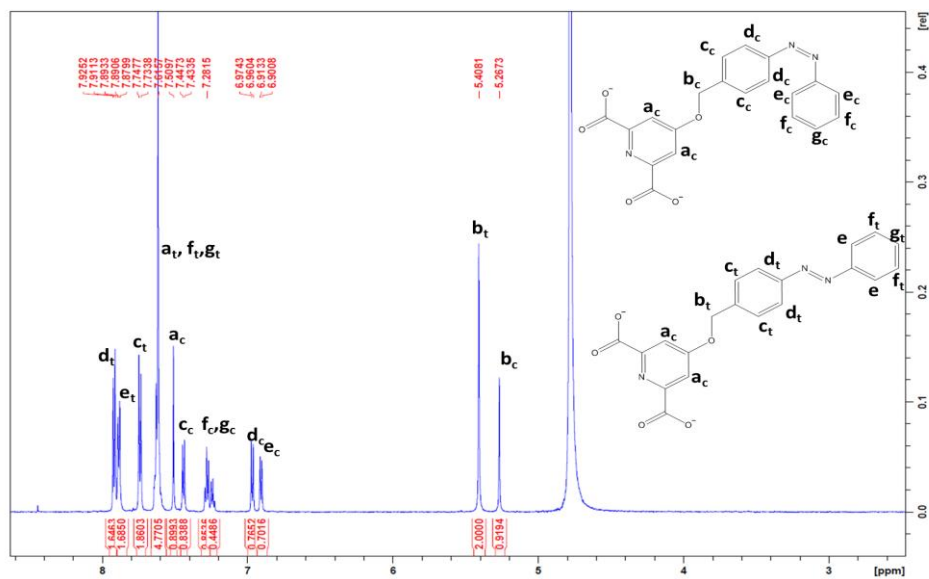


Figure S5.1.  $^1\text{H-NMR}$  of (e)-4-((4-(phenyldiazenyl)benzyl)oxy)pyridine-2,6-dicarboxylic acid (**3**) in  $\text{D}_2\text{O}$ .

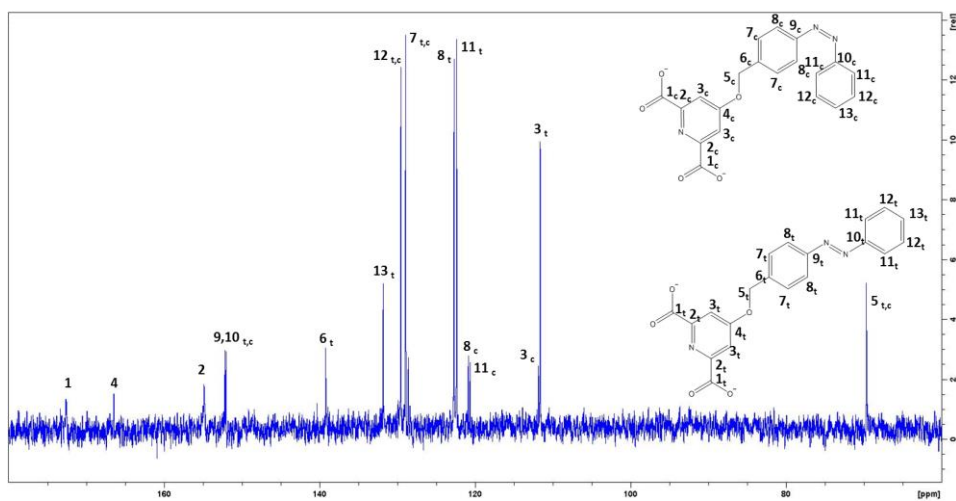
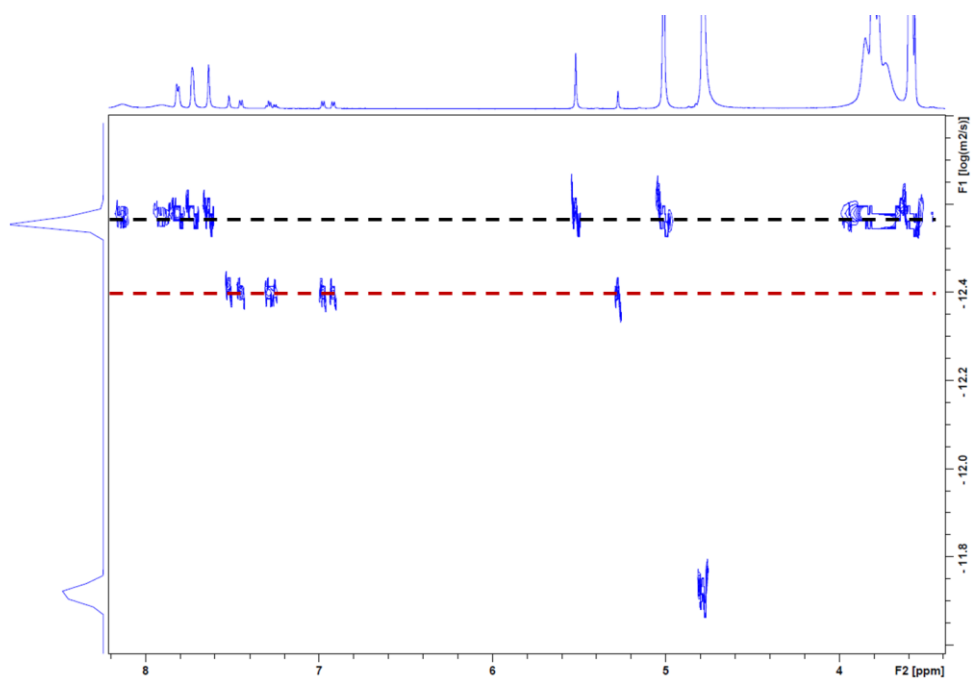
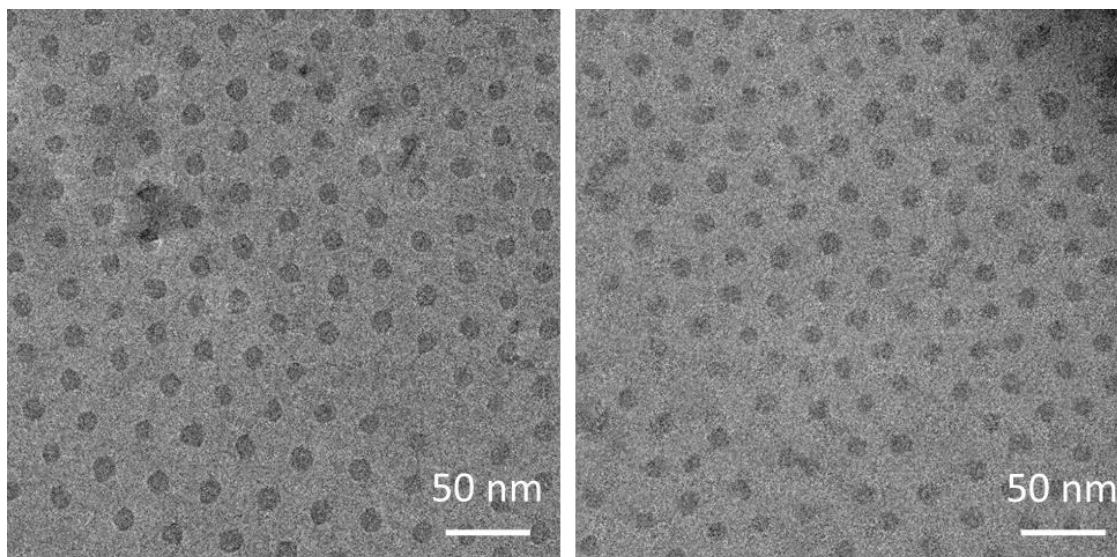


Figure S5.2.  $^{13}\text{C-NMR}$  of (e)-4-((4-(phenyldiazenyl)benzyl)oxy)pyridine-2,6-dicarboxylic acid (**3**) in  $\text{D}_2\text{O}$ .





**Figure S5.5.** DOSY of oligomeric core-unit in  $D_2O$ . Pyridine-2,6-dicarboxylate-modified cyclodextrin (6) and trans azobenzene guest have similar diffusion coefficient (black line), while cis azobenzene does not couple with aCD (red line).



**Figure S5.6.** Cryo-TEM pictures of oligomeric (left) and monomeric (right) based Azo-C4Ms.

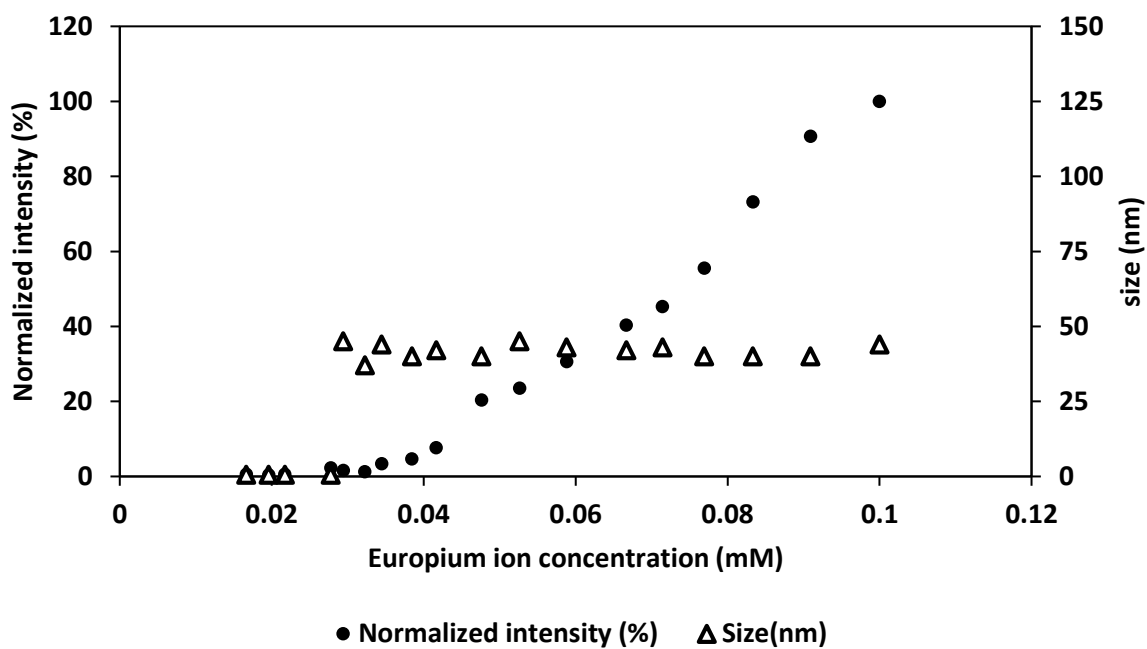


**Figure S5.7.** Critical Micelle Concentration (CMC) of the monomeric micelles with Europium ion concentration (mM) plotted against Intensity (kcps).

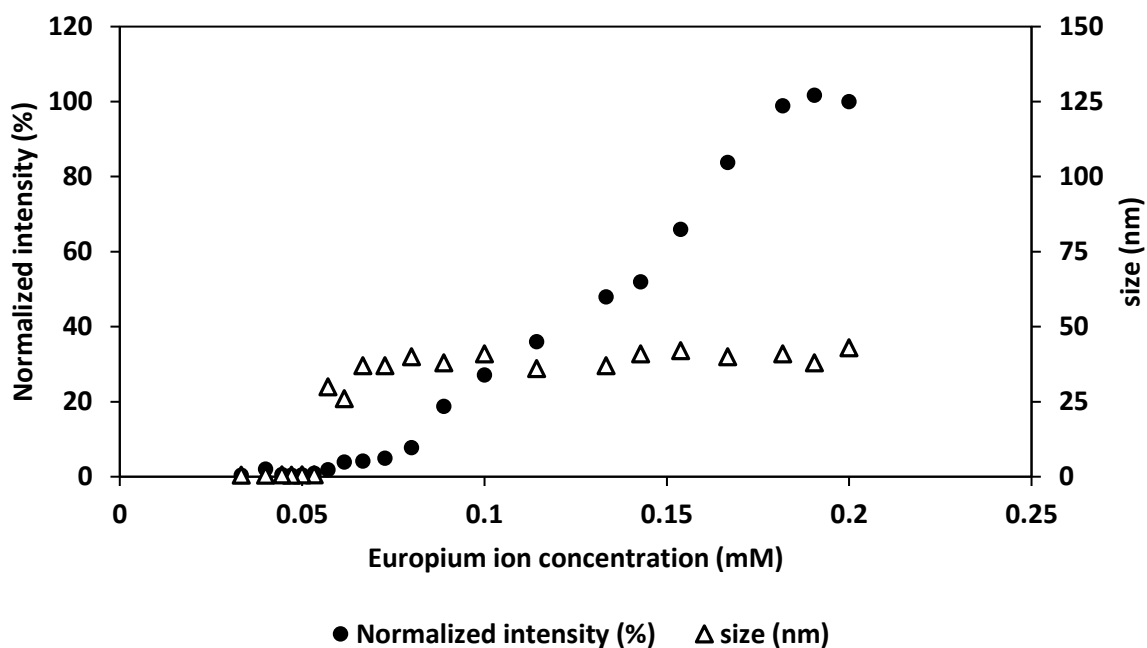


**Figure S5.8.** Critical Micelle Concentration (CMC) of the oligomeric micelles with Europium ion concentration (mM) plotted against Intensity (kcps) and size (nm).

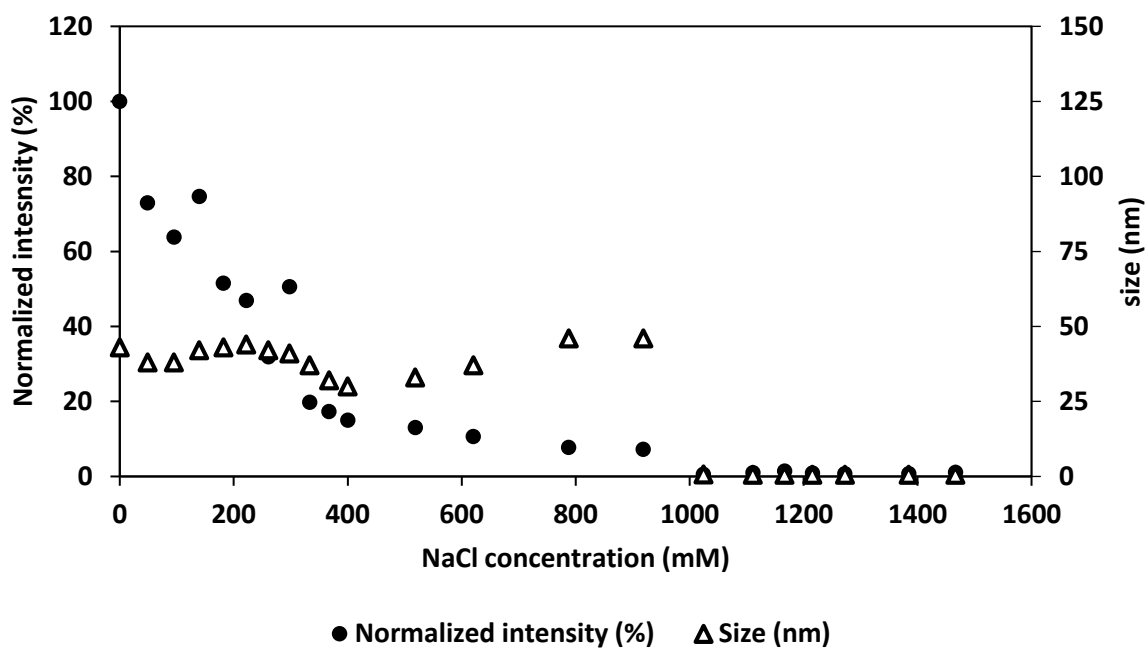


**Figure S5.9.** Critical Salt Concentration (CSC) of the monomeric micelles with NaCl concentration (mM) plotted against intensity (%).

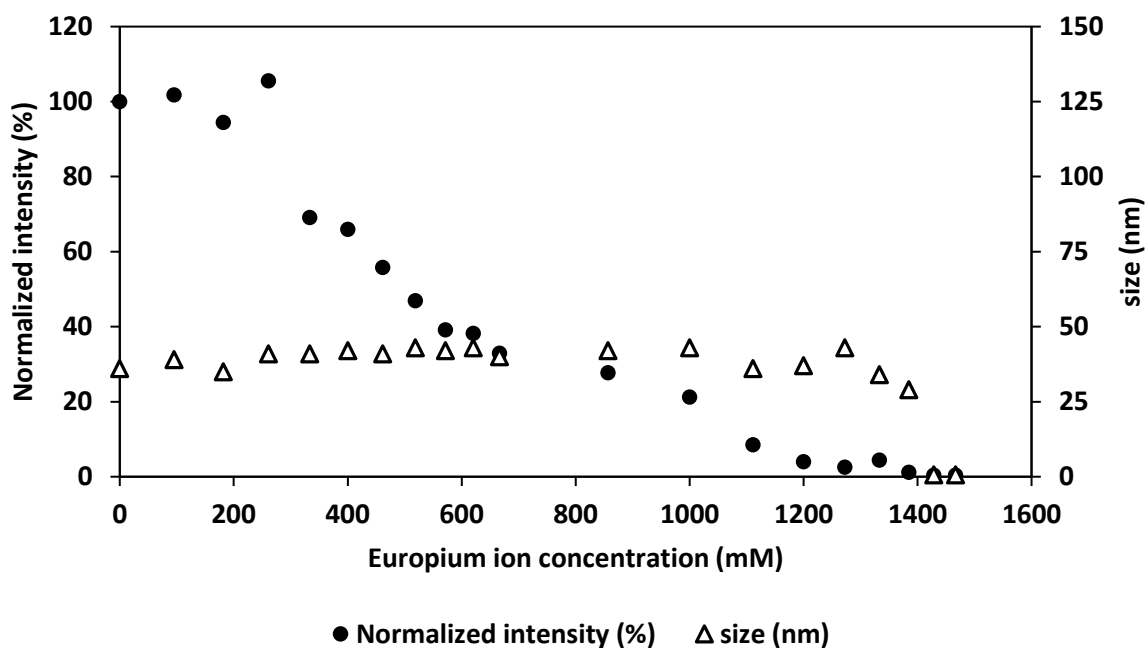


**Figure S5.10.** Critical Salt Concentration (CSC) of the oligomeric micelles with NaCl concentration (mM) plotted against Intensity (%).

Light-response studies

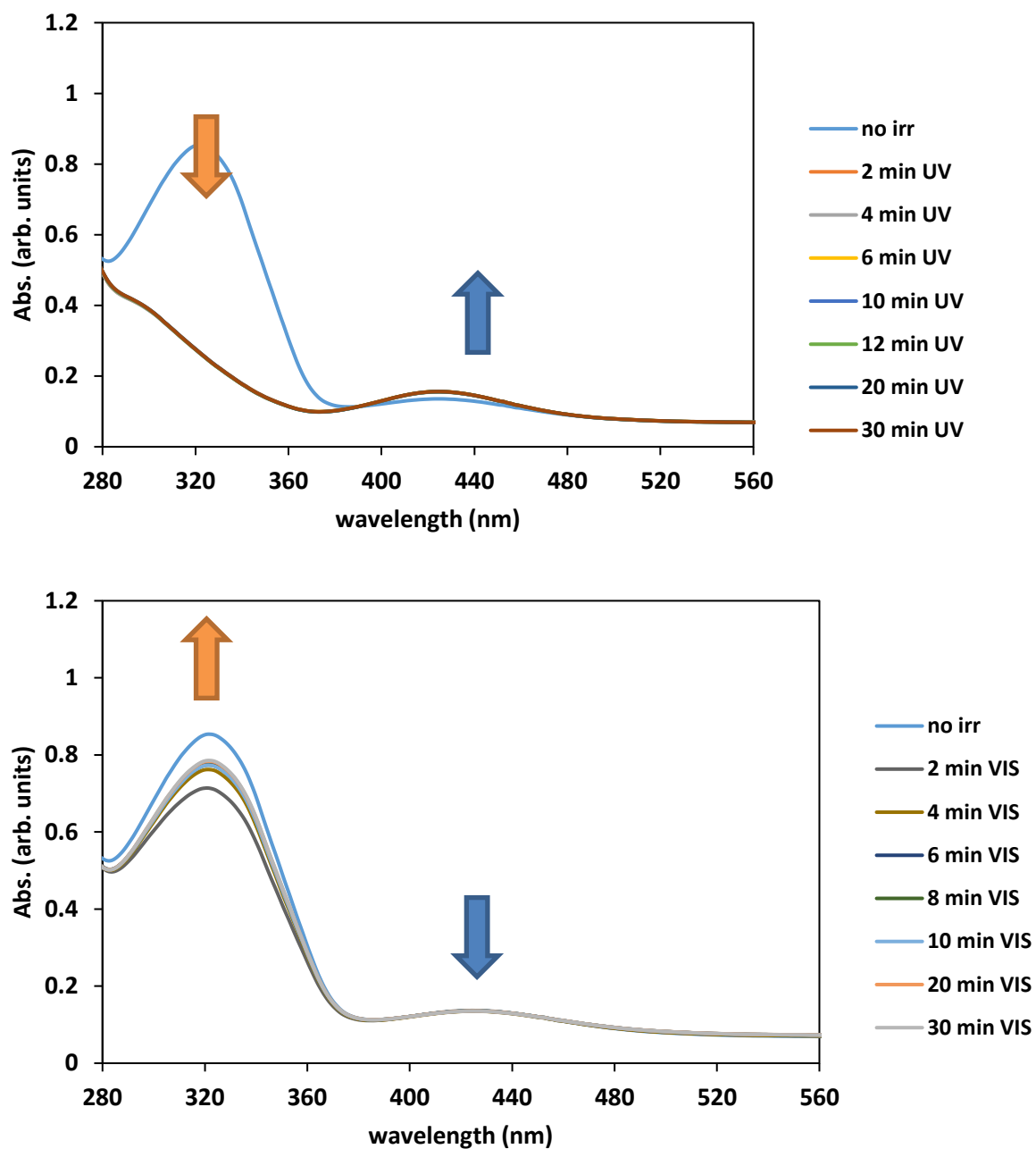
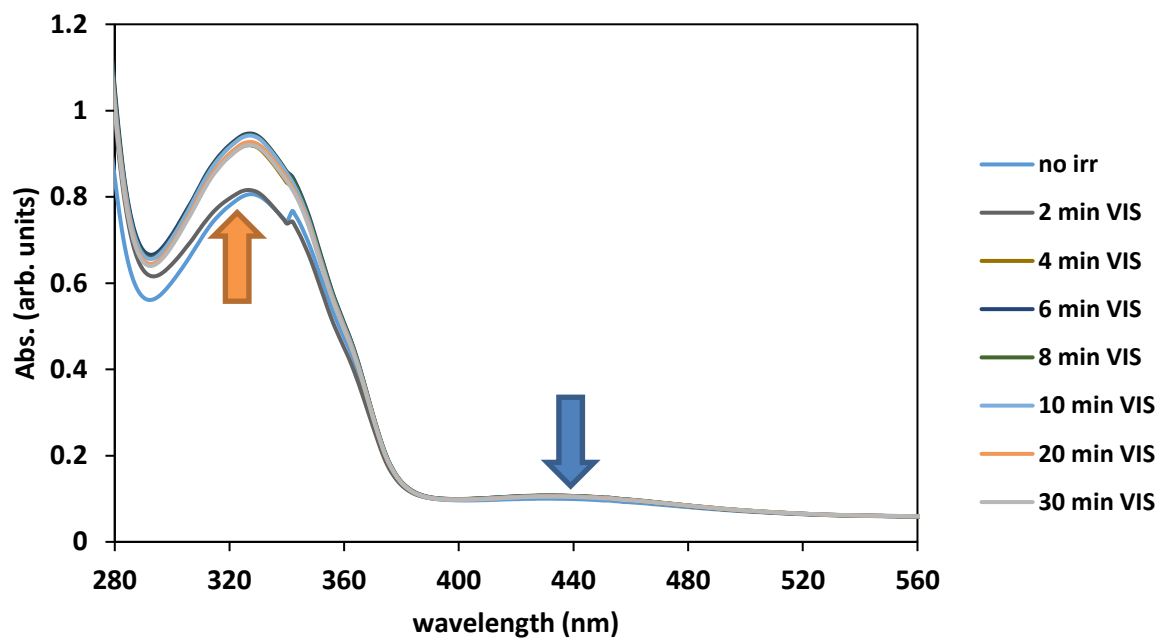
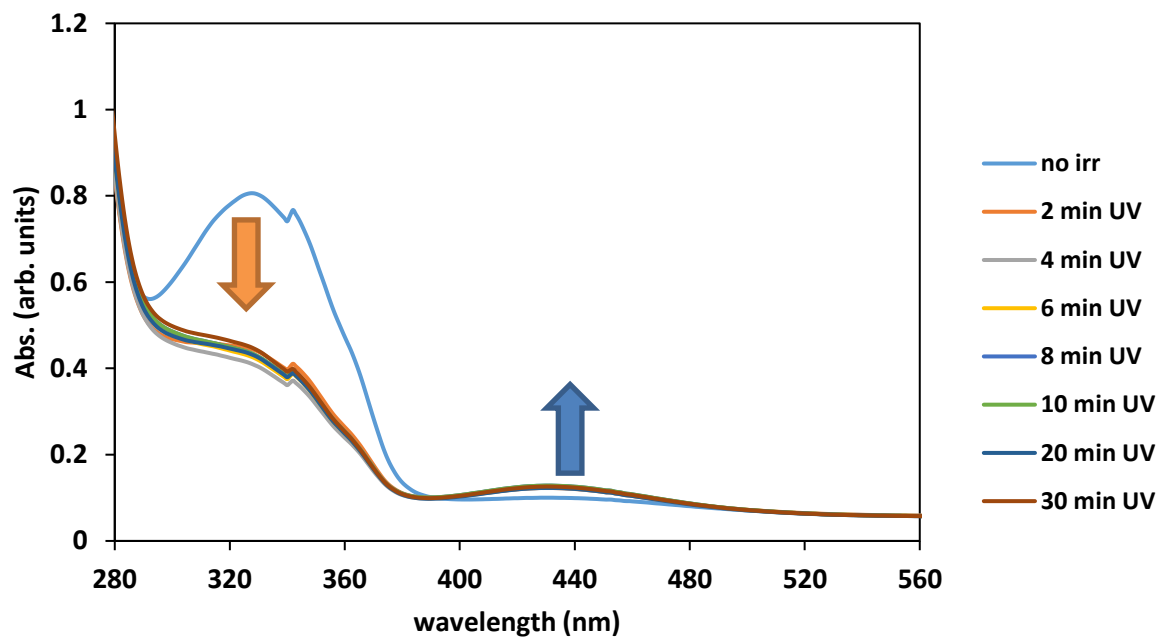
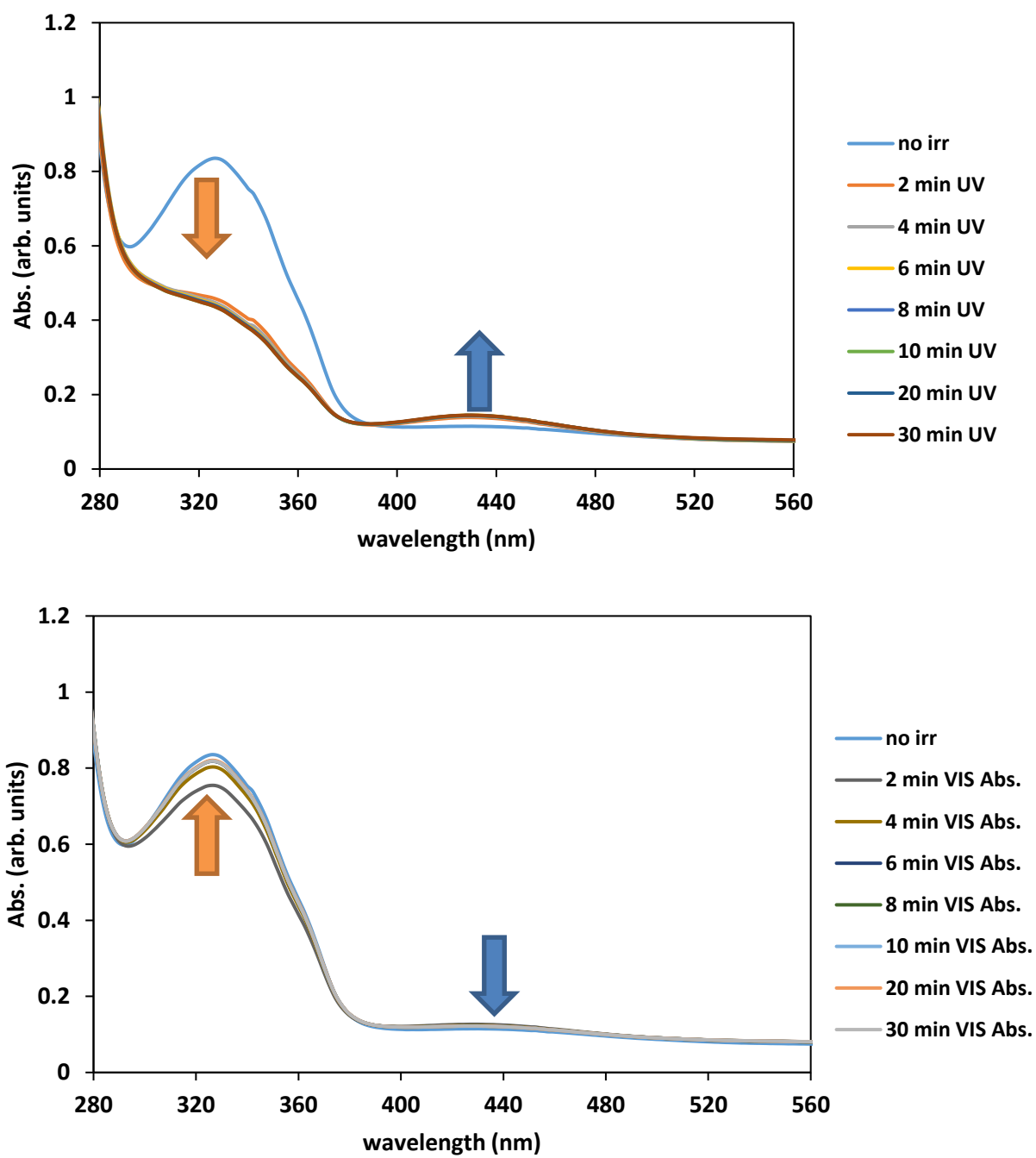


Figure S5.11. UV-Vis spectra of Azo-DPA, exposed to UV (top) and Vis (bottom) light over time.



**Figure S5.12.** UV-Vis spectra of oligomeric Azo-CAMs, exposed to UV (top) and Vis (bottom) light over time.



**Figure S5.13.** UV-Vis spectra of monomeric Azo-CAMs, exposed to UV (top) and Vis (bottom) light over time.

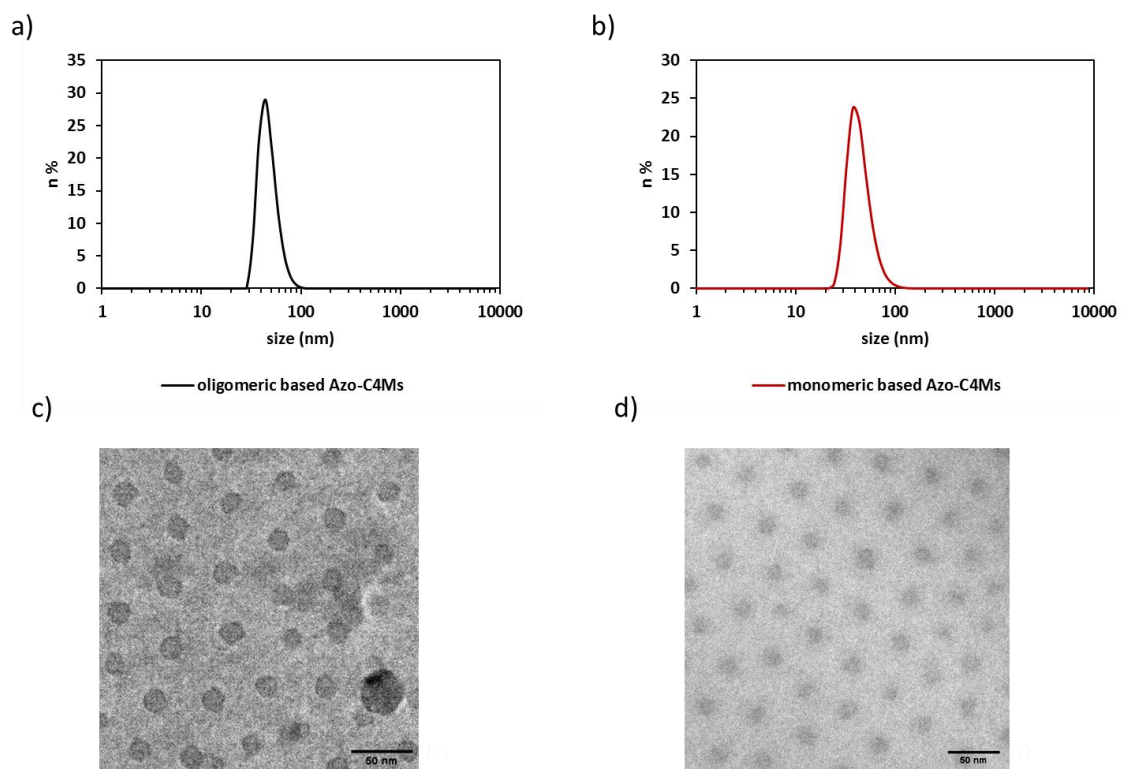


**Figure S5.14.** Top: size distributions at the DLS of oligomeric a) and monomeric b) core-unit- based Azo-C4Ms. Bottom: and Cryo-TEM images of oligomeric c) and monomeric d) core-unit- based Azo-C4Ms, after 10 minutes of 365 nm treatment. The samples were added to the TEM grid and immediately freeze under liquid  $N_2$ , for the Cryo-TEM study.

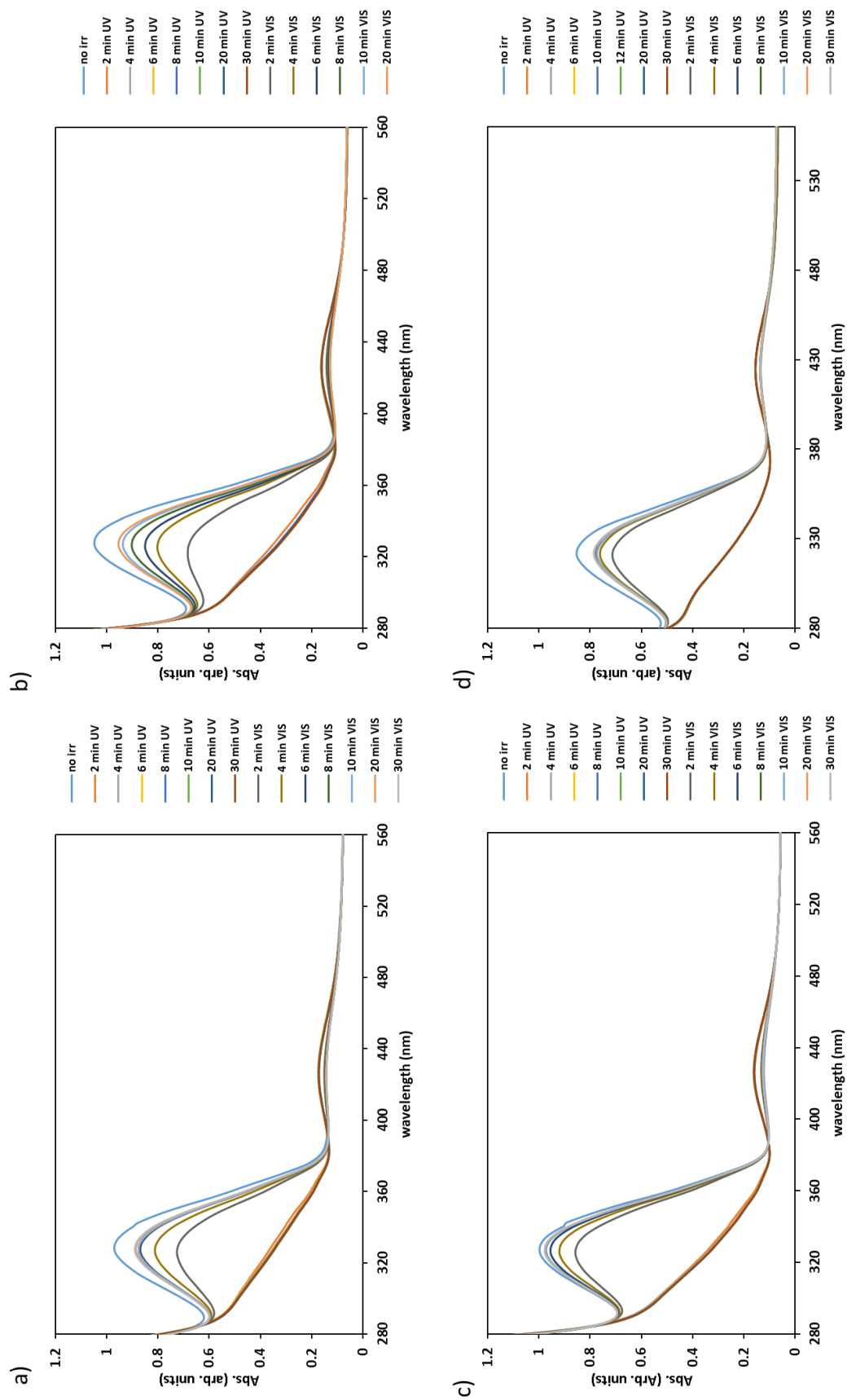


**Figure S5.15.** UV-Vis spectra of Azo-C4Ms, of Azo-C4Ms, by increasing the amount of Azo-ma substituted, 33% a), 90% b), 100% c) and Azo-DPA(control) d), exposed to UV and Vis light over time.

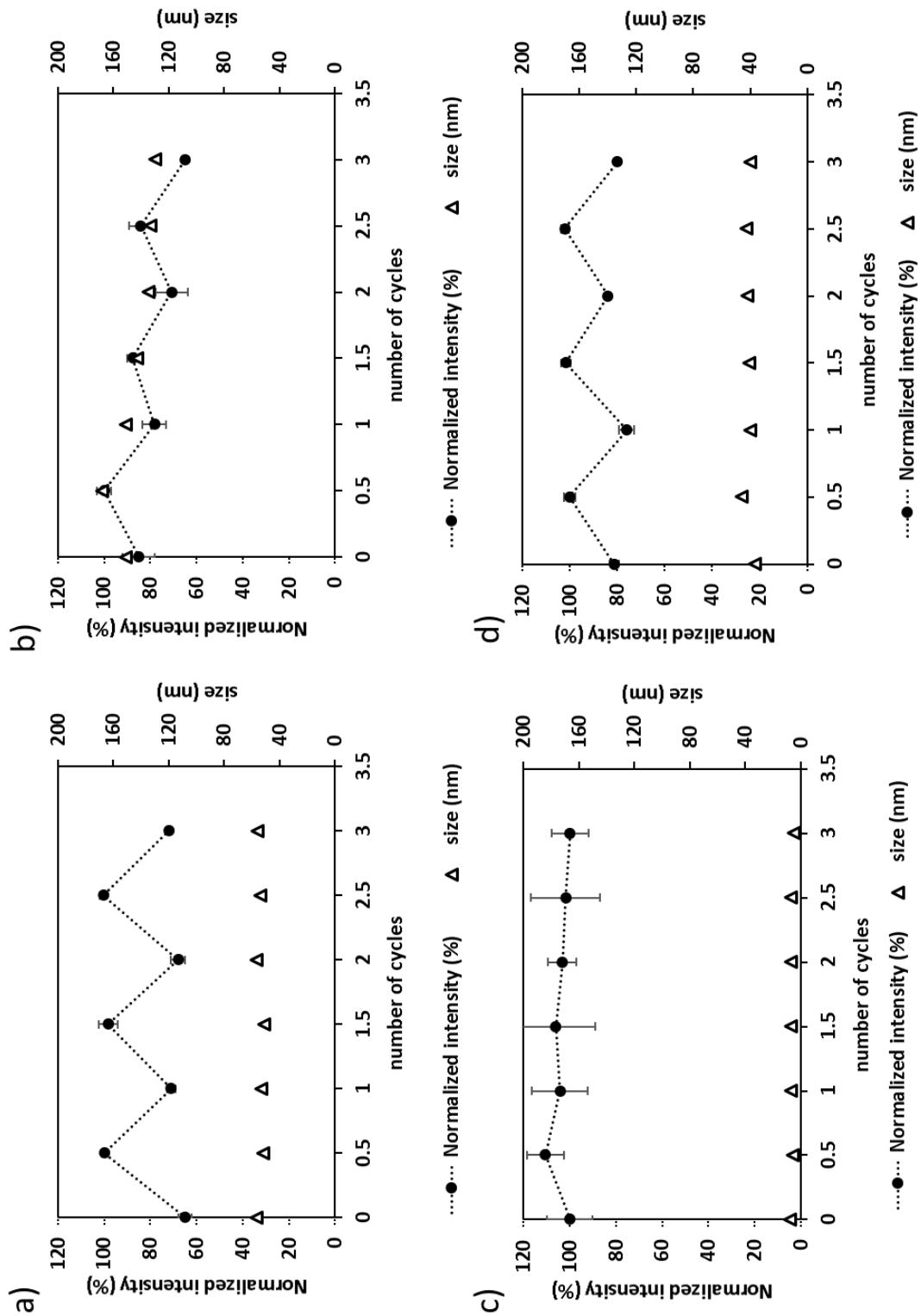


**Figure S5.16.** DLS cycle of Azo-C4Ms, by increasing the amount of Azo-ma substituted 33% a), 90% b), 100% c) and Azo-DPA (control) d). The normalized intensity and size are plotted over the number of repeated cycles.

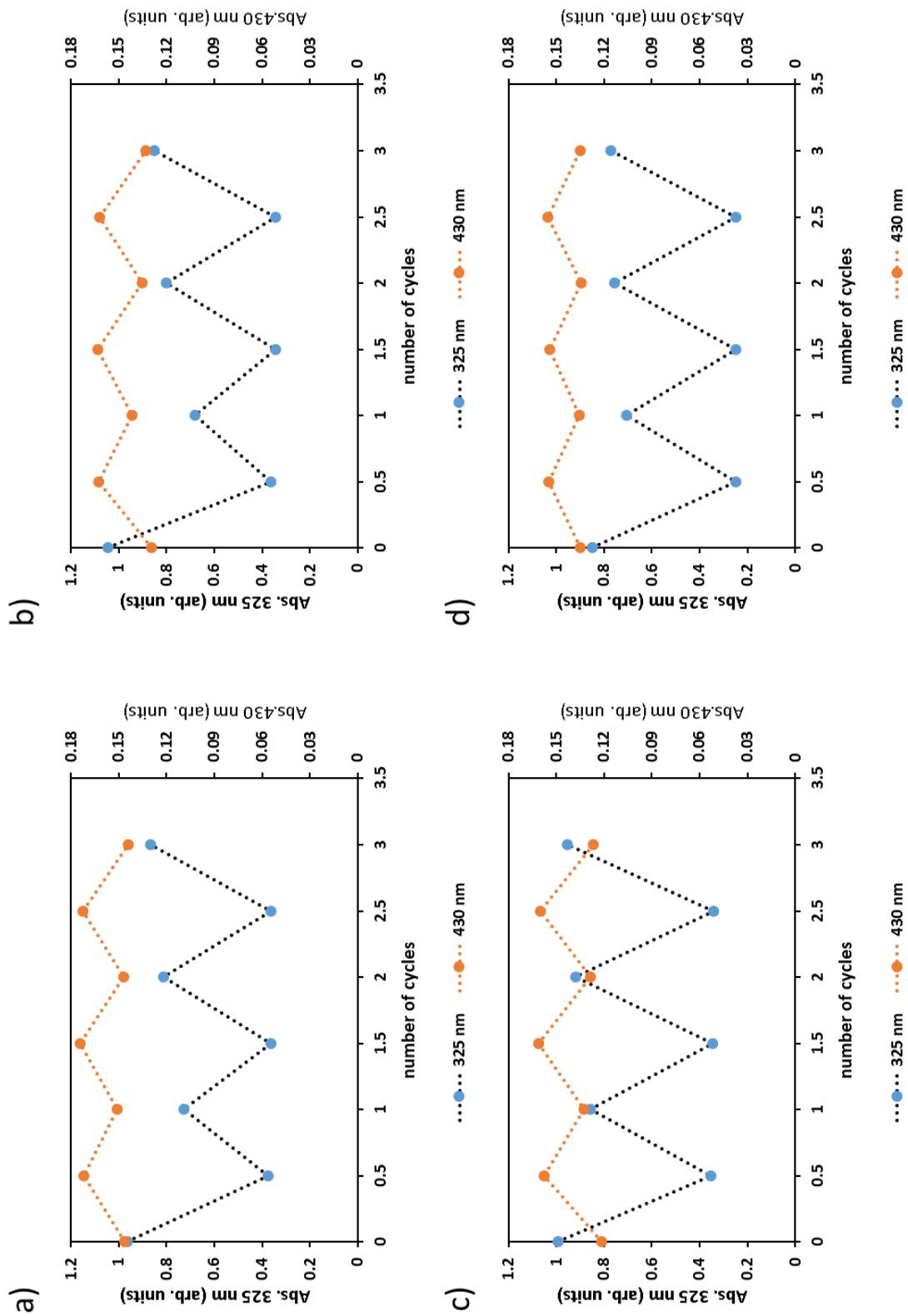


**Figure S5.17.** UV-Vis cycle of Azo-C4Ms, by increasing the amount of Azo-ma substituted, 33% a), 90% b), 100% c) and Azo-DPA(control) d). The absorption at 325 nm and 430 nm is plotted over the number of repeated cycles.

**Table S5.1.** Values of Scattered intensity, polydispersity index and size for all the micelle controls.

<i>Controls</i>	<i>PdI</i>	<i>Dh (nm)</i>	<i>I (Mcps)</i>
<i>Eu-<math>\alpha</math>CD</i>	<i>na</i>	<i>na</i>	<i>na</i>
<i>Eu-AZO</i>	<i>na</i>	<i>na</i>	<i>na</i>
<i>Eu-BP</i>	<i>na</i>	<i>na</i>	<i>na</i>
<i><math>\alpha</math>CD-AZO</i>	<i>0.9</i>	<i>722</i>	<i>0.9</i>
<i><math>\alpha</math>CD-BP</i>	<i>0.4</i>	<i>na</i>	<i>na</i>
<i>AZO-BP</i>	<i>0.6</i>	<i>na</i>	<i>na</i>
<i>EU-<math>\alpha</math>CD_AZO</i>	<i>0.8</i>	<i>na</i>	<i>na</i>
<i>Eu-CD_BP</i>	<i>0.3</i>	<i>na</i>	<i>na</i>
<i><math>\alpha</math>CD-AZO_BP</i>	<i>0.7</i>	<i>437</i>	<i>2.2</i>
<i>AZO-Eu-BP</i>	<i>na</i>	<i>na</i>	<i>na</i>
<i>MES-Eu</i>	<i>na</i>	<i>na</i>	<i>na</i>
<i>MES-<math>\alpha</math>CD</i>	<i>na</i>	<i>na</i>	<i>na</i>
<i>MES-Azo</i>	<i>na</i>	<i>na</i>	<i>na</i>
<i>MES-BP</i>	<i>na</i>	<i>na</i>	<i>na</i>
<i>monomeric-based Azo-C4Ms</i>	<i>0.12</i>	<i>40</i>	<i>12</i>
<i>oligomeric-based Azo-C4Ms</i>	<i>0.15</i>	<i>43</i>	<i>30</i>

## 5.6. REFERENCES

1. Zhao, Y., *Photocontrollable block copolymer micelles: what can we control?* J. Mater. Chem., 2009. **19**(28): p. 4887-4895.
2. Feng, Z., Lin, L., Yan, Z., and Yu, Y., *Dual Responsive Block Copolymer Micelles Functionalized by NIPAM and Azobenzene*. Macromol. Rapid Commun., 2010. **31**(7): p. 640-644.
3. Ahmad, Z., Shah, A., Siddiq, M., and Kraatz, H.-B., *Polymeric micelles as drug delivery vehicles*. RSC Adv., 2014. **4**(33): p. 17028-17038.
4. Ye, Q., Huo, M., Zeng, M., Liu, L., Peng, L., et al., *Photoinduced Reversible Worm-to-Vesicle Transformation of Azo-Containing Block Copolymer Assemblies Prepared by Polymerization-Induced Self-Assembly*. Macromolecules, 2018. **51**(9): p. 3308-3314.
5. Zhang, X., Ma, X., Wang, K., Lin, S., Zhu, S., et al., *Recent Advances in Cyclodextrin-Based Light-Responsive Supramolecular Systems*. Macromol. Rapid Commun., 2018. **39**(11): p. e1800142.
6. Biswas, S., Kumari, P., Lakhani, P.M., and Ghosh, B., *Recent advances in polymeric micelles for anti-cancer drug delivery*. Eur. J. Pharm. Sci., 2016. **83**: p. 184-202.
7. Deshmukh, A.S., Chauhan, P.N., Noolvi, M.N., Chaturvedi, K., Ganguly, K., et al., *Polymeric micelles: Basic research to clinical practice*. Int. J. Pharm., 2017. **532**(1): p. 249-268.
8. Tang, Z., He, C., Tian, H., Ding, J., Hsiao, B.S., et al., *Polymeric nanostructured materials for biomedical applications*. Prog. Polym. Sci., 2016. **60**: p. 86-128.
9. Jochum, F.D. and Theato, P., *Temperature- and light-responsive smart polymer materials*. Chem. Soc. Rev., 2013. **42**(17): p. 7468-7483.
10. Zhou, Q., Zhang, L., Yang, T., and Wu, H., *Stimuli-responsive polymeric micelles for drug delivery and cancer therapy*. Int. J. Nanomedicine, 2018. **13**: p. 2921-2942.
11. Huang, Y., Dong, R., Zhu, X., and Yan, D., *Photo-responsive polymeric micelles*. Soft Matter, 2014. **10**(33): p. 6121-6138.
12. Wang, Y., Ma, N., Wang, Z., and Zhang, X., *Photocontrolled Reversible Supramolecular Assemblies of an Azobenzene-Containing Surfactant with  $\alpha$ -Cyclodextrin*. Angew. Chem. Int. Ed. Engl., 2007. **119**(16): p. 2881-2884.
13. Dong, J., Wang, Y., Zhang, J., Zhan, X., Zhu, S., et al., *Multiple stimuli-responsive polymeric micelles for controlled release*. Soft Matter, 2013. **9**(2): p. 370-373.
14. Mura, S., Nicolas, J., and Couvreur, P., *Stimuli-responsive nanocarriers for drug delivery*. Nat. Mater., 2013. **12**(11): p. 991-1003.
15. Bai, Y., Liu, C.P., Song, X., Zhuo, L., Bu, H., et al., *Photo- and pH- Dual-Responsive beta-Cyclodextrin-Based Supramolecular Prodrug Complex Self-Assemblies for Programmed Drug Delivery*. Chem. Asian J., 2018. **13**(24): p. 3903-3911.
16. Zhang, Q., Ko, N.R., and Oh, J.K., *Recent advances in stimuli-responsive degradable block copolymer micelles: synthesis and controlled drug delivery applications*. Chem. Commun. (Camb), 2012. **48**(61): p. 7542-7552.
17. Nalluri, S.K. and Ravoo, B.J., *Light-responsive molecular recognition and adhesion of vesicles*. Angew. Chem. Int. Ed. Engl., 2010. **49**(31): p. 5371-5374.
18. Bandara, H.M. and Burdette, S.C., *Photoisomerization in different classes of azobenzene*. Chem. Soc. Rev., 2012. **41**(5): p. 1809-1825.
19. Dong, M., Babalhavaeji, A., Collins, C.V., Jarrah, K., Sadowski, O., et al., *Near-Infrared Photoswitching of Azobenzenes under Physiological Conditions*. J. Am. Chem. Soc., 2017. **139**(38): p. 13483-13486.
20. Merino, E., *Synthesis of azobenzenes: the coloured pieces of molecular materials*. Chem. Soc. Rev., 2011. **40**(7): p. 3835-3853.
21. Molla, M.R., Rangadurai, P., Antony, L., Swaminathan, S., de Pablo, J.J., et al., *Dynamic actuation of glassy polymersomes through isomerization of a single azobenzene unit at the block copolymer interface*. Nat. Chem., 2018. **10**(6): p. 659-666.
22. Lu, Y., Zou, H., Yuan, H., Gu, S., Yuan, W., et al., *Triple stimuli-responsive supramolecular assemblies based on host-guest inclusion complexation between  $\beta$ -cyclodextrin and azobenzene*. Eur. Polym. J., 2017. **91**: p. 396-407.
23. Schumers, J.M., Fustin, C.A., and Gohy, J.F., *Light-responsive block copolymers*. Macromol. Rapid Commun., 2010. **31**(18): p. 1588-1607.
24. Harnoy, A.J., Slor, G., Tirosh, E., and Amir, R.J., *The effect of photoisomerization on the enzymatic hydrolysis of polymeric micelles bearing photo-responsive azobenzene groups at their cores*. Org. Biomol. Chem., 2016. **14**(24): p. 5813-5819.
25. Xu, Y., Cao, J., Li, Q., Li, J., He, K., et al., *Novel azobenzene-based amphiphilic copolymers: synthesis, self-assembly behavior and multiple-stimuli-responsive properties*. RSC Advances, 2018. **8**(29): p. 16103-16113.

26. Jochum, F.D. and Theato, P., *Thermo- and light responsive micellation of azobenzene containing block copolymers*. Chem. Commun. (Camb), 2010. **46**(36): p. 6717-6719.
27. Facciotti, C., Saggiomo, V., Bunschoten, A., Fokkink, R., Hove, J.B.T., et al., *Cyclodextrin-based complex coacervate core micelles with tuneable supramolecular host-guest, metal-to-ligand and charge interactions*. Soft Matter, 2018. **14**(47): p. 9542-9549.
28. Biesalski, M., Johannsmann, D., and Ruhe, J., *Electrolyte-induced collapse of a polyelectrolyte brush*. J. Chem. Phys., 2004. **120**(18): p. 8807-8814.
29. Wang, J., Groeneveld, A., Oikonomou, M., Prusova, A., Van As, H., et al., *Revealing and tuning the core, structure, properties and function of polymer micelles with lanthanide-coordination complexes*. Soft Matter, 2016. **12**(1): p. 99-105.
30. Wang, Y., Ma, N., Wang, Z., and Zhang, X., *Photocontrolled reversible supramolecular assemblies of an azobenzene-containing surfactant with alpha-cyclodextrin*. Angew. Chem. Int. Ed. Engl., 2007. **46**(16): p. 2823-2826.
31. Wang, J., Voets, I.K., Fokkink, R., van der Gucht, J., and Velders, A.H., *Controlling the number of dendrimers in dendrimicelle nanoconjugates from 1 to more than 100*. Soft Matter, 2014. **10**(37): p. 7337-7345.
32. Ten Hove, J.B., van Oosterom, M.N., van Leeuwen, F.W.B., and Velders, A.H., *Nanoparticles reveal Extreme Size-Sorting and Morphologies in Complex Coacervate Superstructures*. Sci. Rep., 2018. **8**(1): p. 13820-13827.
33. Ten Hove, J.B., Wang, J., van Oosterom, M.N., van Leeuwen, F.W.B., and Velders, A.H., *Size-Sorting and Pattern Formation of Nanoparticle-Loaded Micellar Superstructures in Biconcave Thin Films*. ACS Nano, 2017. **11**(11): p. 11225-11231.
34. Poutanen, M., Guidetti, G., Groschel, T.I., Borisov, O.V., Vignolini, S., et al., *Block Copolymer Micelles for Photonic Fluids and Crystals*. ACS Nano, 2018. **12**(4): p. 3149-3158.
35. Holder, S.J. and Sommerdijk, N.A.J.M., *New micellar morphologies from amphiphilic block copolymers: disks, toroids and bicontinuous micelles*. Polym. Chem., 2011. **2**(5): p. 1018.
36. Voets, I.K., de Keizer, A., and Cohen Stuart, M.A., *Complex coacervate core micelles*. Adv. Colloid Interface Sci., 2009. **147-148**: p. 300-318.
37. Chen, C.-J., Liu, G.-Y., Liu, X.-S., Li, D.-D., and Ji, J., *Construction of photo-responsive micelles from azobenzene-modified hyperbranched polyphosphates and study of their reversible self-assembly and disassembly behaviours*. New J. Chem., 2012. **36**(3): p. 694-701.





# CHAPTER 6

---

General discussion

---

## ABSTRACT

---

In this chapter, we summarize the most important findings of each chapter and discuss the current challenges and the future developments of C4Ms. We consider that C4Ms contributed to the progress of polymeric micelles, revealing the mechanism of assembly and disassembly under controlled redox, H<sub>2</sub>O<sub>2</sub> and light stimuli. The encapsulation and release results, discussed in this thesis, suggest that C4Ms might be a promising tool for drug delivery applications. However, biologically relevant studies, such as toxicity tests, glutathione and near infrared responses, should be more deeply researched for applying C4Ms in biomedical field.

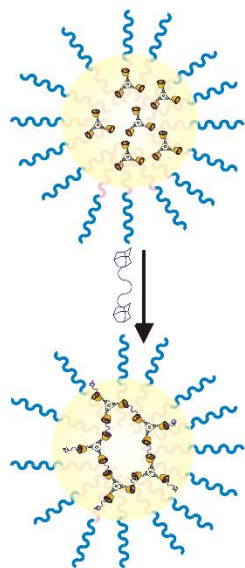
## 6.1. MAIN FINDINGS

In this thesis we presented a new class of micelles, called “Cyclodextrin-based Complex Coacervate Core Micelles” (C4Ms), integrating host-guest interactions inside the core of Complex Coacervate Core Micelles (C3Ms). C4Ms allowed to determine the minimum number of charges per core-units required for coacervation and brought new insights on the micellar ability to assemble and disassemble under precise and controlled stimuli. C4Ms were formed, mainly, by combining three supramolecular interactions: i) metal-to-ligand coordination, by mixing europium ions and cyclodextrin-modified dipicolinic acid, ii) host-guest interaction, by adding different guest moieties, e.g. adamantane, ferrocene or azobenzene, to the cyclodextrin host, and iii) coacervate electrostatic interaction, by adding an oppositely charged block copolymer. We designed and synthesized a cyclodextrin-modified dipicolinic acid (CD-DPA) as the key molecule to bridge between the metal-to-ligand coordination and host-guest interaction. Throughout the entire thesis, we combined CD-DPA with different guests:

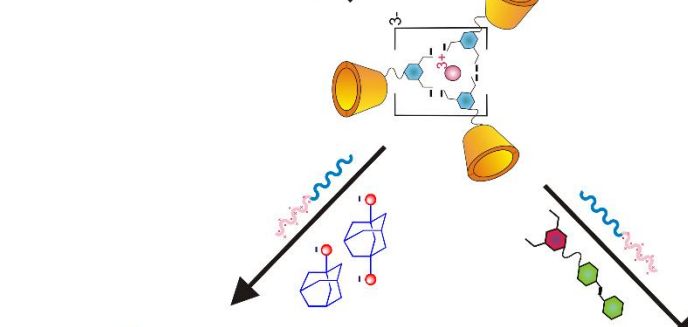
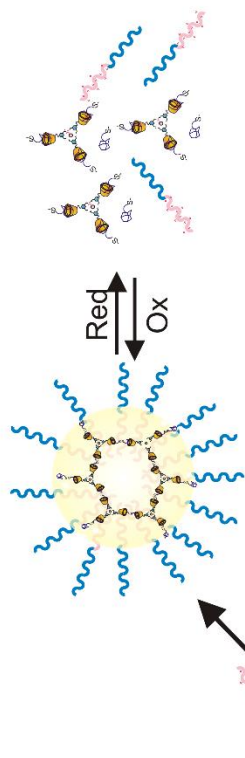
- i) charged monoligand adamantanes (**Ad-ma**<sup>1-</sup> and **Ad-ba**<sup>2-</sup>) in chapter 2, to determine the lowest limit of charges per core-unit required for coacervation
- ii) a redox-responsive bisadamantane (**Ad-SS-Ad**) in chapter 3, to investigate the ability of C4Ms to reversibly disassemble under redox-stimuli and, consequently, release a cargo
- iii) a H<sub>2</sub>O<sub>2</sub>-responsive ferrocene-modified dipicolinic acid (**Fc-DPA**) in chapter 4, to investigate the ability of C4Ms to precipitate under oxidative treatments
- iv) an azobenzene-modified dipicolinic acid (**Azo-DPA**) in chapter 5, to investigate the ability of C4Ms to reversibly disassemble under light treatment.

The different interactions are summarized in Figure 6.1. and their host-guest association constants in water are listed in Table 6.1.

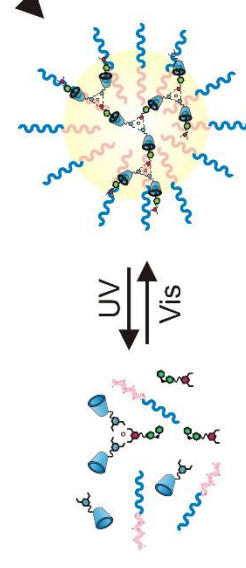
**Chapter 2**  
Cyclodextrin-based Complex Coacervate Core Micelle  
with tuneable supramolecular host-guest,  
metal to ligand and charge interactions.



**Chapter 3**  
Assembly, disassembly and reassembly of  
Cyclodextrin-based Complex Coacervate Core Micelles  
with Redox-Responsive Supramolecular Cross Linkers



**Chapter 5**  
Light-responsive  
Cyclodextrin-based Complex Coacervate Core Micelles



**Chapter 4**  
Oxidant-responsive Ferrocene-based  
Cyclodextrin Complex Coacervate Core Micelles

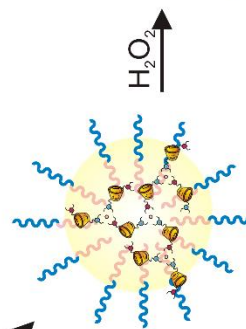


**Figure 6.1.** Schematic representation of the different host-guest interactions throughout this thesis.

**Table 6.1.** Association constant values between  $\alpha$  and  $\beta$ -cyclodextrin and the guest moieties used in this thesis.

<i>Host/Guest</i>	<i>Adamantane</i>	<i>Ferrocene</i>	<i>Ferrocenium</i>	<i>Azobenzene</i>	<i>Azobenzene</i>
				<i>trans</i>	<i>cis</i>
<i><math>\alpha</math>CD</i>	(2:1) <i>na</i>	(2:1) $10^2 M^{-1}$	(2:1) $2 M^{-1}$	$2 \cdot 10^3 M^{-1}$	$35 M^{-1}$
<i><math>\beta</math>CD</i>	$10^3 - 10^5 M^{-1}$	$3 \cdot 10^3 M^{-1}$	$10^1 M^{-1}$	$7 \cdot 10^2 M^{-1}$	$2 \cdot 10^2 M^{-1}$

i) **Chapter 2** represents the fundamental design, development and study of a novel class of C3Ms, C4Ms.

The ability to tune the number of core charges remains a key tool for the following chapters. For the first time, in this chapter, C4Ms were formed in three progressive steps: 1) the formation of a metal-to-ligand coordination, by mixing europium ions and cyclodextrin-modified dipicolinic acid ( $\beta$ CD-DPA), 2) the complexation of host-guest interactions, by adding adamantane guests to the metal-to-ligand coordination and 3) the core charge neutralization, by adding the block copolymer. In the first step, the metal-to-ligand coordination structure carries three negative charges, derived from the interaction between one  $\text{Eu}^{3+}$  with three  $\beta\text{CD-DPA}^{2-}$  molecules. In step 2), Ad-ma<sup>1-</sup> and Ad-ba<sup>2-</sup> guest molecules were added, in different ratios, to the metal-to-ligand coordination structure and the new-formed structure was called “monomeric core-unit”. The number of negative charges of the core-unit was tuned from six up to nine, mixing Ad-ma<sup>1-</sup> and Ad-ba<sup>2-</sup> in different ratios. In step 3), the PMVP<sub>128</sub>-PEO<sub>477</sub> was added until core-charge neutralization. The results on size, shape and stability indicated that seven negative charges might be the minimum number of charges per core-units required to form well-defined and stable micelles. While, core-units with six negative charges formed undefined elongated aggregates. By adding the adamantane bisligand Ad-Glu-Ad, monomeric core-units were combined into dimeric and polymeric networks. This addition enhanced the stability of C4Ms, especially against salt and competing  $\beta$ CD. Dynamic Light Scattering (DLS), Static Laser Scattering (SLS and polarized-SLS), and Transmission Electron Microscopy (cryo-TEM) were the main techniques used to study the size, shape and stability of these micelles.

However, few experiments done by using Small Angle X-Ray Scattering (SAXS) revealed that this technique is also suitable for determining the size, gyration radius, structure and shape of C4Ms, (Figure 6.2.), requiring only small volume and low concentration samples.[1]

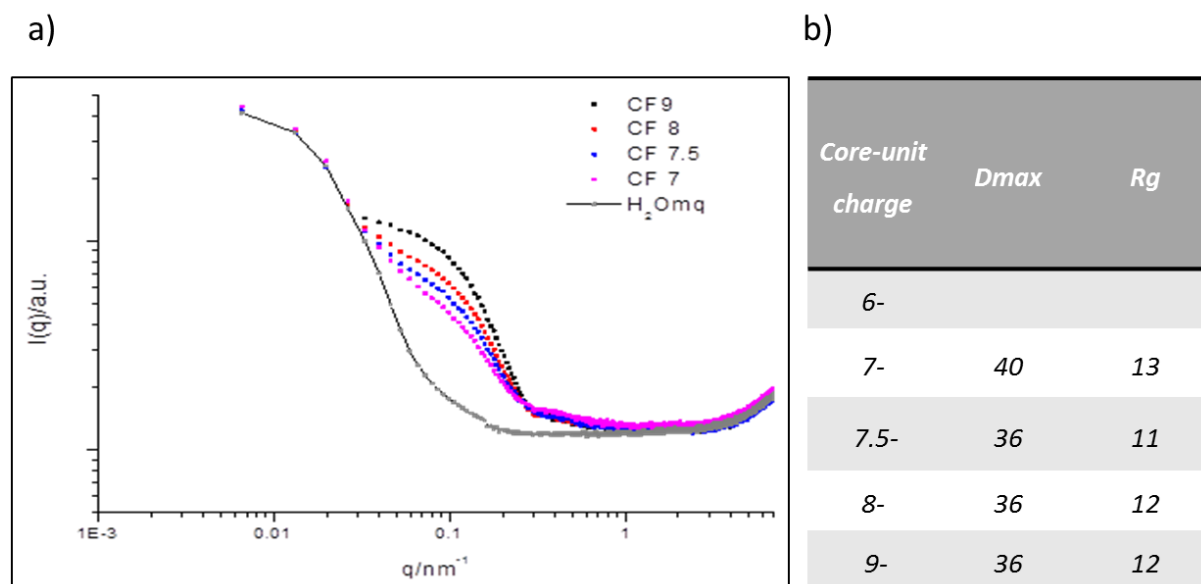


**Figure 6.2.** Plot of intensity vs  $q$  vector for different core-unit-based micelles a) and values of hydrodynamic size and radius of gyration b), measured at SAXS. These measurements were performed at the Institut de Science et d'Ingenierie Supramoleculaires I.S.I.S. under the supervision of Prof. Luisa De Cola.

ii) In **chapter 3**, the aim was to design and develop redox-responsive C4Ms.

We still used adamantane as guest molecule for its medium-high association constant with  $\beta$ CD.[2, 3] Nevertheless, we designed a cleavable disulfide bond in the center of an adamantane bisligand (Ad-SS-Ad). Ad-SS-Ad promoted the assembly of C4Ms, by combining multiple coordination structures together. By adding DTT as reducing agent, the disulfide bond was cleaved into thiolates, provoking the breaking of polymeric core-units into low charged monomeric units. As previously demonstrated, monomeric units based on six negative charges are too low to form stable micelles and, therefore, the micellar disassembly is favored. Over few hours, the disassembly is reversed due to the re-oxidation of thiolates to disulfides, promoted by oxygen. The reversible disassembly process can be controlled by varying two parameters: 1) the DTT concentration and 2) the ratio between responsive and non-responsive bislinker. By increasing the DTT concentration from 3 equivalents to 30 equivalents, the time required to re-assembly increased from ca. 2 hours to 7 hours. Moreover, by substituting the redox-responsive bislinker

with the Ad-Glu-Ad non-redox responsive bislinker, not only the disassembly process was delayed, but also the number of disassembled micelles decreased. Preliminary studies, by using water and dichloromethane biphasic system, showed that Ad-SS-Ad-based C4Ms promote the solubilization of methyl red (MR) in water and its release to the organic phase upon micelle dissociation via DTT treatment. These results suggested that stimuli-responsive C4Ms could be promising for future drug-solubilization and delivery applications.

iii) In **chapter 4**, ferrocene-based C4Ms are designed to respond to H<sub>2</sub>O<sub>2</sub> oxidation.

H<sub>2</sub>O<sub>2</sub> is a Reactive Oxygen Species (ROS) that originates from aerobic metabolism by-products and therefore is relevant in stress-related biological studies.[4-9] The key molecule for the oxidant-response property of C4Ms is the ferrocene-modified dipicolinic acid, (Fc-DPA). In its reduced form, Fc-DPA can complex with βCD with medium-strong  $k_a$ . [10, 11] However, when oxidized, the complexation does not occur, leaving the core-unit with a low number of charges, thus, favoring the micellar destabilization.

By simply changing the europium/ligand ratio, we can tune the core structure of Fc-C4Ms from monomeric to oligomeric-based. Fc-C4Ms, based on these two core structures, present different responses towards oxidant treatments. The stability against the oxidant can be tuned in three ways: 1) by changing monomeric-units into oligomeric branched networks, 2) by varying the oxidant concentration and 3) by adding a non-responsive guest.

Oligomeric-based Fc-C4Ms show higher stability against oxidant treatment, compared to monomeric-based Fc-C4Ms, respectively 970 and 325 equivalents of H<sub>2</sub>O<sub>2</sub>. By increasing the oxidant equivalents to 1300, both types of micelles destabilize, by first aggregating and, then, precipitating. We substituted the Fc-DPA with increasing amount of a non-responsive bislinker (Ad-Glu-Ad). By substituting 90% of Fc-DPA with Ad-Glu-Ad, the stability of C4Ms against the oxidant was improved. These Fc-C4Ms, with well-controllable and tunable response to oxidant, could be interesting for future *in vitro* stress-related studies.

iv) In **chapter 5**, azobenzene-modified dipicolinic acid (Azo-DPA) and  $\alpha$ CD-DPA were used as light-responsive host-guest couple.

Light is considered an ideal external stimulus, because time, space, intensity, size spot, etc. can be regulated externally by an user.[12, 13] In its *trans* isomer, Azo-DPA can complex with  $\alpha$ CD-DPA with medium-high association constant.[11, 14] Given 365 nm light excitation for few minutes, Azo-DPA was able to isomerize to its *cis* isomer, leaving the  $\alpha$ CD cavity. In this chapter, the knowledge on the charge, acquired in chapter 2, was crucial to weaken the assembly of Azo-based C4Ms and favor the micellar disassembly, under light stimuli. Indeed, by simply introducing Azo-DPA as light-responsive guest, the disassembly of C4Ms was not occurring. This system had to be weakened from oligomeric core-unit structures to monomeric ones, to be significantly responsive. For a similar stability reason, the  $\beta$ CD host molecule had to be substituted by  $\alpha$ CD. Initial results showed that C4Ms based on Azo-DPA and  $\beta$ CD were very stable in both forms, *trans* and *cis*. We attributed this stability to the high association constant between  $\beta$ CD and azobenzene, in both isomers. While the  $k_a$  between  $\alpha$ CD and azobenzene differs much more between the two isomers, compared to the  $\beta$ CD (Table 6.1.). This change in  $k_a$ , combined with the weakening of the oligomeric core-units to monomeric ones, favors the micellar disassembly. Uniquely, in this chapter,  $\alpha$ CD-DPA and Azo-DPA were the key host-guest couple for light responsive disassembly. To synthesize  $\alpha$ CD-DPA, we applied the same synthetic protocol of the  $\beta$ CD-DPA, based on click chemistry. Interestingly, the yield of  $\alpha$ CD-DPA was significantly lower than the yield of  $\beta$ CD-DPA. As preliminary experiment, we mixed AZO-DPA with a Gd-DOTA-modified azobenzene molecule in different concentrations. Gd-DOTA-Azo is an additional guest that can weaken the micelles, by making monomeric core-units and provide the MRI property. Results showed that by using 100% of Gd-DOTA-Azo, no C4Ms formation occurred. However, by properly mixing Gd-DOTA-Azo and Azo-DPA, well-defined light-responsive micelles formed. This last study was performed in collaboration with Prof. Dr. Bart Jan Ravoo and the PhD candidate Julian Simke, from the University of Munster.

**Table 6.2.** Summary of the main findings divided per chapter.

<b>Chapter</b>	<b>2</b>	<b>3</b>	<b>4</b>	<b>5</b>
<b>Host-guest couple</b>	$\beta$ CD-DPA Ad-ma, Ad-ba	$\beta$ CD-DPA Ad-SS-Ad	$\beta$ CD-DPA Fc-DPA	$\alpha$ CD-DPA Azo-DPA
<b><math>k_a</math></b>	$10^3 - 10^5 M^{-1}$	$10^3 - 10^5 M^{-1}$	$3 \cdot 10^3 M^{-1}$	$2 \cdot 10^3 M^{-1}$
<b>CMC Eu (<math>\mu</math>M)</b>	40	50	4	35
<b>CSC NaCl (mM)</b>	30	30	25-100	300-600
<b>Size (nm)</b>	$45 \pm 6$	$70 \pm 10$	$60 \pm 8$	$40 \pm 8$
<b>Destabilization trigger</b>	Core-unit < 6 charges	Redox stimuli ( $\Delta I = 70\%$ )	Oxidant stimuli ( $\Delta I = 100\%$ Size change)	Light stimuli ( $\Delta I = 10-35\%$ )
<b>Tunable parameters</b>	Ad-ma/Ad-ba Ad-ma/ Ad-Glu-Ad	(DTT) stimuli Ad-SS-As/ Ad-Glu-Ad	( $H_2O_2$ ) stimuli Monomeric vs oligomeric	Light wavelength Azo-DPA/Azo-ma Monomeric vs oligomeric
<b>Reversibility</b>	na	Yes Multiple cycles	na	Yes Multiple cycles
<b>Encapsulation and release</b>	na	Methyl red Biphasic system	na	Methyl red Biphasic system (not optimized)

## MAIN COMPARISONS

Table 6.2. summarizes the main outcomes of each chapter, such as  $k_a$ , CMC, CSC, size, type of trigger, tunable parameters, reversibility, encapsulation and release ability of C4Ms. The CMC value, for the C4Ms based on adamantane and azobenzene guests, is similar, around 35  $\mu\text{M}$  of europium ions (Chapter 2, 3 and 5). However, Fc-C4Ms showed a CMC of ca. 4  $\mu\text{M}$  of europium ions, approximately 10 times lower than the value mentioned above. This result could be related to the interaction between Fc-DPA and the block copolymer, occurring at very low component concentration as confirmed by DLS. The CMC is one of the most important parameter for the micelle formation, however, it remains one of the least studied parameter, according to literature.[1] Moreover, in the case of C4Ms, the addition of host-guest interactions makes the studying of CMC not straightforward. Perhaps a systematic investigation of the CMC, by varying the concentration of multiple combined components, might be essential.

CSC represents an additional important key factor, in physiological-mimicking conditions. Table 6.2. shows that C4Ms based on Fc-DPA and Azo-DPA have a higher stability against salt, compared to C4Ms based on adamantane guest. This result could be related to the difference between the monomeric and oligomeric structures. Indeed, Fc-DPA and Azo-DPA have the ability to form oligomeric structures, due to their guest-ligand designed structure, while, C4Ms based on Ad-ma or Ad-ba can only form monomeric core structures.

The size of coacervate micelles is not easily changeable by varying the core structures. This finding was reported by changing the core structure of C3Ms from dimeric to polymeric[15] and by changing the generation of dendrimers encapsulated inside coacervate micelles.[16] However, in our case, the change of the core structure results in a difference in size, respectively of 40 nm for the monomeric Ad-ma and Ad-ba based C4Ms and 70 nm for the Ad-SS-Ad-based C4Ms. Uniquely, the Cryo-TEM images of Azo-DPA-based C4Ms showed an almost perfect crystalline distribution of these micelles on the TEM grid. All the other C4Ms showed a conventional size distribution, with the typical “size-sorting” distribution pattern.[17, 18] We do not have a clear reason for the size difference and the crystal structure results. However, it is known that there are several factors involved in the size distribution of coacervate micelles, such as the block copolymer length

(Ncorona/Ncore), the quaternization ratio, the solubility of the components in the given solvent, the ionic strength, etc.[1, 19, 20] Each guest moiety has a specific pKa, solubility and interaction, that can affect the micelle size and morphology, e.g. Azo-DPA  $\pi$ - $\pi$  stacking.

The micelle destabilization was deeply discussed in each chapter. However, it is interesting to compare the responses of the different C4Ms. As discussed in chapter 3, micelles based on Ad-SS-Ad were responsive towards DTT stimuli, due to cleavage of the disulfide bond in the center of the adamantane bislinker. The intensity difference, at the DLS, could be estimated around 70%. However, after few hours, the oxygen present in the cuvette triggered the disulfide re-oxidation and, thus, the micelle re-assembly. This redox trend could be repeated for more than 4 cycles. This assembly, disassembly and re-assembly tendency was also seen in Azo-C4Ms, in which UV light isomerized the azobenzene molecules from trans to cis and, thus, favored the micelle disassembly. The reversed reaction was triggered by visible light, by isomerizing back to trans azobenzene. The difference between the two micelle states is not very marked, especially for oligomeric-based micelles. However, by lowering the number of charges, we reach 35% difference in scattered intensity. The reason for such a limited difference can be related to three main factors: i) the isomerization of the azobenzene is not 100%, as is clear from the UV-Vis spectra in chapter 5, ii) the azobenzene is an hydrophobic molecule that still prefers to be in the coacervate core, rather than in contact with water molecules and iii) we are working at high concentrations compared to the CMC. A higher difference in stability could be visible by lowering the concentration of the components (working at the edge of the CMC value).

Basic studies on the ability of C4Ms to encapsulate and release a cargo are fundamental for future biomedical applications. We tested the encapsulation and release of methyl red dye, in chapter 3 and in chapter 5. In chapter 3, we encapsulated 5% of methyl red inside Ad-SS-Ad-based C4Ms and we studied the dye release, by adding 30 equivalents of DTT and by using a water/DCM biphasic system. The preliminary results show that Ad-SS-Ad-based C4Ms seem a promising platform to encapsulate and release poor water soluble drugs, based on a controlled stimuli. However, the encapsulation and release ability of Azo-C4Ms should be deeper investigated. These results showed that the dye is transferred into the organic phase upon 10 min of light stimuli. However, it is also

clear that the dye itself has a tendency to move towards the organic phase, already in the control. Despite the fact that the difference between the control and the sample is visible, more measurements are needed, e.g. by monitoring the time that the dye requires to move to the organic phase.

Further discussions on the encapsulation and release studies and the future prospects are given in the following sections.

## 6.2. CURRENT CHALLENGES AND FUTURE POTENTIAL

Despite the knowledge we acquired on the ability to assemble and disassemble C4Ms under specific stimuli, more understanding on the response mechanisms to different situations should be achieved.

Redox remain the most investigated stimulus for biomedical application, since tumor cells have high concentrations of GSH reducing agent and low oxygen. Therefore the design of micelles having cleavable disulfide bonds might be promising for drug delivery systems. Light is also considered a valuable stimulus, because its wavelength, excitation time, spot size etc. can be controlled externally. Designing a multi-stimuli responsive system able to controllably disassemble under subsequent redox and light stimuli could be valuable for a well-controlled drug delivery system.

## 6.3. REDOX STIMULI

In chapter 3, we gained new insights on the ability of Ad-SS-Ad-based C4Ms to assemble, disassemble and re-assemble, given redox stimuli.

However, to make these micelles more relevant in biomedical field, DTT treatment should be substituted with glutathione (GSH). It is, indeed, well-reported in literature that cancer cells have a higher concentration of GSH, compared to healthy cells.[21, 22] Therefore, designing micelles with cleavable disulfide bonds, upon GSH stimuli, could be more concrete, than upon DTT stimuli. A preliminary experiment was performed by treating Ad-SS-Ad-based C4Ms with GSH. However, the scattered intensity and size, after the re-oxidation of thiolates to disulfides was not reaching the initial values. We speculated that GSH might form intermediates with higher stability, compared to DTT intermediates.[23] More insights on the reaction process should be gained for both reducing agents (Figure 6.3.). Moreover, for a practical application of Ad-SS-Ad-based C4Ms in biomedical field, the buffer solution at pH 10, used in chapter 3, could be substituted with a buffer solution at lower pH, to better mimic *in vivo* conditions.[24-26]

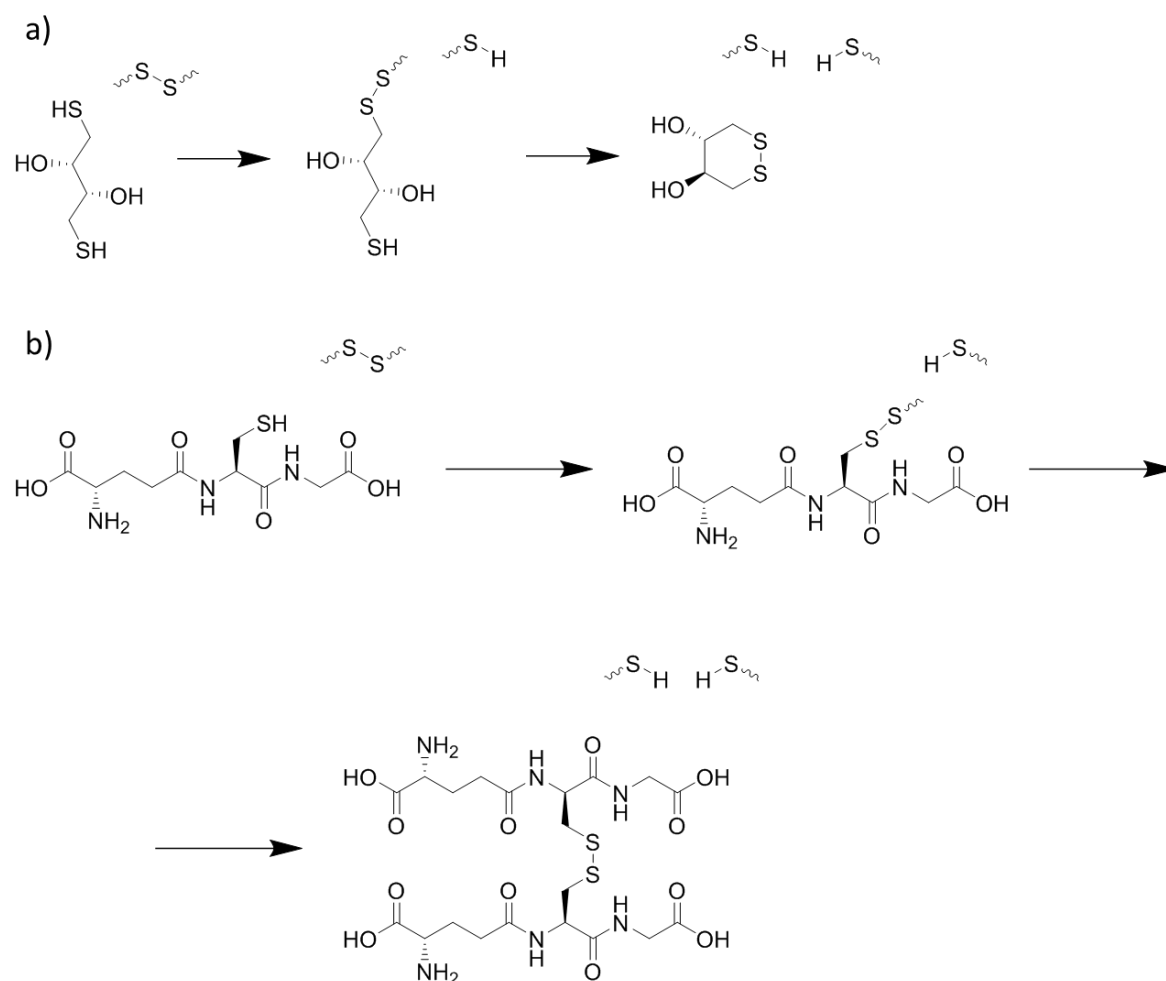


**Figure 6.3.** Reduction reaction scheme of a disulphide-containing molecule, mediated by DTT a) and by GSH b).

In chapter 4, we discuss  $\text{H}_2\text{O}_2$ -responsive C4Ms, based on ferrocene molecules.  $\text{H}_2\text{O}_2$  is defined as Reactive Oxygen Species (ROS) that originates from aerobic metabolism by-products. Testing the micelle disassembly upon contact with  $\text{H}_2\text{O}_2$ -producing bacteria could be relevant for drug delivery application in stress conditions.

The oxidation of ferrocene to ferrocenium ( $\text{Fc}^+$ ) could also be investigated by electrochemistry or by changing  $\text{H}_2\text{O}_2$  with different oxidants, such as iron chloride (III), silver nitrate (I) and iodine.[11, 27, 28] From our preliminary results, none of these oxidant allowed the reversible assembly of C4Ms. Most of them were inducing a one way micelle destabilization and precipitation, as shown in Figure 6.4. It would be interesting to understand the limiting conditions to the reversibility of Fc-based C4Ms. Nevertheless, the reversibility property is not always required for drug-delivery applications.

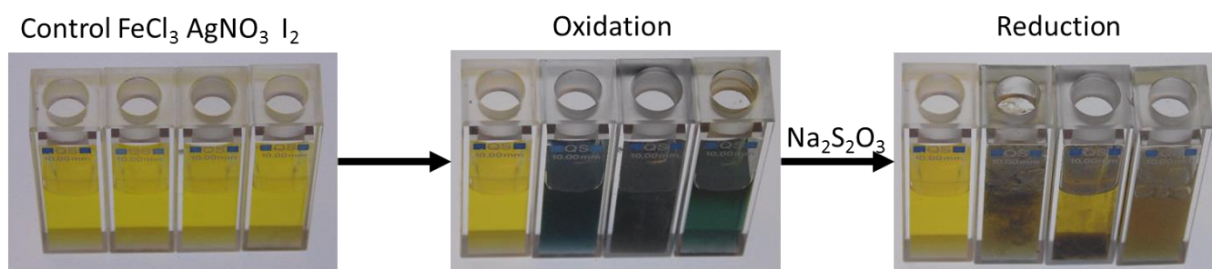


**Figure 6.4.** Sequential oxidation and reduction reactions of ferrocene molecules in water. The oxidation to ferrocenium was investigated by adding iron chloride (III), silver nitrate (I) and iodine. The reduction reaction was investigated by adding sodium thiosulfate.

## 6.4. LIGHT STIMULI

In chapter 5, we used azobenzene molecules and UV light to trigger the micellar disassembly. UV is, generally, the wavelength at which most of the aromatic molecules absorb, such as DPA, BP, Azo, etc. Therefore, using this wavelength in our system, to promote dye release, might not be very selective. Moreover, UV exposure is well-known to cause skin damages, once *in vivo*. [12, 13, 24] By modifying the azobenzene guest with the substituents shown in the Figure 6.5, it would be possible to shift the absorption wavelength towards longer wavelengths. [29] However, the pH and the steric hindrance are important factors to maintain the isomerization ability of the azobenzene guest.

		Structure (R)	$\lambda$ (nm)
		1	569
		2	560
		3	580
		4	595
		5	575
		6	597

**Figure 6.5.** Molecular structures of an azobenzene-based molecule with different substituents (left). The wavelength values are listed on the right.

## 6.5. MULTI-STIMULI

In recent studies, the combination of different stimuli, into so-called “multi-stimuli-responsive systems”, is gaining more attention.[30] The advantage of multi-stimuli-responsive systems relies on the possibility to have a two-step release, firstly, by disassembling the nanocarrier via biologically internal stimuli and, secondly, by external stimuli, controlling remotely the parameters.[12, 31-33] Moreover, multi-stimuli responsive micelles have usually higher versatility, tunability and control, compared to uni-stimuli-responsive micelles.[30, 32, 34, 35]

An example of a multi-stimuli responsive micelle is the system described by Watanabe et al. that can assemble and disassemble under the combination of specific temperature and light stimuli.[36] The light stimulus induces a transition from micelles to unimeric structures. While the temperature triggers opposite behaviour. An additional example of multi stimuli responsive system is the micelle reported by Lu et al., in which i) light, ii) temperature and iii) redox stimuli were used to change the morphology and the properties of the micelles.[37] UV light induced their disassembly, due to a misbalance between the hydrophobic/hydrophilic polymer ratio. Upon DTT addition, spherical micelles changed their shape into small and irregular structures. Temperature turned the spherical micelles into aggregations above a certain critical temperature. Surprisingly, these stimuli were never tested in contemporary combination with each other.

In our case, the design of multi-stimuli-responsive C4Ms was not straightforward.

- The combination of **redox and light-responsive** stimuli, such as chapter 3 and 5, would imply the mixing of i)  $\alpha$ CD and ii)  $\beta$ CD guests, with iii) the adamantane disulfide bislinker (for the redox response) and iv) the azobenzene moiety (for the light response). This multiple mixing increases the complexity of the system. Despite the fact that the adamantane molecules can complex only with  $\beta$ CD, the azobenzene molecules can complex with  $\alpha$ CD only in its *trans* isomer and with  $\beta$ CD, in both *cis* and *trans* isomers. We previously proved that C4Ms based on  $\beta$ CD and azobenzene molecules cannot undergo dissociation. Therefore, mixing the two cyclodextrins with the redox and light responsive bislinker would probably not cause an efficient micelle dissociation.

- The combination of **oxidant and light-response** stimuli, such as chapter 4 and 5, presents a similar problem to the one discussed above. This system would require the presence of i)  $\alpha$ CD and ii)  $\beta$ CD guests, iii) the ferrocene molecule (for the oxidant response) and iv) the azobenzene moiety (for the light response). However, Fc-DPA can form 2:1 complex with  $\alpha$ CD (Figure 6.6.) and the azobenzene molecules can complex with  $\beta$ CD, in both *cis* and *trans* isomers. Therefore, probably also in this case, mixing the two cyclodextrins with the oxidant and light responsive bislinker would probably not cause an efficient nor straightforward micelle dissociation.

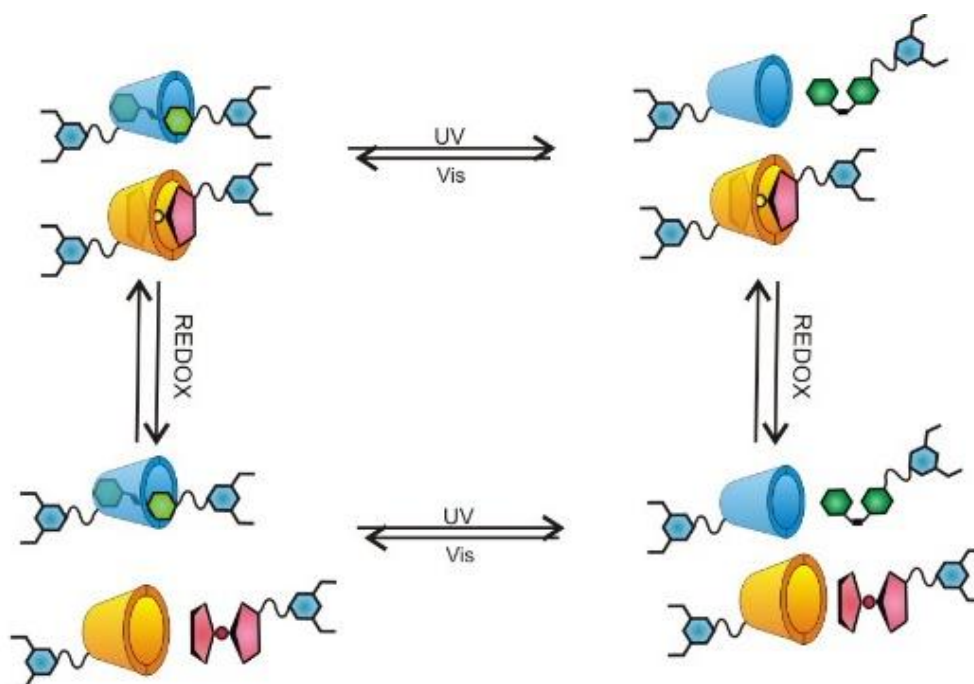


**Figure 6.6.** Representation of a multi-stimuli responsive system, by combining light and oxidant-responsive guests. Azobenzene can complex with  $\beta$ CD in both isomers, *cis* and *trans*. Ferrocene molecules can complex with  $\beta$ CD forming 1:1 complex, and with  $\alpha$ CD, forming 1:2 complex.

To bypass this challenge related to host-guest complexation in different isomers and in different ratios, we designed a guest that would be responsive for **multiple-stimuli in one: Azo-SS-Azo bislinker**, (Figure 6.7. a). The synthesis was simple and successful; however, the water-solubility was too poor to prepare a stock solution at the usual mM concentrations.

We, therefore, corrected the design of this bislinker, by implementing a cystine-based Azo-SS-Azo, more water-soluble. However, this synthesis was not straightforward, neither by mechanochemistry [38, 39] and neither by phase-transfer approaches, (Figure 6.7. b).

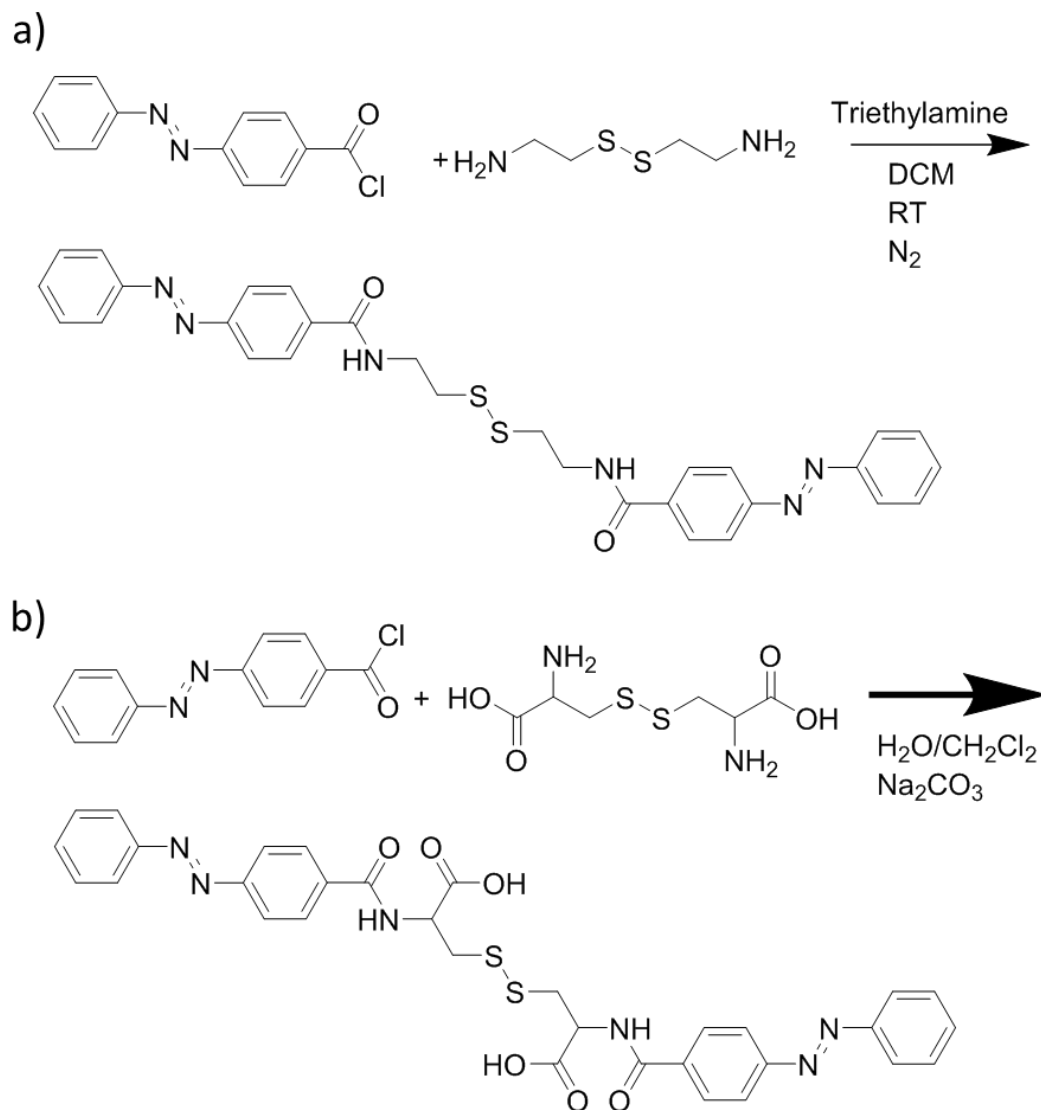


**Figure 6.7.** Synthetic schemes of Azo-SS-Azo linker for light and redox multi stimuli-responsive micelles.

An additional approach to form multi-responsive C4Ms was to combine the redox-responsive core-guest with a **temperature-responsive** block copolymer. A preliminary trial combining C3Ms and a temperature responsive block copolymer was performed, by using PNIPAM<sub>44</sub>-DMEMA<sub>216</sub>. The PNIPAM<sub>44</sub> block represents the temperature responsive part, due to its low solubility in water above 32°C, (Figure 6.8. a).[24] The DMEMA<sub>216</sub> block is pH sensitive, due to its positive charge above pH 7, (Figure 6.8. b).

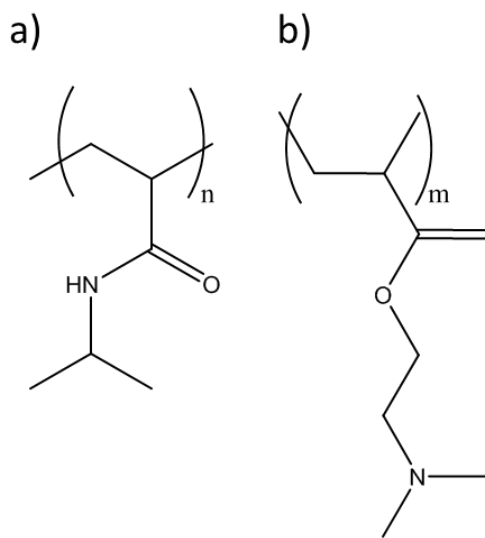


**Figure 6.8.** PNIPAM( $n=44$ ) a) and DMEMA ( $m=216$ ) b) molecular structures.

Preliminary results from 3°C to 55°C shows that the temperature responsive block copolymer forms undefined aggregates with high polydispersity, rather than well-defined micelles, Figure 6.9. No significant change in size was seen above and below 32°C. However, more experiments are necessary to define the optimum block copolymer length and concentration.

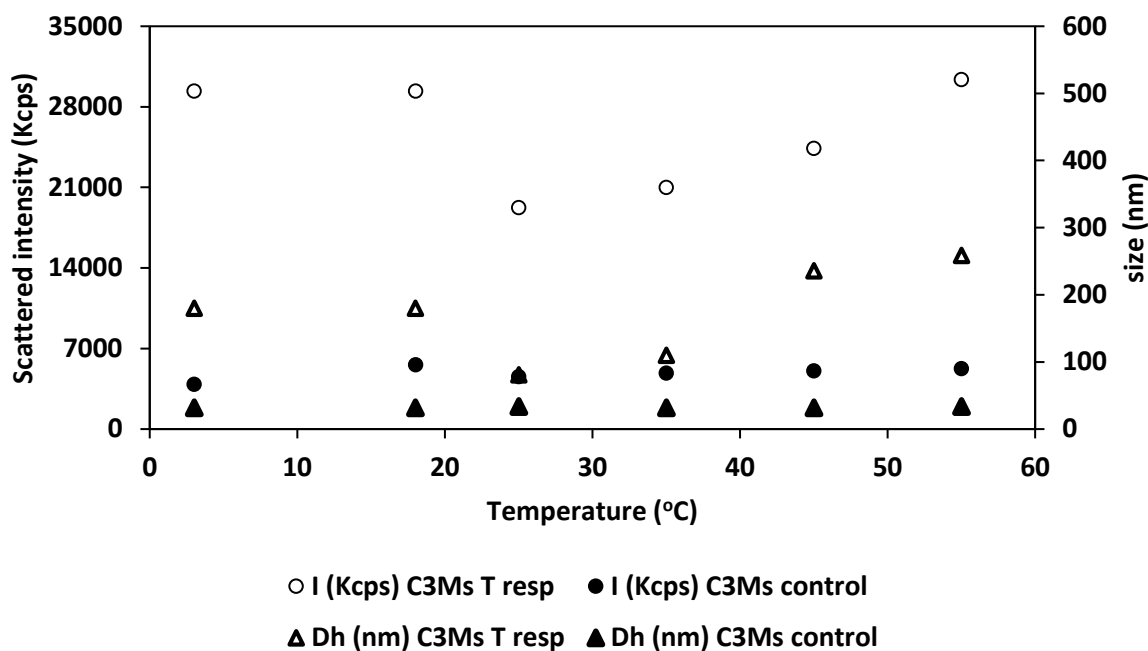


**Figure 6.9.** Graph representing C3Ms controls (blue) and temperature-responsive-based C3Ms (red) intensities (Kcps) and size(nm) as function of the temperature, by using DLS. C3Ms were used as a starting point for future application studies on C4Ms.

## 6.6. ENCAPSULATION AND RELEASE

The ability of C3Ms to encapsulate different cargoes, such as DNA, RNA, proteins, is well-known in literature.[1, 40-42] However, the ability to selectively disassemble C4Ms under specific stimuli and, consequently, release the cargo was not known before. Host-guest interactions, based on cyclodextrin-host and stimuli-responsive guests, were addressed by us as the keystone to combine dye encapsulation and release in a controlled fashion. Cyclodextrins were already known for their ability to encapsulate poor water-soluble dyes.[43] However, the combination of CD with the DPA ligand allowed CD-DPA to play a fundamental role in the micelle formation (by the metal-to-ligand coordination) and, at the same time, in the micelle disassembly (by the host-guest interaction).

In chapter 3, we studied C4Ms as preliminary drug-delivery systems, by releasing a cargo upon micelle dissociation. As explained in chapter 3, Methyl Red (MR) was used as drug model for its medium-high association constant with CD.[44-46] A biphasic system based on water/DCM allowed for an easy and visual detection of the MR release after micelle dissociation. However, the choice of

MR as dye and the biphasic system as tool were not straightforward. Several other types of i) dyes, ii) techniques and iii) stimuli were investigated.

### **i) Dyes**

Several dyes are poor water-soluble and, thus, it is a challenge to prepare very precise stock solutions, especially, at relatively high dye concentrations (mM) in water. An alternative approach could be to prepare a stock solution by mixing directly CD and dyes.

Dyes, such as naphthalene and anthracene, can form 1:1 complex with CD, however, their low solubility and their similar absorption peak to DPA made them not the suitable dyes for our study (Figure 6.10. and Table 6.3).[47, 48] Phenolphthalein is a pH responsive dye; which fluorescence can go OFF upon association with CD. At high pH, usually micelles disassemble and the dye is released from the CD, turning ON its fluorescence.[49, 50] However, C4Ms are very stable at high pH and no significant difference in fluorescence was detectable in our case. Phenanthroline had not only a similar absorption peak to DPA, but also it is able to coordinate europium ions. For this reason, it was excluded from our encapsulation-release study. Several other studies were limited by the dye solubility, for example cholesterol. Cholesterol is a principal sterol synthesized in the body and it is the precursor of several fundamental steroid hormones.[51] Therefore, controlling its concentration and biodistribution in the human body is crucial. Cholesterol has one of the highest  $k_a$  with cyclodextrin due to its highly hydrophobic nature.[52] Due to this, it is able to form micelles in solution at very low concentrations, below  $\mu\text{M}$ . [51, 53, 54] These factors limited its application in C4Ms.

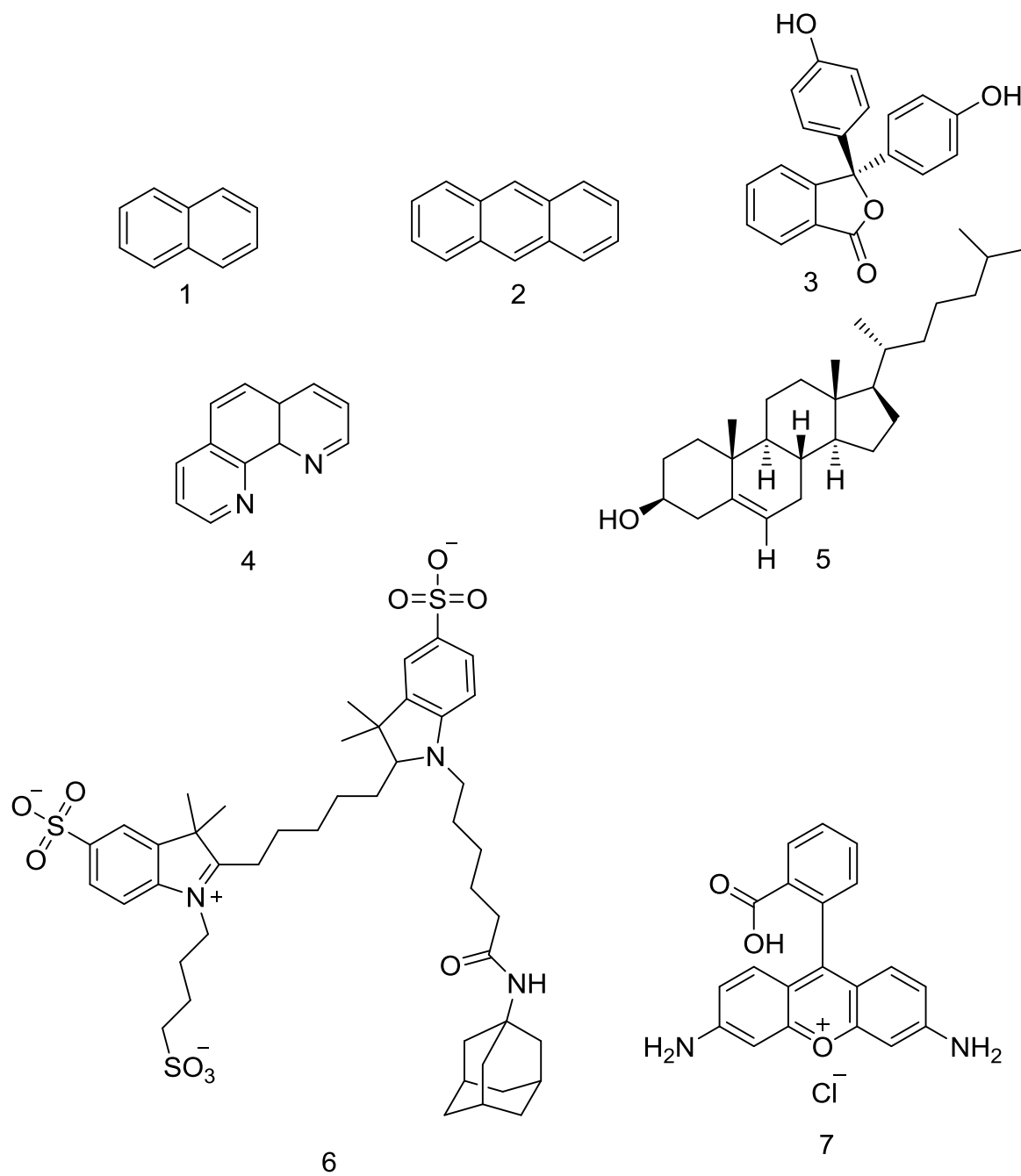


**Figure 6.10.** Molecular structures of several cargoes that were investigated for the encapsulation and release experiment. The number corresponds to the properties listed in the table below.

**Table 6.3.** List of pros and cons of several cargoes that were investigated for the encapsulation and release experiment.

<i>Number</i>	<i>Name</i>	<i>Pros</i>	<i>Cons</i>
1	<i>Naphthalene</i>	<i>CD guest 1:1</i>	<i>Similar abs. to DPA Low solubility</i>
2	<i>Anthracene</i>	<i>CD guest 1:1</i>	<i>Similar abs. to DPA Low solubility</i>
3	<i>Phenolphthalein</i>	<i>pH responsive dye on/off fluorescence</i>	<i>Micelle stability above pH 10</i>
4	<i>Phenanthroline</i>	<i>CD guest 1:1</i>	<i>Europium coordination</i>
5	<i>Cholesterol</i>	<i>Relevant in biomedical field</i>	<i>Forming cholesterol micelles</i>
6	<i>Adamantane-Cy5</i>	<i>K<sub>a</sub> comparable with Ad-SS-Ad bislinker High solubility High ext. coeff.</i>	<i>DTT influences its emission</i>
7	<i>Rhodamine 110</i>	<i>High ext. coeff. Well-known properties</i>	<i>H<sub>2</sub>O<sub>2</sub> influences the dye emission Low solubility</i>

## ii) Techniques

To quantify the dye encapsulation and release, the most common techniques used in literature are the UV-Vis and fluorescence spectroscopy.[55, 56] With these techniques, the dye peak is monitored over time and its shift or change in intensity can be quantitatively related to the dye encapsulation and release. In some cases, dialysis or centrifugations are combined with these techniques to physically separate between encapsulated dye and released dye. Fluorescence Correlation Spectroscopy (FCS) is also commonly used to distinguish the free dye from the encapsulated dye, based on the different diffusion coefficients.[57, 58] In our case, the concentration of C4Ms was too high and FCS was not the ideal technique to handle such concentrated samples.

We used different purification methods, such as dialysis and centrifugation, to remove and quantify a new dye Ad-Cy5, free in solution, (Figure 6.10.).

### iii) Stimuli

In Chapter 2, the dye release was triggered by DTT addition. However, during the preliminary experiments, DTT was affecting the dialysis and centrifugation tubes, by reacting with the cellulose filter cover and causing misleading results.

H<sub>2</sub>O<sub>2</sub> has also been applied as a trigger for micelle disassembly and dye release.[5, 59] Despite all the experiments reported in literature, any extensive controls have been done on the influence of H<sub>2</sub>O<sub>2</sub> on the fluorescence of these dyes. We proved that H<sub>2</sub>O<sub>2</sub> affects the fluorescence of the rhodamine dye over time and, therefore, it might not be a good candidate to study the dye release (Figure 6.11). However, by making a precise calibration curve and by correcting the emission for it, it might still be possible to use H<sub>2</sub>O<sub>2</sub> for drug release studies.

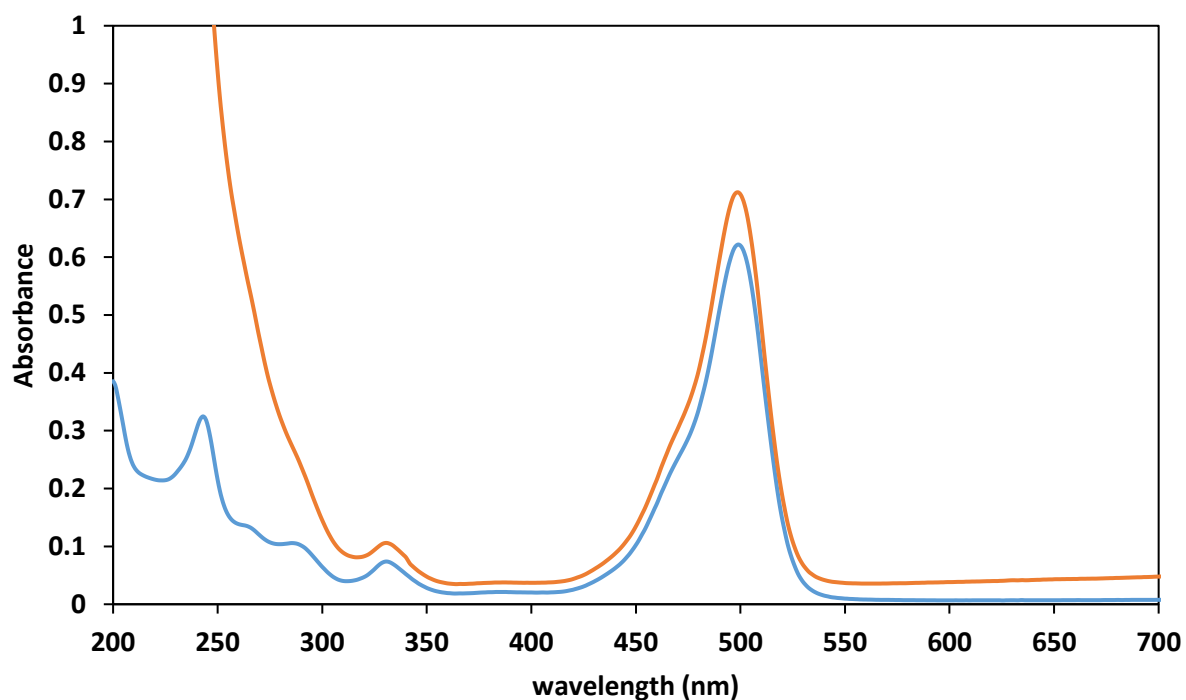


**Figure 6.11.** Absorption spectra of Fc-C4Ms before (blue) and after (orange) the addition of 1300 equivalents of H<sub>2</sub>O<sub>2</sub>.

## 6.7. TOWARDS IN VITRO STUDIES

Since the last decade, there have been some polymeric micelles in **clinical trials**, namely Genexol-PM, NK105, SP1049C, DTXL-TNP, NC6004, NK012 and NK911, (Table 6.4).[60] [56] All these polymeric micelles are considered good candidates in biomedical fields, due to their ability to dissolve poor water-soluble anticancer agents, such as doxorubicin, cisplatin and paclitaxel, and make them more biocompatible. Despite these beneficial properties, many micelles are not evaluated for clinical trials, especially for their low stability in physiologically relevant media. This problem highlights the necessity to promote deeper understanding of disassembly mechanism of these micelles and stability characterization, especially in biologically relevant environments.[12, 30]

**Table 6.4.** List of properties of polymeric micelles in clinical trials.

<i>Name</i>	<i>Drug</i>	<i>Polymer</i>	<i>Size (nm)</i>	<i>Loading (%)</i>	<i>Phase</i>
<i>Genexol</i>	<i>Paclitaxel</i>	<i>mPEG-PDLLA</i>	<i>50</i>	<i>17</i>	<i>III, IV</i>
<i>NK105</i>	<i>Paclitaxel</i>	<i>PEG-P(Asp)</i>	<i>85</i>	<i>23</i>	<i>II, III</i>
<i>SP1049C</i>	<i>Doxorubicin</i>	<i>Pluronic</i>	<i>30</i>	<i>8</i>	<i>III</i>
<i>DTXL-TNP</i>	<i>Docetaxel</i>	<i>PLA-PEG</i>	<i>100</i>	<i>10</i>	<i>I</i>
<i>NC6004</i>	<i>Cisplatin</i>	<i>PEG-P(Glu)-Cisplatin</i>	<i>30</i>	<i>40</i>	<i>I, II</i>
<i>NK012</i>		<i>PEG-P(Glu)</i>	<i>20</i>	<i>20</i>	<i>II</i>
<i>NK911</i>	<i>Doxorubicin</i>	<i>PEG-P(Asp)-Dox</i>	<i>40</i>	<i>Na</i>	<i>II</i>

To achieve a practical application of C4Ms in biomedical fields, new insights on their toxicity, biodistribution, *in vivo*-functioning, etc. should be achieved. Previous C3Ms were studied as fluorescent imaging and MRI contrast agents with high tunability between these two

properties.[61] Animal experiments, using C3Ms for *in vivo* imaging, proved their negligible toxicity.[62]

We performed a preliminary study on the **toxicity** of C4Ms, by monitoring the viability of HeLa cells, upon the addition of C4Ms. HeLa cells were left in the incubator under 5% CO<sub>2</sub> and 95% atmosphere gasses at 37°C, over two days. 1 mL of C4Ms solution (0.5 mM Eu(III) ion concentration) was added to the DMEM cell medium. The cell viability was calculated around 6% after 24 hours (Figure 6.12). This low count in cell viability is not in good agreement with the previous toxicity studies on C3Ms. However, additional controls on each single component and repetitive measurements are needed to confirm the toxicity (or not) of C4Ms.

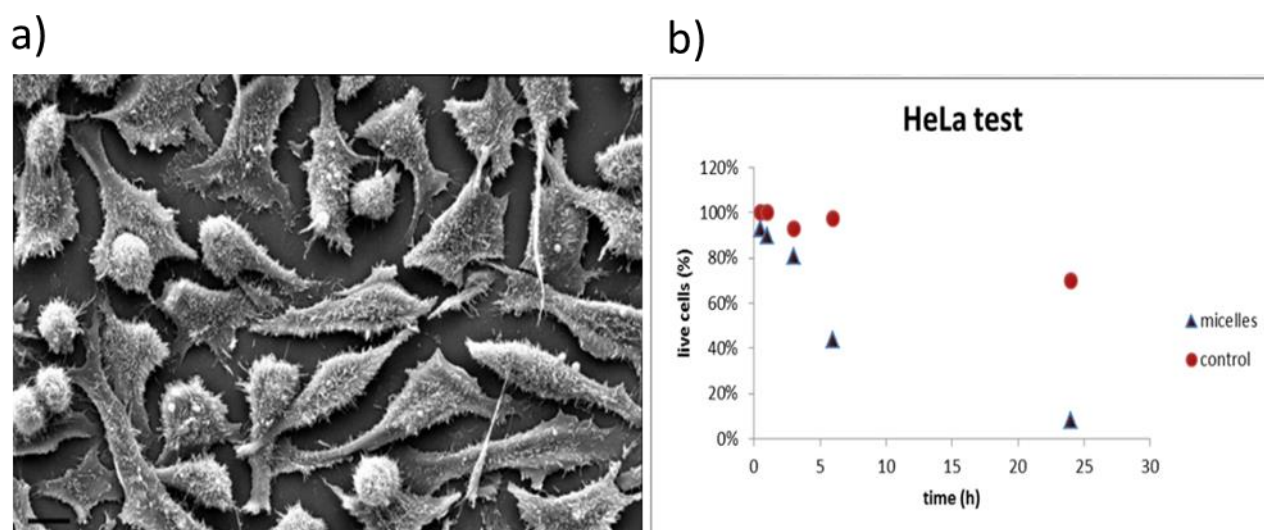


**Figure 6.12.** Image of HeLa cells acquired with an optical microscope a) and plot of the number of living HeLa cells against time b). These measurements were performed at the Institut de Science et d'Ingenierie Supramoleculaires I.S.I.S. under the collaboration with prof. Luisa De Cola.

## 6.8. FINAL CONSIDERATIONS

Over the last decades, polymeric micelles have become progressively more sophisticated. From a simple mixing of two oppositely charged block copolymer, to a metal-to-ligand coordination and dendrimers driven assembly, until host-guest-based Complex Coacervate Core Micelles.

In this thesis, we reported the contribution of C4Ms to the progress on polymeric micelles, revealing the mechanism of assembly and disassembly under controlled stimuli, by finely tuning the component core charges. The CD-DPA has been a fundamental instrument to bridge between micelle formation, via metal-to-ligand coordination and the micelle disassembly, via host-guest interaction. It allowed to finely tune the charge of the core-units and acquire a deep understanding of the number of charges required for coacervation. Based on that, we were able to exploit the number of charges to tune the stability of the C4Ms and make them more prone to disassemble and release a cargo. Cyclodextrin was not only valuable for encapsulating the cargo, but was also fundamental for the responsivity of coacervate micelles. By changing the guest, C4Ms can be responsive for different stimuli, from redox to light. More studies are required to combine these different stimuli and the design of multi-stimuli-responsive C4Ms. However, biologically relevant studies, such as toxicity tests, GSH and NIR responses should be deeply researched. Based on the response studies and the encapsulation and release preliminary results shown in this thesis, we believe C4Ms might be a promising tool for drug delivery systems.

**Translational work** and **interdisciplinary studies** between chemists, computational chemists, physicists, biologists and doctors might be the key to bridge fundamental science on nanotechnology and disease-approach research, gaining different points of view and achieving a broad and deep understanding of their properties and potentials.[63]

**Reproducibility** still remains a limiting process for most of the nanotechnology lab-based research, especially for scaling up the research.[24, 26]

Nonetheless, making nanomedicines **affordable, transportable, and easy to use** should be a complementary research focus.

## 6.9. REFERENCES

1. Voets, I.K., de Keizer, A., and Cohen Stuart, M.A., *Complex coacervate core micelles*. Adv. Colloid Interface Sci., 2009. **147-148**: p. 300-318.
2. Tran, D.N., Colesnic, D., Adam de Beaumais, S., Pembouong, G., Portier, F., et al., *Cyclodextrin-adamantane conjugates, self-inclusion and aggregation versus supramolecular polymer formation*. Org. Chem. Front., 2014. **1(6)**: p. 703-706.
3. Tošner, Z., Aski, S.N., and Kowalewski, J., *Rotational Dynamics of Adamantanecarboxylic Acid in Complex with  $\beta$ -cyclodextrin*. J. Incl. Phenom. Macrocycl. Chem., 2005. **55(1-2)**: p. 59-70.
4. Huo, M., Yuan, J., Tao, L., and Wei, Y., *Redox-responsive polymers for drug delivery: from molecular design to applications*. Polym. Chem., 2014. **5(5)**: p. 1519-1528.
5. Liu, L., Rui, L., Gao, Y., and Zhang, W., *Self-assembly and disassembly of a redox-responsive ferrocene-containing amphiphilic block copolymer for controlled release*. Polym. Chem., 2015. **6(10)**: p. 1817-1829.
6. Dong, Z., Kang, Y., Yuan, Q., Luo, M., and Gu, Z., *H<sub>2</sub>O<sub>2</sub>-Responsive Nanoparticle Based on the Supramolecular Self-Assemble of Cyclodextrin*. Front. Pharmacol., 2018. **9**: p. 552-562.
7. Fu, Y.-H., Chen, C.-Y., and Chen, C.-T., *Tuning of hydrogen peroxide-responsive polymeric micelles of biodegradable triblock polycarbonates as a potential drug delivery platform with ratiometric fluorescence signaling*. Polym. Chem., 2015. **6(47)**: p. 8132-8143.
8. Lisanti, M.P., Martinez-Outschoorn, U.E., Lin, Z., Pavlides, S., Whitaker-Menezes, D., et al., *Hydrogen peroxide fuels aging, inflammation, cancer metabolism and metastasis: the seed and soil also needs "fertilizer"*. Cell Cycle, 2011. **10(15)**: p. 2440-2449.
9. Liu, B., Wang, D., Liu, Y., Zhang, Q., Meng, L., et al., *Hydrogen peroxide-responsive anticancer hyperbranched polymer micelles for enhanced cell apoptosis*. Polym. Chem., 2015. **6(18)**: p. 3460-3471.
10. Osella, D., Carretta, A., Nervi, C., Ravera, M., and Gobetto, R., *Inclusion Complexes of Ferrocenes and Cyclodextrins Critical Appraisal of the Electrochemical Evaluation of Formation Constants*. Organometallics 2000. **19**: p. 2791-2797.
11. Harada, A., Takashima, Y., and Nakahata, M., *Supramolecular polymeric materials via cyclodextrin-guest interactions*. Acc. Chem. Res., 2014. **47(7)**: p. 2128-2140.
12. Ding, C., Tong, L., Feng, J., and Fu, J., *Recent Advances in Stimuli-Responsive Release Function Drug Delivery Systems for Tumor Treatment*. Molecules, 2016. **21(12)**: p. 1-30.
13. Gohy, J.F. and Zhao, Y., *Photo-responsive block copolymer micelles: design and behavior*. Chem. Soc. Rev., 2013. **42(17)**: p. 7117-7129.
14. Wang, Y., Ma, N., Wang, Z., and Zhang, X., *Photocontrolled Reversible Supramolecular Assemblies of an Azobenzene-Containing Surfactant with  $\alpha$ -Cyclodextrin*. Angew. Chem. Int. Ed. Engl., 2007. **119(16)**: p. 2881-2884.
15. Wang, J., Groeneveld, A., Oikonomou, M., Prusova, A., Van As, H., et al., *Revealing and tuning the core, structure, properties and function of polymer micelles with lanthanide-coordination complexes*. Soft Matter, 2016. **12(1)**: p. 99-105.
16. Wang, J., Voets, I.K., Fokkink, R., van der Gucht, J., and Velders, A.H., *Controlling the number of dendrimers in dendrimicelle nanoconjugates from 1 to more than 100*. Soft Matter, 2014. **10(37)**: p. 7337-7345.
17. Ten Hove, J.B., van Oosterom, M.N., van Leeuwen, F.W.B., and Velders, A.H., *Nanoparticles reveal Extreme Size-Sorting and Morphologies in Complex Coacervate Superstructures*. Sci. Rep., 2018. **8(1)**: p. 13820-13827.
18. Ten Hove, J.B., Wang, J., van Oosterom, M.N., van Leeuwen, F.W.B., and Velders, A.H., *Size-Sorting and Pattern Formation of Nanoparticle-Loaded Micellar Superstructures in Biconcave Thin Films*. ACS Nano, 2017. **11(11)**: p. 11225-11231.
19. Voets, I.K., *Electrostatically Driven Assembly of Polyelectrolytes*. 2016. **16**: p. 65-89.
20. van der Kooij, H.M., Spruijt, E., Voets, I.K., Fokkink, R., Cohen Stuart, M.A., et al., *On the stability and morphology of complex coacervate core micelles: from spherical to wormlike micelles*. Langmuir 2012. **28(40)**: p. 14180-14191.
21. Giustarini, D., Galvagni, F., Tesei, A., Farolfi, A., Zanoni, M., et al., *Glutathione, glutathione disulfide, and S-glutathionylated proteins in cell cultures*. Free Radic. Biol. Med., 2015. **89**: p. 972-981.
22. Gamcsik, M.P., Kasibhatla, M.S., Teeter, S.D., and Colvin, O.M., *Glutathione levels in human tumors*. Biomarkers, 2012. **17(8)**: p. 671-691.
23. Bindoli, A., Fukuto, J.M., and Forman, H.J., *Thiol chemistry in peroxidase catalysis and redox signaling*. Antioxid. Redox Signal., 2008. **10(9)**: p. 1549-1564.
24. Alvarez-Lorenzo, C. and Concheiro, A., *Smart drug delivery systems: from fundamentals to the clinic*. Chem. Commun. (Camb), 2014. **50(58)**: p. 7743-7765.
25. Bae, Y., Fukushima, S., Harada, A., and Kataoka, K., *Design of Environment-Sensitive Supramolecular Assemblies for Intracellular Drug Delivery: Polymeric Micelles that are Responsive to Intracellular pH Change*. Angew. Chem. Int. Ed. Engl., 2003. **115(38)**: p. 4788-4791.

26. Biswas, S., Kumari, P., Lakhani, P.M., and Ghosh, B., *Recent advances in polymeric micelles for anti-cancer drug delivery*. Eur. J. Pharm. Sci., 2016. **83**: p. 184-202.
27. Astruc, D., *Why is Ferrocene so Exceptional?* Eur. J. Inorg. Chem., 2017. **2017**(1): p. 6-29.
28. Gu, H., Mu, S., Qiu, G., Liu, X., Zhang, L., et al., *Redox-stimuli-responsive drug delivery systems with supramolecular ferrocenyl-containing polymers for controlled release*. Coord. Chem. Rev., 2018. **364**: p. 51-85.
29. Dong, M., Babalhavaeji, A., Collins, C.V., Jarrah, K., Sadovski, O., et al., *Near-Infrared Photoswitching of Azobenzenes under Physiological Conditions*. J. Am. Chem. Soc., 2017. **139**(38): p. 13483-13486.
30. Mura, S., Nicolas, J., and Couvreur, P., *Stimuli-responsive nanocarriers for drug delivery*. Nat. Mater., 2013. **12**(11): p. 991-1003.
31. Ge, Z. and Liu, S., *Functional block copolymer assemblies responsive to tumor and intracellular microenvironments for site-specific drug delivery and enhanced imaging performance*. Chem. Soc. Rev., 2013. **42**(17): p. 7289-7325.
32. Zhang, Q., Ko, N.R., and Oh, J.K., *Recent advances in stimuli-responsive degradable block copolymer micelles: synthesis and controlled drug delivery applications*. Chem. Commun. (Camb), 2012. **48**(61): p. 7542-7552.
33. Motornov, M., Roiter, Y., Tokarev, I., and Minko, S., *Stimuli-responsive nanoparticles, nanogels and capsules for integrated multifunctional intelligent systems*. Prog. Polym. Sci., 2010. **35**(1-2): p. 174-211.
34. Tayo, L.L., *Stimuli-responsive nanocarriers for intracellular delivery*. Biophys. Rev., 2017. **9**(6): p. 931-940.
35. Zhou, Q., Zhang, L., Yang, T., and Wu, H., *Stimuli-responsive polymeric micelles for drug delivery and cancer therapy*. Int. J. Nanomedicine, 2018. **13**: p. 2921-2942.
36. Wang, C., Hashimoto, K., Zhang, J., Kobayashi, Y., Kokubo, H., et al., *Micellization/Demicellization Self-Assembly Change of ABA Triblock Copolymers Induced by a Photoswitchable Ionic Liquid with a Small Molecular Trigger*. Macromolecules, 2017. **50**(14): p. 5377-5384.
37. Lu, Y., Zou, H., Yuan, H., Gu, S., Yuan, W., et al., *Triple stimuli-responsive supramolecular assemblies based on host-guest inclusion complexation between  $\beta$ -cyclodextrin and azobenzene*. Eur. Polym. J., 2017. **91**: p. 396-407.
38. Holler, M., Stoerkler, T., Louis, A., Fischer, F., and Nierengarten, J.-F., *Mechanochemical Solvent-Free Conditions for the Synthesis of Pillar[5]arene-Containing [2]Rotaxanes*. Eur. J. Org. Chem., 2019. **2019**(21): p. 3401-3405.
39. Metro, T.X., Bonnamour, J., Reidon, T., Sarpoulet, J., Martinez, J., et al., *Mechanosynthesis of amides in the total absence of organic solvent from reaction to product recovery*. Chem. Commun. (Camb), 2012. **48**(96): p. 11781-11783.
40. Narang, A.S., Delmarre, D., and Gao, D., *Stable drug encapsulation in micelles and microemulsions*. Int. J. Pharm., 2007. **345**(1-2): p. 9-25.
41. Nolles, A., van Dongen, N.J.E., Westphal, A.H., Visser, A., Kleijn, J.M., et al., *Encapsulation into complex coacervate core micelles promotes EGFP dimerization*. Phys. Chem. Chem. Phys., 2017. **19**(18): p. 11380-11389.
42. Zhou, H., Sun, X., Zhang, L., Zhang, P., Li, J., et al., *Fabrication of biopolymeric complex coacervation core micelles for efficient tea polyphenol delivery via a green process*. Langmuir, 2012. **28**(41): p. 14553-14561.
43. Crini, G., *Review: a history of cyclodextrins*. Chem. Rev., 2014. **114**(21): p. 10940-10975.
44. Khouri, S.i.J., Abdel-Rahim, I.A., and Shamaileh, E.M., *A thermodynamic study of  $\alpha$ -,  $\beta$ -, and  $\gamma$ -cyclodextrin-complexed m-methyl red in alkaline solutions*. J. Incl. Phenom. Macrocycl. Chem., 2012. **77**(1-4): p. 105-112.
45. Kuwabara, T., Nakajima, H., Nanasawa, M., and Ueno, A., *Color Change Indicators for Molecules Using Methyl Red-Modified Cyclodextrins*. Anal. Chem., 1999. **71**(14): p. 2844-2849.
46. Thendral, P. and Thulasidhasan, J., *Inclusion complexation of methyl orange and methyl red with  $\alpha$ - and  $\beta$ -cyclodextrin: spectral and theoretical study*. I. J. C. P. S., 2018. **9**(1): p. 25-33.
47. Alvariza, C., Usero, R., and Mendicuti, F., *Binding of dimethyl 2,3-naphthalenedicarboxylate with  $\alpha$ -,  $\beta$ - and  $\gamma$ -cyclodextrins in aqueous solution*. Spectrochim. Acta A Mol. Biomol. Spectrosc., 2007. **67**(2): p. 420-429.
48. Pastor, I., Marino, A.D., and Mendicuti, F., *Complexes of dihexyl 2,6-naphthalenedicarboxylate with  $\alpha$ - and  $\beta$ -cyclodextrins: Fluorescence and molecular modelling*. J. Photochem. Photobiol. A, 2005. **173**(3): p. 238-247.
49. Bibby, D.C., Davies, N.M., and Tucker, I.G., *Poly(acrylic acid) microspheres containing cyclodextrin: loading and in vitro release of two dyes*. Int. J. Pharm., 1999. **187**: p. 243-250.
50. Dollendorf, C., Hetzer, M., and Ritter, H., *Polymeric redox-responsive delivery systems bearing ammonium salts cross-linked via disulfides*. Beilstein J. Org. Chem., 2013. **9**: p. 1652-1662.
51. III, R.O.W., Mahaguna, V., and Sriwongjanya, M., *Characterization of an inclusion complex of cholesterol and hydroxypropyl- $\beta$ -cyclodextrin*. Eur. J. Pharm. Biopharm., 1998(46): p. 355-360.

52. Sun, Q., Fang, S., Fang, Y., Qian, Z., and Feng, H., *Fluorometric detection of cholesterol based on beta-cyclodextrin functionalized carbon quantum dots via competitive host-guest recognition*. *Talanta*, 2017. **167**: p. 513-519.
53. Mitra, S. and Dungan, S.R., *Cholesterol Solubilization in Aqueous Micellar Solutions of Quillaja Saponin, Bile Salts, or Nonionic Surfactants*. *J. Agric. Food Chem.*, 2001. **49**: p. 384-394.
54. Haberland, M.E. and Reynolds, J., *Self-association cholesterol*. *Proc. Nat. Acad. Sci.*, 1973: p. 2313-2316.
55. Blanco-Fernandez, B., Concheiro, A., Makwana, H., Fernandez-Trillo, F., Alexander, C., et al., *Dually sensitive dextran-based micelles for methotrexate delivery*. *RSC Advances*, 2017. **7**(24): p. 14448-14460.
56. Deshmukh, A.S., Chauhan, P.N., Noolvi, M.N., Chaturvedi, K., Ganguly, K., et al., *Polymeric micelles: Basic research to clinical practice*. *Int. J. Pharm.*, 2017. **532**(1): p. 249-268.
57. Nolles, A., Westphal, A.H., de Hoop, J.A., Fokkink, R.G., Kleijn, J.M., et al., *Encapsulation of GFP in Complex Coacervate Core Micelles*. *Biomacromolecules*, 2015. **16**(5): p. 1542-1549.
58. Zhang, X., Poniewierski, A., Jelinska, A., Zagozdzon, A., Wisniewska, A., et al., *Determination of equilibrium and rate constants for complex formation by fluorescence correlation spectroscopy supplemented by dynamic light scattering and Taylor dispersion analysis*. *Soft Matter*, 2016. **12**(39): p. 8186-8194.
59. Wei, X., Dong, R., Wang, D., Zhao, T., Gao, Y., et al., *Supramolecular Fluorescent Nanoparticles Constructed via Multiple Non-Covalent Interactions for the Detection of Hydrogen Peroxide in Cancer Cells*. *Chemistry*, 2015. **21**(32): p. 11427-11434.
60. Lu, Y. and Park, K., *Polymeric micelles and alternative nanonized delivery vehicles for poorly soluble drugs*. *Int. J. Pharm.*, 2013. **453**(1): p. 198-214.
61. Wang, J., Velders, A.H., Gianolio, E., Aime, S., Vergeldt, F.J., et al., *Controlled mixing of lanthanide(III) ions in coacervate core micelles*. *Chem. Commun. (Camb)*, 2013. **49**(36): p. 3736-3738.
62. Xu, L., Feng, L., Han, Y., Jing, Y., Xian, Z., et al., *Supramolecular self-assembly enhanced europium(III) luminescence under visible light*. *Soft Matter*, 2014. **10**(26): p. 4686-4693.
63. Hu, Q.D., Tang, G.P., and Chu, P.K., *Cyclodextrin-based host-guest supramolecular nanoparticles for delivery: from design to applications*. *Acc. Chem. Res.*, 2014. **47**(7): p. 2017-2025.





# CHAPTER 7

---

---

## Summary

---

---

## 7.1. SUMMARY

The treatments of chronic and severe disorders, such as heart diseases, cancer and diabetes still remain challenging for health care researchers, due to the severe side effects and the limited efficacy.[1, 2] Drugs have often low targeted specificity, non-selective bio-distribution and poor water-solubility, leading to increase the drug quantity and, thus, also the unwanted side effects. Nanotechnology is emerging as an alternative approach to conventional disease treatments, applicable in early diagnosis, therapy monitoring, drug delivery, and guided surgery.[3-5] Nanotechnology has several advantages, compared to conventional treatments, such as i) high surface to volume ratio, ii) favorable and controlled drug release profile, iii) possibility to functionalize the surface and iv) long time circulation in the blood stream.[6-9] Those properties allow nanocarriers to interact more efficiently with tumor cells, release drugs in a precise and localized way and avoid premature drug release.[10] Polymer-based micelles seem promising in nanomedicine, due to their ability of solubilizing poorly water-soluble drugs and to their biocompatibility.[11] Within polymer-based micelles, Complex Coacervate Core Micelles, or C3Ms, demonstrated to encapsulate a wide range of cargoes, such as DNA, RNA, protein, enzymes, etc.[12-18]. The ability of encapsulating several charged cargoes relies on their self-assembly, based on electrostatic interactions between oppositely charged block copolymers. However, more insight on controlling and fine tuning the assembly and disassembly behavior of coacervate core micelles is still needed. Cohen Stuart's group has achieved a higher control of the core assembly, compared to the first C3Ms micelles, by using coordination chemistry. The negatively charged polymer was substituted by a negatively charged metal-to-ligand coordination, between dipicolinic acid molecules (DPA) and metal ions. Di-cationic transition metal ions (II), such as Fe, Ni, Co or Zn, can be coordinated by two DPA<sup>2-</sup> molecules.[19] This coordination forms core-units with a residual negative charge in the core. By adding a neutral and positively charged block copolymer, the residual negative charge can be neutralized, thus, leading to the formation of metal-to-ligand-based C3Ms. C3Ms, based on these metal-to-ligand coordination structures, are very versatile, di-cationic transition metal ions can be substituted with lanthanides (III), tuning the core structure from linear to branched and adjusting the derived properties of the micelle.[20-23] In 2014 Wang *et al.* reported an elegant approach to achieve new insight on the assembly of C3Ms, on their aggregation

number and their packing density, by encapsulating negatively-charged PAMAM dendrimers into C3Ms, forming the so-called dendrimicelles.[24-27] While the size and the structure of these dendrimicelles are independent of the dendrimer generation, the aggregation number varied from 100 to 1, by increasing the dendrimer generation from 2 to 9. Moreover, dendrimers of generation below 2 were not able to form any dendrimicelles, indicating that there might be a minimum amount of charges required for coacervation. A novel approach to investigate this concept, is described in chapter 1.

In **chapter 1**, we discussed the current challenges in the biomedical field and we introduced C3Ms as possible candidates to overcome these challenges, due to their ability to solubilize poorly water-soluble drugs, the high stability against salt and dilution and the great versatility. A special attention was put on the progressive developments of well-controlled C3Ms assembly, by combining metal-to-ligand coordination and dendrimers inside coacervate micelles. The encapsulation of dendrimers inside micelles shined new light on the aggregation number and the packing density of different dendrimer generations inside micelles. Found that dendrimers of low generations were not able to form any dendrimicelles, we hypothesized that there might be a minimum amount of charges required for coacervation. Determining that value by using dendrimers would be limited by the dendrimer generation and, therefore, not possible in a precise way. The goal of this thesis was to integrate host-guest interactions inside the core of complex coacervate micelles, and bring new insights in the micellar ability to assemble and disassemble under precise and controlled stimuli, by finely tuning the charge.

In **chapter 2** we focused on the design of a new class of micelles, called Cyclodextrin-based Complex Coacervate Core Micelles or C4Ms. The self-assembly of C4Ms consists of three steps: i) the formation of a metal-to-ligand coordination, by mixing europium ions and cyclodextrin-modified dipicolinic acid ( $\beta$ CD-DPA), ii) the complexation of host-guest interactions, by adding adamantane guests to the metal-to-ligand coordination and iii) the final micelle formation, by adding the block copolymer until charge neutralization. In step i) the metal-to-ligand coordination structure

presents three negative charges, derived from the interaction of one europium ions (3+) and three  $\beta$ CD-DPA (2-) molecules. In step ii), two charged adamantane guest, Ad-monoacid (1-) or Ad-bisacid (2-) are added to the metal-to-ligand coordination, forming the host-guest core-unit structure. By adding Ad-monoacid or Ad-bisacid in different ratios, the charge of the coordination structure was increased from 3- to 6- up to 9-. In step iii), the residual core charges are neutralized, by adding the block copolymer to the host-guest structure. By comparing the different core-unit structures, we determined that seven were the minimum number of charges per core-unit, required for coacervation. Six negative charges per core-unit were not able to form well-defined spherical micelles, but rather undefined aggregates. C4Ms stability against salt and dilution was enhanced by adding an adamantane guest bislinker, able to combine multiple monomeric core-units into strong polymeric networks.

In **chapter 3**, we designed redox-responsive C4Ms, called Ad-SS-Ad-based C4Ms, based on the knowledge acquired in **chapter 2**. Redox is considered an “**internal stimulus**”, because the response is triggered by intrinsic characteristics of tumor cells.[28-30] Therefore, designing smart C4Ms, able to disassemble upon high concentration of reducing agent, could be advantageous for future biomedical applications. In this chapter, Ad-SS-Ad-based C4Ms were designed combining four orthogonal interactions, namely i) metal-to-ligand coordination, ii) host-guest interaction, iii) electrostatic interaction and iv) disulfide cross-link. Upon reducing agent treatment, the disulfide cross-link is cleaved into thiolates, favoring the micellar disassembly. This disassembly is reversible over time, due to the re-oxidation of thiolates to disulfides. The rate of re-assembly was controlled by varying the DTT concentration and the ratio between redox-responsive and non-redox-responsive bislinkers. Preliminary studies showed that Ad-SS-Ad-based C4Ms promote the solubilization of Methyl Red in water and its release (i.e. to the organic phase) upon micelle dissociation. These results suggested that stimuli-responsive C4Ms could be promising for future drug delivery applications.

In **chapter 4**, ferrocene-based C4Ms were designed to respond to  $H_2O_2$  oxidation.  $H_2O_2$  is a Reactive Oxygen Species (ROS) that originates from aerobic metabolism by-products and therefore is

relevant in stress-related biological studies.[31, 32] The key molecule for the oxidant-response property was the ferrocene–modified dipicolinic acid, (Fc-DPA). In its reduced form, Fc-DPA can form a medium-strong complex with  $\beta$ CD. However, when oxidized, the complexation does not occur, favoring the micellar destabilization. The stability against the oxidant was controlled in three ways: i) by changing monomeric-units into polymeric branched networks, ii) by varying the oxidant equivalents and iii) by adding a non-responsive guest.

In **chapter 5**, azobenzene-modified dipicolinic acid (Azo-DPA) and  $\alpha$ CD-DPA were used as light-responsive host-guest couple. Light is considered an ideal external stimulus, because time, space, intensity, size sport, etc. can be regulated by an external user. In its *trans* isoform, Azo-DPA can complex with  $\alpha$ CD-DPA with medium-high association constant. Upon 365 nm light excitation, Azo-DPA isomerizes to its *cis* isoform, leaving the  $\alpha$ CD cavity. In this chapter, the knowledge on the charge, acquired in chapter 2, was crucial to weaken the assembly of Azo-based C4Ms and favor the micellar disassembly, under light stimuli.

**Chapter 6** summarises the most important findings of each chapter, the current challenges and the future developments of C4Ms. We consider that C4Ms contributed to the progress of polymeric micelles, allowing a better control on the micelle formation and dissociation, driven by redox,  $H_2O_2$  and light stimuli. The encapsulation and release results, discussed in this thesis, suggest that C4Ms might be a promising tool for drug delivery applications. However, additional studies should be performed, such as the combination of multiple stimuli, e.g. redox and light, and biologically relevant experiments, e.g. toxicity tests, glutathione and near infrared responses, for a concrete application of C4Ms in biomedical field.

## 7.2. REFERENCES

1. Bjornmalm, M., Thurecht, K.J., Michael, M., Scott, A.M., and Caruso, F., *Bridging Bio-Nano Science and Cancer Nanomedicine*. ACS Nano, 2017. **11**(10): p. 9594-9613.
2. Blanco, E., Hsiao, A., Mann, A.P., Landry, M.G., Meric-Bernstam, F., et al., *Nanomedicine in cancer therapy: innovative trends and prospects*. Cancer Sci., 2011. **102**(7): p. 1247-1252.
3. Liu, Y., Miyoshi, H., and Nakamura, M., *Nanomedicine for drug delivery and imaging: a promising avenue for cancer therapy and diagnosis using targeted functional nanoparticles*. Int. J. Cancer, 2007. **120**(12): p. 2527-2537.
4. Muthu, M.S., Leong, D.T., Mei, L., and Feng, S.S., *Nanotheranostics - application and further development of nanomedicine strategies for advanced theranostics*. Theranostics, 2014. **4**(6): p. 660-677.
5. Heath, J.R., *Nanotechnologies for biomedical science and translational medicine*. Proc. Natl. Acad. Sci. U. S. A., 2015. **112**(47): p. 14436-14443.
6. Lee, J.J., Saiful Yazan, L., and Che Abdullah, C.A., *A review on current nanomaterials and their drug conjugate for targeted breast cancer treatment*. Int. J. Nanomedicine, 2017. **12**: p. 2373-2384.
7. S., T.A. and S., G.S., *Nanooncology: The Future of Cancer Diagnosis and Therapy*. CA Cancer. J. Clin., 2019. **63**: p. 398-418.
8. Lembo, D. and Cavalli, R., *Nanoparticulate delivery systems for antiviral drugs*. Antivir. Chem. Chemother., 2010. **21**(2): p. 53-70.
9. Tran, S., DeGiovanni, P.J., Piel, B., and Rai, P., *Cancer nanomedicine: a review of recent success in drug delivery*. Clin. Transl. Med., 2017. **6**(1): p. 1-21.
10. Jahangirian, H., Lemraski, E.G., Webster, T.J., Rafiee-Moghaddam, R., and Abdollahi, Y., *A review of drug delivery systems based on nanotechnology and green chemistry: green nanomedicine*. Int. J. Nanomedicine, 2017. **12**: p. 2957-2978.
11. Ahmad, Z., Shah, A., Siddiq, M., and Kraatz, H.-B., *Polymeric micelles as drug delivery vehicles*. RSC Adv., 2014. **4**(33): p. 17028-17038.
12. Kim, J.O., Nukolova, N.V., Oberoi, H.S., Kabanov, A.V., and Bronich, T.K., *Block Ionomer Complex Micelles with Cross-Linked Cores for Drug Delivery*. Polym. Sci. Ser. A Chem. Phys., 2009. **51**(6): p. 708-718.
13. Voets, I.K., de Keizer, A., and Cohen Stuart, M.A., *Complex coacervate core micelles*. Adv. Colloid Interface Sci., 2009. **147-148**: p. 300-318.
14. S., L., R., d.V., W., N., and A., C.S.M., *Structure and Stability of Complex Coacervate Core Micelles with Lysozyme*. Biomacromolecules, 2007. **8**: p. 2219-2227.
15. Obermeyer, A.C., Mills, C.E., Dong, X.H., Flores, R.J., and Olsen, B.D., *Complex coacervation of supercharged proteins with polyelectrolytes*. Soft Matter, 2016. **12**(15): p. 3570-3581.
16. Nolles, A., Westphal, A.H., Kleijn, J.M., van Berkel, W.J.H., and Borst, J.W., *Colorful Packages: Encapsulation of Fluorescent Proteins in Complex Coacervate Core Micelles*. Int. J. Mol. Sci., 2017. **18**(7): p. 1-19.
17. Nolles, A., Westphal, A.H., de Hoop, J.A., Fokkink, R.G., Kleijn, J.M., et al., *Encapsulation of GFP in Complex Coacervate Core Micelles*. Biomacromolecules, 2015. **16**(5): p. 1542-1549.
18. Bourouina, N., de Kort, D.W., Hoeben, F.J., Janssen, H.M., Van As, H., et al., *Complex Coacervate Core Micelles with Spectroscopic Labels for Diffusometric Probing of Biopolymer Networks*. Langmuir, 2015. **31**(46): p. 12635-12643.
19. Wang, J., de Keizer, A., Fokkink, R., Yan, Y., Cohen Stuart, M.A., et al., *Complex coacervate core micelles from iron-based coordination polymers*. J. Phys. Chem. B, 2010. **114**(25): p. 8313-8319.
20. Yang, L., Ding, Y., Yang, Y., Yan, Y., Huang, J., et al., *Fluorescence enhancement by microphase separation-induced chain extension of Eu<sup>3+</sup> coordination polymers: phenomenon and analysis*. Soft Matter, 2011. **7**(6): p. 2720-2724.
21. Hernandez-Garcia, A., Velders, A.H., Stuart, M.A., de Vries, R., van Lent, J.W., et al., *Supramolecular Virus-Like Nanorods by Coassembly of a Triblock Polypeptide and Reversible Coordination Polymers*. Chemistry, 2017. **23**(2): p. 239-243.
22. Wang, J., Velders, A.H., Gianolio, E., Aime, S., Vergeldt, F.J., et al., *Controlled mixing of lanthanide(III) ions in coacervate core micelles*. Chem. Commun. (Camb), 2013. **49**(36): p. 3736-3738.
23. Wang, J., Groeneveld, A., Oikonomou, M., Prusova, A., Van As, H., et al., *Revealing and tuning the core, structure, properties and function of polymer micelles with lanthanide-coordination complexes*. Soft Matter, 2016. **12**(1): p. 99-105.
24. Wang, J., Voets, I.K., Fokkink, R., van der Gucht, J., and Velders, A.H., *Controlling the number of dendrimers in dendrimicelle nanoconjugates from 1 to more than 100*. Soft Matter, 2014. **10**(37): p. 7337-7345.
25. Ten Hove, J.B., Wang, J., van Leeuwen, F.W.B., and Velders, A.H., *Dendrimer-encapsulated nanoparticle-core micelles as a modular strategy for particle-in-a-box-in-a-box nanostructures*. Nanoscale, 2017. **9**(47): p. 18619-18623.

26. Ten Hove, J.B., Wang, J., van Oosterom, M.N., van Leeuwen, F.W.B., and Velders, A.H., *Size-Sorting and Pattern Formation of Nanoparticle-Loaded Micellar Superstructures in Biconcave Thin Films*. ACS Nano, 2017. **11**(11): p. 11225-11231.
27. Ten Hove, J.B., van Oosterom, M.N., van Leeuwen, F.W.B., and Velders, A.H., *Nanoparticles reveal Extreme Size-Sorting and Morphologies in Complex Coacervate Superstructures*. Sci. Rep., 2018. **8**(1): p. 13820-13827.
28. Giustarini, D., Galvagni, F., Tessei, A., Farolfi, A., Zanoni, M., et al., *Glutathione, glutathione disulfide, and S-glutathionylated proteins in cell cultures*. Free Radic. Biol. Med., 2015. **89**: p. 972-981.
29. Mura, S., Nicolas, J., and Couvreur, P., *Stimuli-responsive nanocarriers for drug delivery*. Nat. Mater., 2013. **12**(11): p. 991-1003.
30. Katayose, S. and Kataoka, K., *Water-Soluble Polyion Complex Associates of DNA and Poly(ethylene glycol)-Poly(L-lysine) Block Copolymer*. Bioconjug. Chem., 1997. **8**: p. 702-707.
31. Huo, M., Yuan, J., Tao, L., and Wei, Y., *Redox-responsive polymers for drug delivery: from molecular design to applications*. Polym. Chem., 2014. **5**(5): p. 1519-1528.
32. Liu, L., Rui, L., Gao, Y., and Zhang, W., *Self-assembly and disassembly of a redox-responsive ferrocene-containing amphiphilic block copolymer for controlled release*. Polym. Chem., 2015. **6**(10): p. 1817-1829.



# Acknowledgments

Among the propositions, the papers and all the chapters, the acknowledgment section was the hardest part to write. This is probably due to the roller-coaster of feelings that I experienced during the PhD.

The 26<sup>th</sup> of August 2015 I took a one-way ticket for the Netherlands: without knowing anyone, neither friends nor colleagues, without having a clue about the weather, landscape, food and Dutch work-life balance. Especially, I had no clear idea of what it meant to do a PhD.

The day after I landed, I walked to the top of the “mountain”, at the Dreijen, to meet Professor Aldrik Velders. Aldrik, you are the first person I would like to thank. I truly admire the passion you have in teaching a new generation of curious students and the perseverance for doing always the “right thing”. Thank you for the endless discussions on the paper versions, but especially for your humanity beyond science.

I would like to thank my co-promotor, Vittorio Saggiomo, for the organic chemistry lessons and the time and efforts spent in giving me feedback on power point presentations and papers. Especially after the first year, we clicked in a pretty strong and unique brotherhood bond.

Anton, thank you for the prompt feedback on the thesis and on the papers. Thanks especially for your unconditional loyalty and constant help. (Thanks for refilling always a stock of chocolate and chewing gums in the first drawer)

Banu, thank you for making my day every single day. I admire you as a woman, as a mother and as a friend.

Thanks Gerben, the songs you were constantly singing made the soundtrack of my PhD. ♪ *The final countdown* ♪ Thanks to Sander(s) for the nerd jokes and the *lekker* coffee. Thanks to the craziest and loudest people in the BNT group, Stan, Laura and JB, you are the core of the BNT group. Rebecca, thanks for the (non) scientific talks in front of the DLS. Koen, the Friday meetings with you were more politically correct! Thanks to Pieter for the help and patience during my private NMR lessons and to Fatemeh and Rosa for the nice chats during the breaks. Thanks to the new entries, Yurdanur and Ningyi, it was nice to spend time with you! Isabelle, Ebru, Ravin, Karthik,

Simon: this work would not have been possible without your help. We grew up together! I want to thank some special ex BNT members: Lars, Samuel, Maria, Jeroen and Junyou.

I want to thank the PCC group, for the financial support when we were on the “mountain” and for the friendly atmosphere. Special thanks to Mara and Josie, you took care of me like your daughter! I want to thank Remco for the DLS discussions, it was such a pleasure to work with you in the DLS lab. Ilse, Lione and Diane for the shared talks during CHAINS!

My PCC-Volleyball mates: Anton, Joshua, Sven, Nik, Henk, Joshua, Martijn and Hui, come on guys let's conquer the last field!

Thanks to the PI's involved in the Marie Curie ITN for the constructive feedback on my presentations. Thanks to my PhD colleagues in the ResMoSys ITN: Vanessa, Giuseppe, Ligia, Albano, Antanas, Guille, Marion, Qiang, Zhang, John. I will never forget our meetings, the first in Cambridge, the serious one in Amsterdam and the (very) informal one in Budapest. Looking forward for the next ones!

Pascal Hervé, tu étais un bon mentor pour moi! Matthieu, Guillaume, Hélène, Jordy, Justine, Alois, Charles, Arnaud, Hamza, Celeste and Leila, c'était une expérience merveilleuse de travailler avec vous! 😊

Monica, una splendida amicizia nata a Bordeaux e continuata sul lago!

♪ *With a little help from my friends* ♪

A special thanks to “La casa del popolo”; it would have been hard to survive without the home-made tagliatelle, gnocchi, cannelloni, limoncello, finocchietto, spritz, etc... Quando mi mancava il calore, il sapore e il profumo di casa... lo trovavo alla casa del popolo con voi. Un grazie speciale al fondatore Fabian e a tutti gli adepti Marco, Enrico, Nicolò, Riccardo, Nicola, Giulia, Lavinia, Stefano, Pietro, Erika, Francio, Cata, Agatina. Vi aspetto sul lago di Garda. ♪ *Country roads, take me home* ♪

Thanks to Tanya with whom I had a special connection from the very first moment we met. And thanks to Chris, Maartje and Claudio, with whom I connected deeply in Frankfurt for a very special wedding.

Fede, the movies and documentaries were more funny with you :) Thanks to my Herenstraat friends: Erika, Ben, Tatiana and Dora. Gracias por mi locas amigas: Juliana, Paty, Elvira, Raisa, Claudine por almuerzos y cenas de Josephine! Thanks to Renske, Sjosh, Eleni, Simha, Mattia and Bastian for the chats in front of a coffee!

Grazie a Marco ed Elisa, per la pizza, le chiacchierate e gli sfoghi. Mi avete fatto sentire più vicina a casa!

Special thanks to the Amnesty International and the Story Telling groups in Wageningen.

Thanks to Ingi for the hard work-out at the Bongerd. ♪I say, take me out! ♪

Friendship without borders, thanks to my Italian supporters from home:

Cicci, Gio, Betta, Pedo, Spa, Marti, Modi, Eli, Amby, Andrei, Paciu: grazie ragazzi del supporto e di essere venuti a trovarmi in quel di Wag e per aver fatto un viaggio di 12 h in macchina per rimanere solo 24 h! Ma almeno l' antico vaso é in salvo <Amarone> ;)

Grazie Amby, hai sempre creduto nelle mie capacità. Grazie per essere venuta a trovar<mi> così spesso. Ogni volta era una nuova avventura. Grazie soprattutto ad Elisa, per le lunghe telefonate e il supporto durante le mie ripetute crisi all' aeroporto di Malpensa. Grazie davvero. Grazie a Betta per rappresentare un forte role model di donna in carriera. ♪*Respect* ♪

Grazie a Marina, Manuel, Anna, Erik, Mery e Arban per le indimenticabili serate sul lago e ad Amsterdam!

Grazie a Donatella e Luigi per essere la mia seconda famiglia e soprattutto per i pacchi da giu'! :)

Grazie Eleonora per il tempo passato insieme a Leiden e le lunghe chiacchierate al Hoge Veluwe Park. Grazie Carlo Alberto, tornare in Italia e cambiare le cose é un dovere.

Grazie Silvia per aver messo ordine in tutto questo.

Casa é casa, anzi casa é dove c' é la mia famiglia. Durante il dottorato ho perso due persone molto care e che credevano molto in me, la nonna Bruna e la zia Aureliana. Voglio ringraziare le altre persone che mi appoggiano tutti i giorni: gli zii, Tullio, Morena, Papi, Dany, Norma e i cugini, Nicola, Carlotta, Anna e Riccardo. Un grazie speciale alla mia nonna Maria, che credo abbia sofferto più di tutti la mia lontananza. E che dopo ogni mia cartolina diceva: "Ndo ela adeso quelal la?!"

♪*We are family*♪ Grazie anche ad Argo che mi aspetta dopo questa lunga Odissea.

Grazie a mia mamma. La prima femminista io abbia conosciuto nella mia vita, “Puoi essere chi vuoi nella vita, fare qualsiasi lavoro, non ci sono barriere per noi donne, se non quelle che ci mettiamo noi stesse!”. Ricordo ancora la mia crisi del secondo anno di dottorato, quando mi hai riagganciato il telefono dicendo “L’ hai iniziato e lo porti a termine, non mollare. Lo sai che puoi farcela!”. Le prime vere lezioni di vita le ho imparate da te.

Grazie a mio papà. Sapevo di aver preso la testardaggine, ma ora mi é chiaro che anche l’ ambizione e la passione per i viaggi e la voglia di lavorare in un ambiente internazionale.

Un grazie speciale alle mie testimoni di dottorato: Julia e Raquel, siete qui perché non siete solo colleghe, ma parte della mia famiglia. ♪ *Sisters Are Doin' It for Themselves* ♪

Julia you remain an incredible friend, colleague and person. I learnt so much from you, that I cannot even explain it in these few sentences. You are my lighthouse, the person I want to resemble.

Raquel, I met you “only” last year during the “Women In Science Conference”. Since then our friendship consolidated very fast and strong. Between coffees and #niunamas parades, tu vuelves en mi media naranja.

Today, 26<sup>th</sup> of October 2019, it’s time for a showdown.

This PhD experience involved very hard moments and great memorable times. It strengthened my personality and made me reschedule a whole new priority list in my life.

I will leave the Netherlands with an open ticket: having met a lot of great people, nice friends, funny colleagues and two sisters, an hot lead on the weather (bleah), the landscape (berg?! tzz), food (which one?- the Italian home-made one!) and the Dutch work-life balance (great, except for the last year of PhD) and of course a clear idea of what it meant to do a PhD.

Thank you all for being a part of this journey. ♪ *It's a long way to the top...* ♪

E con questo si concludono i miei tre cantici, triennale, specialistica e dottorato, proprio come l’ inferno, il purgatorio e il paradiso. Anche se non nello stesso ordine.

E infine grazie a te, Mirko, che hai sopportato i miei *roller-coaster* moments, dai miei momenti bui e a quelli euforici, le mie cadute e i miei successi... sei l’amor che move il sole e l’altre stelle.





## ABOUT THE AUTHOR

The author of this thesis was born in 1990 in Peschiera Del Garda, Italy. She moved to Verona to study Biotechnology and obtained her bachelor degree with a thesis entitled “Study and characterization of Selenium nanoparticles from *Stenotrophomonas maltophilia* bacteria, through AFM technique”, under the supervision of Prof. Romeo. She completed *cum laude* the Master in Science and Technology of Bio-Nanomaterials at the Ca' Foscari University of Venice with the thesis “Development of lanthanide doped alkaline earth fluorides core-shell nanoparticles for nanothermometry and drug delivery”, on upconverting nanoparticles, under the supervision of Prof. Speghini. She spent also part of her master at the *Institute National De La Recherche Scientifique* of Montreal, Canada, under the supervision of Prof. Vetrone.



Since September 2015 she has been working in the ResMoSys ITN Marie Curie network as PhD student, in the BioNT group of Prof. Velders at the University of Wageningen, the Netherlands. During her PhD, she worked at the I.S.I.S. in Strasbourg, under the supervision of Prof. De Cola and at Solvay, in Bordeaux, under the supervision of Dr. Pascal Herve'. Her focus was to investigate the assembly and disassembly behaviours of stimuli-responsive supramolecular polymer-based micelles, for future drug delivery and contrast agent applications.

The outcomes of her research are described in this thesis.



## OVERVIEW OF COMPLETED TRAINING ACTIVITIES (VLAG)

### CATEGORY A: TRAINING PROGRAMME

<i>Name of the course</i>	<b>Organization</b>	<b>City</b>	<b>Year</b>
<i>CHAINS conference</i>	NWO	Veldoven (NL)	2015
<i>CHAINS conference</i>	NWO	Veldoven (NL)	2016
<i>CHAINS conference</i>	NWO	Veldoven (NL)	2017
<i>CHAINS conference</i>	NWO	Veldoven (NL)	2018
<i>Cambridge conference ISMSC</i>	RCS	Cambridge (GB)	2017
<i>Marie Curie ITN workshop-spectroscopy</i>	Resmosys	Strasbourg (F)	2016
<i>Marie Curie ITN workshop-scattering</i>	Resmosys	Wageningen (NL)	2016
<i>Marie Curie ITN workshop-crystallography</i>	Resmosys	Cambridge (GB)	2017
<i>Marie Curie ITN workshop-IP patent</i>	Resmosys	Copenhagen (DK)	2018
<i>Marie Curie ITN workshop-quartz microbalance</i>	Resmosys	Stockholm (SE)	2018
<i>Strasbourg secondment</i>	Resmosys	Strasbourg (F)	2016
<i>Solvay internship-organogels</i>	Resmosys	Bordeaux (F)	2018
<i>Biobusiness summer school</i>	Hyphen	Amsterdam (NL)	2019
<i>International conference ISMSCS + SUPRAMOL</i>	RSC	Lecce (Italy)	2019
<i>Advance organic chemistry</i>	VLAG	Wageningen (NL)	2015-2017
<i>Women in science conference Insight-out</i>	NOW	Ede, Amersfoort (NL)	2016, 2018

### CATEGORY B: GENERAL COURSES

<i>Name of the course</i>	<b>Organization</b>	<b>City</b>	<b>Year</b>
<i>The essentials of writing and presenting</i>	WGS	Wageningen (NL)	2016
<i>Scientific publishing</i>	WGS	Wageningen (NL)	2017
<i>Efficient writing strategies</i>	WGS	Wageningen (NL)	2017
<i>Interpersonal communication</i>	VLAG	Wageningen (NL)	2017
<i>Stress identification management</i>	WGS	Wageningen (NL)	2017
<i>Scientific writing</i>	WGS	Wageningen (NL)	2017
<i>Publishing with impact</i>	WGS	Wageningen (NL)	2017
<i>Brain training</i>	WGS	Wageningen (NL)	2017
<i>PhD day</i>	Radboud University	Nijmegen (NL)	2017
<i>Career orientation</i>	VLAG	Wageningen (NL)	2019
<i>Utrecht career workshop</i>	Hyphen	Utrecht (NL)	2017-2019

**CATEGORY C: OPTIONALS**

<b>Name of the course</b>	<b>City</b>	<b>Year</b>
<i>Preparation of research proposal</i>	Wageningen	2016
<i>PhD study tour to Denmark and Sweden*</i>	Copenhagen, Lund, Malmo	2018
<i>Weekly group meetings with the entire group (Fridays)</i>	Wageningen	2015-2019
<i>Weekly group meetings with the students (Mondays)</i>	Wageningen	2017-2018
<i>Monthly groups meetings (research topic micelles)</i>	Wageningen	2017-2018
<i>Literature updates (fridays)</i>	Wageningen	2015-2019

\* organization of the PhD trip

**I: Practicals - TEACHING OBLIGATIONS**

<b>Name and code of the course</b>	<b>Year</b>
<i>Bionanotechnology introduction BNT50806</i>	2015-2018
<i>Bionanotechnology towards nanomedicine BNT30306</i>	2015-2019

**II: Supervision of MSc- and BSc-students and internships (90 hrs major thesis, 60 hours minor thesis and 30 hours internship)**

<b>Name of the MSc student</b>	<b>Year</b>
<i>Isabelle Povel</i>	2015-2016
<i>Ebru Acun</i>	2017-2018
<i>Ravin Sharma</i>	2017-2018
<i>Simon van Hurne</i>	2018-2019
<i>Karthik Gangadharaiiah</i>	2018-2019





## SCIENTIFIC PUBLICATIONS

- \* **C. Facciotti**, V. Saggiomo, A. Bunschoten, R. Fokkink, J. B. T. Hove, J. Wang and A. H. Velders, *Soft Matter*, 2018, 14, 9542, “Cyclodextrin-based complex coacervate core micelles with tuneable supramolecular host-guest, metal-to-ligand and charge interactions.” DOI: 10.1039/c8sm01504j, **(Chapter 2)**
- \* **C. Facciotti**, V. Saggiomo, A. Bunschoten, J. B. ten Hove, M. T. M. Rood, F. W.B. van Leeuwen, A. H. Velders “Assembly, Disassembly and Reassembly of Complex Coacervate Core Micelles with Redox-Responsive Supramolecular Cross-Linkers.” under revisions in *ChemSystemsChem*, **(Chapter 3)**
- \* **C. Facciotti**, V. Saggiomo, A. Bunschoten, S. van Hurne, R. Kaup, A. H. Velders “Oxidant-responsive ferrocene-based Complex Coacervate Core Micelles.” accepted in *SupramolChem*. DOI: 10.1080/10610278.2019.1685094, **(Chapter 4)**
- \* **C. Facciotti**, V. Saggiomo, K. Gangadharaiyah, A. Bunschoten, R. Kaup, S. Jansen, A. H. Velders “Light-responsive Cyclodextrin-based complex coacervate core micelles.” manuscript in preparation, **(Chapter 5)**

## ADDITIONAL PUBLICATIONS

- \* P. Cortelletti, **C. Facciotti**, I. X. Cantarelli, P. Canton, M. Quintanilla, F. Vetrone, A. Speghini and M. Pedroni, *Optical Materials*, 2017, 68, 29, “Nd<sup>3+</sup> activated CaF<sub>2</sub> NPs as colloidal nanothermometers in the biological window.”
- \* P. Cortelletti, A. Skripka, **C. Facciotti**, M. Pedroni, G. Caputo, N. Pinna, M. Quintanilla, A. Benayas, F. Vetrone and A. Speghini, *Nanoscale*, 2018, 10, 2568, “Tuning the sensitivity of lanthanide-activated NIR nanothermometers in the biological windows.”





The research described in this thesis was financially supported by the European Union's Horizon 2020 research and innovation programme under the Marie Skłodowska-Curie grant agreement No. 642192.

Cover designed by Carola Speri

Printed by Proefschriften.nl